CRANFIELD UNIVERSITY

RAVI SHANKAR DHARMARAJ RAM MANOHAR

JOURNEY PREDICTIVE ENERGY MANAGEMENT STRATEGY FOR A PLUG-IN HYBRID ELECTRIC VEHICLE

SCHOOL OF ENGINEERING

PhD THESIS

CRANFIELD UNIVERSITY

SCHOOL OF ENGINEERING

PhD THESIS

Academic Year 2012 - 2013

RAVI SHANKAR DHARMARAJ RAM MANOHAR

Journey Predictive Energy Management Strategy for a Plug-in Hybrid Electric Vehicle

Supervisors: Dr. James Marco and Prof. Francis Assadian
May 2013

This thesis is submitted in partial fulfilment of the requirements
for the degree of Doctor of Philosophy

Abstract

The adoption of Plug-in Hybrid Electric Vehicles (PHEVs) is widely seen as an interim solution for the decarbonisation of the transport sector. Within a PHEV, determining the required energy storage capacity of the battery remains one of the primary concerns for vehicle manufacturers and system integrators. This fact is particularly pertinent since the battery constitutes the largest contributor to vehicle mass. Furthermore, the financial cost associated with the procurement, design and integration of battery systems is often cited as one of the main barriers to vehicle commercialisation. The ability to integrate the optimization of the energy management control system with the sizing of key PHEV powertrain components presents a significant area of research. Further, recent studies suggest the use of "intelligent transport" infrastructure to include a predictive element to the energy management strategy to achieve reductions in emissions. The thesis addresses the problem of determining the links between component-sizing, real-world usage and energy management strategies for a PHEV. The objective is to develop an integrated framework in which the advantages of predictive energy management can be realised by component downsizing for a PHEV.

The study is spilt into three sections. The first part presents the framework by which the predictive element can be included into the PHEV's energy management strategy. Second part describes the development of the PHEV component models and the various energy management strategies which control the split in energy used between the engine and the battery. In this section a new control strategy is presented which integrates the predictive element proposed in the first part. Finally, in the third section an optimisation framework is presented by which the size of the components within the PHEV are reduced due to the lower energy demands of the new proposed energy management strategy.

The first part of the study presents a framework by which the energy consumption of a vehicle may be predicted over a route. The proposed energy prediction framework employs a neural network and was used off-line for estimating the real-world energy consumption of the vehicle so that it can be later integrated within the vehicles energy management control system. Experimental results show an accuracy within 20%–30% when comparing predicted and measured energy consumptions for over 800 different real-world EV journeys.

The second part of the study is to develop a model with scalable PHEV components for evaluation. The base data was obtained from a real-world electric vehicle evaluation programme. A scalable engine was built using Willan's line

method. A number of different "charge-blended" control strategies were developed and evaluated based on an established instantaneous optimal control strategy. Two benchmarks were used for analysing the performance of the controllers. The global-optimal solution using dynamic programming was developed along with a well-known rule-based thermostat control strategy. On comparing two weeks of driving data from 40 different drivers, the new proposed control strategy was within 3% of the global optimal solution while the rule based controller was only within 12%. The non-applicability of "charge-blended approaches" for benchmarking PHEVs using legislative procedures were considered.

The final part of the thesis consists of an optimisation study in which the new proposed "charge-blended" controller is used to facilitate the downsizing of the electrical machine, the internal combustion engine and the high voltage battery. For a target gCO_2/km value and drive-cycle, results show that this approach can yield significant downsizing opportunities, with cost reductions on the order of 2%–9% being realisable.

The conclusion of the present work is that, by making use of real-world data and a "charge-blended" controller it is possible to achieve significant downsizing opportunities with no additional financial cost and "intelligent-transport" infrastructure. This would aid in further decarbonisation of the transport sector and make PHEVs more commercially viable.

Acknowledgements

I am very grateful to my supervisors Dr James Marco and to Professor Francis Assadian for their guidance and for believing in me. I am also thankful for their commitment to a high academic standard, which has inspired me to improve my work ethic.

I wish to thank Morgan Motor Company for giving me this learning opportunity and in particular Mr Robert Gibson who helped me with the LifeCar2 project. I wish to acknowledge and appreciate the valuable information from Cenex specifically with Mr. Steve Carroll for his helpful discussions.

I would like to thank my wife, Vidya, who kept pushing me forward and motivating me without losing sight of the end result. Her hard work ethic has been an inspiration for me and I would have to thank her for the long hours she sat with me to read the work I had produced.

I would also like to thank everybody in Cranfield who gave me a warm welcome and kind support. I am very grateful to my mates with whom I have shared both office and home: Stamatis Angelinas, Ganesh Mohan, Cian Harrington, Kevin Stevens, Michele Vianello and Stergios Topouris for their invaluable discussions, sparkling jokes and friendship.

Last but not the least I would like to thank Prof. James Whidbourne for his extensive help and believing in me to produce a high quality standard Thesis.

Finally, I would like to thank my family for always believing in me and making sure I never lost sight of my objectives during the tough moments.

Contents

List of Figures

List of Tables

List of Abbreviations

Advisor	Advanced Vehicle Simulator
ARTEMIS	Assessment and Reliability of Transport Emission Models and Inventory Systems
BIS	Department for Business, Innovation and Skills
CAN	Controller Area Network
CB	Charge blending mode
CD	Charge depletion mode
Cenex	Centre of Excellence for Low Carbon and Fuel Cell Technologies
CS	Charge sustaining mode
CSV	Comma Separated Value
DC/DC	Direct Current to Direct Current power converter
Defra	Department for Environment, Food and Rural Affairs
DP	Dynamic Programming
ECE	Economic Commission for Europe
ECMS	Equivalent Consumption Minimisation Strategy
ECU	Electronic control unit
EM	Electrical Machine
EOL	End of life
EPA	Environmental protection agency
EV	Electric Vehicle

GA	Genetic Algorithm
GIS	Geographical Information System
HV	High voltage
ICE	Internal Combustion Engine
INV	Inverter
JC08	JC08 chassis dynamometer test cycle for light vehicles
LV	Low voltage
mpg	miles per gallon
NEDC	New European Driving Cycle
NN	Neural Network
PF	Power follower strategy
PHEV	Plug-in Hybrid Electric Vehicle
PI	proportional integral controller
PSAT	Powertrain System Analysis Toolkit
RMSE	Root Mean Squared Error
SOC	State of Charge
TCO	Total cost of ownership
TTW	Tank to wheel
UDDS	Urban Dynamometer Driving Schedule
UK	United Kingdom
UNECE	United Nations Economic Commission for Europe
US	United States of America
WTW	Well to wheel

List of Symbols

α	Slope of the road
η_{em}	Efficiency of the EM
γ	Number of stops per microtrip
ω_{em}	Rotational speed of the electric machine (rad/s)
$\sigma_{v_{avg}}$	standard deviation of vehicle speed within the microtrip
ζ	Equivalence ratio
T_e	Torque of engine (Nm)
$\dot{m}_f(t)$	Mass of fuel flow (g/s)
η_e	Efficiency of Engine
ω_e	Speed of Engine (rad/s)
$c_m(t)$	Mean Piston Speed (m/s^2)
e	Thermodynamic Efficiency
F_r	Resistive force acting on the wheels of the vehicle (N)
g	Instantaneous consumption of fuel (g)
g_{equiv}	Equivalent amount of fuel used by the battery (g)
H_l	Fuel's Lower Heating Value
I_i	measure of intersection based traffic events
i_b	Current at the terminals of the battery (A)
i_{em}	Current at the terminals of the EM (A)

J	Minimisation Function
M_c	Mass of the chassis (kg)
M_v	Mass of the vehicle (kg)
M_{bat}	Mass of the battery (kg)
M_{cell}	Mass of the battery cell (kg)
M_{em}	Mass of the EM (kg)
M_{ice}	Mass of the ICE (kg)
N	Number of strokes
np	Number of cells in parallel
ns	Number of cells in series
P_{aux}	Auxiliary power load (W)
P_{bat}	Power drawn or supplied to the battery (W)
$P_{em(peak)}$	Peak power of the scaled EM (W)
P_{fuel}	Indicated Power (W)
P_{ice}	Power delivered by the integrated ICE and EM (W)
p_{loss}	Mean Mechanical Losses Pressure (N/m^2)
$p_{me}(t)$	Piston Mean Effective Pressure (N/m^2)
$p_{mf}(t)$	Fuel Mean Effective Pressure (N/m^2)
Q_b	Capacity of the battery (Ah)
Q_{cell}	Capacity of the cell (Ah)
r_w	Radius of the wheels of the vehicle (m)
R_b	Resistance of the battery (Ω)
R_{cell}	Resistance of the cell (Ω)
S	Engine Stroke (m)
SOC	State of charge of the battery(%)

SOC_{init}	Initial state of charge of the battery (%)
T_e	Torque of engine (Nm)
T_w	Torque at the wheels (Nm)
T_{em}	Torque at the EM (Nm)
v	Speed of the vehicle (m/s)
V_d	Volumetric Size of Engine (m^3)
v_x	distance travelled by the vehicle within the microtrip (m)
v_{avg}	average speed of the vehicle within the microtrip (m/s)
v_b	Voltage at the terminals of the battery (V)
v_{em}	Voltage at the terminals of the EM (V)
v_{oc}	Open circuit voltage of the battery (V)

Chapter 1

Introduction

This thesis addresses the problem of determining the links between component-sizing, real-world usage and energy management for a plug-in hybrid electric vehicle (PHEV). The objective is to develop an integrated framework in which the advantages of a predictive energy management strategy can be realised by component downsizing for a PHEV. Further, recent legislation such as Regulation 101 in Europe which is used to benchmark the emissions of PHEVs are misleading because PHEV performance depends on the usage profile and charging behaviour in the real-world. Therefore, a secondary objective is to compare the performance of these vehicles in the real-world against the legislative benchmark figures.

1.1 Background

Within the automotive sector one of the main drivers for technological development and innovation is the need to reduce the vehicle's fuel consumption and the emissions of carbon dioxide (CO_2) [10]. Legislative requirements are motivating manufacturers and subsystem suppliers to develop new and innovative electric vehicles (EV)and hybrid electric vehicle (HEV) concepts. In recent years, PHEVs have also attracted considerable interest from both academia and industry [94].

In a conventional vehicle, the internal combustion engine (ICE) burns fuel and converts chemical energy to mechanical energy. The wheels use this power to overcome inertia, rolling resistance and aerodynamic drag to accelerate the vehicle. The improvement of a vehicle's fuel consumption and tank to wheel (TTW) emissions can be achieved by improving the efficiency of the drive-train and using alternate energy sources. Since EVs use electricity from the grid and produce zero TTW emissions they are an appropriate solution to reduce CO_2 emissions. However, it has to be realised that the inclusion of a large battery pack to the powertrain has a significant cost and weight implication [7]. Further, issues such as battery

degradation and "range-anxiety", have always deterred the adoption of EVs by consumers [21].

In order to address the contradicting requirements between TTW CO_2 reduction and range / cost limitation of EVs, the PHEV was developed [4]. It is widely seen as an interim solution for the decarbonization of the transport sector [6]. A PHEV is comprised of a traditional EV with a small ICE which works as an on-board charger. Augmenting the electrical components of the powertrain with a small ICE helps to overcome the limited range of existing EVs [6]. This improvement in range can be achieved without significant financial investment for new recharging infrastructure or a step-change improvement in the energy density of the storage technology being required [75].

The distance a PHEV can travel using only the battery is typically known as the vehicle's all electric range (AER). Generally AER values are represented in miles and can typically range from 20-40 miles [53]. For journeys that are shorter than the AER of the vehicle, the PHEV will have zero TTW CO_2 emissions. However, recognising that one of the primary drivers for the adoption of PHEVs is the ability to use the vehicle for travelling extended distances, the design challenge is therefore one of:

1. correctly sizing the powertrain components to balance the powertrain cost and the reduction in TTW emissions for varied usage profiles and,

2. managing the energy flows between the ICE and the battery to maximise the operating efficiency and the reduction of CO_2 tail-pipe emissions.

The traditional method of sizing a battery for a PHEV or an EV is through a combination of numerical modelling and physical testing of the target vehicle over a subset of legislative drive-cycles. These include the Urban Dynamometer Driving Schedule (UDDS) in North America and the JC08 Cycle in Japan. In Europe, the homologation of EVs, HEVs and PHEVs are based on the requirements of Regulation 101 [87] that specifies the use of the New European Drive-cycle (NEDC). It is acknowledged that the NEDC is unrepresentative and fails to emulate realistic driving conditions [2, 9]. As a result, a number of different research publications have attempted to evaluate the performance of a vehicle through a better understanding of how that vehicle is used in the real-world [9, 39, 64].

For distances longer than the AER, a new area of research has been suggested in [39] where if a level of journey predictability can be used then the ICE can be employed "optimally" throughout the journey. Similarly, [64] suggests that by blending both energy sources smaller components can be utilised with almost no change in PHEV performance and only a small increase in fuel consumption.

Therefore, in summary, typically the performance of the PHEV is affected by three key considerations :

1. The real-world usage profile of the PHEV.
2. The supervisory controller or energy management strategy of the PHEV
3. The component size selection of the PHEV.

In isolation all three areas of research strive for the development of the "optimal" PHEV to reduce TTW emissions. However, as a holistic approach it becomes apparent that there are many links between the three areas of research and an understanding of all the three areas are needed to develop the "optimal" PHEV.

1.2 Motivation and Objectives

Although PHEVs show promise with the reduction of TTW emissions, it is unlikely that there is a single solution of PHEV component sizes to address the different usage scenarios. Indeed, the influence of the usage profile on component sizes has been investigated in [39]. The idea was further extended in [64], where it has been suggested that by using advanced control approaches the components can be downsized. The paper compared the fuel consumption of two PHEVs where one PHEV had a considerably smaller Electrical Machine (EM) and battery in terms of power and energy ratings. However, since these studies used a global optimal control trajectory, which demands a high computational load, the PHEV component sizes were pre-selected for comparison and could not be selected within an optimisation framework.

As an alternative to studying the complete design space of different component sizes, a sizing methodology was developed by the Argonne National Laboratory within a commercially available tool called Powertrain System Analysis Toolkit (PSAT). This tool sized and compared a myriad of different components using a rule based methodology and results are published in [46, 24]. However, due to the computational load per model execution, the control strategy was limited to a simple rule-based controller. The study was improved in [96], where an optimisation technique was employed to determine the "optimal" PHEV for a given drive-cycle. This research was also limited to a simple rule-based control strategy. A summary of these limitations for component sizing has been listed in [6]. The author was critical of the previous literature since these design exercises considered a single automotive technology, a specific type of architecture and a simple control strategy to reduce computational load [6]. Therefore, the first objective of this thesis is to develop

an optimisation based framework by which the advantages of an advanced control strategy can be compared to a simple rule-based strategy for different powertrain designs. It is envisaged that the benefits of the control strategy would be realised as a financial cost benefit by adopting smaller components.

Since PHEVs have been developed, several advanced control strategies have been designed which are discussed further in Chapter 2. Among the various strategies, an important consideration are control approaches that have a predictive element in their design. Predicting the speed profile in advance has led to fuel consumption benefits of around 10% [28] over a simulated real-world drive-cycle. However, on reviewing existing literature, one of the main drawbacks of this approach is the additional computational load encountered to implement such a control strategy in real-time. It has been assumed that due to this consideration these strategies have not been used in conjunction with component size optimisation. The second objective of this thesis is therefore to design a predictive energy management controller to maximise the benefits of a PHEV which can be used in real-time and has a comparatively lower computational load.

Finally, in order to predict the speed or demand profile for a PHEV, a framework has to be developed. However, these methods have been previously developed for the creation of drive-cycles [2]. The objective is to extend this work so that a novel framework can be developed by which the power demand of the PHEV or energy consumption of an EV may be predicted over a route.

The author acknowledges that some of these areas of research have been investigated before with varying levels of complexity. However, the understanding of the interaction between these areas of research has not been fully undertaken.

Therefore in summary, the three key areas of research are listed by the Venn diagram in Figure 1.1. The research objectives are:

- Development of a novel framework by which real-world data can be analysed and the energy demand can be predicted for a PHEV.

- Secondly, to develop a prediction based control strategy and to compare the performance of the PHEV in the real-world to legislative tests.

- Thirdly, to develop a sizing methodology and optimisation framework using which the advantages of a prediction based control strategy can be extended by the downsizing of components in the PHEV.

Novel methods were developed to address each of the individual areas of research. These include a road-type prediction methodology, an energy management strategy and a sizing framework for a PHEV. The methods are discussed in Chapters 4, 7 and

9. A summary of the new methods and the achievements compared to benchmarks are presented in the Conclusions in Chapter 10.

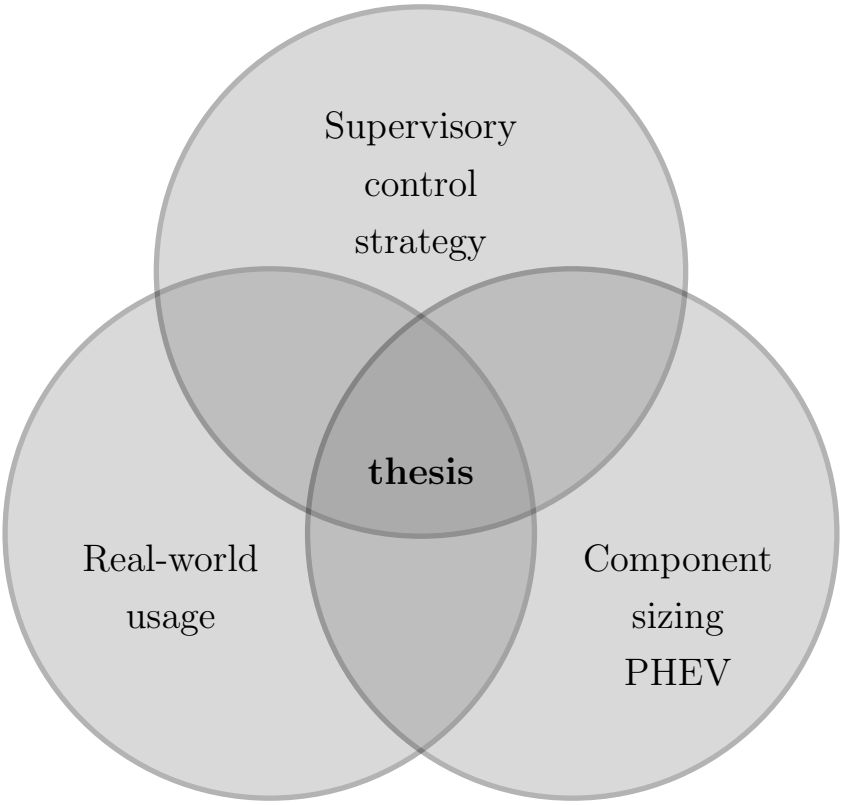

Figure 1.1: Area of research

1.3 Published Work

During this research several papers were published in journals and presented in conferences, these have been listed in this section. Specifically, each journal paper addresses a specific area of novelty.

Conferences

[1] R. Shankar and J. Marco. Performance of an ev during real-world usage. In *Cenex Hybrid Electric Vehicles Conference 2011*. Cenex, 18th – 19th May 2011

[2] R. Shankar, J. Marco, and F. Assadian. A methodology to determine drivetrain efficiency based on external environment. In *IEEE International Electric Vehicle Conference (IEVC)*, pages 1 – 6. IEEE, 2012

[3] R. Shankar, J. Marco, and F. Assadian. Design of an optimized charge-blended energy management strategy for a plugin hybrid vehicle. In *UKACC International Conference on Control*, pages 619 – 624. IEEE, 2012

Journals

[4] R. Shankar, J. Marco, and F. Assadian. The novel application of optimization and charge blended energy management control for component downsizing within a plug-in hybrid electric vehicle. *Energies*, 5(12):4892 – 4923, 2012

[5] R. Shankar and J. Marco. A method for estimating the energy consumption of electric vehicles and plug-in hybrid electric vehicles under real-world driving conditions. *IET Intelligent Transport Systems*, 2013

1.4 Thesis Structure

This thesis comprises of ten chapters.

Chapter 2 discusses existing work on real-world usage data analysis, component sizing of PHEVs and energy management strategies. Particular emphasis is paid to literature which studies the links and implications of these three interrelated areas of research.

The research undertaken is based on the data obtained from two field-trials conducted by others. Chapter 3 evaluates the data available, the important features of the trials and the limitations of the respective datasets. Chapter 3 also discusses the the drive-cycles tradionally used during evaluation.

Chapter 4 describes the data-analysis phase of the research. A neural network (NN) based framework has been developed to analyse the usage profile obtained from the first field trial. The NN is used to predict the energy consumption of an EV which was used in the trial introduced in Chapter 3.

Chapter 5 presents the EV model. The experimental data used for development and verification of the EV model is from the field-trial.

Chapter 6 extends the model developed in Chapter 5 to a PHEV. Particular

emphasis is given to the scaling parameters and methodology used for the development of an ICE model.

Chapter 7 evaluates the various control strategies developed as part of the research. It includes a global optimal solution using dynamic programming (DP). An instantaneous optimal solution with predictive capabilities is presented based on the NN developed in Chapter 4. Finally, to compare the various controllers a rule-based controller is also developed.

Chapter 8 evaluates the performance of the PHEV over the current European legislative procedure (Regulation 101). The legislative tests are compared to the results obtained using real-world data from the second field trial described in Chapter 3.

Chapter 9 involves the development of an optimisation framework by which the various components are sized for different drive-cycles. The framework is developed with the objective of component downsizing by the use of the novel energy management strategy developed in Chapter 7.

Chapter 10 addresses the primary conclusion of the work and areas for further research.

Chapter 2

Literature Review

The objective of this chapter is to evaluate the pertinent research published relating to the thesis objectives listed in Section 1.2. The chapter has been divided into four parts:

1. The first section (Section 2.1) details the analysis of real-world data. The data can be analysed at a macroscopic level in which entire trips over a large time-period are analysed. Conversely, the second type of analysis is in a microscopic level where the data is split into smaller sections and clustered for analysis.

2. The second section (Section 2.2) considers the importance of different operating modes of the PHEV. The choice of modes affects the energy management strategy adopted.

3. The third section (Section 2.3) presents the energy management strategies developed for the PHEV. Recent research highlights the advantages of predictive energy management strategies.

4. The last section (Section 2.4) addresses the various powertrain component size determination techniques.

2.1 Review of Real-World Vehicle Usage

The objective of this section is to derive a methodology through which data obtained from the real-world operation of a vehicle can be analysed. Specifically, the objective is to form a framework by which the power demand / energy consumption of the vehicle across different driving environments can be predicted. The proposed advantage of such an approach is discussed in detail in the control strategy review Section 2.3.

A majority of the literature publications obtain data from on-board vehicle loggers for analysis. This data universally includes speed and depending on the application several additional vehicle parameters such as fuel consumption and battery energy. The analysis of this real-world data is typically undertaken for three reasons.

- Researchers analyse real-world data to derive a representative drive-cycle that captures the predominant characteristics of the data collected. For example, in [2] 58 cars were monitored for $73000km$. This data was then analysed for development of the Assessment and Reliability of Transport Emission Models and Inventory Systems drive-cycle (ARTEMIS).

- The second reason for analysing real-world data such as vehicle speed and acceleration is often to estimate the emissions and fuel consumption in the real-world and compare them to results obtained by performing legislative tests. It has been argued in [23] that fuel consumption and emissions can vary by as much as 20% from legislative tests due to varying operating parameters in the real-world.

- The third avenue of research is relatively new and deals with analysing real-world data directly to aid in the development of advanced powertrains and/or their control strategies. For example, an initial study done in [48] shows the establishment of a battery stress factor using the driving environment. This can be useful in estimating the size of the battery needed for typical journeys.

As stated at the beginning of the Chapter, the data is analysed in existing literature at a macroscopic level where entire trips are analysed over several months or a large user-base [9] or at a microscopic level where trips are deconstructed to smaller portions known as microtrips [2].

2.1.1 Macroscopic Review of Trip Data

The macroscopic studies are undertaken to understand the consumer requirements when adopting PHEVs. Some of the parameters which are typically recorded to analyse consumer behaviour are charging duration, distance travelled between charge events and energy consumption per unit distance. However, the first prototype PHEV was built only in 1996 and mass-produced commercial PHEV such as the Chevrolet Volt, Toyota Prius PHEV, Ford C-Max Energi, BYD F3DM and Fisker Karma have become available only since 2010. Therefore, these consumer studies make use of only a few vehicles and clearly defined market segments. Therefore, the

results of the studies cannot be held as best representative for a typical driver. For completeness, current demonstration vehicles from other manufactures include Ford Escape Plug-in Hybrid, Volvo V70 Plug-in Hybrid, Suzuki Swift Plug-in, Audi A1 e-tron, Dodge Ram 1500 Plug-in Hybrid, and Volkswagen Golf Variant Twin Drive. It has been assumed the data from these vehicles have been analysed in-house and hence data is not available in the public domain.

However, there are several EV trials among which two are listed here. The next two programmes presented are from a retro-fitted PHEV trial and a website report of customers using PHEVs [45, 89].

The MINI E Consumer Study

There have been several EV user studies around the Mini-E programme [15, 86]. It is one of the largest studies to date. The programme consisted of two 6 month periods where during each period 40 EVs were given to different households for evaluation. The vehicle used was a Mini Cooper powered by a 150 kW EM and a 35 kWh battery pack. The expected range of the EV was 250 km over the NEDC. An important finding is that 94% of the users drove less than 160 km per trip. However, an interesting consideration is that these cars were used as second cars and 14% of the trips could not be completed on average because of range or cargo space limitations. It is argued that this issue has to be addressed due to the high cost implications of purchasing a zero CO_2 emission powertrain. In such a scenario a PHEV with an optimised AER to address the majority of the trips would have been better suited.

Cenex Smart ED Trial Programme

This study forms one of the source data for this research. The details of the study are discussed further in Section 3.1. The objective of the study was to analyse the driving patterns of EVs [9]. Among the trips 93% of them were started with over 50% battery SOC. This attributes to the fact that the majority of the users charged the vehicle every day.

PHEV Demonstration and Consumer Education, Outreach, and Market Research Program

This study involved the evaluation of retro-fitted hybrid vehicles to include a plug-in capability [45]. A standard Toyota Prius with a 1.4 kWh battery was upgraded by the company Hymotion to a 5kWh battery pack with a plug-in capability. The vehicle had a 30 mile (48.2 km) theoretical EV range. The vehicles were given to

67 different households which were using them as their second car for four to six weeks each. An interesting outcome of the research is that the charging behaviour is related to infrastructure issues rather than user behaviour. A subset of the results due to their varied performance is shown in Figure 2.1. The area of the circles represent the mileage covered during the trial programme for each household. The x axis shows the percentage of miles driven in charge depletion (CD) mode. In this mode the use of the battery is maximised. The y axis shows the corresponding fuel consumption in miles per gallon (mpg). From the figure, although it is obvious that the percentage of miles driven in CD mode improves the fuel consumption, there does not seem to be a relationship between miles covered and fuel consumption. This fact reiterates the point that in a PHEV the charging profiles and the AER have a significant effect on fuel consumption compared to total distance covered.

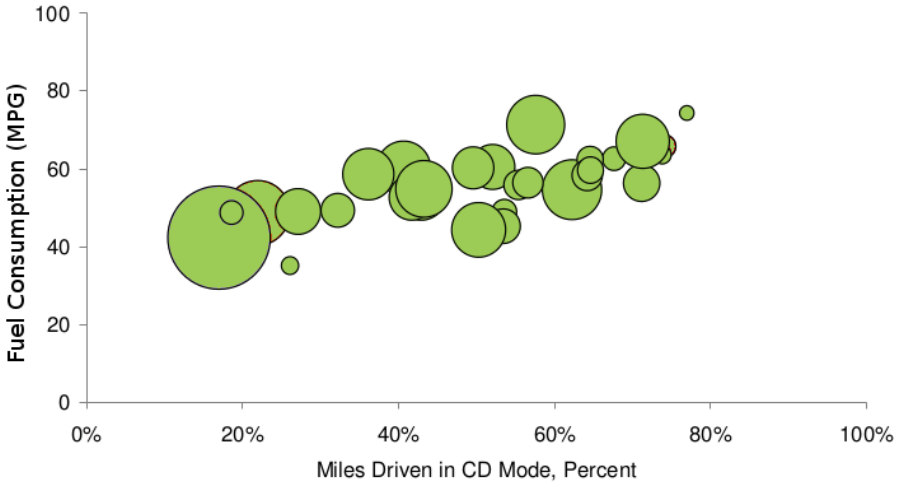

Figure 2.1: Fuel economy recorded during a PHEV trial programme [45]

VoltStats.com

The website has reports from the live datalogs of the PHEV Chevrolet Volt sold in the US [89]. The on-board logger gives trip-wide statistics which are then displayed on the website. Trends can be determined such as electric range driven and the average fuel economy achieved. Figure 2.2 shows the fuel consumption of the Chevrolet Volt among 1400 drivers listed on the website to date. However, the duration for which the vehicle has been driven is not known. Since it is an active website with each new addition to the fleet of cars signed-on, the data changes. The fuel consumption is a definite function of the amount of electric miles driven, as seen by the green line which shows the percentage of miles driven electrically.

Although data and trends could be analysed at the trip level with large data-sets they do not contain sufficient resolution to predict energy consumption for specific

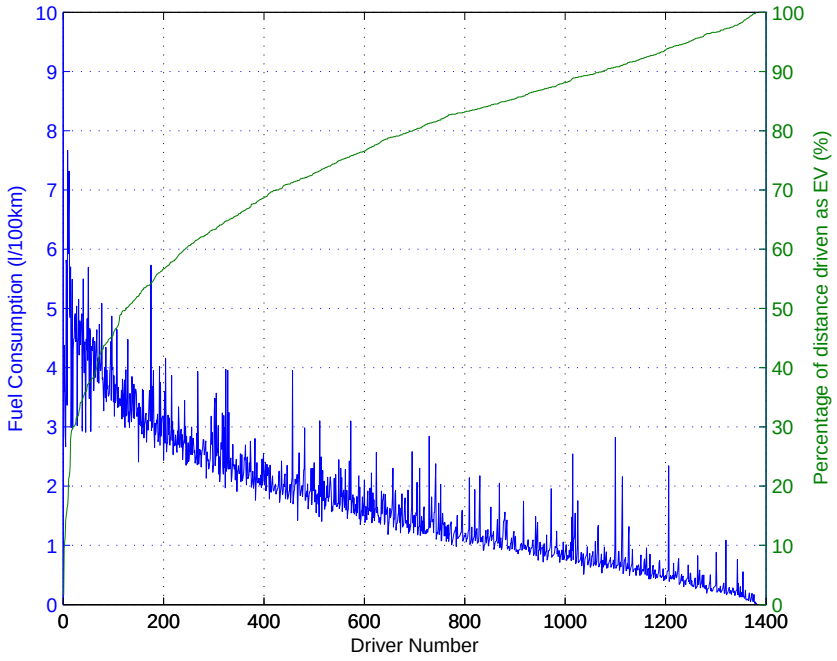

Figure 2.2: Fuel economy of Chevrolet Volt

scenarios based on road-type and traffic condition. Therefore, in the next stage of the review of real-world usage, examples are shown as to how the data maybe split into smaller sections for analysis.

2.1.2 Review of Microtrip Level Analysis

A microtrip can be considered as a split or portion of the main trip. The research presented in [2, 82] splits trips based on vehicle rest periods. Each microtrip is the amount of time spent between two rest periods. Each microtrip is then classified into different groups based on road-types and traffic conditions. The identification of these various road-types and traffic conditions is done by the adoption of these typical processes :

- Euclidean distance based methods [82, 2]
- Neural Network based methods [23]
- Fuzzy Logic based methods [50]

Irrespective of the tool chosen to classify the data, the two key pre-processing tasks are as follows :

- Identification of the method of splitting the data into microtrips with sufficient resolution for analysis [2].

- Identification of parameters within the microtrip such that sufficient variability is shown for the accurate identification of the driving environment [23].

The classification of real-world data was started as early as 1978 by Kuhler and Karstens when ten different driving pattern parameters were used: average speed, average speed excluding stop, average acceleration, average deceleration, mean length of a driving period, average number of acceleration-deceleration changes within one driving period, proportion of standstill time, proportion of acceleration time, proportion of deceleration time, and proportion of time at constant speed [44]. The study was undertaken to determine a realistic legislative cycle for the USA.

The number of parameters chosen for identifying the various driving environments vary based on the fidelity needed. For example, in [23] during the investigation of relationships between fuel consumption and driver behaviour, 62 different parameters were identified per microtrip for classification of the data into 12 groups of varying road-types and traffic congestion. As a contradiction; in [80] only two parameters; average trip speed and average distance between stops were used to cluster driving cycles into three categories : highway, suburban, and urban. The work was extended in [50] to establish a battery "stress factor" based on the predicted power and driving environment. Interestingly, in case of the work done by [80] there is no verification procedure to check the validity of the identification process. The objective was only to identify three dissimilar groups. However, in contrast the work done by [23] had an objective to identify homogeneous groups and they were verified by identifying the corresponding area on a map. Urban trips were verified using geographical information system databases (GIS) on whether they were located inside city limits.

It is noteworthy that there is a trade-off between computational load, number of parameters chosen and accuracy of the classification process [90]. Indeed, for studies where the objective is to have an on-line implementation of the system, the number of parameters are reduced at the expense of accuracy. For example, the authors in [36] develop a NN based framework to differentiate six representative driving patterns (drive-cycles). Finally, based on the driving environment identified the energy management strategy is tuned. Compared to [23] in [36], 62 parameters have been reduced to 24 and 12 groups have reduced to 6 and the drive-cycles identified were still consistent. The work was extended in [61] where a NN is used to match the driving profile to pre-established USA driving cycles (Facility Specific cycles). The NN makes use of 14 different parameters to recognise the cycles.

Similar to [61], several papers have been published with varying numbers of parameters. The selection largely depends on the training data available and the amount of road-categories to be identified. In [61] a key point which is addressed is the trade-off between prediction accuracy and determination of road-types for new datasets. Several similar research papers have addressed this issue and are listed here in Table 2.1 for completeness. 17 different parameters with a NN tuned fuzzy logic method is used in [97]. However, the dataset consisted of microtrips from only two local driving cycles (urban and highway) and accuracy of prediction is not discussed. The authors of [12] make use of 3 different parameters to differentiate the same level-of-service (LOS) cycles split into 6 subgroups using NN. Finally [51] and [58] makes use of 2 and 1 parameters to analyse microtrips. A summary of the different parameters was published in [90] and extended here in Table 2.1. The parenthesis is given for papers where the authors had to include additional parameters for improvements in accuracy.

Table 2.1: Classification considered for real-world data [90]

Parameter	[36]	[61]	[97]	[35]	[12]	[51]	[58]
Average speed	*	*	*	*			
Average running speed except stop	*						*
Stop time/total time	*			*		(*)	
Positive acceleration kinetic energy change per unit mass per unitdistance	*						
Average acceleration	*	*	*				
Average deceleration	*	*	*				
Average positive gradient	*						
Average negative gradient	*						
Positive gradient time/total time	*						
Negative gradient time/total time	*						
Number of stops per kilometer	*						
Average micro-trip time(from start to stop)	*						
Acceleration time/total time	*						
Deceleration time/total time	*						
Standard deviation of acceleration	*	*	*	(*)			
Standard deviation of deceleration	*		*				
Maximum speed	*	*	*	(*)			
Standard deviation of speed	*		*	(*)			
Average gradient	*						
Maximum gradient	*						
Minimum gradient	*						

Table 2.1: Classification considered for real-world data [90]

Parameter	[36]	[61]	[97]	[35]	[12]	[51]	[58]
Standard deviation of gradient	*						
Standard deviation of positive gradient	*						
Standard deviation of negative gradient	*						
Trip distance		*					
Maximum acceleration		*	*	*			
Minimum deceleration		*	*	*			
% of time in certain speed intervals		*	*				
% of time in certain acceleration intervals			*				
% of time in certain deceleration intervals		*	*				
# of acceleration/deceleration shifts per 100m where the difference of adjacent local max-speed and min-speed was > 2 km/h		*					
Maximum product of velocity and acceleration				(*)			
Minimum product of velocity and acceleration				(*)			
Average product of velocity and acceleration				(*)			
Standard deviation of product of velocity and acceleration				(*)			
Current velocity					*		
Driver power demand					*		
SOC					*		
Average positive power demand						*	
Average negative power demand						(*)	
Standard deviation of positive power demand						*	

After the identification of parameters, the data has to be processed and classified. There are several methods available to classify *microtrips* into different road types. Among the literature studied, the common method to classify data is by using a NN [36, 61, 97, 35, 12]. This could be attributed to the fact that traditionally NNs have been used for pattern recognition in several industries [61]. However, for completeness other methods are discussed here and include a rule-based method, Euclidean method and fuzzy logic.

The rule based method is the simplest method to identify the type of road. The speed limits on the road can be used as limits on the average microtrip speed to identify the road type [2]. However, the idea was abandoned by the author due to poor accuracy among the test data recorded. The authors acknowledged realistically a complex set of rules with a number of different parameters would have to be tuned

to improve the accuracy of the approach. The authors then adopted a NN since it was more suited for the application.

In the Euclidean method, microtrips with similar parameters are grouped under each category [82, 52]. The chosen parameters typically include average vehicle speed and acceleration [82, 83]. A complete list of the parameters which can be considered is given in Table 2.1. This method is relatively quick to implement with any scientific programming language such as Matlab's Statistical Toolbox. The methodology and implementation of this method is discussed further in Section 4.3.1.

In [50], the authors use fuzzy logic to classify microtrips into different road types based on average vehicle speed, distance of microtrip and the vehicle's acceleration. It is argued that one of the biggest advantages of using fuzzy logic for pattern recognition is its qualitative approach rather than defined datasets. One of the drawbacks of this method is that the author must visually inspect the data to modify the fuzzy logic rule base to achieve the three distinct groups that are homogeneous. The accuracy of this method for tuning was not verified by the author [50].

2.2 Different Operating Modes of PHEV

PHEVs are classified as HEVs with a battery pack that can be charged from the electric grid. Therefore, the vehicle has the capability of running as an EV while it has sufficient state of charge (SOC). Typically, based on the AER of the vehicle the PHEV is denoted as *PHEVx* where x is the AER of the vehicle [88]. For example, a *PHEV10* has the ability to drive a predefined drive-cycle using only electric energy for 10 miles (16 km).

The objective of a PHEV is to offset the use of the ICE by using stored energy from the electric grid. By using these two sources of energy appropriately the PHEV can be driven with lower TTW emissions than a comparable HEV [6]. The control algorithm which arbitrates the use of these two energy sources is commonly known as the energy management strategy. The strategies which are often employed in PHEVs are discussed in Section 2.3. The different modes in which the energy management system can operate generally includes :

Electric Vehicle Mode (EV) Charge Depleting Mode (CD)

In this mode the vehicle is driven predominantly as an EV. The ICE is used only when the battery is not able to provide enough power. This mode is of particular importance since this mode corresponds with the published AER value. In existing literature EV mode and CD mode are differentiated depending on the operation of the ICE. In a pure EV the use of ICE is completley prohibited [59].

Charge Blending Mode (CB)

In this mode the battery SOC is controlled so as to decrease during vehicle operation. In this mode the engine may be on or off, but most of the tractive energy is provided by the battery. The CB mode is different from the CD mode because the rate of decrease of battery SOC is lesser in CB mode.

Charge Sustaining Mode (CS)

This operating mode is used when the SOC of the battery is depleted. The SOC is often controlled within a narrow operating band. This mode is similar to the operation of a HEV because, the level of battery SOC does not decrease with time [40]. The net source of energy is from the ICE.

Figure 2.3 shows the various modes of operations. Simple rule based strategies may operate in EV mode until the battery energy is depleted. After the depletion of the battery the vehicle transitions to the CS mode of operation.

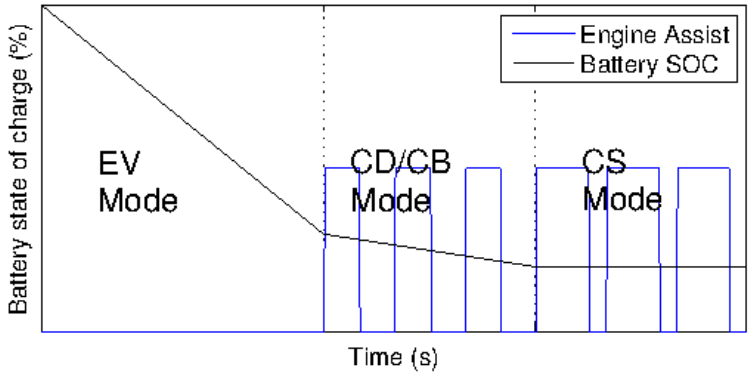

Figure 2.3: PHEV different operating modes

As far as legislation and manufacturing are concerned the two key variables which are used to compare the performance of PHEVs are fuel consumption which directly correspond to TTW emission figures and the AER of the vehicle. As an incentive in the UK, a £5000 subsidiary is being offered by the Department for Transport, for PHEVs with an AER of 10 miles and CO_2 emissions less than $75gCO_2km^{-1}$ between charges [55]. Similar to the UK in the USA, federal income tax credit is available up to \$7500 for vehicles with battery packs larger than $4kWh$.

Surprisingly, there is no penalty for the consumption of electric grid power in the UK [87]. For full well-to-wheel (WTW) CO_2 emission studies, varied results are reported depending on the efficiency of the electric grid and the grid-mix. The grid-mix is the split of CO_2 emitted by the various power sources powering the generation network. It has been envisaged that in the future by adopting "cleaner"

power sources such as wind energy and tidal energy the percentage of CO_2 emitted by the grid would gradually reduce making the WTW emissions lower.

For the purpose of this research TTW CO_2 emission is given prime importance since it is being actively reduced using incentives. However, for the sake of completeness, comparisons are made among the various PHEVs using the grid mix figures of the UK published by DEFRA [20]. The DEFRA report states that per kWh of electric energy usage $594gCO_2$ are emitted by various UK power sources.

2.3 Review of Energy Management Control Strategies

One of the aims of this research is to realise an energy management strategy which can be deployed on a PHEV. It is one of the main functions which has to be developed for the PHEV, since it arbitrates the amount of power provided from the ICE or the battery. The aim of this section is to determine the most appropriate energy management strategy for development, which will then be later extended and used for component sizing of the PHEV powertrain.

The classification of the different energy management controllers is shown in Figure 2.4. At the first level, the controllers are classified as rule-based and optimisation based [93]. Rule based controllers are deterministic and they include methods such as thermostat type control strategy, power-follower and fuzzy logic. They typically require a considerable amount of off-line tuning before deployment [43]. These controllers are used for real-time applications for their ease of deployment and within component sizing optimisation frameworks for their speed [95]. The two sub-categories discussed within rule-based controllers are deterministic and fuzzy logic.

Optimisation based controllers include global optimisation methods and instantaneous optimal methods. Global optimal solutions analytically obtain the best possible control solution [39]. However, since the method iteratively determines the solution, the driving-cycle needs to be known apriori. Since the trips are known before hand the strategies can also be classified as acausal methods.

The instantaneous optimal methods include the equivalent consumption minimisation strategy (ECMS). It involves the optimisation of the drive-train at each time instant. They are referred to as causal systems since they minimise a cost function based on the real-time feedback of past information. The complete classification is shown in Figure 2.4.

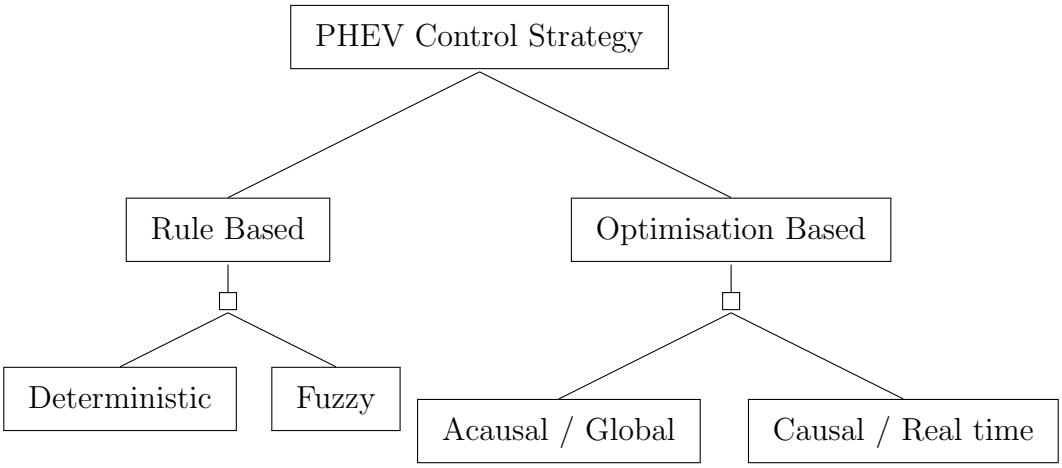

Figure 2.4: PHEV control strategy classification

2.3.1 Rule-Based Control Strategies

Typically the main objectives of rule based control strategies is to operate the PHEV at the ICE's highest efficiency point. Rule-based control strategies can be a combination of EV, CD, CB and CS modes of operation. The common rule based methods include deterministic and fuzzy logic based methods.

Deterministic rule based controllers

Rule based controllers are commonly described with state diagrams and flow charts. They are usually tuned or calibrated for specific driving schedules. The most basic form of the rule-based controller is a switching on-off control [22]. These controllers were first proposed for HEVs and then extended for PHEVs [22]. During a trip a PHEV starts with a full SOC. At the beginning of the trip the battery is used until the SOC reaches a lower threshold. When the SOC reaches the lower threshold the engine is switched on and operated at its maximum efficiency point. Further, the engine is turned off when the SOC reaches an upper threshold point.

The switching on-off controller has been extended as the power follower strategy (PF). This controller was implemented on HEVs, including production cars such as the first generation Toyota Prius [8]. The power follower strategy consists of the switching on-off controller and an additional set of rules. These rules include conditions such as when the vehicle is to operate only using electric energy when travelling below a certain speed (EV mode). A similar strategy is implemented for a PHEV in [91]. The PF strategy was extended in [53], in this case the base vehicle chosen is under-powered and rules were added to turn the engine on when the battery power was exceeded.

The PF strategy has been made available in commercial software such as

ADVISOR and PSAT which are used to model hybrid drive-trains. Therefore, they are adapted and used for benchmarking purposes such as in [26] where, the controller is compared to a DP based CB approach. The other purpose of these controllers is that because of their simple construction and fast execution time, they are used often within component sizing research [71].

The power follower while being a practical and successful solution, does not focus on optimisation of the complete drive-train for a PHEV, however it does provide a useful benchmark for comparison with more advanced control techniques.

Fuzzy rule based controllers

Fuzzy logic defines a subset of deterministic rule-based controllers with a higher level of abstraction. Due to this level of abstraction they are intuitive and easier to define and tune compared to rule-based strategies [43]. An example of this controller implementation is presented in [43] where, the controller improves the fuel consumption over the PF strategy for a parallel HEV. However, it was observed that the controller had to be tuned depending on the drive-cycle to give a fuel consumption improvement [48]. Therefore, the controller would not achieve its optimal performance in the real-world.

To overcome this drawback, research has been reported in [48], in which the fuzzy logic controller is able to discern the roadway type, driving style and other parameters such as traffic congestion. Based on this data the fuzzy logic controller is able to change the rule base online with the current vehicle operation. The research has been published in a two-part paper series [48] and [49] where the design of the fuzzy logic controller has been published in [48].

A fuzzy logic controller is developed for a PHEV in [98]. It varies the amount of engine assist based on driver commands and SOC. The authors address a specific application, which is a city bus route, they state that tuning the controller for the specific drive-cycle is appropriate. The functioning of the controller is similar to a power follower strategy and the authors acknowledge tuning for a specific drive-cycle is essential to improve the performance of the controller. The controller is able to shift between CD and CS modes of operation depending on the SOC of the battery.

2.3.2 Optimisation Based Control Strategies

Optimisation based control strategies are designed to improve the performance of the drive-train as a whole. They are usually based on the minimisation of a cost function. Typically, these cost functions aim to reduce fuel consumption, CO_2, emissions [39] and improve drivability [62]. As shown in Figure 2.4, optimisation based control strategies can be split as global and real-time based optimisation approaches [77].

In general, the energy management problem for a HEV can be expressed as the minimisation of the performance index J as follows :

$$J(SOC(t_0), P_{ICE}, SOC(t_f)) = \phi(SOC(t_0), SOC(t_f) + \int_{t_0}^{t_f} L(SOC(t), P_{ICE}, t) \tag{2.1}$$

where

t is time

t_0 is time at start of drive-cycle

t_f is time at end of drive-cycle

P_{ICE} is control action, in this case amount of power from ICE

$L(\cdot)$ is the instantaneous cost function

$\phi(\cdot)$ is terminal cost

SOC is considered as the only state in the system and it has been assumed all other dynamics are faster and does not affect the energy management problem. The instantaneous cost function $L(\cdot)$ is typically the mass flow rate of fuel, and sometimes other considerations are included such as other pollutants, battery life degradation etc. Using a powertrain model, which typically contains a quasi-static engine model, the mass flow rate of fuel is related to the control action $P_{ICE}(t)$, the driver's power demand $P_{dmd}(t)$, the amount of power drawn from the battery $P_{batt}(t)$ and the vehicle speed $v(t)$. For a majority of the problems the vehicle speed and the P_{dmd} are considered as external measured inputs and are a fixed vector of time for a specific drivecycle. Finally, ϕ is the terminal cost at the end of the drive-cycle and is typically included to maintain the SOC of the battery for a HEV. However, for a PHEV since the vehicle will be charged from the electric grid ϕ can be considered as zero.

Global optimisation based controllers

An overview of different global optimisation control techniques for HEVs discussing the advantages and disadvantages of each is published in [76]. For global optimisation techniques the drive-cycle needs to be known ahead of time. They can also be classified as acausal systems since the minimisation is based on future events and results. This type of controller is primarily used for benchmarking purposes or for the comparison of different powertrains.

One of the common optimisation techniques, in general, is linear programming. One example of which was applied for a series HEV in [84]. However, the authors acknowledge that linearising the model is complex, specifically for special conditions such as engine startup or cranking and gear-ratio changes.

Another approach discussed for PHEVs is to optimise control parameters of a real-time controller so as to tune it for minimum fuel consumption. Within [72], a PF based strategy is tuned for different drive-cycles using evolutionary techniques such as genetic algorithms (GA). The result of this optimisation is a SOC trajectory similar to that found in CD-CS modes. This technique can be extended when including component sizing parameters [19]. However, it is noteworthy that this solution is the best achievable solution with a PF strategy and further improvements are possible by adoption of a different control strategy. The advantage of using this approach is, though it does not give the global optimal solution, it is possible to determine the tuning parameters for a real-time implementable strategy and maximise the capabilities of that strategy .

Several authors have considered DP as an effective approach to determine the "optimal" control trajectory over time [39, 64]. DP is based on the Bellman's principal of optimality, a theoretical background on the subject is given in [41]. In case of DP the state SOC, the control action P_{ICE} are all discretised; thus many possible solutions are considered. The performance index J is given as a function of sequence of control decisions (π) of P_{ICE} for each discretised time step t, where N_t is the total number of time steps. Therefore the performance index is given as :

$$J_0(\pi) = \phi(SOC(N)) + \sum_0^{N-1} \dot{m}_f(SOC_k, P_{apu,k}, t_k) \tag{2.2}$$

and the optimal policy is

$$\pi^* = \arg\min\ J_0(\pi) \tag{2.3}$$

Typically in a PHEV the objective is to deplete the battery completely at the end of the cycle so that it can be charged from the electric grid for the start of the next cycle. Therefore it is assumed $\phi(SOC(N)) = 0$. In [39], when the optimal control policy was calculated over several drive-cycles, it was determined with DP, the CB mode of operation achieved a relatively lower fuel consumption than CD-CS modes. That is, the optimal control policy always caused the state SOC to decrease progressively throughout the trip and the SOC was at its lowest value at the end of the trip. Further, [64] compare PHEVs with different component sizes with DP based CB approach. They conclude, downsizng of powertrain components of a PHEV reduces the financial cost of the drive-train but does not have a significant influence on the fuel consumption if a global optimal strategy is adopted.

One of the key points raised in [76] is the required fidelity of the model to sufficiently capture the reductions in TTW emissions. Typically, when implementing the DP algorithm, the model has to be discrete and the resolution of the states affects the accuracy of the final solution. Universally, among the published literature the

optimal trajectory is calculated for discretised values of time and SOC [76, 39, 64]. The cost functions used vary from optimising for fuel and other constraints such as Engine ON-OFF time.

In order for the DP to function the cumulative cost of the cost function for each discretised state is calculated backwards. A complete working of the approach is presented in Chapter 7. The objective is to obtain a cost-to-go matrix which can be used to determine the minimal cost path across time. For example, Figure 2.5 shows the operation of a HEV over the ECE cycle, for a time duration of 196s, a target terminal SOC of 0.7, a time step of 1 s, and an SOC discretisation of 0.01% of full charge. The plant model used in this study consisted of only one state, which is the SOC. It can be observed based on the number of states, the number of dimensions of the cost-to-go matrix would increase.

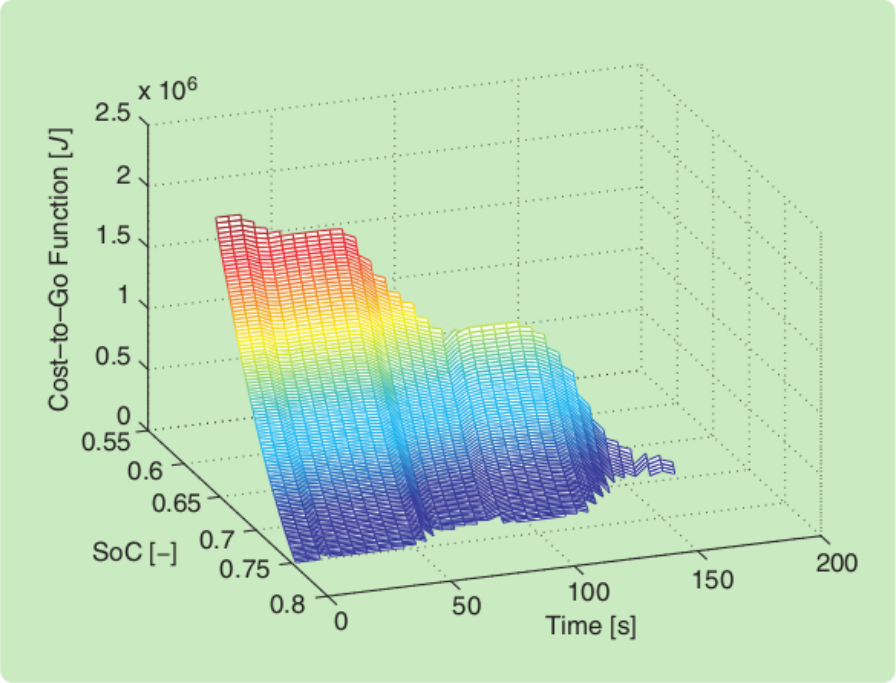

Figure 2.5: Example cost matrix using DP [76]

The resolution of this matrix or grid is exponential to the number of states in the system and proportional to the discretisation. Due to this reason a problem as shown above can take several hours to solve depending on the amount of computing power available [76].

DP has also been implemented stochastically by using Markov chains [60]. Markov chains give a probability distribution of various speeds from which the power demand can be constructed. The advantage of this method is that for a give drive-cycle the derived cost-to-go function can be implemented in real-time by means of 'look-up tables'.

Some of the other optimisation techniques which have been implemented are introduced here for completeness. Similar to the research done by [72] other optimisation techniques can be adopted to tune the power-follower based control strategy parameters [74] and [96].

Therefore, global optimisation methods are computationally heavy. Although drive-cycle dependency can be avoided by the use of Markov chains, on reviewing existing literature they have never been used in experimental setups. However, they provide the best feasible result for a given drive-train and the result of this research suggests a CB approach is more suited to maximise the performance of the drive-train.

Real-time optimisation based controllers

Real-time optimisation is similar to global approaches, except the drive-cycle is not known. Therefore the optimisation problem has to be reduced to a problem which can be solved every time step. These controllers have altered cost functions to make decisions based on past or predicted information and therefore they can be classified as causal systems.

A series of papers have been published [28, 29, 31, 30] in which the drive-cycle is predicted using various techniques including simple rules based on the speed limit and NN approaches. On predicting the trip, DP is applied for obtaining the ideal control trajectory across time. Finally, the trajectory is applied to the vehicle when it is simulated across the drive-cycle. The authors [28] obtain varied results depending on the accuracy of the trip model. Finally, a two scale DP technique is used in [27]. By two-scale, the authors advocate the use of two DP layers or loops. In the outer loop, based on the trip predicted, a low resolution DP grid is applied to calculate a high level SOC trajectory. After this calculation, relying on data from local traffic information centres a finer grid DP is applied for the small section of the trip using the high level SOC trajectory as a reference. The performance of the predicted DP solution is close to the global optimal solution (11%). However, the authors have not addressed the possibility of inaccuracies / non-availability of source data to predict the drive-cycle.

Another frequently used strategy developed for real-time application is ECMS. The strategy was first proposed for a parallel HEV in [68]. A detailed history of ECMS is given in [33]. The ECMS method was developed to reduce the global optimisation problem to an instantaneous optimal problem without use of information regarding the future. The strategy is based on the CB approach to regulate the SOC around a reference point while providing the required power and achieving minimum fuel consumption. The strategy is based on the ideaology all

energy eventually comes from the fuel therefore use of the battery power P_{batt} can be worked out to an equivalent amount of fuel used. ECMS is based on the concept of optimising the fuel used including the equivalent amount of fuel which will be lost in the past or future by charging the battery and vice-versa every time instant. Therefore, it is a real-time optimisation based on amount of fuel used and equivalent amount of fuel used to charge or discharge the battery. If J is considered as the performance index then the optimisation problem can be written as :

$$\begin{aligned} & \min_{SOC, P_{ICE}} J \\ J \quad = \quad & \dot{m}_f(P_{ICE}(t)) + \dot{m}_{equiv}(P_{batt}(t)) \cdot \zeta \end{aligned}$$

where

$\dot{m}_f$	is the fuel flow rate of ICE
$\dot{m}_{equiv}$	is the equivalent amount of fuel used by battery
ζ	is the equivalence ratio

(2.4)

subject to

$$P_{dmd}(t) = P_{ICE}(t) + P_{batt}(t)$$

where

$P_{dmd}(t)$	is the Power Demand at time t
$P_{ICE}(t)$	is the Control action, Power from APU at time t
$P_{batt}(t)$	is the Power from battery

(2.5)

The term $\dot{m}_f$ is the amount of fuel used by the ICE at that time instant. $\dot{m}_{equiv}$ is the equivalent amount of fuel lost or gained by charging and discharging the battery by using the engine in the future. Obviously, the cost of using the battery would vary depending on the amount of free energy recovered through regenerative braking in a HEV or the amount of energy gained from the electric grid in the case of a PHEV. Therefore, the second term is tuned based on past information using a term called the equivalence ratio (ζ). The strategy has to be tuned such that the cost of using the battery is sufficiently expensive, so that battery will not be drained before the end of the trip. The strategy was further improved by a function where ζ was varied based on SOC at that time [67] for a HEV. It was improved in [66] where the vehicle was made to charge sustain using the battery SOC as a reference.

One of the cited drawbacks of the ECMS strategy is the inaccuracy in estimating the equivalence ratio [62]. This issue is studied in detail in [62]. The authors suggest an optimisation routine to obtain the equivalence ratio for a given drive-cycle. A number of different approaches have been suggested each employing a different combination of equations and look-up tables based on battery SOC to calculate the equivalence ratio for different HEVs. A complete list is given in [33, 76] and is therefore not repeated here.

The ECMS is compared to DP solutions for a PHEV in [85]. The authors conclude that for distances much longer than the AER and for vehicles employing larger batteries, the ECMS and DP provide similar fuel economy and SOC profiles. The authors determine that the DP operation is similar to a CS operation during very long drive-cycles.

Recently, there has been much interest in real-time optimisation controllers and their links with GPS/GIS technologies. It has been assumed on estimation of the future power demand by means of a trip preview, it would be possible to calculate the equivalence ratio (ζ) analytically [99, 100]. The first stage of the strategy is to use an average speed value profile based on road-type to generate an equivalence ratio map with distance and SOC on the x and y axis respectively. This lookup table can then be used within a forward facing ECMS strategy with the appropriate ζ value. The main drawback which is observed by the authors is the accurate calculation of the ζ is determined by the resolution of the discretisation of the DP algorithm and the accuracy of the predicted trip. A high resolution of 0.0001% SOC was adopted for every 1 second for discretisation which led to a large computational load during DP execution. To overcome this issue, the authors developed an iterative algorithm where different values of ζ that are constant throughout the trip are used backwards in time to calculate the change in SOC. Finally, the corresponding SOC to the start of the trip is selected by interpolation of the value ζ. The authors claim that this process is faster than the DP algorithm. However, it is important to note that in such an implementation, the feedback path through SOC is removed and therefore the controller cannot correct the value of ζ during execution of the simulation.

2.4 Review of Component Sizing Strategies

There is no recognised set of requirements for the sizing of components for a PHEV. Typically, the component selection for a PHEV can be broken down into two requirements that are given as :

1. **Energy Requirements** of the battery are primarily dictated by the needed AER for the PHEV. The NEDC is usually chosen in Europe to calculate the AER [87].

2. **Power Requirements** for the battery will depend on the peak power encountered by the PHEV when it is being driven in EV mode. There is a possibility of turning on the engine to meet peak power demands. In [64], it is suggested that component sizing is possible with a CB approach with minimal impact on fuel consumption. This could lead to down-sized components and therefore a smaller financial cost of the powertrain.

Requirements can also be addressed such as acceleration times, passing manoeuvre times, gradeability capability of the vehicle.

An interesting consideration is that although the first prototype of a PHEV was developed in 1996, a production intent vehicle was developed only in 2010. Due to this reason, only a very few design studies exist and the requirements are typically defined by emissions rather than typical manufacturer constraints such as cost and driveability [78, 71]. Table 2.2 lists prototype vehicles built that are in the public domain. An interesting point to note that is relevant to this study is the shift from Nickel based batteries to Lithium based batteries.

Typically, component sizing algorithms can be broken into two groups, analytical methods and optimisation based methods. Analytical methods make use of iterative rule based algorithms to calculate the component sizes and optimisation based methods make use of optimisation techniques to determine the component sizes.

2.4.1 Analytical Methods

A number of research publication have been presented by the Argonne National Laboratory [25] and National Renewable Energy Laboratory [78, 71] on component sizing. Although the powertrain architecture, cost projection, requirements and technology vary, the underlying sizing methodology is the same. Both make use of laboratory maps for the development of the PHEV models. Various scaling factors are applied for resizing the components and finally a simple iterative routine is used along with a power follower energy management strategy to make the vehicle achieve a given AER when the vehicle is operating in EV mode. This component sizing routine is available in the software Advisor and PSAT. A complete breakdown of the working of the routine is provided in [78, 71].

2.4.2 Optimisation Routines

There are limited research publications that present a structured approach to component sizing and control optimisation [6]. Furthermore, typically only a particular subset of technology options is evaluated. In [95], chaos optimisation is used to size the various components of the PHEV. Again, the base model that is underneath for component scaling is given by the software PSAT. Therefore, this is potentially a large new area of research which is critical to address the development of PHEV.

Table 2.2: List of prototypes of PHEVs

Vehicle	Year	EV range (km)	Notes
UC Davis Joule	1996	105 (EV)	0.66L IC engine, NiMH battery
Audi Duo	1997	50 (EV)	1.9L IC engine, Pb-acid battery
PSA Dynavolt	1998	100 (EV)	0.2L IC engine, NiCd
Renault Scenic	1998	20 (EV)	1.6L IC engine, NiCd battery
UC Davis Coulomb	1998	97 (EV)	0.66L IC engine, NiMH battery
GM EV1 HEV concept	1998	65 (EV)	1.3L Diesel engine, NiMH battery
GM EV1 HEV concept	1998	65 (EV)	Natural gas turbine, NiMH battery
WWU Viking 23	1998	113 (EV)	0.993L IC engine, NiCd battery
Fiat Multipla	1999	80 (EV)	1.6L IC engine, NiMH battery
UC Davis HEV1	1999	97 (EV)	0.57L IC engine, NiMH battery
UC Davis Sequoia	2000	94 (EV)	1.9L IC engine, NiMH battery
Suzuki EV Sport	2000	150 (EV)	0.393L IC engine, NiMH battery
Citroen Xsara Dynactive	2000	20 (EV)	1.4L IC engine, NiMH battery
UC Davis MD CVT Suburban	2001	58 (EV)	2.2L IC engine, Pb-acid battery
UC Davis Yosemite	2002	79 (EV)	1.9L IC engine, NiMH battery
Renault Kangoo Electric road	2003	60 (EV)	0.5L IC engine, NiCd battery
AC Propulsion PHEV Jetta	2003	64 (EV)	1.4L IC engine, Pb-acid battery
UC Davis Trinity	2004	64 (EV)	1.5L IC engine, Li-ion battery
DaimlerChrysler Sprinter PHEV	2005	32 (EV)	2.3L IC engine, NIMH batteries
CS Energy Prius conversion	2006	71 (CD)	1.5L IC engine, LiFePO4 battery
Hymotion Prius conversion	2006	50 (EV)	1.5L IC engine, LiPolymer battery
Hymotion escape conversion	2006	80 (EV)	2.3L IC engine, LiPolymer battery
GM Volt concept	2006	64 (EV)	1.0L E85 IC engine, Li-ion battery
GM Saturn Vue concept	2006	>16 (EV)	3.6L IC engine, Li-ion battery
Ford PHEV Fuel Cell concept	2006	40 (EV)	Fuel cell engine, Li-ion battery

2.5 Conclusions

The studies presented in this chapter describe the work progressing in each area of research. It is noteworthy that most research publications focus either on control strategies or component sizing but do not consider a holistic approach to the design of the PHEV. As discussed in Section 2.1, neural networks have been predominantly used for the identification of the different road-types, however a consistent framework for integration of this method into an energy management strategy is not addressed. This area of research has been expanded in Chapter 4 where a NN is used to predict the energy consumption of the vehicle across a trip.

The second area of research was the control strategy employed on the PHEV. As reviewed, the traditional optimisation techniques such as DP give the best solution but are not feasible for real-time application. However, there are several instantaneous optimal solutions which can be implemented in real-time. But these solutions have to be tuned for specific drive-cycles for best performance. Therefore, the ideal trade-off would be to use a global optimal solution to generate a trajectory which can then be used to tune the performance of the instantaneous optimal solution. The application of such an approach is discussed in Chapter 7.

Finally, a relatively new area of research is the co-optimisation of the sizing of the PHEV and the energy management strategy. Typically, even instantaneous optimal solutions are avoided within a component sizing optimisation framework due to high computational load. Some studies which attempt "co-optimisation" is discussed in Section 2.4. A novel framework is described in Chapter 9 where the predictive energy management strategy is compared to a rule-based strategy while sizing the components of the PHEV.

Chapter 3

Review of Available Data and Drive-Cycles Employed

The aim of this chapter is to give a detailed introduction of the type of data available for real-world usage analysis and modelling of the various powertrain components. The real-world usage data employed as the foundation for this study was recorded from two different data sources. The first source of data is from an EV trial programme and is used to determine the energy consumption of a typical C segment passenger car under different operating regimes in the real-world with different driver behaviour. This data has been used to develop the backward model of the PHEV which is subsequently used by the optimisation routine in Chapter 9. However, within the EV trial programme it is not possible to identify individual drivers. Therefore, individual driver profiles such as daily distance cannot be determined from this dataset. The second source of data is used to analyse driver behaviour. Specifically, to look at the typical operating regimes such as daily distance covered by different commuters. In the last section of this chapter the various drive-cycles used during this research is presented. The next two sections discuss the main features of the two trials and the vehicles used within each programme.

3.1 The Smart Move 2 Electric Vehicle Trial

This trial was conducted within the UK in 2011 as part of the Smart Move 2 Electric Vehicle Trial programme [9]. The evaluation programme was being managed by Cenex (the UK's Centre of Excellence for low carbon and fuel cell technologies) and was being funded by the UK Department for Business, Innovation and Skills (BIS).

A summary of the relevant statistics for the evaluation programme are presented in Table 3.1. The scope of this research has been restricted to the Smart ED from this programme due to the limited data available from the Mitsubushi i-Miev. Whenever

any of the vehicles were used, key vehicle parameters were automatically recorded from the vehicle's Controller Area Network (CAN) bus and uploaded to a central database for analysis. Some of the key parameters which have been used in this analysis are vehicle speed, battery voltage, battery current and vehicle mode. Vehicle mode includes information such as whether the vehicle was in drive, neutral, park or charging. It is noteworthy that during charging, the sample rate employed for data collection was 0.017 Hz or 1 minute, whereas during vehicle drive a faster sampling rate of 1 Hz was employed. This latter figure was deemed appropriate for measuring the energy usage profile of the vehicle. However, it is not sufficient to record those power flows associated with fast transient driving events such as regenerative braking.

Trial program parameters	**Data**
Number of vehicles	8
Types of Vehicles	7 Smart EVs and 1 Mitsubishi i-Miev
Duration of Vehicle Test Program	6 Months
Total kilometres driven by Smart EVs during program	4268 km
Number of days in demonstration events	12 days

Table 3.1: Summary of Smart Move 2 Electric Vehicle Trail programme

3.1.1 The Vehicle (Smart ED)

The Smart ED is an EV designed for an urban environment. The layout of the drive-train is given in Figure 3.1.

The Smart ED is a compact vehicle powered by a $16.5kWh$ Lithium-Ion Battery with a peak power rating of $30kW$. The top speed of the vehicle is limited to $100km/h$ (62 mph). The EMs were supplied by Zytec Automotive, the peak power rating of the motor is $55kW$ and the continuous power rating of the motor $42.5kW$. However, the peak power of the drive-train of the smart is $30kW$. This peak power is much lower than a typical saloon (a standard C segment vehicle with an ICE typically produces $75kW$). A typical saloon has a power to weight ratio of $50W/kg$ while the smart with a kerb weight of 1036kg has a power to weight ratio of $29W/kg$. Since the Smart ED is a compact car and is underpowered compared to a standard saloon, the ARTEMIS drive-cycle is also used as a reference which represents a more representative drive-cycle for the vehicle.

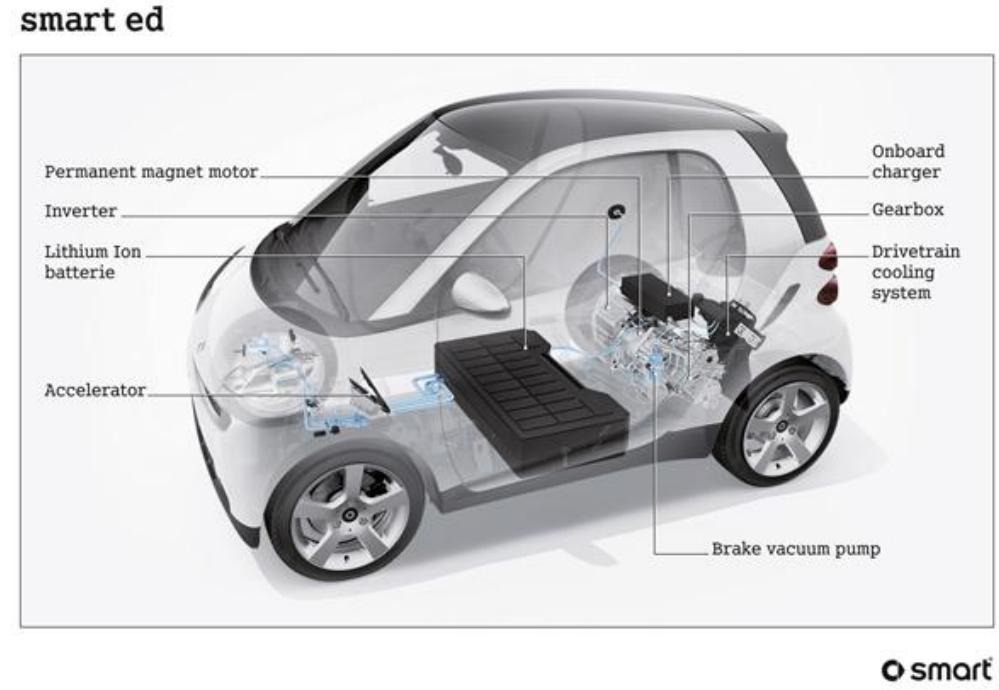

Figure 3.1: Smart ED [57]

Recording of the data is initiated based on the ignition key flag or the charging cover flag on the CAN bus. The data has been made available on servers for downloading as comma separated value files (CSV). A script was written in MATLAB to post-process this data, remove erroneous files and to convert the CSV files to MAT files for subsequent analysis. A summary of the data available in the CSV file is given in Table 3.2, the schematic layout of the drive-train is given in Figure 3.2 [9]. Some of the parameters are directly measured by sensors and others are calculated by the on-board ECU.

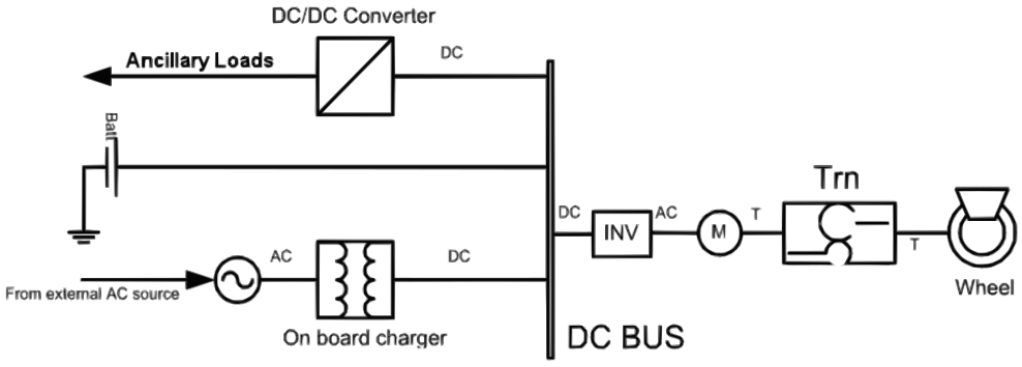

Figure 3.2: Smart ED Layout [57]

Table 3.2: Recorded parameters on the Smart

	Parameter	Unit	Description
1	Segment ID		
2	IMEI		International Mobile Equipment Identity number used to identify GSM device in logger
3	Time		YYYY-MM-DD HH:MM:SS
4	Interval	secs	Time interval between current and previous data point
5	Latitude	deg	Decimal degree. Northern hemisphere is positive.
6	Longitude	deg	Decimal degree. Eastern hemisphere is positive.
7	Altitude	m	Height above mean sea level in meters
8	Ignition	0/1	Ignition status 0 = Off 1 = On
9	Temperature	deg C	Ambient temperature
10	Speed	kph	Vehicle speed calculated from motor speed
11	Energy Transferred Key On	kWh	Total energy transferred from the battery during drive. Starts at key on. Stops at Key off
12	Energy Transferred Charging	kWh	Total energy transferred during charging. Charging started - contactors closed. Charging finished - contactors opened
13	SOC	%	State of charge of HV battery
14	Charging Lead	0/1	Battery being charged by HV battery charger
15	Battery Voltage	Volts	HV battery voltage as measured by the BMS at the battery HV connection
16	Battery Current	Amps	HV battery current as measured by the BMS at the battery HV connection. Negative current is energy being delivered from the battery.
17	Motor Voltage	Volts	HV battery voltage as measured by the Drive-train at the HV connector on the drive-train
18	Motor Current	Amps	HV battery current as measured by the Drive-train at the HV connector on the Drive-train. This signal includes motor demands and DC-DC converter demands
19	Drive Battery Temperature	deg C	Maximum temperature within the HV Battery. Accuracy upto a degree
20	Cooling Request	%	Cooling request from the battery to the EVCM. 0 % = No cooling / 100% = maximum cooling. The cooling of the system is provided by the AC system.
21	Motor Speed	rpm	Motor speed as measured by the Drive-train

Table 3.2: Recorded parameters on the Smart

	Parameter	Unit	Description
22	Motor Torque	Nm	Motor torque requested from the Drive-train
23	Auxiliary Power	kW	Power used for cabin heating/cooling and battery cooling. This includes cabin heating and cooling plus battery cooling demands.
24	Charger Voltage	Volts	AC Mains voltage as measured by the charger.
25	Charger Current	Amps	AC Mains current as measured by the charger.

3.2 The Mini Data Programme

The Mini Data programme focuses on the measurement and analysis of the driving styles and journey profiles of 40 different drivers over a seven-day period. All of the drivers reside within an urban, European environment. Driver selection was conducted by an independent third party with the intent of ensuring a representative demographic sample within the cohort. The vehicle employed for this study was a commercially available C-segment passenger car. Direct measurements were made on the usage of the vehicles either by adding new instrumentation or by recording data from the vehicles CAN bus. In total, over $8400km$ of driving data were recorded for analysis. Details on the evaluation programme and previous work which aimed to size the energy storage requirements of a HEV/EV are given in [82]. The authors acknowledge that this is a modest sample size and as a result is not statistically significant. However, as will be discussed in Chapter 8, even with this limitation a number of conclusions can be drawn based on the distance travelled per day. Figure 3.3 shows the total distance travelled by each driver during the seven-day period. From the figure it is obvious that the use case scenarios are quite different. The objective of this research would be to analyse the performance of the PHEV for a set of legislative drive-cycles and these 40 drivers.

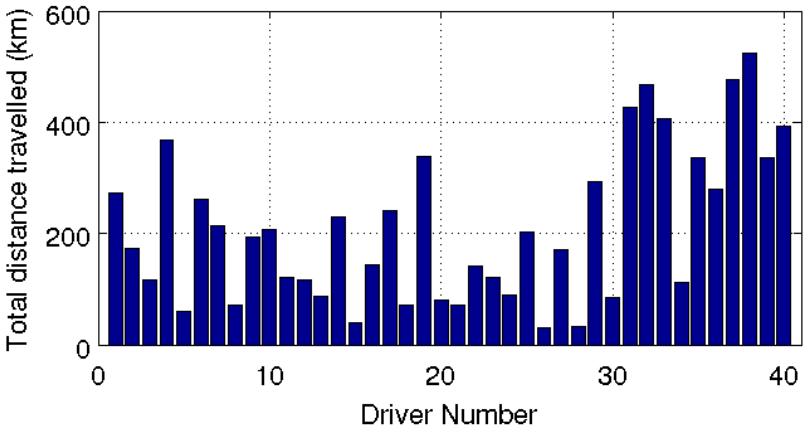

Figure 3.3: Distance travelled per week during the Mini Programme

3.3 Drive-Cycles Used in the Thesis

The three different drive-cycles which are considered throughout the research are discussed in this section. The various case-studies will involve the performance of the PHEV over these three drive-cycles. It has been presented in [38] that drive-cycles can be classified into two categories based on their formulation.

The first category of cycles is made up of a series of repetitions of a number of vehicle operating conditions normally encountered when driving. These types of cycles are known as modal cycles. The drive-cycles developed by the Economic Commission of Europe and the Japanese Cycles represent this category. Figure 3.4 NEDC , represent the test cycles for Europe. Japan uses a similar cycle known as Japanese 10-15 Mode Cycle. From the Figure it can be seen that there are a number of repeating smaller cycles and constant speed sections. The NEDC is the first drive-cycle considered for this research.

One of the reasons for adopting these simplified modal cycles is the ease of operation of the dynamometer to perform emission tests on vehicles. This kind of approach where the fuel consumption / emission is based on a number of average operating speeds does not adequately describe the underlying distribution of speeds and accelerations that are encountered in the real-world. This underlying distribution will lead to higher acceleration levels which will imply higher power and energy requirements. The work done in [23] suggests that these higher acceleration levels will lead to increased fuel consumption and emissions in a conventional vehicle by 20 to 40 percent. Furthermore, the NEDC cycle was formulated when the average power output of the engine was lower, therefore the acceleration rates on the NEDC are comparatively lower than the acceleration rates encountered in the real-world [79].

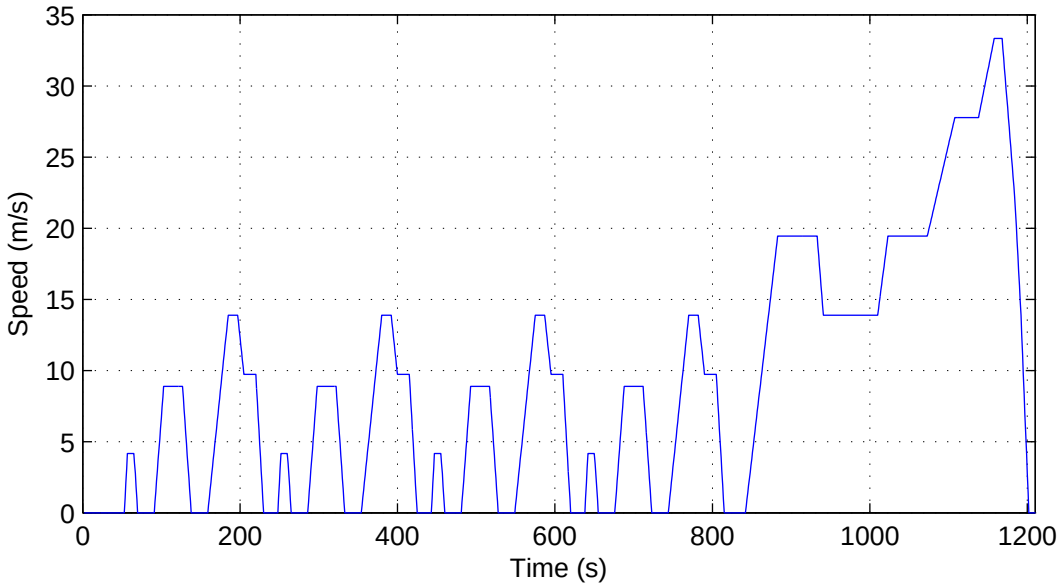

Figure 3.4: NEDC

The second category of cycles consists of an actual simulation of a typical road route. These cycles can be classified as transient cycles. The United States (US) , Canada, Australia and Switzerland use these cycles within their legislative procedure to establish emissions of the vehicle. Since the test cycle emulates real-world driving, the test cycle has more speed variations when compared to modal cycles. The speed and acceleration distribution of these drive-cycles are more representative of real-world driving and hence tests performed with these drive-cycles give a better representation of fuel consumption / emission figures [18]. An accurate representation of a real-world driving scenario for a typical passenger car in Europe would be the ARTEMIS drive-cycle. The drive-cycle is represented in Figure 3.5. A background on the formulation of these representative cycles can be found in [2] and [82]. Furthermore it has been argued in [23] that in urban conditions the driving profile varies based on the vehicle, driving behaviour, road conditions and the level of traffic congestion. All of these factors lead to large variations in emission levels and fuel consumption. Due to these factors the ARTEMIS is another drive-cycle used within this research for evaluation of the PHEV.

The third drive-cycle used in this research is one of the trips recorded during the Cenex trial programme as discussed in Chapter 4. It was part of the training data set employed for the NN. Figure 3.6 shows the drive-cycle. It is noteworthy that compared to the data recorded in the EV trial programme which is from a compact vehicle with limited range, the ARTEMIS drive-cycle is more representative of a conventional saloon. This variation would be discussed further when comparing these two real-world cycles.

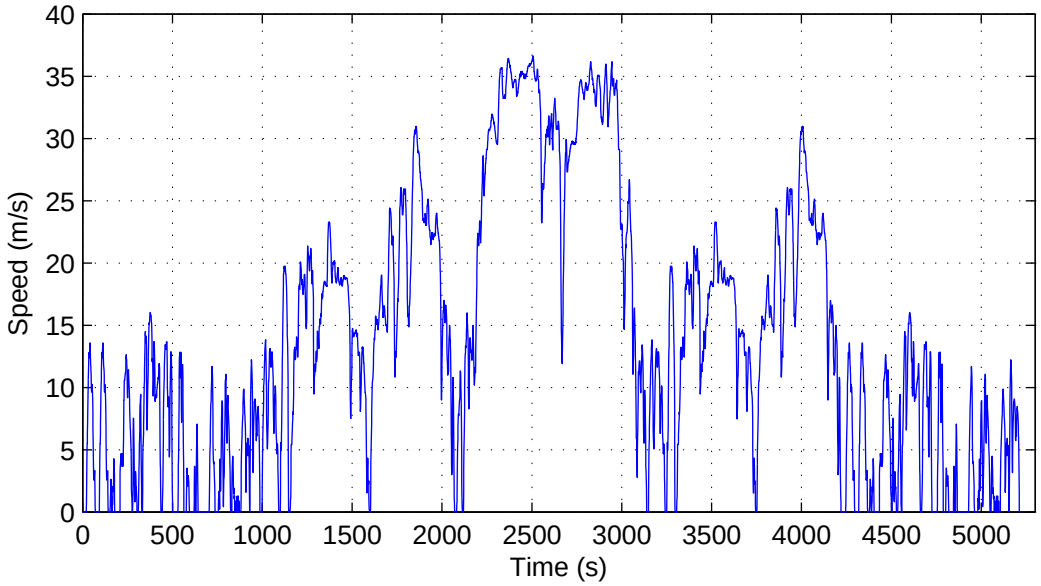

Figure 3.5: ARTEMIS urban, rural road and motorway cycles combined [2]

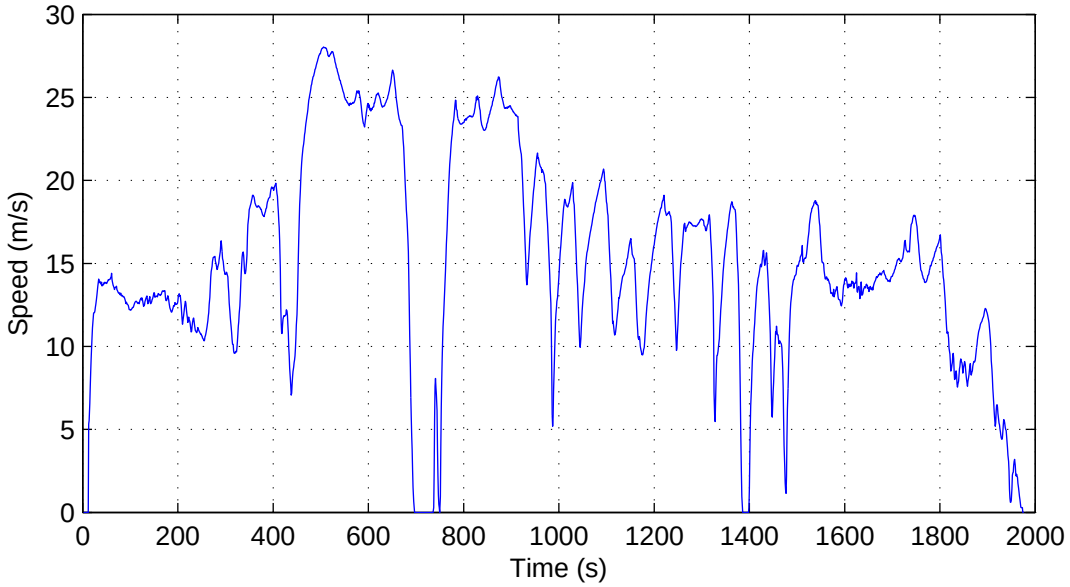

Figure 3.6: Example of real-world drive-cycle from EV trial programme

In conclusion, the standard modal drive-cycles can be useful as a tool to benchmark vehicle performance. However, they do not necessarily depict the performance of the vehicle in the real-world. Table 3.3 shows a comparison of key parameters (speed, acceleration levels) among the various drive-cycles. The average acceleration of the ARTEMIS cycle when compared to the NEDC cycle varies by more than 8 % and the peak acceleration varies by more than 104 %. This drastic variation in acceleration is one of the primary causes for variations in emissions between the real-world and legislative cycles. Furthermore, compared to the NEDC, it can be argued that the ARTEMIS cycle is a closer representation of a typical real-world cycle for all vehicles in Europe. An interesting point to note is that the average acceleration of the real-world cycle is lower than the NEDC. This could be due to the factor that the EV had comparatively very low power compared to a conventional vehicle.

Table 3.3: Comparison of key parameters of various drive-cycles

Parameters	NEDC	Real-world	Artemis
Distance	$10.93km$	$29.83km$	$73.02km$
Top Speed	$33.33m/s$	$28.04m/s$	$36.6m/s$
Mean Speed	$12.32m/s$	$15.64m/s$	$15.97m/s$
Maximum Acceleration	$1.04m/s^2$	$3.23m/s^2$	$2.86m/s^2$
Mean Acceleration	$0.53m/s^2$	$0.24m/s^2$	$0.55m/s^2$

Chapter 4

Framework for Real-World Data Analysis

4.1 Introduction

The objective of this chapter is to present two different methodologies by which a given drive-cycle can be analysed based on road-type, traffic congestion and driver aggression. In the first part of the chapter the data is analysed at the trip level; analysing average distance covered. The second part of the chapter presents the two tools used for microtrip data classification. They are based on euclidean distance and a NN approach. The training data for the NN is based on a one month study, which is a subset of the Smart Trial programme described in Section 3.1. After the formulation of the framework it is then further extended to predict the energy consumption of the vehicle. The work is conducted such that this framework can then be used as a part of a predictive control strategy which is described further in Chapter 7.

4.2 Analysis of the Data at the Trip Level

As described in Section 2.1, the analysis of the data at the trip level is quite critical to establish the needed AER of the PHEV. This requirement essentially dictates the percentage of distance driven electrically and hence the amount of fuel energy which can be offset [71]. During this research it has been assumed that the vehicles are charged on a daily basis or at the start of each trip. Early adoption demonstrations show users charge the vehicle overnight to reduce fuel consumption [45].

Figure 4.1 shows the cumulative distribution of the trips for the Smart ED and also the Mini dataset. The Mini dataset has been included to compare an unlimited range conventional vehicle to a range limited EV such as the Smart ED. Based on

this, trip distance to cover the 90% of the average daily mileage the AER has to be 50km. It is based on the assumption that two trips of average trip distance 25 km are undertaken per day, that is, one trip to work and one trip from work [11]. It is interesting to note that it was suggested in [9], that range anxiety could be a reason for the adoption of short trips in the case of an EV. However, from the comparison of the Mini trial to the Cenex trial, it can be seen that the majority of the trips are similar in terms of distance.

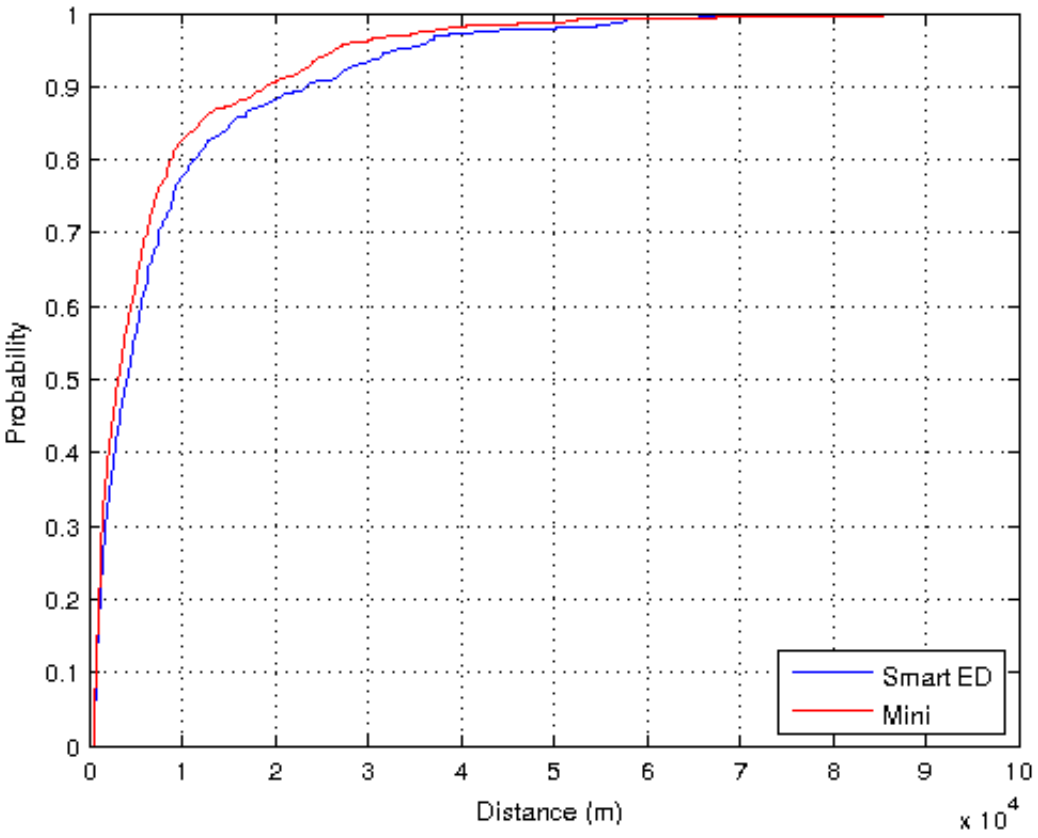

Figure 4.1: Cumulative distribution of trip length

4.3 Analysis of the Data Using Microtrips

On investigation of existing literature, as described in Section 2.1, the primary means of analysing real-world vehicle usage data is to deconstruct the complete dataset for a trip into smaller portions known as microtrips. The primary motivation is to improve the road definition of the trip data. It has been envisaged that splitting the data into microtrips facilitates a more robust prediction of parameters, such as average energy consumption relative to the amount of time the vehicle spends in a

particular mode of operation or environment. Within [82] a microtrip is defined as the non-zero vehicle speed profile between two vehicle stops. Figure 4.2(a) shows a section of a trip split into smaller microtrips. A concern raised in [82] is that this method results in the under representation of motorway or highway sections. This is because for highway conditions there may be large sections of the journey in which the vehicle never stops. This problem is further compounded because the vehicle may not stop when entering or exiting a highway or motorway. As a result, different road types may be merged into a single microtrip. In order to overcome this limitation a solution proposed by [1] in which each microtrip is then further segmented as a function of time has been employed here. In this study a microtrip is defined as the non-zero vehicle speed profile between two vehicle stops for a time period of up to 30 seconds. Very short (start-stop) microtrips are accumulated into adjacent microtrips until the 30 second time limit is reached. Figure 4.2(b) shows the new microtrip split solution. The classification of these microtrips can be done using two very different approaches.

- In the first approach, the data is clustered into similar homogeneous groups. This is done by euclidean distance classification. It is noteworthy that the groups that are finally identified may not coincide with any previous classification.

- The second approach consists of identifying data and comparing them to a pre-identified training data-set. For this approach a NN was formulated for the identification of the different road-types.

4.3.1 Categorisation of Microtrips Based on Euclidean Distance

This method is useful to identify clusters of microtrips that have similar characteristics. The clustering approach has been implemented in MATLAB using a clustering tool called k-means [56]. The algorithm is an iterative process with the following steps :

Step 1: Random points in the dataset are selected as the centres of each cluster.

Step 2: The distance of each point to the centres is calculated. The cluster number to the nearest centre is assigned for each point.

Step 3: The centres are adjusted by calculating the centroid of each cluster with the corresponding points.

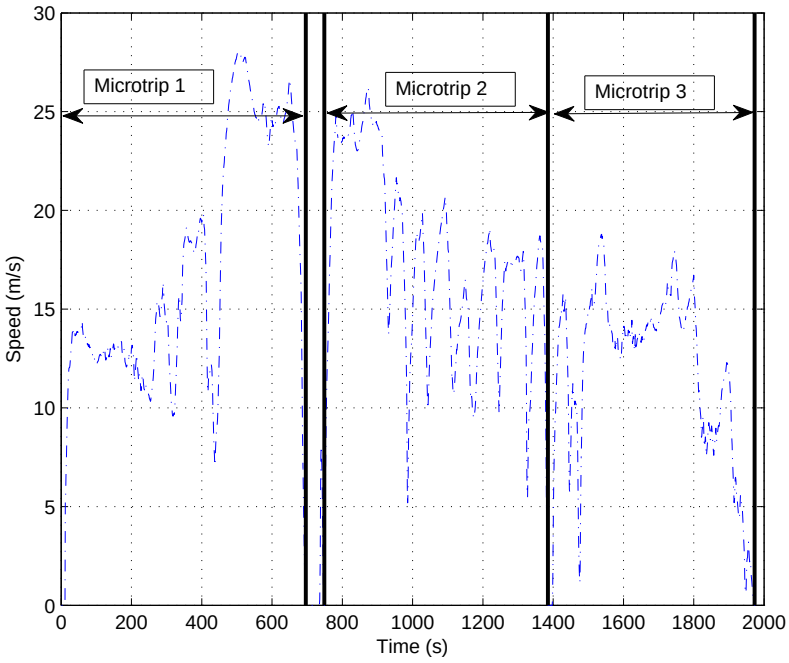

(a) Based on rest Periods

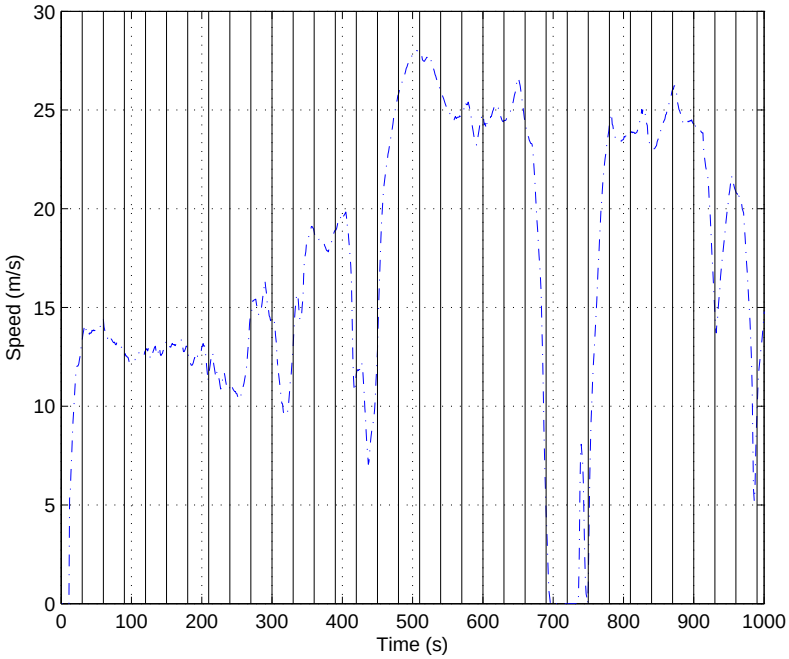

(b) Split every 30 seconds

Figure 4.2: Splitting to microtrips

Step 4: Steps 2 and 3 are repeated until there is no net change in total distance for each cluster.

Based on the work done in [2] it can be deduced that the two key factors which are useful for the detection of roadtype are speed and acceleration. The approach was adopted by [82] to classify the data of the Mini programme and develop a methodology to size batteries for a HEV. The same classification groups and input parameters have been used so that the data obtained from the Smart ED programme can be compared to the Mini programme. The total dataset represents 4,268km of driving. The parameters used for the study were :

- average speed of each microtrip
- average acceleration of each microtrip
- congestion index of each microtrip

Congestion index is defined as the ratio between the mean speed and standard deviation of the mean speed. Further details of the congestion index are given in Section 4.3.2. Before, classifying the data, the data for each parameter is normalised to the maximum value of each parameter. Figure 4.3 shows the mean speed and acceleration for each microtrip of the complete Smart ED dataset and the clusters that they belong to.

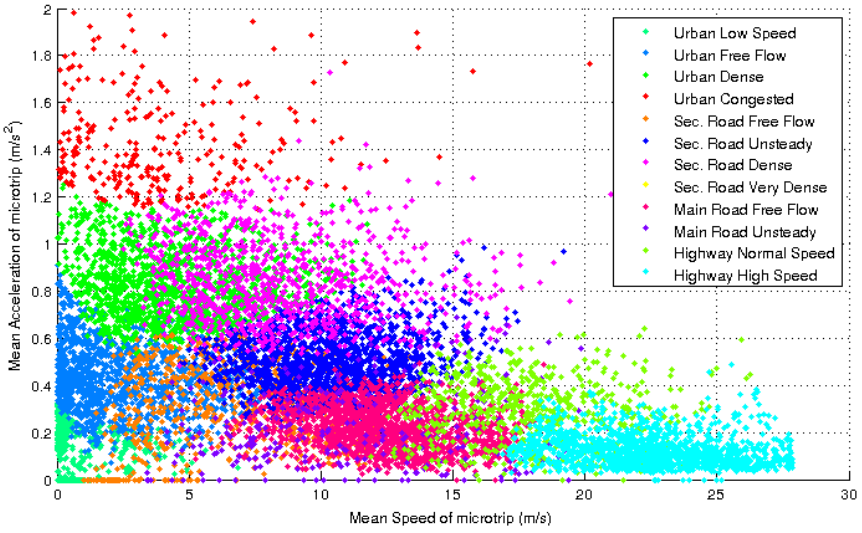

Figure 4.3: Distribution of microtrips - classification based on Euclidean distance

Table 4.1 shows the centroid values for each cluster and for comparison of the Smart ED dataset and the Mini dataset obtained from [82]. Figure 4.3 shows the

classification of the various microtrips. The classification groups are selected based on [82] for comparison to the Mini dataset. From Table 4.1 it is noteworthy that the speeds are similar between the Smart ED dataset and the Mini dataset in the urban environment. The maximum variation is found in the highway group. This can be attributed to the top speed limitation of the Smart ED. However, when comparing accelerations in Table 4.1 the acceleration of the Smart ED is much lower than that of the Mini across all classification groups. This could be attributed to the fact that the Smart ED is an underpowered vehicle. However, it also has to be noted from Figure 4.3 there are microtrips which have accelerations above $0.65m/s^2$ which is the maximum mean acceleration of all the categories. Therefore, the low acceleration values in each group are definitely a function of the classification scheme as much as the functioning of the vehicle in the real-world. Indeed on further investigation it was determined that the initial centres chosen for the k-means algorithm affected the final results. In order to further investigate the performance of the k-means algorithm for classification two key metrics were compared. The first metric is the ratio of the sum of the variance of each cluster to the total variance of the cluster. This is shown in the following equation :

$$\text{variance ratio} = \frac{\sum_{j=1}^{k}\sum_{i=1}^{n}\|x_i^{(j)} - c_j\|}{\sum_{i=1}^{N}\|x_i - C\|} \tag{4.1}$$

Where k represents the number of clusters, n represents the total number of samples in each cluster, x is each sample, c is the centroid of each cluster, N is the total number of samples and C is the centroid of all the samples. The resultant variance ratio is shown in Figure 4.4. As it can be seen the variance reduces as the number of clusters increase. However, this happens only until a specific number of clusters, after which the introduction of additional clusters does not add any valuable information to the classification. The selection of number of clusters from this point is still ambiguous but for this research in order to compare with previous work 12 cluster groups are chosen [82]. The other metric used is the entropy of the cluster. The entropy of a cluster is given as

$$H(X) = -\sum_{i=1}^{n} P(x_i) \cdot \log_2 P(x_i) \tag{4.2}$$

The summation of entropies represent the quality of the classification. The lower the total entropy, it means the clustering groups are well defined. However, in this case on classification the lowest value of entropy was found to be a cluster group of 1. There have been other metrics introduced which give better representation of assessing the quality of the classification, however, that was not the intention of this Thesis. The objective is to match the existing data to a pre-defined set training

data-set therefore neural networks was adopted. The neural network is described in detail in the next section.

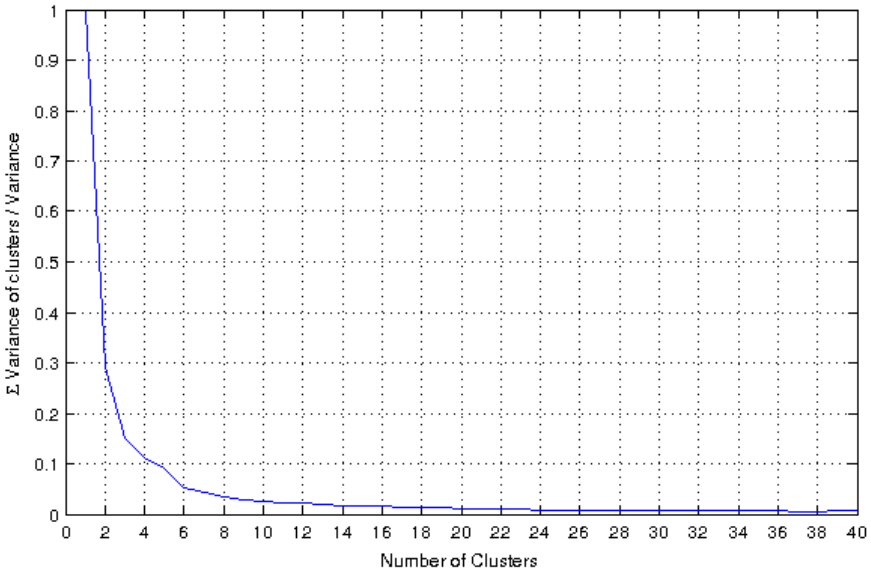

Figure 4.4: Variance ratio for different number of clusters

On comparing the values to the other two drive-cycles, it can be seen that the Mini is relatively closer to the ARTEMIS dataset than the Smart ED. However, this variation could again be due to the selection criteria. Further, the classification data may not have any relation to the real-world. For example, if the data was heavily biased towards urban trips in the real-world, the classification scheme will not be able to differentiate these nuances. There are limitations with this approach, however for completeness it has been discussed here. In the next stage, to overcome these limitations a NN framework was developed to classify the real-world data.

Table 4.1: Centroid values for each cluster and comparison against the Mini

		Cluster Number	SMART ED		Mini		NEDC		ARTEMIS	
			Average Speed (m/s)	Average Accel (m/s^2)	Average Speed (m/s)	Average Accel (m/s^2)	Average Speed (m/s)	Average Accel (m/s^2)	Average Speed (m/s)	Average Accel (m/s^2)
Urban	Low Speed	1	0.25	0.04	1.56	0.49	5.05	0.64	5	0.75
	Free flow	2	2.49	0.43	5.5	0.78				
	Dense	3	4.44	0.83	6.97	1.18				
	Congested	4	4.74	1.50	2.37	1.37				
Secondary road	Free flow	5	6.63	0.31	13.5	0.59			16	0.58
	Unsteady	6	10.35	0.5	10.55	0.69				
	Dense	7	8.42	0.84	13.1	1.08				
	Very Dense	8	8.82	4.23	9.57	1.08				
Main road	Free flow	9	12.48	0.21	24.36	0.39				
	Unsteady	10	11.33	0.21	15.78	0.49				
Highway	Normal Speed	11	17.99	0.29	27.14	0.29	17.35	0.37	30	0.52
	High Speed	12	22.57	0.12	32.1	0.39				

4.3.2 Categorisation of Microtrips Based on Neural Networks

Classification groups

In order to classify the data so that it can be related back to real-world geographic profiles, the UK road-type classification scheme was adopted. Table 4.2 presents the road type classification or groups employed within this research. For reference, a short description of each road type is provided and a comparison is made to analogous terms used within research papers published in both the US and mainland Europe.

Table 4.2: Road type classification

Road-type classification	Description	Comparable US road-type	Comparable EU road-type
Motorway or Highway	They are the main roads connecting the important regions of UK. They usually have a speed limit of 70 mph.	Freeway	Highway / Motorway
A-Road	Usually the road is as straight as possible, and has a speed limit of 60 or 70 mph. They are usually dual carriageway, but can be single lane.	Arterial Roads	Main Road
B-Road	B roads are numbered local routes, which have lower traffic densities than the main A roads. They are typically less than 15 miles long. B roads can range from dual carriageways to single track roads with passing places.	Arterial Roads	Secondary Road
Urban Road	These roads have a speed limit of 20 mph to 40 mph and are the inner city roads.	Local Roadways	Urban

In the UK the geographic information system (GIS) data for the entire road network is available as Environmental Systems Research Institute (ESRI) shape files [65]. For a given road section, the corresponding shape files contain specific information on; road name, road type and its GPS-coordinates. As a result, by

comparing the GPS data received from the different EVs while they are being driven with the information contained within the Ordinance Survey database, it is possible to identify the road-type for each microtrip. However, due to inaccuracies in GPS data and software limitations, the comparisons were done manually. Although a small dataset could be analysed in this way, a different tool was needed to facilitate automation and comparison of the entire dataset. Therefore, a training based pattern recognition tool was adopted. A training dataset in which different drivers drove the car over a specific route in which the road-type was known in advance was created. This training dataset was then used to "train" the NN to determine the road-type.

In order to predict the real-world energy consumption of the EVs and PHEVs it is necessary to ascertain not only the nature of the road type the vehicle is travelling through, but also the level of congestion experienced [2]. As described in the literature review, the traffic conditions and driver aggressiveness can cause variations by as much as 20% [17]. Therefore, as a result, each microtrip is further classified in accordance with the level of traffic congestion experienced. Partly due to its subjective nature, the definition of traffic congestion varies greatly between different research studies. For example [2] segments each road type into three different levels of congestion, resulting in 12 unique groups overall. The method of splitting the trip data is based on the relative congestion computed within the dataset. In [61] another approach is adopted in which congestion levels are identified by examining the similarity of each microtrip to drive-cycles published within the US by the environmental protection agency (EPA).

In this research, the approaches recommended by [82] and [63] have been adopted. Both authors advocate measures of congestion that are readily discernible from the vehicle speed profile:

- Intersection based traffic events
- Vehicle congestion based traffic events

Within [63] the authors describe intersection based traffic events as those where the speed of the vehicle reduces to one-third of its initial value or when the vehicle comes to a complete standstill. This phenomenon often occurs during traffic queues or at a road junction. In this research a measure of intersection based traffic events (I_i) is proposed as the number of vehicle stops per one km of driving. The value of I_i can therefore be calculated using the following expression:

$$I_i = \gamma \cdot \frac{1000}{v_x} \tag{4.3}$$

In Equation 4.3, v_x denotes the distance travelled by the vehicle within the microtrip and the number of recorded vehicle stops. A microtrip is designated as a start-stop microtrip if the number of I_i exceeds 2 stops per km. Given that each microtrip is based on a 30 second period, if the measured distance travelled is less than 1 km, then a weighted number of vehicle stops is used in the calculation of I_i.

Within [82], for a given microtrip the authors choose to define traffic congestion as the variation in vehicle speed from the mean vehicle speed. A Congestion Index (C_i) is calculated as follows:

$$C_i = \frac{v_{avg}}{\sigma_{v_{avg}}} \tag{4.4}$$

In Equation 4.4, $\sigma_{v_{avg}}$ defines the standard deviation of vehicle speed within a microtrip and v_{avg} defines the mean vehicle speed within the microtrip. The equation is based on [82], where it is implied when operating on a motorway at high speed, the speed is fairly constant and slight variation in speed would be considered as a congested traffic. The threshold of C_i above which a microtrip is deemed to represent congested traffic conditions is subjective. For this research it was determined that the simplest method of splitting the categories was to determine the mean congestion index of the entire dataset after removing the start-stop microtrips. The microtrips having a congestion index higher than this mean value were defined as congested and the rest were classified as free flowing. The mean value of C_i for the entire dataset was determined as 0.32. However it is interesting to note that the mean value of C_i for the training data set was much lower (0.14). This is primarily because the training dataset was obtained in a rural section of the UK where the average traffic conditions were low. Based on the two metrics of I_i and C_i, Table 4.3 summaries the three different measures of traffic congestion employed in this study.

Table 4.3: Summary of congestion metrics and thresholds

Measure of Congestion	Threshold
Congestion Index (C_i)	$C_i \geq 0.32 \Rightarrow$ congested traffic conditions
	$C_i < 0.32 \Rightarrow$ uncongested traffic conditions
Intersection Event Index (I_i)	$I_i \geq 2 \Rightarrow$ start-stop microtrip
	$I_i < 2 \Rightarrow$ congested or free-flowing microtrip.

Training the NN

Ten drivers were asked to drive along a prescribed route at three different times of the day. The three different times of day (9:45 AM, 1:15 PM and 4:45PM) were chosen so that the vehicle would be driven in varying traffic conditions. It was found

when completing the trips, generally the traffic was maximum on the 4:45 PM trip and least in the 9:45 AM trip. The route shown in Figure 4.5 was chosen such that a variety of different road types are encountered. The resulting thirty trips of known road-type have been taken as a training dataset for the NN classification method. A complete schedule of the usage of the Smart ED is given in Appendix 11.1. The training data consists of 688km driving and 1691 microtrips.

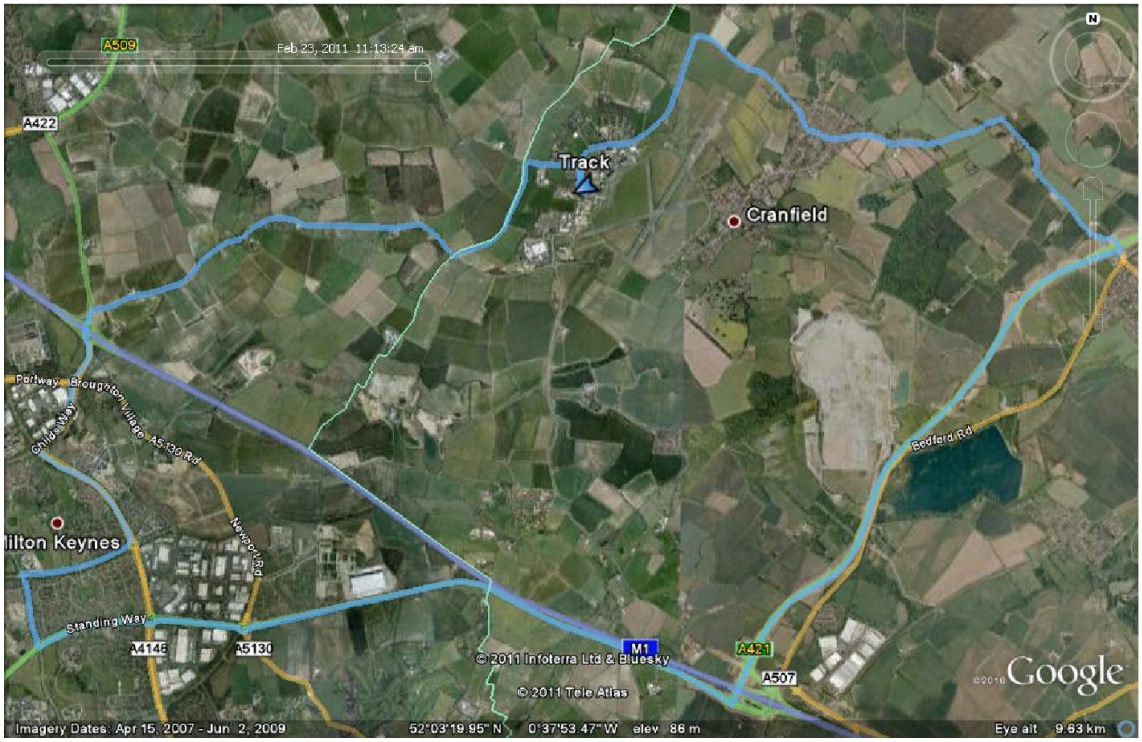

Figure 4.5: Training trip made at Cranfield University

Figure 4.6 shows a sample speed profile and road type determination from the ESRI shape files. The resulting distribution of microtrips is shown in Figure 4.7. There is an uneven distribution of microtrips even if the route is the same because among the thirty trips there was varying time durations due to traffic conditions and three of the trips had to be discarded due to faults in the measurement of data.

Figure 4.8 shows the mean speed and acceleration distribution for all different road types and traffic conditions of the training dataset. The mean values of each cluster are shown in Table 4.4. The classification values are as expected for different road types. The average speed increases as the road-type reaches motorway conditions and the acceleration values increase with traffic increases. The trends in this research are similar to the work done in [23] where a much larger dataset is used.

The stop start congested motorway road-types occur primarily on ramps to the motorway. On the motorway itself, it was found by observation that the Smart

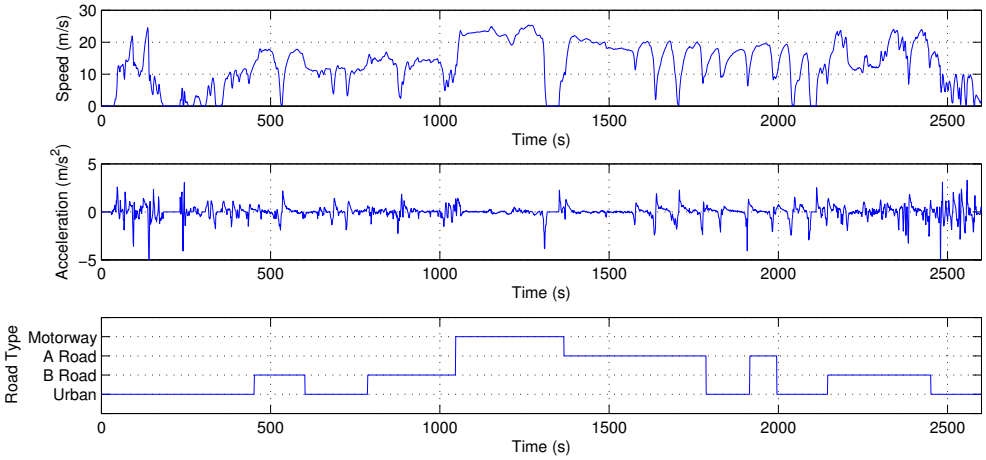

Figure 4.6: Sample trip taken from reference data

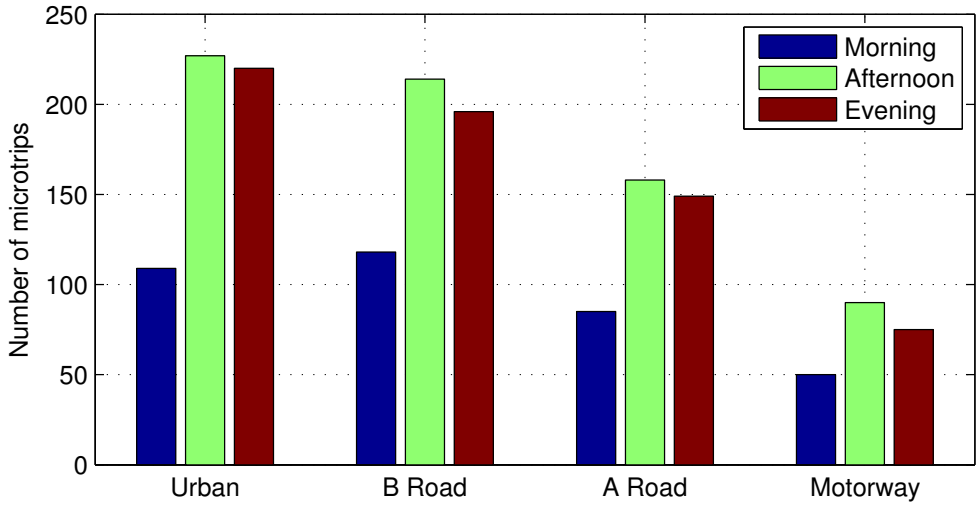

Figure 4.7: Microtrip distribution for reference data

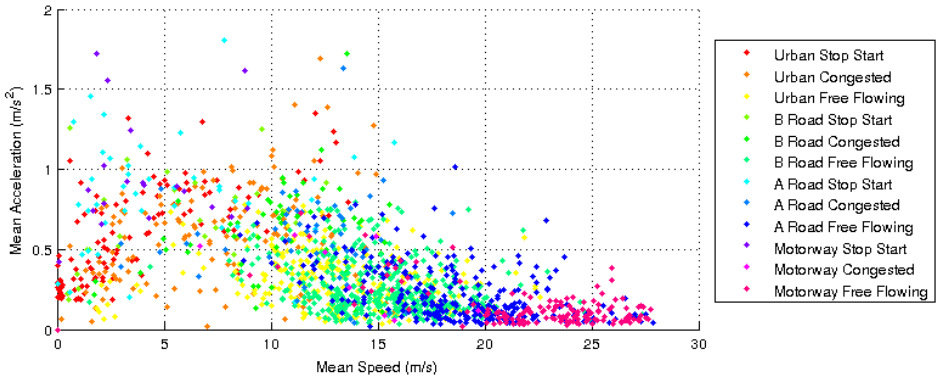

Figure 4.8: Distribution of microtrips for different road types and traffic conditions

Table 4.4: Mean values for different road-types for Reference Data

Road Category	Traffic Congestion	Cluster Number	Average Speed (m/s)	Average Acceleration (m/s^2)	Congestion Index
Urban	Stop and Go	1	3.48	0.91	1.02
	Congested	2	8.26	0.51	0.26
	Free Flowing	3	12.61	0.16	0.03
B Road	Stop and Go	4	3.74	1.06	1.01
	Congested	5	10.49	0.50	0.19
	Free Flowing	6	15.43	0.17	0.03
A Road	Stop and Go	7	3.32	1.09	1.18
	Congested	8	12.23	0.63	0.19
	Free Flowing	9	21.50	0.11	0.01
Motorway	Stop and Go	10	2.97	0.94	1.23
	Congested	11	9.50	0.62	0.28
	Free Flowing	12	25.12	0.06	0.01

ED with a top speed of $100km/h$ struggles to keep up with traffic flow, therefore the congestion index is lower and all trips are classified as free flowing. Figure 4.9 shows the number of microtrips under different road types. As discussed in [82], the threshold of classifying trips as congested is sensitive to the method of classification.

NN Classification

NNs have been used on a wide range of applications as a pattern recognition technique in speech recognition, robotics, process control and telecommunications [42]. The algorithms used mimic the working of a biological nervous system. A theoretical background on the subject can be obtained in [42]. However, from an application-oriented point of view, the algorithm can be implemented in MATLAB using the NN Toolbox.

Typically the goal of a NN can be defined as a model which is able to map a set of given inputs to a set of training output variables. In this case the microtrip parameters such as the list presented in the literature review Section 2.1 is obtained from the training dataset and used as input signals. The road-type data during the trip are used as output variables. After training, the model will be able to identify road-types for a set of microtrip input parameters.

Every NN is layered and is said to be made up of neurons. Figure 4.10 shows the structure of a simplified NN. Each circle can be considered to represent a

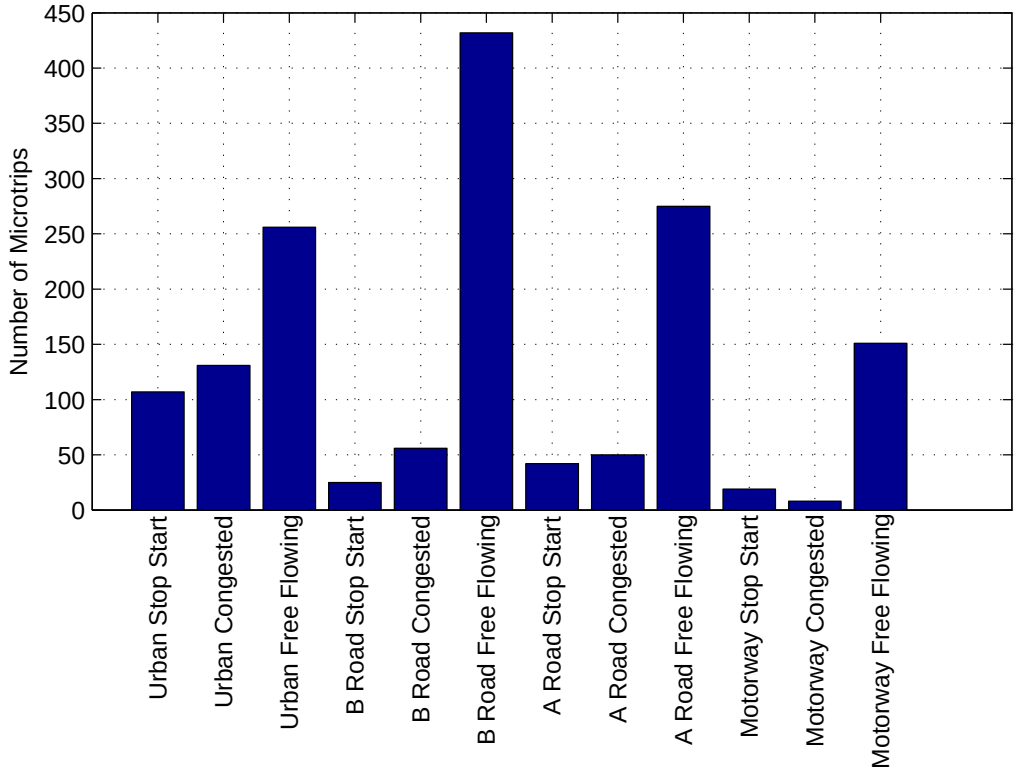

Figure 4.9: Number of microtrips for different road types and traffic conditions

neuron. The connections between each neuron are known as synapses. Each neuron consists of a mathematical function which is localised to that neuron, that is, the mathematical function is strictly dependent only on the input signal to that neuron. Every layer of neurons comprises the same mathematical function. The connections between neurons (synapse) can be altered by altering the weight of the input. Thus the output of the neuron can be altered by altering the weight of the input (synapse). By supervised alteration of these weights the desired output (training output) can be attained. At a minimum, a NN is made up of three layers; the input layer, a hidden layer and an output layer.

From this discussion it becomes clear that the architecture of the network has a significant influence on the results obtained. The architecture could be feed-forward and feed-back type depending on their construction. Further, based on the training method adopted and the architecture of the network the NN are classified into different types. A detailed discussion into the types of NNs and their construction are beyond the scope of this research. However, a complete overview of the different NN types are given in [42]. The type of network architecture adopted for this research is

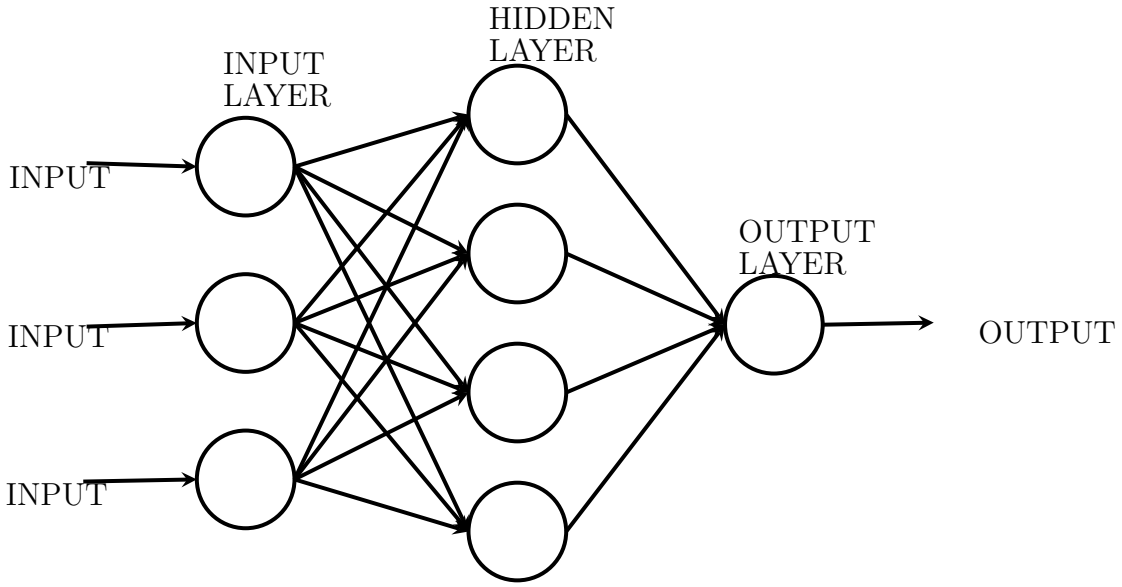

Figure 4.10: A simple NN

predominantly used for pattern recognition [42]. It is a feed-forward network with a competitive learning algorithm. It is also known as a Self Organising Map [1]. The mathematics behind self-organising maps has not been dealt with in this thesis due to detracting from the subject and time constraints, but a short overview of the working is presented for completeness. Figure 4.11 shows the structure of the NN.

The weight matrix IW in Figure 4.11 is initialised by a random selection among the training data. The elements of output S^1 is the distance between the input vector p and each row of the input weight matrix. The competitive transfer function outputs one (winner) for the neuron containing the least euclidean distance between IW and the training data. The weight matrix is altered based on the row which produced the wining neuron. The weights are altered such that the distance of that row to the input vector further reduces. Thus the competitive layer works similar to k-means by forming cluster groups based on the weight matrix to reduce the overall distance.

The linear layer forms the relationship between the winning neurons and the training output. Both the competitive layer and linear layer at a minimum have to contain the same number of target classification groups. Each class of the competitive layer is assigned to a target class. It is possible to have more competitive layer classes and depending on training they are assigned to respective target classes. For example if neurons 1,2,3 in the competitive layer all learn for target class 2, the linear layer outputs 1 if any of the neurons are activated.

The design of the NN for driving pattern recognition extends the work published

by [23] and [1]. Within [23], the author identifies 40 parameters that can be calculated, per microtrip, to quantify those vehicle and environmental attributes that affect fuel economy. Within [1], the author employs a subset of these parameters as the input vector to a NN with the aim of constructing different drive-cycles that emulate specific driving environments.

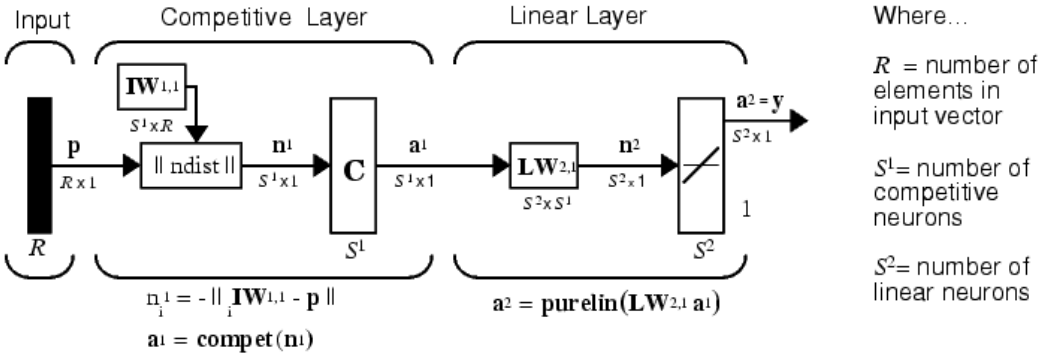

Figure 4.11: Structure of NN

Figure 4.12 presents the overall experimental set-up that was used not only for training the NN, but also for classifying the EV fleet data.

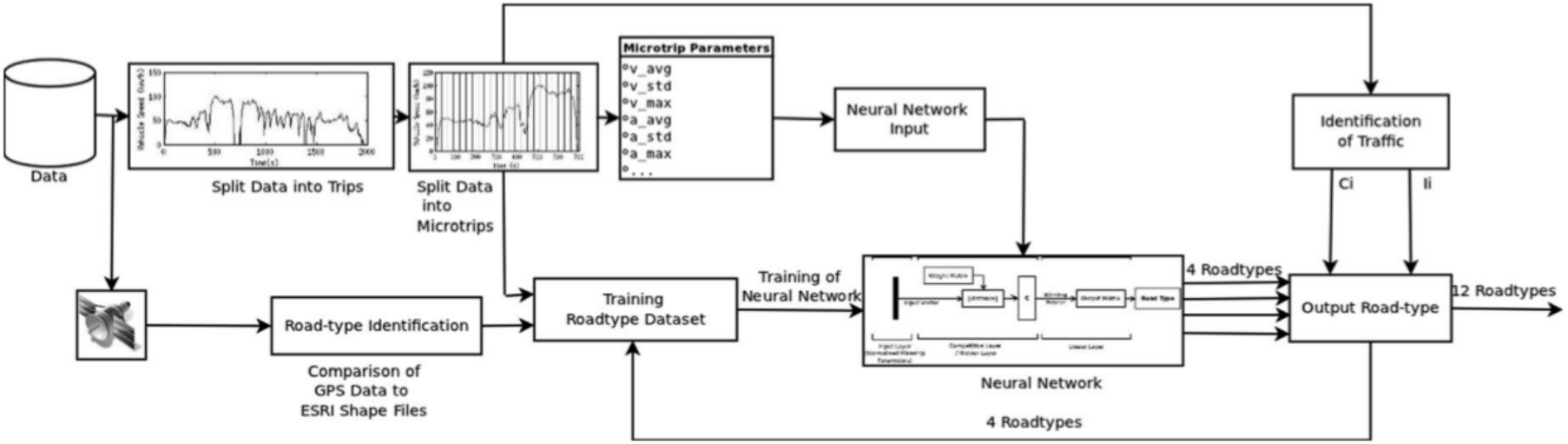

Figure 4.12: Experimental set-up for the training and use of the NN

Table 4.5 presents the 28 parameters identified in [1] that were calculated for each microtrip from the training data set and employed as the input vector to the NN. The input vector was first normalised in order to avoid bias within the data set. When training the NN, it is important to avoid a phenomenon known as over training. Over training may occur when the number of hidden neurons is comparatively high and as a result, the network learns not only the basic mapping associated with input and output data, but also the subtle nuances and even the errors specific to the training set [42]. If too much training occurs, the network only memorises the training set and loses its ability to generalise to new data. In order to check for the influence of this phenomenon, 80% of the training data described was used to train the NN with the remaining 20% being used to check for the presence of the over training phenomena. The result of this test highlights an insensitivity of the accuracy of the NN, for a hidden layer which has 10-40 neurons. Figure 4.13 shows the accuracy of the neural network for different amount of neurons in the competitive layer. As it can be seen the increase in number of neurons does not improve the classification behaviour.

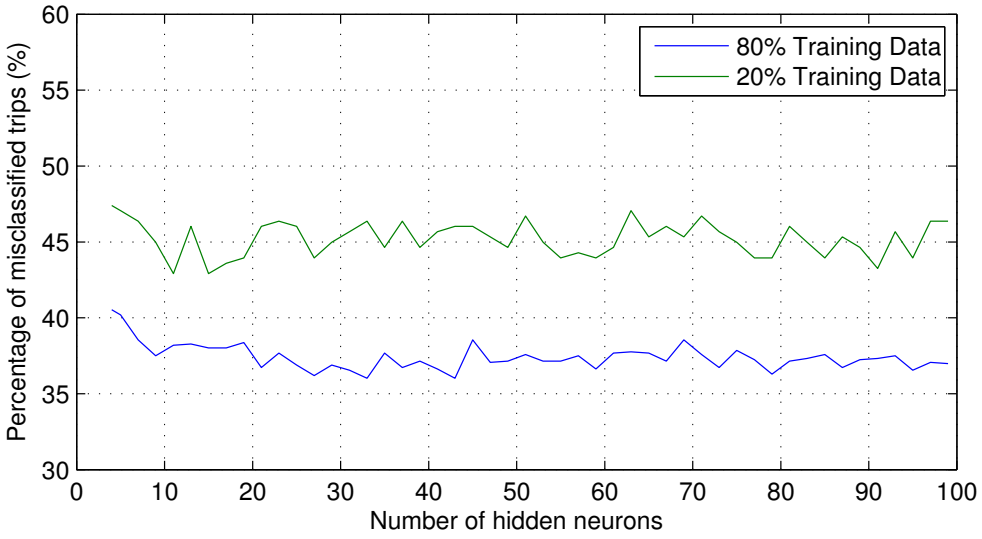

Figure 4.13: Classification accuracy based on number of neurons in competitive layer

The ability of the NN to predict the roadtype with the training data set is shown in Table 4.6. The highlighted values on the leading diagonal of the matrix denote those microtrips that have been properly classified. The low power rating of the vehicle implies that there is little discernable difference between the vehicle's performance over both A and B roads. This is thought to be the primary reason for the relatively poor performance of the NN. When A and B roads are combined, the average prediction accuracy of the NN rises to 80%. Table 4.7 shows the improvement in network performance when A and B roads are combined. It also

has to be considered that the training dataset was obtained in a region of the UK where traffic is fairly minimal. This leads to similar datasets for A and B roads.

Therefore, the author recommends a longer training dataset with roads which show much more variation between A and B roads to correctly identify these two road categories. The subtle dependency between vehicle performance attributes and the validity of the training data set is discussed further during the prediction of power demand in Chapter 7 and Chapter 8. Whereas it is favourable to limit the number of neurons to maintain the networks ability to abstract new data, if the number of the neurons is too low, then the initial random selection of the weighting matrix significantly affects the deterministic nature of the NN. However, as the number of neurons increases the random selection of initial weights has less influence on the final result of the NN. Based on these contradictory requirements and through experimenting with the training data set and the NN, 20 neurons were selected for use within the hidden layer.

In summary, there are a total of 4 neurons for the output layer of the NN in which each represents one of the four possible road types from the network, namely; motorway, A-road, B-road and Urban.

Finally, the results of the training are given in Figure 4.14(a) and (b). Figure 4.14(a) shows the original training dataset which was input into the NN. Figure 4.14(b) shows the output of the NN. On visual inspection the NN recognises the data similar to the training dataset.

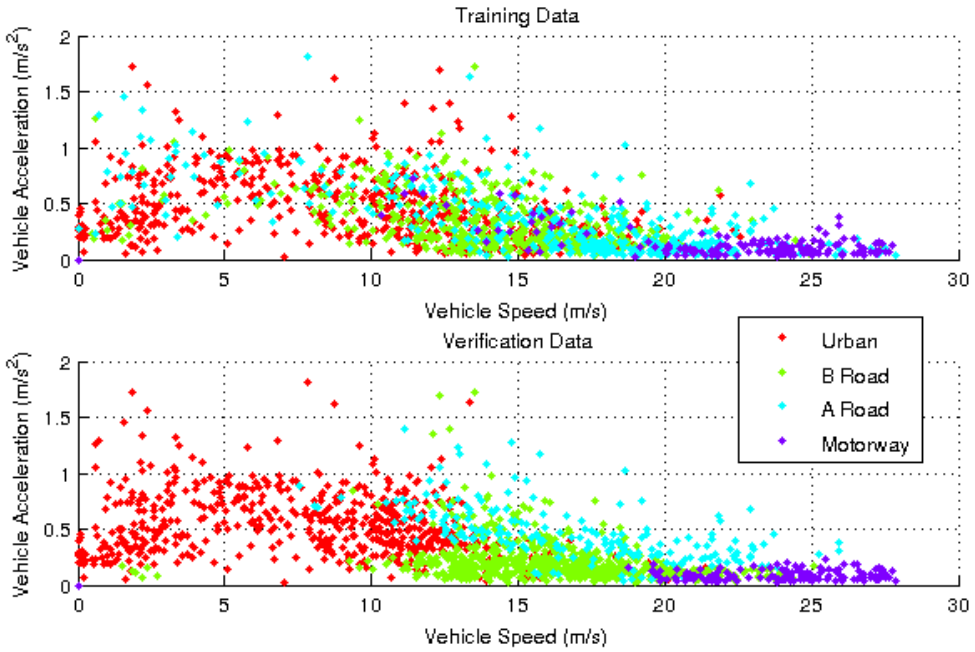

Figure 4.14: Comparison of network output to training data

Table 4.5: Parameters calculated for each microtrip

Parameter	Denotation
Average Speed	v_avg
Standard Deviation of Speed	v_std
Maximum Speed	v_max
Average Acceleration	a_avg
Standard Deviation of Acceleration	a_std
Maximum Acceleration	a_max
Average Deceleration	r_avg
Standard Deviation of Deceleration	r_std
Maximum Deceleration	r_max
Relative Positive Acceleration $1/x \int v \cdot a^{+} dt$ x = total distance	rpa
Number of Stops per km	stp_p_km
Stop Duration per km	sdur_p_km
% of time in speed interval 0-15 km/h	v0_15
% of time in speed interval 15-30 km/h	v15_30
% of time in speed interval 30-50 km/h	v30_50
% of time in speed interval 50-70 km/h	v50_70
% of time in speed interval 70-90 km/h	v70_90
% of time in speed interval 90-110 km/h	v90_110
% of time in speed > 110 km/h	v110_200
Positive Kinetic Energy $(\sum(v_f^2 - v_i^2))/x$ when $dv/dt > 0$	pke
% of time when (va) < 0	va_0
% of time when (va) is 0-3	va_0_3
% of time when (va) is 3-6	va_3_6
% of time when (va) is 6-10	va_6_10
% of time when (va) is 10-15	va_10_15
% of time when (va) > 15	va_15
Total Duration (s)	tdur
Total Distance (m)	tdist

Table 4.6: Classified microtrips for different categories

		Data		**Output Data**			
		Number of micro trips	% Correct	Urban	B Road	A Road	Motorway
Training Data	Urban	486	70.00%	**339**	119	24	4
	B Road	470	71.00%	79	**344**	35	12
	A Road	344	24.00%	56	125	**81**	82
	Motorway	141	86.00%	1	9	10	**121**

Table 4.7: Misclassified microtrips for different categories - Combined A and B roads

		Data		**Output Data**		
		Number of micro trips	% Correct	Urban	A / B Road	Motorway
Training Data	Urban	486	70.00%	339	143	4
	A / B Road	814	72.00%	135	585	94
	Motorway	141	86.00%	1	19	121

Once the NN had been trained it was employed to classify the entire data set from the Smart Move 2 EV fleet evaluation. This equates to over 4,268 km of real-world driving and 11,780 unique microtrips.

Figure 4.15 presents the complete classification of the data set into the 12 different groups of road type and traffic congestion levels. Table 4.8 quantifies the mean values for EV acceleration and speed, in addition to the congestion index (Ci).

Table 4.8 compares the mean values of vehicle speed and acceleration observed from the Smart Move 2 Trial, with those calculated from both the NEDC and the ARTEMIS cycle. Unlike the euclidean method of classification from visual inspection of Figures 4.16 and 4.17 the combined mean values of vehicle speeds and acceleration for A and B roads correlate well with those found within the ARTEMIS drive-cycle. For the ARTEMIS road and urban cycles, the mean values of vehicle speed are 5m/s and 16m/s respectively, whereas the mean values of vehicle acceleration are $0.75m/s^2$ and $0.58m/s^2$. Therefore the EV test data can be considered valid for under urban and extra urban conditions on comparison to the ARTEMIS dive-cycle. The difference in the motorway speeds is attributed to the low power rating of the test EV fleet.

If a comparison is made between the Smart Move 2 fleet data and the characteristics of the NEDC , it can be seen that the legislative urban conditions

are far less demanding than those experienced in the real-world. This is particularly the case for both A and B roads. It is noteworthy, that Table 4.8 only lists the mean values of vehicle acceleration. The peak values of acceleration observed within the measured data vary by more than 120% from those found within the NEDC. This fact further highlights that the European drive-cycle does not properly emulate the dynamic loads on the powertrain.

Unfortunately, the mini dataset could not be analysed using NN due to the lack of a training dataset. It would be possible to apply the trained NN from the Smart Move 2 trial onto the Mini dataset, however the accuracy of the results cannot be validated.

Furthermore, the implications of additional load due to gradients cannot be compared, primarily because of non-availability of data. There is scope for further research in this area, however for the purposes of this thesis, gradient loads have not been considered.

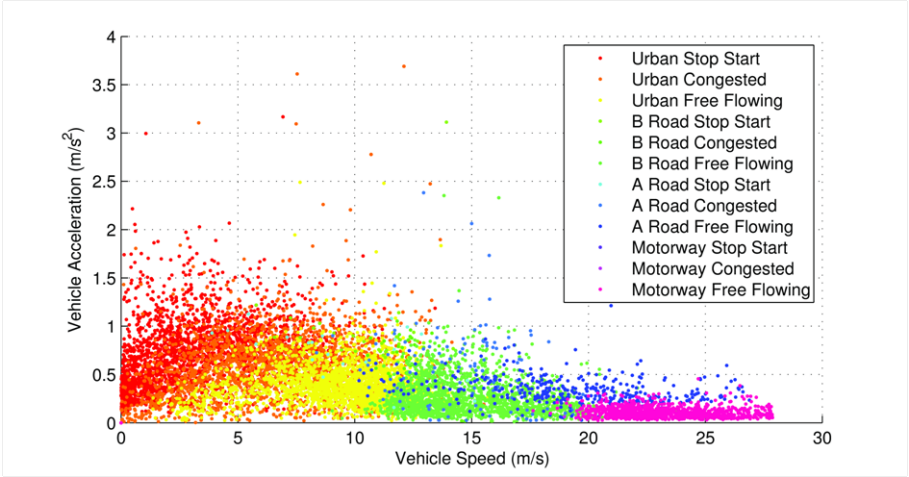

Figure 4.15: Classification of the Smart Move 2 dataset

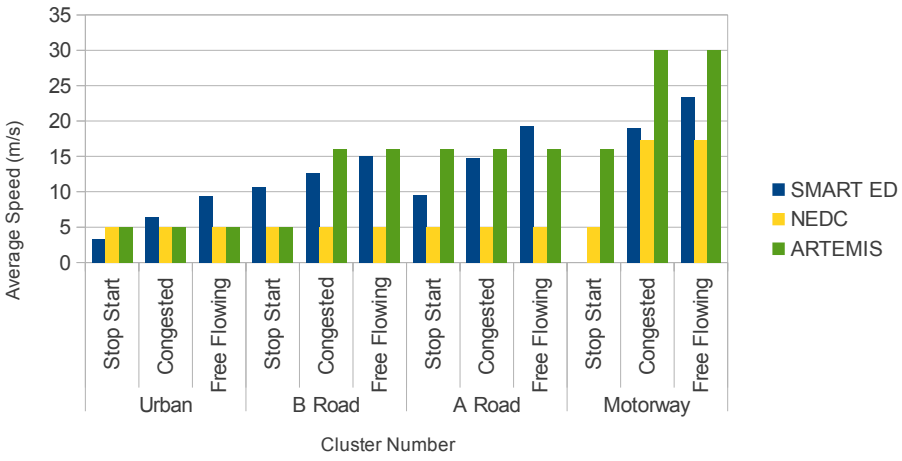

Figure 4.16: Comparison of NN classification to drive-cycles - average speed

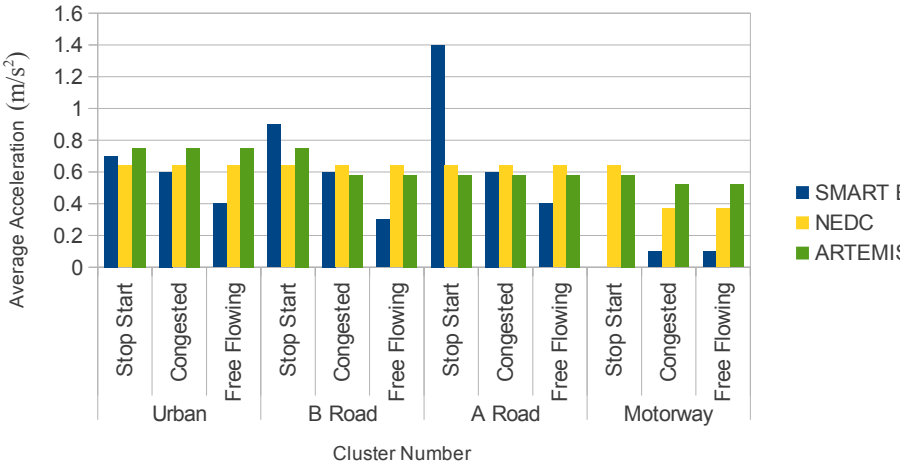

Figure 4.17: Comparison of NN classification to drive-cycles - average acceleration

Table 4.8: Centroid values for each of the categories

Road Category	Traffic Congestion	Smart EV Trial				NEDC		ARTEMIS	
		Average Speed (m/s)	Combined Average Speed (m/s)	Average Accel (m/s^2)	Combined Average Accel (m/s^2)	Average Speed (m/s)	Average Accel m/s^2)	Average Speed (m/s)	Average Accel (m/s^2)
Urban	Stop Start	3.3	6.4	0.7	0.6	5.05	0.64	5	0.75
	Congested	6.4		0.6					
	Free Flowing	9.4		0.4					
B Road	Stop Start	10.7	12.8	0.9	0.6			16	0.58
	Congested	12.7		0.6					
	Free Flowing	15		0.3					
A Road	Stop Start	9.6	14.5	1.4	0.8				
	Congested	14.7		0.6					
	Free Flowing	19.3		0.4					
Motorway	Stop Start	NaN	21.2	NaN	0.1	17.35	0.37	30	0.52
	Congested	19		0.1					
	Free Flowing	23.4		0.1					

4.3.3 Energy Consumption

The energy consumption per unit distance (Wh/km) for each microtrip of the complete dataset is analysed. Figure 4.18 shows the spread of energy consumption for different roadtypes. The negative values result from cases where the vehicle coasts down to a stop and the vehicle is stationary for the rest of the microtrip. The spread of energy consumption decreases in the case of free flowing conditions. This is because acceleration levels become quite low under these conditions. On the motorway during congested conditions the average speed is low (16 m/s), this causes a lower energy consumption within the vehicle. The spread of energy consumption under congested conditions is attributed to driver behaviour [18]. For future studies it would be beneficial to study the data further based on driver behaviour.

Variations between the legislative drive-cycle and real-world usage of the EVs manifest themselves in potentially significant differences in the realisable efficiencies and therefore the range of the vehicles. The EV trial programme sponsor conducted tests with Millbrook to establish the legislative energy consumption values. One of the Smart EVs was tested by Cenex on a dynamometer and its range measured over the NEDC. It was found that the measured range was 136km that correlates well with the manufacturers published figure of 135km. However, the average real-world energy consumption across the entire evaluation programme was 116kW/km. Given a usable battery capacity of 13.2kWh (80% of 16kWh) it can be seen that this equates to an average vehicle range of just 114km, a 15% reduction in the vehicle's range as compared to the manufacturer's cited figure. In reality the range achieved within the vehicle would vary depending on the style of driving, the nature of the road type and traffic congestion levels experienced. Figure 4.18 shows the energy consumption variation for the different microtrips. On each box, the central mark is the median, the edges of the box are the 25th and 75th percentiles, the whiskers extend to the most extreme data points not considered outliers, and outliers are plotted individually. As it can be seen from Figure 4.18, if the vehicle was deployed within a highly congested urban environment such as a European capital city, then the range of the same EV may reduce below 50km.

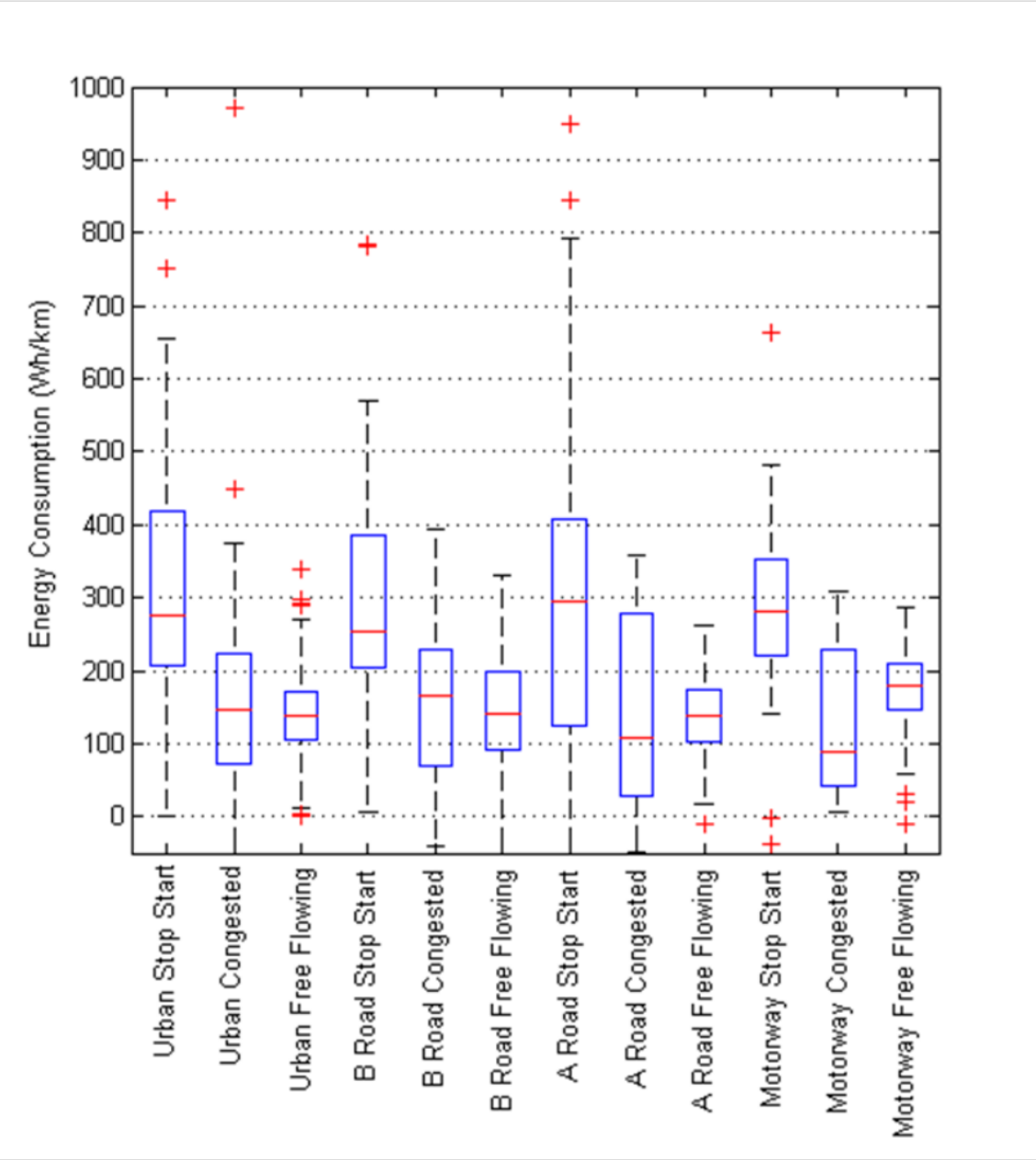

Figure 4.18: Energy consumption for different categories

4.4 Discussion

4.4.1 Repeatability of the Research

The numerical results presented here are derived directly from the Smart Move 2 evaluation programme and as such are constrained to the class of vehicle employed. However, the NN framework designed for recognising the different road types and varying levels of traffic congestion is generic and highly transferable to different vehicle evaluation programmes in which different classifications of vehicles are used. The key point regarding the repeatability of the research is the need to generate a new training data set that is relevant to the target vehicle. It is important that the attributes of the vehicle, namely weight, propulsion power, energy storage etc. are comparable. Furthermore, the decomposition of the route into different road types (urban, A and B roads, motorways) must properly reflect the capabilities of the vehicle and its anticipated use. If this is not the case, it may not be possible to uniquely identify the different conditions appropriate to the usage of the vehicle.

4.4.2 Applications of the Research

Vehicle Fleet Operators

One future direction for the research presented in this Chapter is to codify the NN framework within a software tool that would enable end users to better predict a more realistic EV range. The ability to formulate different scenarios in which the electric range is a function of the different driving styles, traffic congestion levels and road type has obvious advantages when compared to using just legislative drive-cycles for vehicle range prediction. This is particularly pertinent for vehicle fleet operators that may deploy EVs within a specific environment, such as inner-city public transport or the use of urban delivery vehicles. It is argued that the framework presented would not only provide a greater insight as to the real-world range and energy efficiency of the EVs, but also highlight variations between different drivers when the same vehicle is driven over the same route under similar congestion levels.

Transport Sector Forecasting

In addition to meeting the short-term requirements of vehicle fleet operators, the proposed framework can also support those researchers involved in both medium and long term scenario planning. Over the last ten years a number of studies have formulated models for the introduction and market penetration of energy efficient vehicles that include both EVs and PHEVs. These separate studies have been collated and critically evaluated in a recent publication by [16]. The

aim of this recent study is to build a total cost of ownership (TCO) model for different architectures of EVs, PHEVs and conventional ICE powered vehicles. The authors discuss the challenge of developing a representative value for the running costs associated with vehicle ownership (MJ/km). This is primarily due to the complexities of segmentation within the passenger car market and the different usage patterns for different vehicles. As a consequence, within [16] a simple drive-cycle analysis is adopted with a single weighting being applied to represent periods of increased energy demand. As with vehicle fleet operators, given the generation of appropriate training data sets, the same NN approach could be employed to more accurately predict the tank-to-wheel energy demands of different EVs and hybrid derivatives when deployed in different transport environments.

Energy Consumption Prediction

The research presented in this chapter is extended for the formulation of the energy management control system in Chapter 6. A PHEV will typically have two primary modes of operation, namely; a CD mode and a CS mode as described in Section 2.2. However, from studying existing literature [39] it was determined that the CB mode of operation gives the best performance.

In order to implement a CB mode within a real-time energy management controller, the system would need to know the journey route and the energy required to complete the journey. From the data collated from the EV trial, a lookup table of energy consumption values for different road-types has been formulated. The lookup table consists of mean values and upper and lower limits representing the 25th and 75th percentile respectively. In its simplest form, the implementation of the CB strategy would require the driver to enter their desired route. The control system, using the look-up tables, would derive an estimate of the required energy to complete the journey and this would be used as the SOC set-point trajectory within the controller. However, a more robust method of implementation would be to use the NN on-line, in which the speed of the vehicle is used to predict both the road type and congestion levels. This technique would extend the well-established concept of journey prediction [100].

In order to test the feasibility of this concept, a random journey was selected from the trial database and fed into the NN as a 30 second moving window of data. Based on this window of information the NN predicted the road-type and subsequent traffic congestion levels. Figure 4.19 presents the predicted energy consumption and the actual energy consumption measured in the EV. The figure also shows the average energy consumption data from the lookup table. On integration of this data over distance the predicted energy consumption can be calculated. The figure

clearly shows that the predicted energy consumption follows the same trajectory as the measured value and is well within the lower and upper 25% and 75% limits. The same experiment was conducted on over 834 real-world journeys from the EV trial. The results are presented in Figure 4.20, in which the correlation between the actual and estimated energy consumption is presented. Overall, the accuracy of the predicted energy consumption of the EV was 72%. The RMSE value in this case was determined to be 982 Wh. However this figure increases to 82%, if consideration is constrained to trips in which the total energy demand does not exceed 4kWh. The root mean squared error (RMSE) value reduces to 874.14 Wh in this case. Since 90% of the trips recorded were under 4kWh, this represents a more realistic usage scenario for the test urban vehicle. The reason for the drop in prediction in accuracy is due to a number of reasons:

- Prototype vehicles were used for the trial, and their performances improved over time.
- A number of different vehicles were used in the trial program with varying performances.
- The vehicles were used from winter to summer during the test program.This implies the batteries were subjected to temperature variations. The effect of this temperature variation on the performance of the vehicle is not understood.

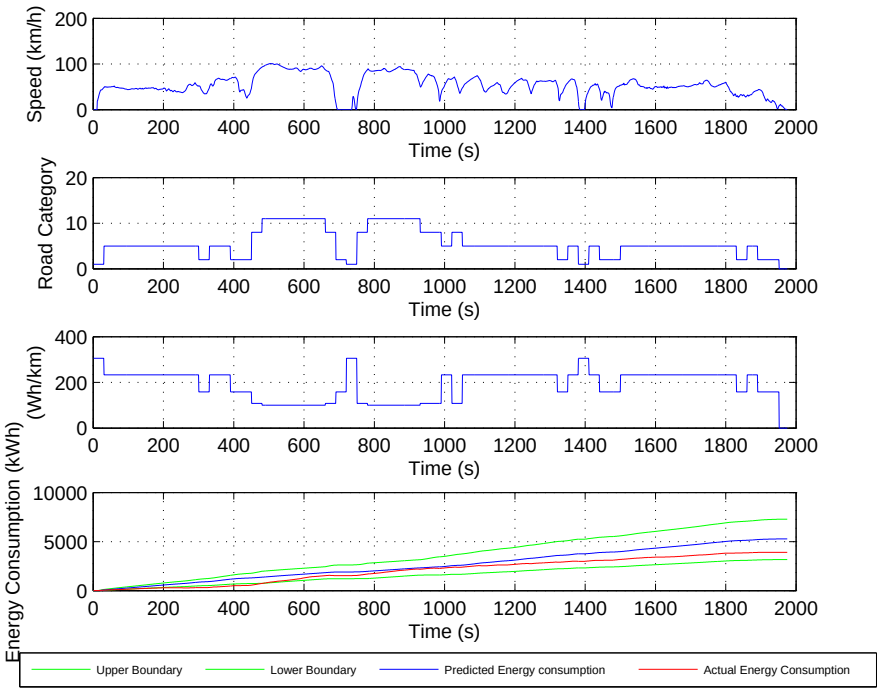

Figure 4.19: Predict energy consumption of a trip

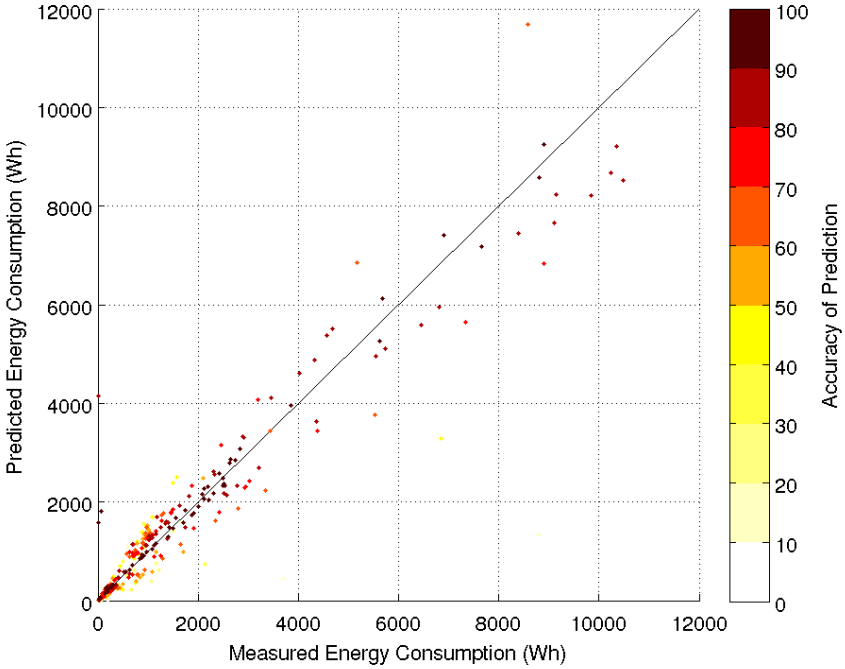

Figure 4.20: Energy consumption for all trips

4.5 Conclusions

A novel framework has been presented where a NN is used to classify the transport environment in which the EV is operating and as such estimate the energy consumption per km of the vehicle. Experimental results, exploring the feasibility of this concept, show a good correlation and accuracy in the order of 70% – 80% when comparing predicted and measured energy consumptions for over 800 real-world journeys. Furthermore, practical limitations are discussed and important criteria are presented that would further improve and extend this method of predicting vehicle energy consumption.

In particular, based on the second objective listed in Chapter 1, emphasis has to be placed on the advantages of using an energy management control system of a PHEV which uses a CB control strategy. The ability to estimate the energy requirements of the vehicle over a given route is a pre-requisite for using a charge blended control strategy. The advantages of such an approach is discussed in existing literature in Section 2.3. Therefore, this framework would be an ideal candidate to be used for a CB strategy for an PHEV. The design of the energy management controller and further results are discussed in Chapter 7.

Chapter 5

Development of EV Model

The second and third objectives of the thesis are the development of a CB energy management strategy and sizing framework for a PHEV. In order to design and evaluate various PHEVs, a set of scalable component model which forms the PHEV must be developed. To achieve this, a prior set of baseline component models were needed for scaling. This chapter introduces the EV powertrain model developed from the data obtained during the Smart Move 2 Trial Programme which will then be extended to a scalable PHEV model in Chapter 6. The secondary aim of the EV model is to verify the accuracy of the component models with the real-world usage data from the trial programme.

This chapter contains an initial summary of the modelling approaches. Then each component is discussed in detail along with the accuracy of the model developed at the component level. The modelling approach is similar to existing modelling software such as ADVISOR or PSAT [92], which are currently used within component sizing frameworks. However, it is noteworthy that the data adopted for these models is from real-world usage data compared to the test data obtained from laboratories. Typically, test data is determined from an experimental setup in a controlled environment to ensure repeatability. The downside of such an approach is that normally the researcher assumes the final intended operating regime and applies the same in the experiment and this approach may not necessarily cover the entire operating conditions of the vehicle. When modelling the vehicle with real-world data this issue is addressed due to the large variation in operating regimes. However, the limitation of such an approach is that the accuracy of the model can be compromised due to these large variations in the environment and additional unforeseen external circumstances. For example the auxiliary loads on the vehicle had a significant influence on the energy consumption per km on the EV. Further discussion about the accuracy of the model is presented in Section 5.10.

5.1 Modelling Approach

Powertrain Modelling approaches can be broadly classified into two different categories depending on the layout of the model [92]:

- Forward Modelling Approach
- Backward Modelling Approach

In a generalised sense forward models are used with the intent of capturing fast transient dynamics and aid in the development of a control system with real-world implementation as the end goal [92]. They typically start from the energy / power source and work "down" the powertrain until the force exerted by the wheel to overcome the inertia of the vehicle is calculated. Finally, using the speed generated by the vehicle and a driver model a new target is given to the energy / power source for the next time step. In contrast a backward model is typically built to evaluate the energy consumption of various drive-trains for comparison by determining the energy and power requirements from the wheel up the powertrain to the energy / power source.

5.1.1 Forward Modelling Approach

In a simplistic sense, vehicle models that include a model of a driver form a forward facing model [92]. It is a closed loop system where the drive-cycle is the target generator and the driver corrects the torque demands to the vehicle to match the drive-cycle profile. In a forward model, typically a driver model is a proportional and integral controller (PI) , which sends positive and negative torque demands to the vehicle plant model so that the vehicle traces the reference drive-cycle. For example, in a conventional vehicle where only the ICE is used to propel the vehicle the throttle command translates to a torque demand which is sent to the engine controller. The engine model produces the required amount of torque within the capabilities of the engine, which is then fed to the transmission model. The transmission model translates the torque depending on the gear ratio to the torque at the wheels. Finally, by using the inertia of the vehicle and the road loads the vehicle speed is calculated by integration. On calculation of the vehicle speed, the speed is calculated upwards through the drive-train back to the engine model. The vehicle speed is fed as feedback to the driver model. Figure 5.1 shows the layout of a typical forward model for a conventional vehicle.

Forward facing models are typically dynamic models that accurately determine torque and speed and manage to capture the limits of the system. They typically are simulated using timesteps of 0.01s or less. Therefore, they are widely used to test

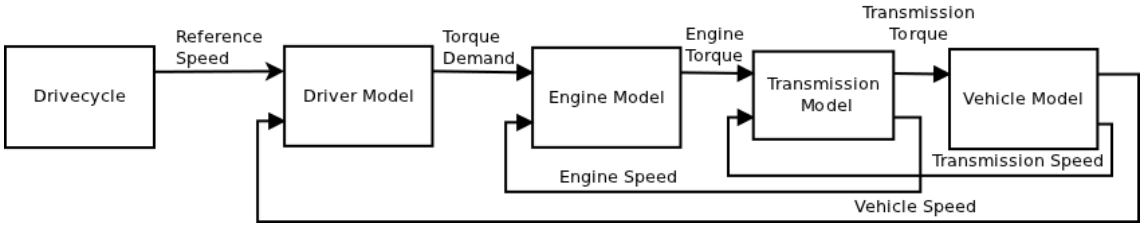

Figure 5.1: Layout of a forward model of a conventional vehicle

scenarios which address driveability issues such as peak acceleration of the vehicle. The layout of the model also helps in the development of hardware interfaces since they adhere to the control signal and true speed and torque demands.

In a forward facing model, since it is a higher fidelity model it comparatively requires a smaller simulation time step than a backward facing model. This results in longer simulation time [92]. Due to the computational demand and longer simulation time, these models are typically not used within an optimisation routine. Further, for a fair comparison of different powertrains the driver model will have to be tuned for every iteration of the optimisation run with different drive-train components making the approach impractical for component sizing.

5.1.2 Backward Modelling Approach

In a backward facing model, it is assumed that the vehicle is powerful enough to meet the drive-cycle speed trace. A driver model is therefore not required. From the drive-cycle, the vehicle road load equation is applied to calculate the speed and torque at the wheels. From the speed and torque at the wheels the speed and torque to the engine is determined backwards through each component by using efficiency models or maps for each component. Since, they use efficiency maps and do not model the dynamic behaviour of the drive-train they can be described as quasi-static models [92]. Finally, the fuel used or electric energy used is calculated. Typically, these values are then used in a minimisation cost function for an optimisation routine. Typically, this type of backward model runs with a large time step ($\approx 1s$) which make them quick to compute. Essentially, the time step chosen depends on the resolution of the drive-cycle. Figure 5.2 shows the layout of a typical backward model for a conventional vehicle.

The drawback associated with the use of backward models is that they do not address the issue of whether the given powertrain can meet the load demands of the drive-cycle. Typically, three different solutions are offered in the literature to solve this issue:

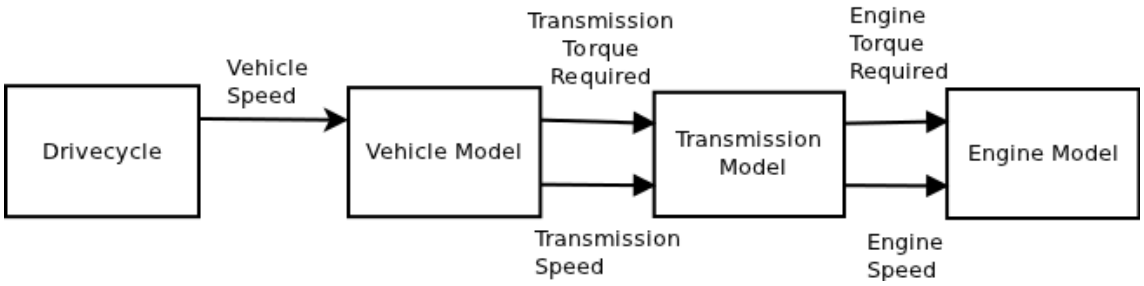

Figure 5.2: Layout of a backward model of a conventional vehicle

Solution 1: It will be possible to constrain the optimisation routine to choose parameters that are deemed as feasible.

Solution 2: The second method has been adopted in this research, constraints are applied for each of the components and if those constraints have been exceeded the simulation is halted and the powertrain is deemed as infeasible.

Solution 3: The third approach has been listed in [92], as a hybrid approach. In this method the limits of each of the components are transmitted downstream so that no component will require more torque or power from its upstream neighbour than it can use. By this method, in the end a new speed trace is calculated which takes into account the capability of the systems in the drive-train. The drawback of this method is that when using optimisation routines it does not give a true picture of the fuel used or electric energy required. For example, a severely down sized model will project the best fuel economy and electric energy required, but still not meet the load demands of the drive-cycle. This implies that the two powertrains are not addressing the same requirements, making the new down-sized powertrain impractical. Figure 5.3 shows the layout of a backward model for a conventional vehicle. The reference speed need not be equal to the vehicle speed.

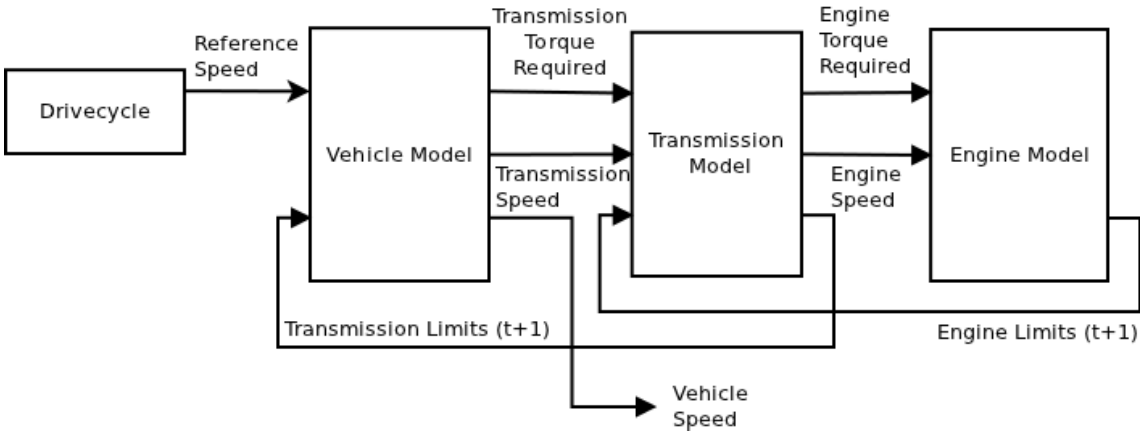

Figure 5.3: Layout of a hybrid model of a conventional vehicle

5.2 Model Objective

The objective is to build a model which is able to accurately capture the change in SOC for a drive-cycle. As described in Equation **??** in the literature review, the only state which is tracked in a HEV energy management problem is the SOC for a given control input of P_{ICE} such that :

$$P_{dmd}(t) = P_{batt}(t) + P_{ICE}(t) \tag{5.1}$$

In this chapter based on the existing data available from the Smart EV trial an model is built to calculate P_{dmd} and P_{batt}. This model is then further expanded in the next chapter to create a scalable PHEV in which depending on the changing component sizes P_{dmd}, P_{batt}, P_{ICE} and SOC is calculated.

5.3 Overall Model

This section deals with the development and verification of the backward model of the pure EV from the Smart Move 2 Trial. The backward model will be expanded to a scalable series PHEV model in Chapter 6. The layout and the components which are modelled to represent an EV are shown in Figure 5.4. [34]. The assumptions for each of the components are stated in their respective subsections.

The components which are modelled are given as :

- Vehicle model
- Integrated electric machine and transmission model
- Battery model

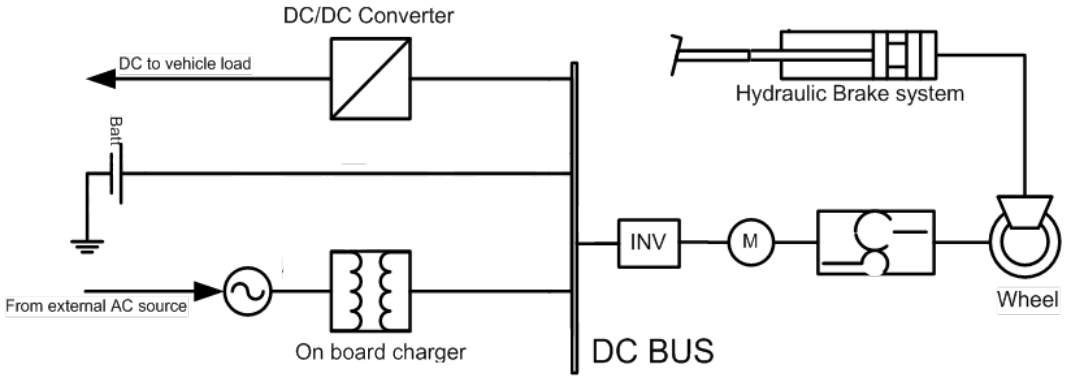

Figure 5.4: Example electric vehicle

- Auxiliary power demands
- Charger model

5.4 Vehicle Model of Smart ED

The objective of this section is to build a pure EV model. The model was built based on several look-up tables which were obtained from experimental data recorded on a vehicle. The next sections describe the equations and the look-up tables formed to match the recorded data. The input into the model includes.

- Vehicle speed v
- Mass of vehicle M_v
- Radius of the wheel r_w
- Auxiliary power demands
- Battery Capacity Qb
- Initial state of charge SOC_{init}

The aim of the model is to verify if the EV drivetrain is able to accurately capture the same change in state of charge of the battery for a given drivecycle. A discretized model is built where the main input is the vehicle speed which is recorded with a time step of 1s. The data available for building the model is shown in Table 3.1. Whenever a recorded channel is used, the variable is shown with an asterix (*).

Since the vehicle model adopted is a backward model, the objective of the vehicle model is to determine the power experienced by the wheel in terms of wheel torque and speed in order to trace the given drive-cycle. The first step is to identify the resistive forces (F_r) acting on the mass of the vehicle for a given speed and acceleration. The vehicle speed and acceleration is determined from data recorded on the CAN bus (Table 3.2 Parameter 10). In order to achieve this a vehicle coast down curve was experimentally obtained for the Smart ED by Millbrook Proving Ground Ltd [9]. The coast-down curve is obtained by accelerating the vehicle to a predetermined speed, turning it off and letting the vehicle 'coast' to a halt based on the drag losses. The vehicle is then fixed to a dynamometer and the amount of force required by the dynamometer to achieve the same speed profile is measured. This force is given as the coast down curve of the vehicle and it is the total drag force of the vehicle. On curve fitting the drag force against the vehicle speed can be obtained [9] Equation 5.2 presents a 3rd order polynomial that defines Fr as a function of vehicle speed (v). This was obtained by using experimental testing in which the vehicle was allowed to coast from various speeds while applying no drivetrain torque [9]. The constant term of 146.8 N represents the tyre rolling resistance. The slope of the terrain (α) could be calculated using the measured height data obtained from the vehicles onboard GPS (Table 3.2 Parameter 7). However, during the simulations performed due to faulty height data from the GPS during this research the value of α was always considered to be zero. The implications of ignoring gradient loads are described in Section 5.5.

$$F_r = 8 \cdot 10^{-5} \cdot v^{*3} + 0.0241 \cdot v^{*2} + 0.1456 \cdot v^{*} + 146.8 \cdot \cos(\alpha) \tag{5.2}$$

For a given vehicle speed, the associated torque at the wheels (T_w) is calculated using Equation 5.3, where r_w defines the rolling radius of the wheel, $grav$ is the gravitational constant and M_v is the total vehicle mass. The values for r_w and M_v were measured as $0.2462m$ and $900kg$ respectively. The $900kg$ includes the weight of the driver.

$$T_w = (M_v \cdot \frac{dv}{dt} + F_r + M_v \cdot grav \cdot sin(\alpha)) \cdot r_w \tag{5.3}$$

5.5 Integrated Electric Machine and Transmission Model of Smart ED

The Smart ED employs a 55 kW brushless DC machine. For the EV model, the electric machine and the associated inverter have been considered as a single integrated system. The values of electric machine terminal voltage (v^*_{em}), electric machine current (i^*_{em}), the rotational velocity of the machine (ω^*_{em}) and electric

machine torque demand ($T^*_{em(dmd)}$) were recorded under a number of different operating conditions during vehicle evaluation. The corresponding CAN messages are listed in Table 3.2 as parameters 17, 18, 21 and 22 respectively. These values were used within Equation 5.4 to calculate the efficiency of the electric drive system and build the EM efficiency map shown in Figure 5.5. For operating points that are repeating within the evaluation dataset the mean value is calculated. An important feature to note is that for the negative axis the efficiency is suitably inverted and regenerative braking strategy contour of the Smart ED is preserved.

$$\eta_{em} = \frac{T^*_{em} \cdot \omega^*_{em}}{v^*_{em} \cdot i^*_{em}} \tag{5.4}$$

The Smart ED consists of a single stage reduction gearbox which has a final

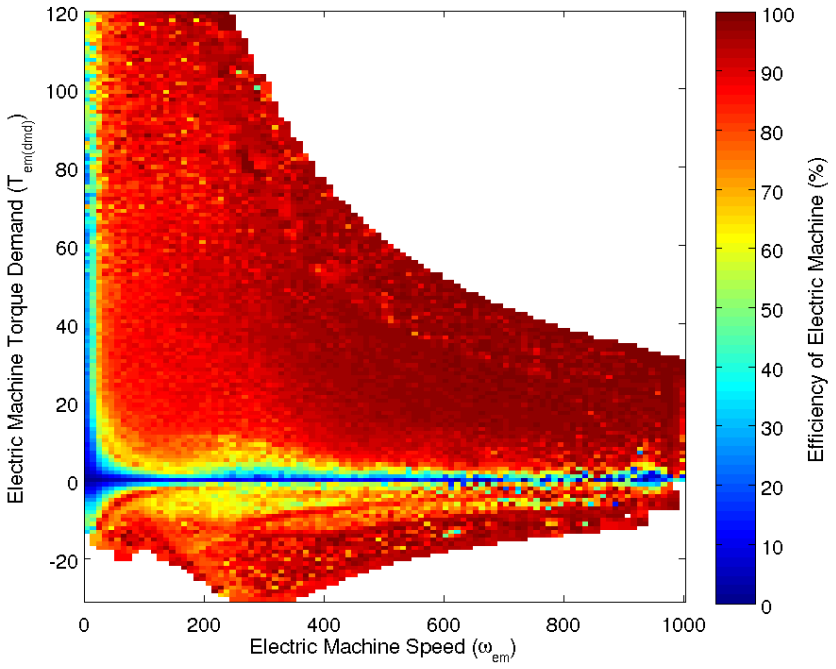

Figure 5.5: Efficiency map of the Smart ED 30 kW Electric Machine

drive ratio (g_{fd}) of 8.67 [57]. Therefore the torque of the electric machine T_{em} was calculated from T_w using Equation 5.5. The objective of using such an approach is to relate all the calculations back to the drive-cycle speed. In order to check the validity of the road load equation and the gear ratio, comparisons are made between the simulation and the recorded data. The speed and torque at the electric machine shaft / gearbox input shaft are compared against measured data. Figure 5.6 shows the speed and torque plots at the gearbox input shaft for one trip. The torque obtained from the CAN data is the demand torque ($T^*_{em(dmd)}$) sent to the electric

machine, therefore it is expected to have been filtered. Further, the negative torque during regenerative braking is limited in the case of the recorded data since it is the demand torque from the control system compared to the simulated torque which is calculated from the wheels.

$$T_{em} = \frac{T_w}{g_{fd}} \tag{5.5}$$

$$\omega_{em} = \omega_w \cdot g_{fd} \tag{5.6}$$

Figure 5.7 shows the accuracy of the prediction of electric machine torque against

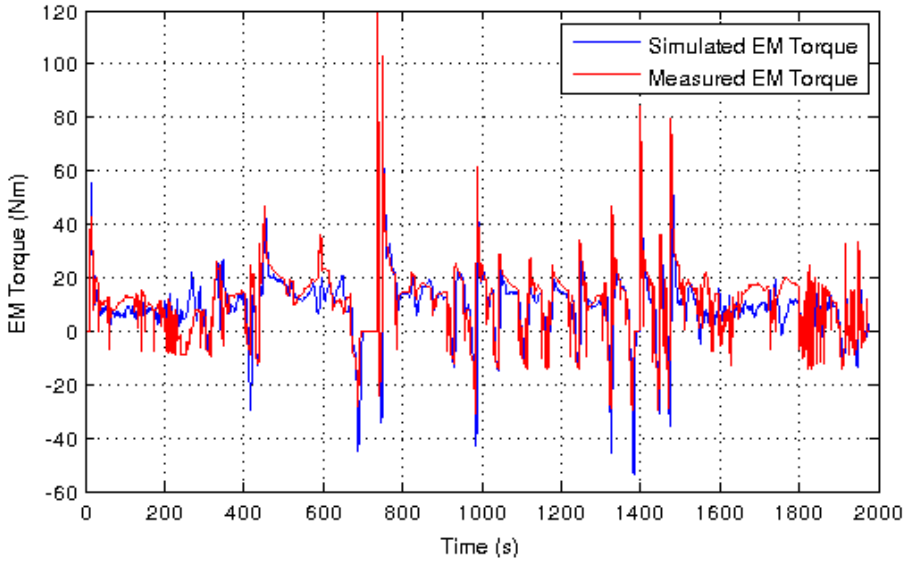

Figure 5.6: Comparison of simulated and measured motor torque

time which has been normalised for a dataset over two months. The average accuracy per trip is 73%. The errors in the prediction of the load torque is primarily because of inaccuracies and resolution of the topographic data stored by the GPS. Unfortunately, the topographic data cannot be corrected. For a verification of the electric machine map shown in Figure 5.5, the recorded speed and torque are fed into the Simulink model and the power at the HV bus is compared to the recorded power. The accuracy of this section of the model is 87%. The inaccuracies in the model are assumed to be due to variations among the prototype vehicles and since temperature differences are not captured.

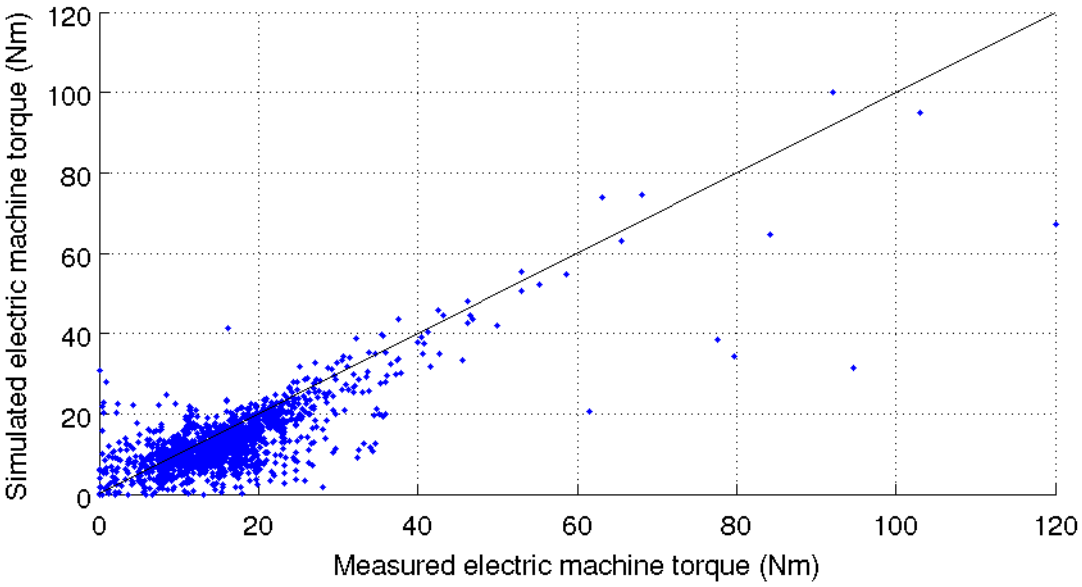

Figure 5.7: Accuracy of simulation of electric machine torque

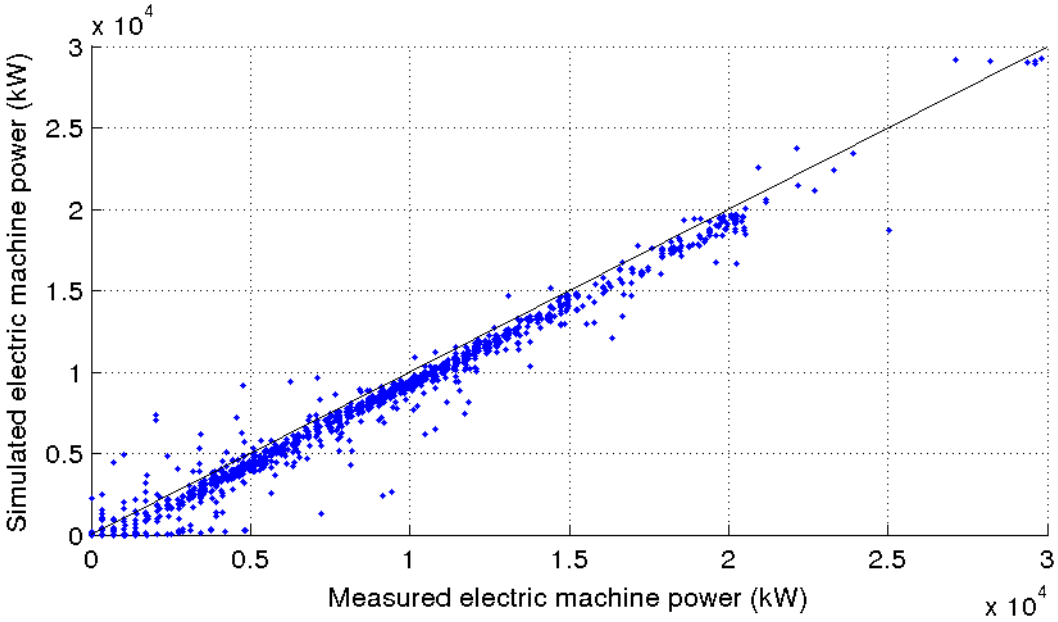

Figure 5.8: Accuracy of simulation of electric machine power

5.6 Auxiliary Power and High Voltage Electric Bus

The auxiliary power is depicted as the power lost through the DC-DC converter and link between the high and low voltage systems in the EV in Figure 5.4. This value is calculated by the vehicles on-board ECU shown in Table 3.2 parameter 23. Usually this load is neglected in the case of legislative tests on the vehicle. In the case of an EV, all driver comfort systems (air conditioner, heater matrix, radio etc) and vehicle electricals (Headlights, Indicators etc.) are drawn from the battery. As a simple study on the additional power requirements needed for auxiliary loads, various devices were turned on in the vehicle for a minute and the steady state power requirement for that device was recorded from parameter 23 in Table 3.2. The average power consumption of various auxiliary loads are given in Table 5.1. As an extreme circumstance when turning on the air compressor the auxiliary power is around 4.5 kW and the peak power is around 7 kW. This power consumption is similar to the power needed for cruising at low speeds. Therefore axillary loads do have a significant impact on the energy utilisation and vehicle range. For the purposes of the simulation an average of $1kW$ is assumed for the model. For a given auxiliary power (P_{aux}) the current at the battery terminals (i_b) using battery terminal voltage (v_b), v_{em} and i_{em} is given by :

$$i_b = \frac{v_{em} \cdot i_{em} + P_{aux}}{v_b} \tag{5.7}$$

Table 5.1: Auxiliary power loads on the vehicle

Auxiliary Load	**Average Power** (W)
Key On Load	220
Park Light	50
Head Lights	180
High Beam	320
Fan Speed 1	50
Fan Speed 2	90
Fan Speed 3	140
Air Conditioner On - 22 degrees - Fan Speed 1	2180
Air Conditioner On - 26 degrees - Fan Speed 1	2650
Air Conditioner On - 18 degrees - Fan Speed 4	4160
Air Conditioner On - 22 degrees - Fan Speed 4	4690
Air Conditioner On - 26 degrees - Fan Speed 4	4890

5.7 Battery Model of Smart ED

As described in the literature review, the battery model contains the only state in the system and it is the SOC. The SOC is defined as the ratio of amount of charge remaining in the battery. Therefore during model execution, SOC is quantified using the generic method of coulomb counting. In this method the change in amount of charge (current) is calculated by integrating the current every time step. Obviously the initial condition of the battery SOC SOC_{init} and Q_b the capacity of the battery expressed in Ah should also be known. Based on this the SOC at time t can be calculated based on the following equation:

$$SOC(t) = \frac{SOC_{init} \cdot Q_b \cdot 3600 - \int_0^t i_b \cdot dt}{Q_b \cdot 3600} \tag{5.8}$$

The model is a discrete model with a time step of 1s, therefore if N is the total number of time-steps the SOC at discrete time step t is :

$$SOC(t) = \frac{SOC(t-1) \cdot Q_b \cdot 3600 - \int_{t-1}^t i_b \cdot dt}{Q_b \cdot 3600} \tag{5.9}$$

In order to ascertain the real-world operating efficiency of the HV battery a Rint type equivalent circuit model was used. This method is widely reported within the literature and comprises of an open circuit voltage (v_{oc}) in series with a charge and discharge resistance (R_b) [32] as shown in 5.9.

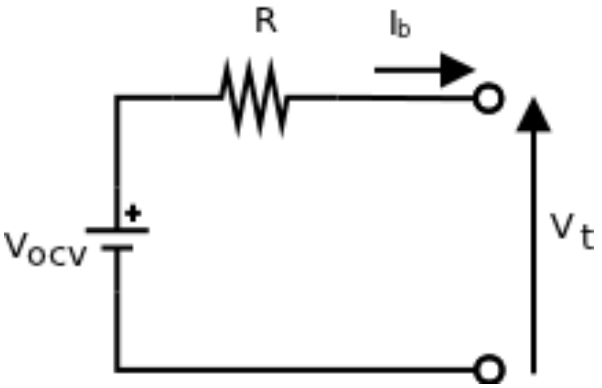

Figure 5.9: Battery Model

The term v_{oc} is the voltage of the battery when there is no losses present, that is the voltage when there is no current flowing from the battery. The value for v_{oc} was estimated based on v_b^*, battery temperature and SOC for the Smart data-set. All three of these values were recorded on the CAN bus on the vehicle. The points in the test data when the i_b^* is equal to zero for 3 seconds and averaging the v_b^*

for that temperature and SOC the v_{oc} of the battery has been determined. Figure 5.10 shows the result of this exercise and presents the estimated value of v_{oc} as a function of measured battery temperature and SOC. The data below 20% SOC becomes unreliable since during the testing programme only a small number of test cases were recorded with low SOC. For a given value of i_b which is the sum of EM current and auxiliary current, the battery terminal voltage can be calculated using Equation 5.10.

Measuring the battery resistance for the vehicle was not possible because the vehicle's battery was sealed for safety reasons and it was not possible to reach the terminals. However, the battery resistance was calculated to be 0.52Ω. This was done by trail and error. For large collection of the journeys recorded different resistance values were attempted on Equations 5.10 and 5.9. It was verified if the resistance value caused for the same amount of current drawn (available on CAN), the change in SOC matched the change recorded by the battery management system. The accuracy of this data cannot be confirmed because the working of the battery management system is not known and the resolution of the CAN data is prohibitive for comprehensive comparison. However, the trend of constant resistance can be clearly seen by comparing the open-circuit voltage based current to terminal voltage based current in Figure 5.11. Figure 5.11 is obtained based on Equation 5.11, where v_{oc} is obtained from the map and i_b and v_b are obtained from the CAN bus.

$$v_t = v_{oc} - i_b \cdot R_b \tag{5.10}$$

$$\eta_b = \frac{v_{oc} \cdot i_b^*}{v_b^* \cdot i_b^*} \tag{5.11}$$

Similar to the EM map, the validity of the battery map is checked by simulating the change in battery SOC for a given battery power input and comparing to the recorded data of the same for a period of 2 months. The mean accuracy of the change in battery SOC per trip is 88%. It is believed that the accuracy could be improved if temperature variation could be accurately captured. However, data such as position of temperature sensors and cooling methods were not available. Therefore this variation has not been considered as part of this research.

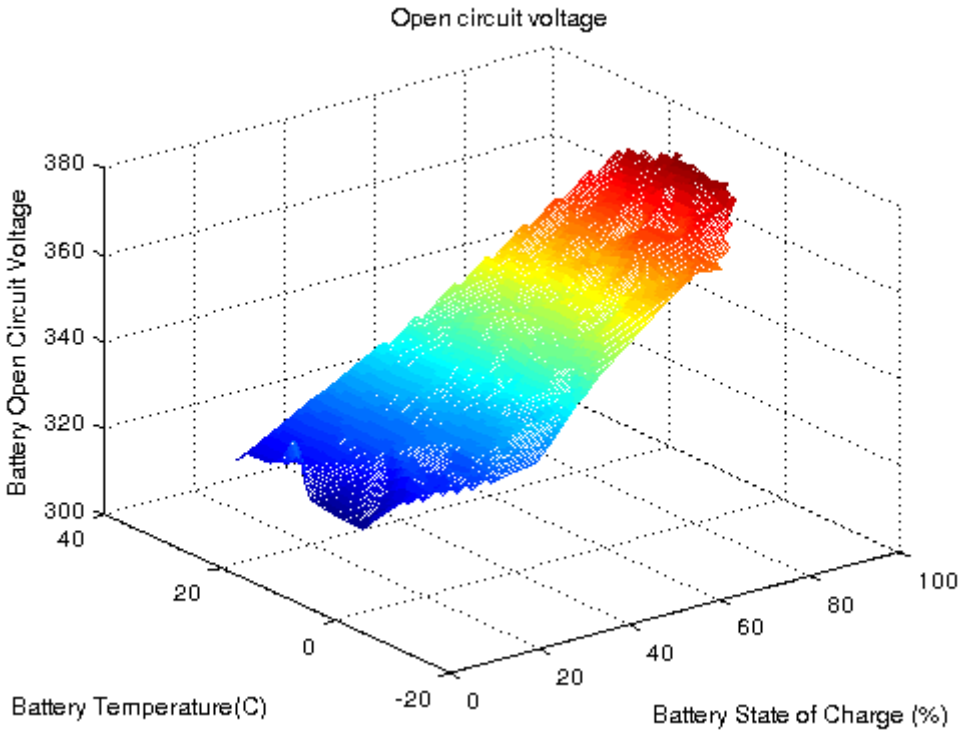

Figure 5.10: Open circuit voltage of battery

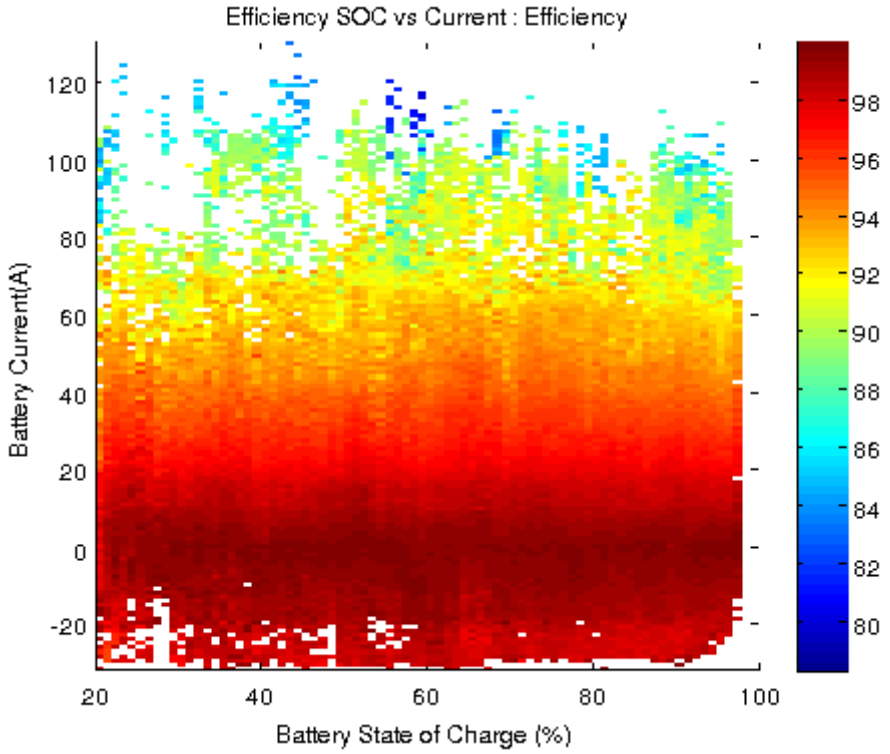

Figure 5.11: Battery efficiency for different SOC

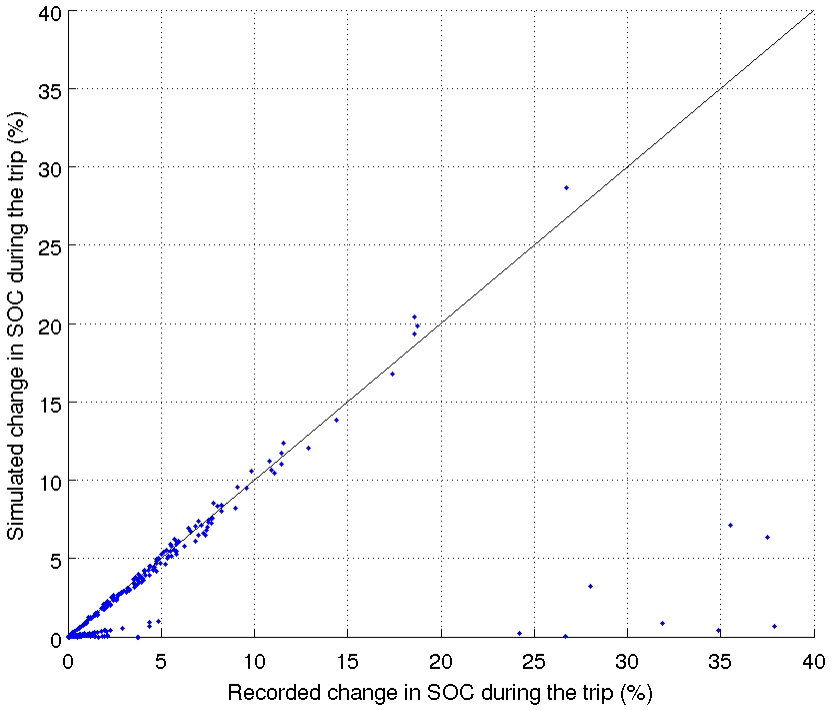

Figure 5.12: Accuracy of simulation of battery component

5.8 Charger

After every simulation run, it is possible to calculate the amount of electric energy required at the plug to charge the vehicle back up to maximum SOC. This is done by applying a constant amount of power into the battery (220 V 15 A) with a charger efficiency of 90%. This calculation is primarily used to calculate the electric energy consumption in Wh/km as stipulated in Regulation 101 [87]. Further information on the application of Regulation 101 is discussed in Chapter 8.

5.9 Model Summary

A complete summary of the equations are given in this section. The model is a discretised model of time $t = 0, 1, 2, 3, 4...$ seconds. The discretisation interval of 1s is chosen because the drive-cycle data available is 1s and energy management problems which track fuel consumption and SOC are fairly low dynamics.

The road tractive force $F_r(t)$ of the EV is given as :

$$F_r(t) = 8 \cdot 10^{-5} \cdot v^3(t) + 0.0241 \cdot v^{*2}(t) + 0.1456 \cdot v(t) + 146.8 \cdot \cos(\alpha) \qquad (5.12)$$

from the tractive force the wheel torque can be calculated as:

$$T_w(t) = (M_v \cdot \frac{dv}{dt} + F_r(t) + M_v \cdot grav \cdot sin(\alpha)) \cdot r_w \tag{5.13}$$

where M_v is mass of vehicle which is $900kg$ and r_w is the wheel radius which is $0.2462m$. The wheel speed can be calculated as:

$$\omega_w(t) = \frac{v(t)}{r_w} \tag{5.14}$$

Based on the wheel speed and torque the electric machine speed and torque can be calculated as :

$$T_{em}(t) = T_w(t) * g_{fd} \tag{5.15}$$

$$\omega_{em}(t) = \frac{\omega w}{g_{fd}} \tag{5.16}$$

where g_{fd} is the final drive gear ratio of 8.67. Now that the electric machine torque and speed are known the electric machine power can be calculated as :

$$P_{em}(t) = \frac{T_{em}(t) \cdot \omega_{em}(t)}{\eta_{em}(T_{em}, \omega_{em})} \tag{5.17}$$

The efficiency of the machine η_{em} is a look-up table based on Figure 5.8. The total power demand P_{dmd} can be calculated as :

$$P_{dmd}(t) = P_{em}(t) + P_{acc}(t) \tag{5.18}$$

In the above equation P_{acc} is the auxiliary power demand which is averaged to $1kW$. In this case because it is a pure EV model P_dmd is equal to P_{batt}. The current at the battery is obtained by solving the equation shown below.

$$R_b \cdot i_b(t)^2 - v_{oc}(SOC(t-1)) \cdot i_b(t) + P_{dmd}(t) = 0 \tag{5.19}$$

where $R_b \cdot i_t(t)^2$ is the battery efficiency losses and R is the resistance of the battery 0.52Ω, $v_{oc}(SOC(t-1))$ is the open circuit voltage of the battery which is a function of the SOC. It is assumed the change in SOC is a relatively slow dynamic and the previous state can be used for the calculation of the v_{oc}. When the current i_b is known the SOC of the battery at time t can be calculated as :

$$SOC(t) = \frac{SOC(t-1) \cdot Q_b \cdot 3600 - \int_{t-1}^{t} i_b \cdot dt}{Q_b \cdot 3600} \tag{5.20}$$

Where Q_b is the capacity of the battery. At the beginning of the drive-cycle time $t = 0$, the SOC is stored as the initial SOC_{init}.

5.10 Verification and Limitations of the Complete Model

In order to verify the complete EV powertrain model, it was run across all the trips recorded and the variation in SOC was compared between the simulation and the actual data. The mean accuracy for all the trips recorded is 68%. Figure 5.13 shows the simulated change in SOC and the actual change in SOC recorded for all trips over a six month period. The frequency of trips where the SOC change is more than 40% is low and they have not been included in the Figure. Although the mean accuracy number is low (68%), it shows the amount of variability in performance of the vehicle in the real-world.

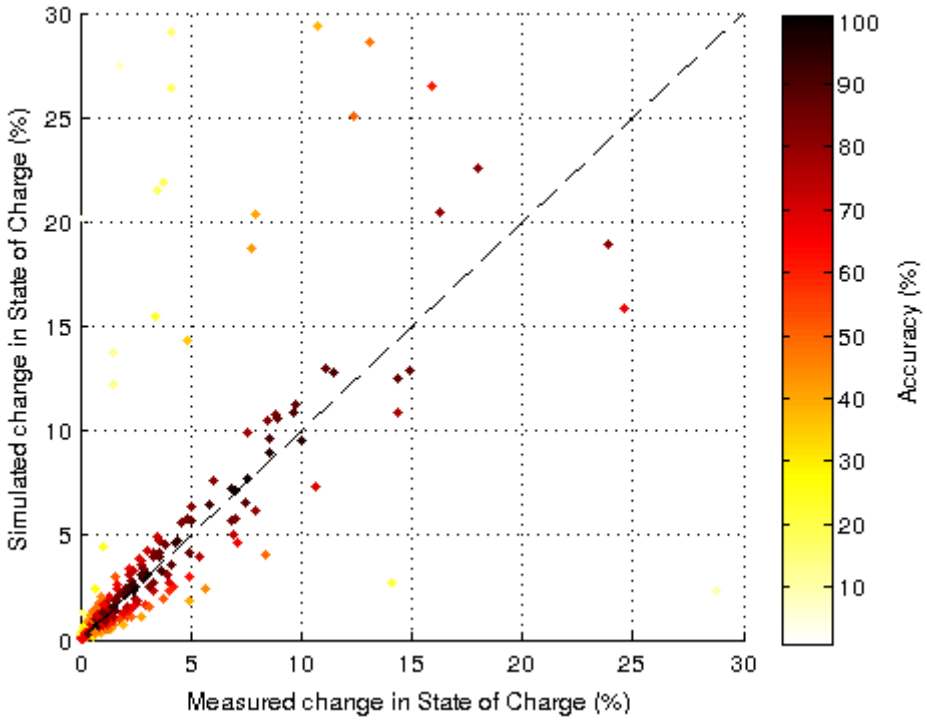

Figure 5.13: Verification of the EV Model

The inaccuracy arises from 5 key areas:

- The beginning and significant contributor to the inaccuracy in the model is ignoring the gradient loads. As stated before this leads to EM torque estimation errors as much as 27%. Further, since the model is a backward facing model, the error in estimation at the first point (at the wheels) which leads to large deviations by the end (at the battery).

- Another key consideration is that only the torque demand is available in the recorded dataset. The variation between the torque demand and actual torque experienced by the electric machine is not known. Due to the control strategy adopted in the Smart ED for functions such as regenerative braking cannot be fully determined. This leads to variations in the energy usage at the electric machine which is then further compounded at the battery.

- The variation in performance of a battery due to temperature is significant. However more data is needed to perform a complete analysis and development of a thermal model. Further the goal is to develop a base model which can then be scaled in chapter 6. And the inclusion of additional complex systems such as a thermal management system, whose scaling parameters are not known, would defeat this objective.

- It was observed that there was a relation between ambient temperature and auxiliary loads. This relationship was explored further in [9]. The ambient temperature during three different case studies was recorded. The corresponding ratio of power to drive the vehicle to the power used by the auxiliaries was calculated. The results are shown in Figure 5.14. In the case of the first study (Indesit), they were a large number of low speed trips with high cabin heating load. Further, variations which affect the ratio between the power consumptions was not discussed such as trip length, duration of journey.

- Another factor to be considered is the payload. There is no mechanism to determine the number of persons travelling in the vehicle. This would affect the vehicle inertia and increase the load experienced by the wheels during acceleration. Finally, the various vehicles used in the trials where all prototype vehicles and due to this, minor variations in calibrations and performance are assumed to exist.

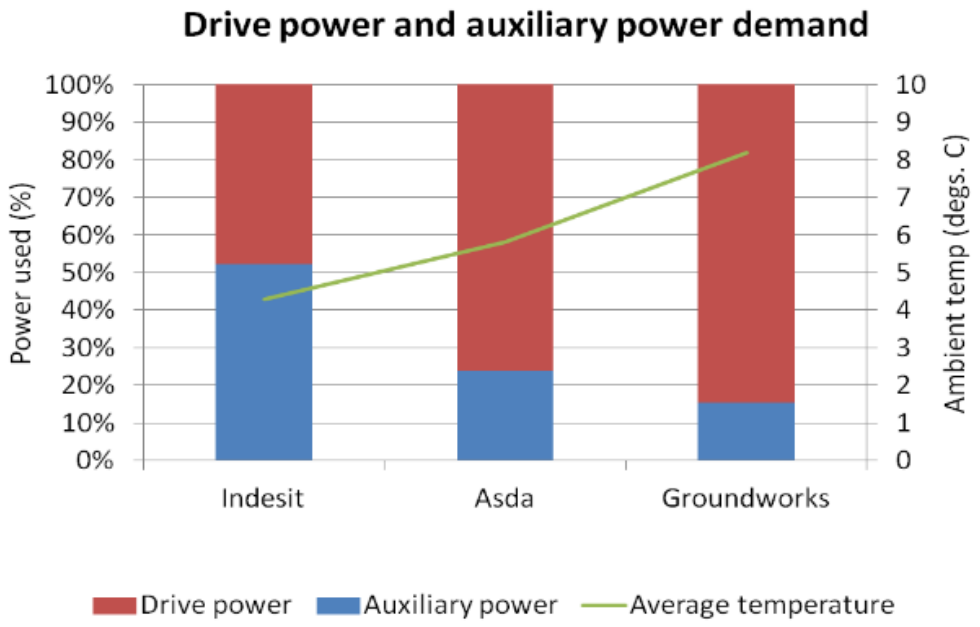

Figure 5.14: Influence of ambient temperature during Smart ED case-study by Cenex [9]

5.11 Conclusion

The chapter describes the methodology employed for the development of the base EV model. The primary motivation for the EV model is to develop a set of base components which can then be scaled and used within an PHEV in chapter 6. Particular emphasis was placed on developing a "simplified model" with low fidelity such that it can then be used within an optimisation framework. Although, the complete vehicle model had an overall accuracy of only 68%, it has to be placed in the context of real-world data obtained during a vehicle trial programme. As described in the previous section a large number of limitations exist since the vehicles were prototypes and some of the data was not accurate / unavailable. However, on comparison to existing tools such as PSAT which are accepted modelling software, the same fidelity has been used. Further, by obtaining the mean values for the various maps the environmental variations are captured and smoothed. Finally, it is noteworthy that the framework developed in this research and the trends observed are valid and improvements in model accuracy / fidelity would give a more accurate trend. The implications of the accuracy of the model and the future work direction is described in chapter 10.

Chapter 6

Scalable Plug-in Hybrid Electric Vehicle

In order to evaluate the performance of various energy management techniques and the component downsizing opportunities associated with their use, an important pre-requisite is the design of a PHEV powertrain model. The layout of a typical series PHEV is shown in Figure 6.1 [33]. The on-board charger, battery (Batt), electrical machine (EM), Inverters (INV), Transmission (Trn), DC/DC converter and wheel have all been modelled based on the EV Model developed in Chapter 5. For each of the powertrain components, the discussion is to *scale* key system parameters as part of the optimization study to enable component sizing.

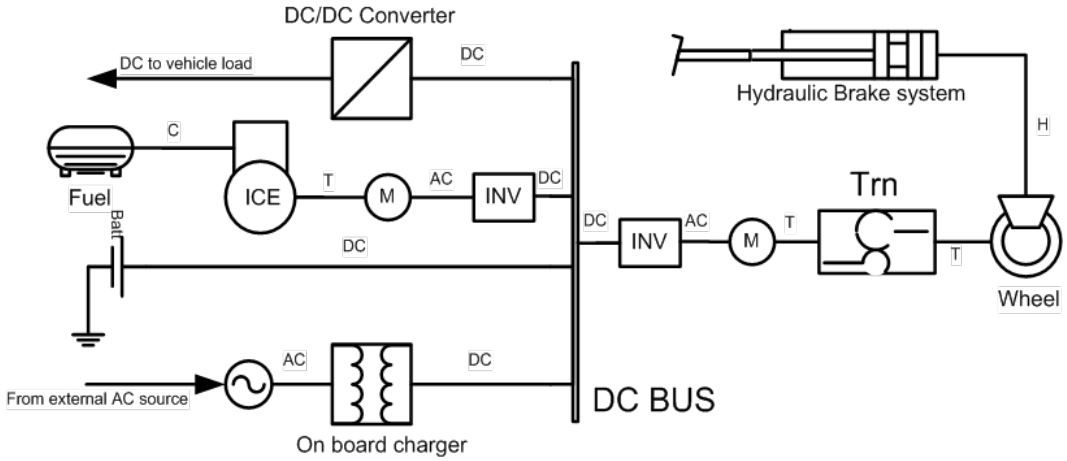

Figure 6.1: Plug-in hybrid electric vehicle schematic

6.1 Modelling Objective and Tasks

The scalable parameters chosen for the PHEV model are engine volumetric size (V_d), peak power of electric machine ($P_{em(peak)}$) and the number of parallel battery strings (n_p). The sequence of steps for the creation of the model and execution over a drive-cycle is given in Figure 6.2 as:

- Stage 1 consists of loading the baseline data obtained from the EV trial.
- Stage 2 represents the generation of a scaled set of PHEV components.
- Stage 3 relates to loading the different drive-cycles and updating the mass of the PHEV based on the respective component mass values.
- Stage 4 is the execution of the model for a selected control strategy and drive-cycle.
- Stage 5 verifies that the component constraints are maintained throughout the simulation. The remainder of the Chapter defines in greater detail, the methods and equations involved at each stage of the process when generating and executing a scalable PHEV model.

After execution for a given control algorithm which is discussed in chapter 7, the results such as the fuel used or the CO_2 emitted are returned to the optimisation framework. The final result of the optimised set of components depends on the formulation of the cost function. The optimisation framework and the associated cost functions are discussed in detail in Chapters 8 and 9 respectively.

The tasks involved to convert the EV model from Chapter 5 to a scalable PHEV model are given as:

- Development of a scalable ICE model.
- Development of a scaling process for the electric machine model developed based on the EV.
- Development of an appropriately sized electric machine connected to the ICE to form the auxiliary power unit (APU).
- Develop equations which relate parameters of each component to their respective masses and financial cost.

The cost function, free parameter set and search routine are given in chapter 8, which describes the optimisation framework.

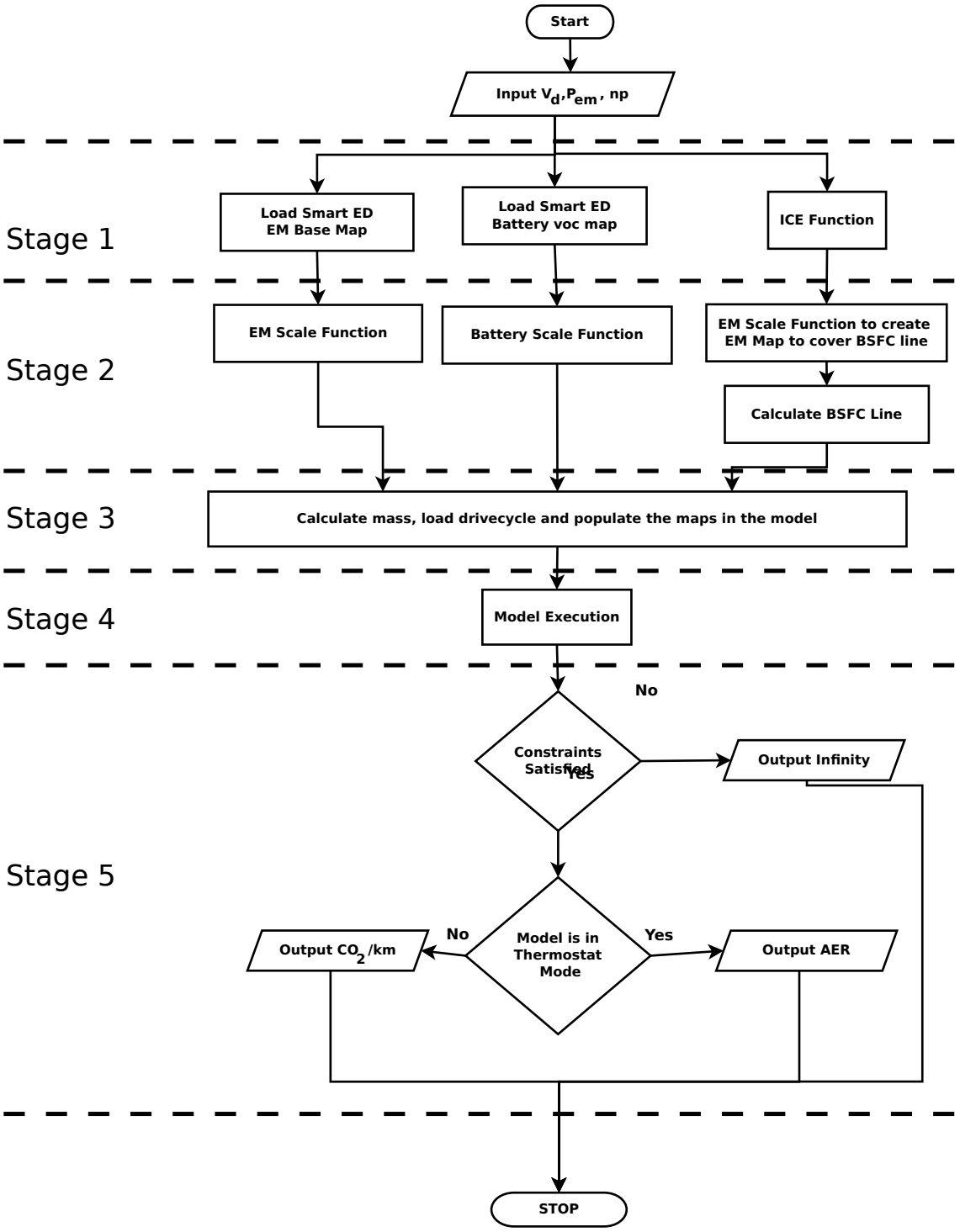

Figure 6.2: Flowchart of execution of the simulation

6.2 Scaling of the Vehicle Model

The function of this component within the PHEV model is to determine the torque and speed at the wheels. The component execution is very similar to the EV model discussed in Chapter 5. The equations of interest are 5.2 and 5.3. The model employs the same radius of the wheel r_w, however the mass of the vehicle M_v has to be adjusted for the varying component sizes. The value of M_v is calculated before the execution of the model at Stage 3 of the simulation and is represented in Equation 6.1. It is the summation of the chassis mass (M_c), and the respective mass contributions from the electrical machine (M_{em}), battery (M_{bat}), and the ICE (M_{ICE}). The mass contribution functions are given for each sub-model in the relvant section. The mass of the vehicle chassis is assumed to be constant at 700 kg:

$$M_v = M_c + M_{em}(P_{em(peak)}) + M_{bat}(P_{bat(peak)}) + M_{ICE}(P_{ICE(peak)}) \tag{6.1}$$

6.3 Scaling of Electric Machine and Transmission

For the PHEV model the same final drive ratio has been adopted as the Smart ED to calculate T_{em} and ω_{em} (Equation 5.5). The power supplied or drawn by the electric machine is given by Equation 6.2. The relationship between ω_{em}, T_{em} and η_{em} is given by the Smart ED efficiency map in Figure 5.5 and has been normalised. In order to employ the model within the optimization study, Equation 6.3 shows how the torque (T_{em}) of the efficiency map can be scaled as a function of the peak power requirements of the subsystem ($P_{em(peak)}$). This equation is represented as the EM scale function at Stage 2 of the simulation:

$$P_{em} = \begin{cases} T_{em} \cdot \omega_{em} \cdot \eta_{em}, & \text{if} T_{em} < 0 \\ \frac{T_{em} \cdot \omega_{em}}{\eta_{em}}, & \text{if} T_{em} > 0 \end{cases} \tag{6.2}$$

$$T_{em} = T_{em(base)} \cdot \frac{P_{em(peak)}}{30,000} \tag{6.3}$$

In the above equation 30 kW is the maximum power of the conventional Smart ED machine. This approach has been successfully applied in a number of comparable optimization studies reported in the literature [95] and [92]. When scaling the torque and efficiency characteristics of the electrical machine, the same regenerative braking strategy observed from Figure 5.5 is maintained. It is acknowledged that the regenerative braking strategy would affect the amount of available "free" energy but, sufficient knowledge of the braking system such as front to rear braking ratio or the percentage of regenerative braking for a given driver demand is not known. Therefore, a detailed study into the optimisation of the regenerative braking strategy

is considered beyond the scope of this research. Finally, using manufacturers published data, the mass of the electrical machine and inverter system are updated using a linear function of peak power (g_{em}) [57]:

$$M_{em} = g_{em}(P_{em(peak)}) \tag{6.4}$$

6.4 Scaling of the Battery Model

The equations shown in 5.8 and 5.10 are used to calculate the SOC of the battery by Coulomb counting. The same set of equations are used in Stage 4 of the model execution. However, it is noteworthy that the power drawn or absorbed by the battery now also depends on the power produced by the ICE. Therefore P_{bat} can be calculated based on Equation 6.5. Similar to the Smart ED model developed in Chapter 5, P_{aux} is taken to be 1 kW. Within the PHEV model, the energy management strategy must control the engine power (P_{ICE}) to ensure that the power constraints and SOC range of the battery are not exceeded.

$$P_{bat} = P_{em} + P_{aux} - P_{ICE} \tag{6.5}$$

As part of the model execution sequence described in Figure 6.2, Equations 6.6 - 6.9 present how the battery is scaled by altering the number of parallel strings (n_p). This set of equations is executed at Stage 2 of the simulation as the battery function employed to create the v_{oc} map. The number of cells in series (n_s) is maintained constant to ensure compatibility with the electrical machine:

$$R_b = R_{cell} \cdot \frac{n_s}{n_p} \tag{6.6}$$

$$v_{oc} = v_{oc(cell)} \cdot n_s \tag{6.7}$$

$$Q_b = Q_{cell} \cdot n_p \tag{6.8}$$

$$M_b = M_{cell} \cdot n_p \tag{6.9}$$

It is noteworthy that the mass of each cell (M_{cell}) includes not just the cell mass but also a weighting term of 2 times to account for the mass compounding effects of introducing large battery systems [3]. For example, the additional weight associated with packaging, thermal management and the electrical isolation of equipment.

6.5 Internal Combustion Engine

The development of a generalised, scalable, ICE is a challenging research problem due to the number of variations available on the market. Therefore, for the purposes of this study a naturally aspirated four cylinder spark ignition engine model has been adopted as the baseline model. One of the main reasons for this selection is that it represents the technology that is commonly available on the market today. As discussed in [32] there are various levels of fidelity that can be adopted for modelling the engine. Typically for a backward model, the fuel consumption of the ICE can be represented by a fuel consumption map or a brake specific fuel consumption (BSFC) map [33]. The fuel consumption map defines the amount of instantaneous fuel used to produce a certain amount of torque at a particular speed. An accepted method of scaling internal combustion engine model is by means of using Willans Lines which are described in the next section [32].

Willans line Modelling Approach

The Willans line modelling approach was first proposed by [73], and later developed in [32]. The aim of this section is to develop a model that can be scaled, based on a few design parameters and sufficiently capture the changes in efficiency of the engine based on these design parameters. The total efficiency of the engine can be expressed as Equation 6.10, where T_e and ω_e represent the torque and speed of the engine respectively and P_{fuel} represents the indicated power / enthalpy power. On calculation of P_{fuel}, the fuel flow ($\dot{m}_f$) is calculated based on Equation 6.11.

$$\eta_e = \frac{T_e \cdot \omega_e}{P_{fuel}} \tag{6.10}$$

$$\dot{m}_f = \frac{P_{fuel}}{H_l} \tag{6.11}$$

The primary motivation for creating a scalable engine model is to establish the efficiency of the engine based on two quantities, piston mean effective pressure (p_{me}) and mean piston speed (c_m). Irrespective of engine size, these two parameters are similar for the same engine technology. When the engine is running in a steady state condition, the two non-dimensional parameters can be calculated based on equations 6.12 and 6.13, where N, V_d and S are the number of strokes, engine volumetric size and stroke length respectively.

$$p_{me} = \frac{N \cdot \pi}{V_d} \cdot T_e \tag{6.12}$$

$$c_m = \frac{S}{\pi} \cdot \omega_e \tag{6.13}$$

By introducing one more term, fuel mean effective pressure p_{mf}, the efficiency of the engine based on these two parameters can be calculated by the use of expressions 6.14 and 6.15 where the values for (e) and (p_{loss}) are a function of mean piston speed (c_m) and (p_{mf}).

$$\eta_e = \frac{p_{me}}{p_{mf}} \tag{6.14}$$

$$p_{me} = e \cdot p_{mf} - p_{loss} \tag{6.15}$$

The term e captures the thermodynamic efficiency of the engine. The term p_{loss} encapsulates all the mechanical losses in the engine. As discussed in [32], it is sufficient to conduct experiments to obtain these two curves (e and p_{loss}) to capture the efficiency of the engine at various operating points. Further, by changing the value of V_d, the size of the engine can be suitably adjusted. Figure 6.3 shows the efficiency (η_e) of the engine for various values of p_{me} and c_m. Typically in high load conditions a real engine will run rich (more fuel is injected than the stoichiometric ratio), causing the efficiency to drop. This detail is not accurately captured by the use of the Willans line approach. However, in the model adopted this has not been addressed, since the engine in the PHEV always operates on the BSFC line. For the purposes of Thesis only the volumetric size of the engine is altered for scaling the engine. Figure 6.4 shows the fuel flow for a $0.710L$ engine.

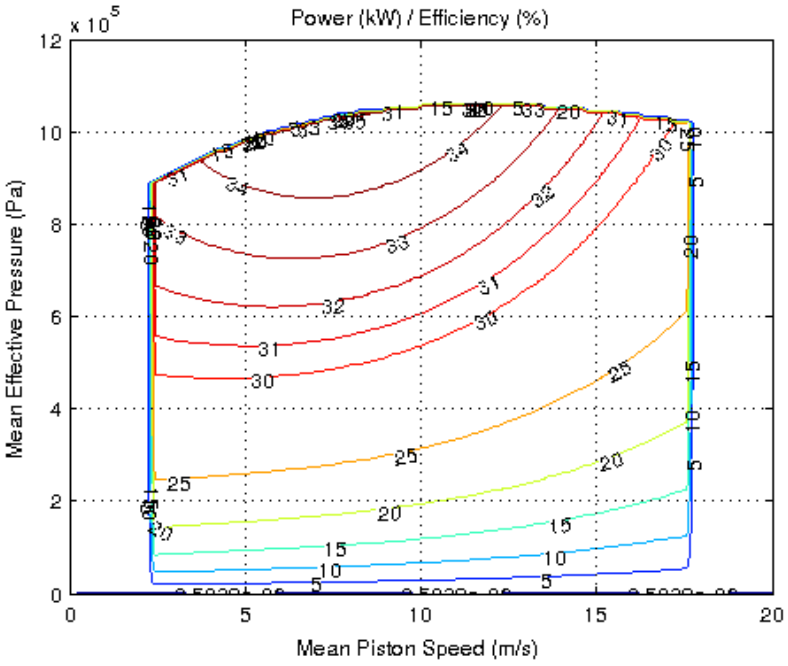

Figure 6.3: Efficiency of the engine based on p_{me} and c_m

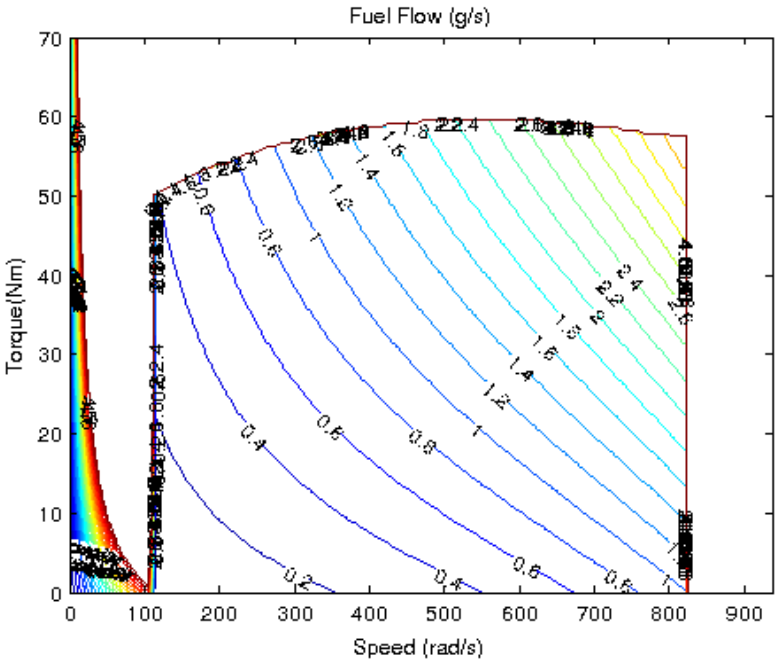

Figure 6.4: Fuel flow of a 0.710l engine

To verify the baseline engine model, the engine model was connected to the smart drive-train model with an automated manual transmission. The gear ratios and shift points were obtained from [54] and [87]. Figure 6.5 shows the fuel flow from the engine for running across the NEDC. The fuel consumption was found to be 5.49 L/100 km. Manufacturers published data for the vehicle cites a value of 5.64 L/100 km, 2% greater than the estimated value. On this basis, the ICE model is deemed to be of sufficient accuracy to be used within an optimisation framework.

The mass of the engine is calculated based on the work published in [32]. This was done by comparing several engine technologies and their corresponding weights. The proportion relating volumetric size to mass is given as $67.6kg/L$.

Identification of best operating line

In the second part, the map of an EM is formulated using the scaling procedure described in Section 6.3. The peak power of the machine is selected such that the EM has sufficient power to match the peak power point along the BSFC line. In order to identify the BSFC line the fuel consumption map is converted to an engine efficiency map and combined with the electric machine efficiency characteristics. The equation to convert fuel consumption to engine efficiency is given in Equation 6.16.

For each power point, the combination of speed and torque values which give the

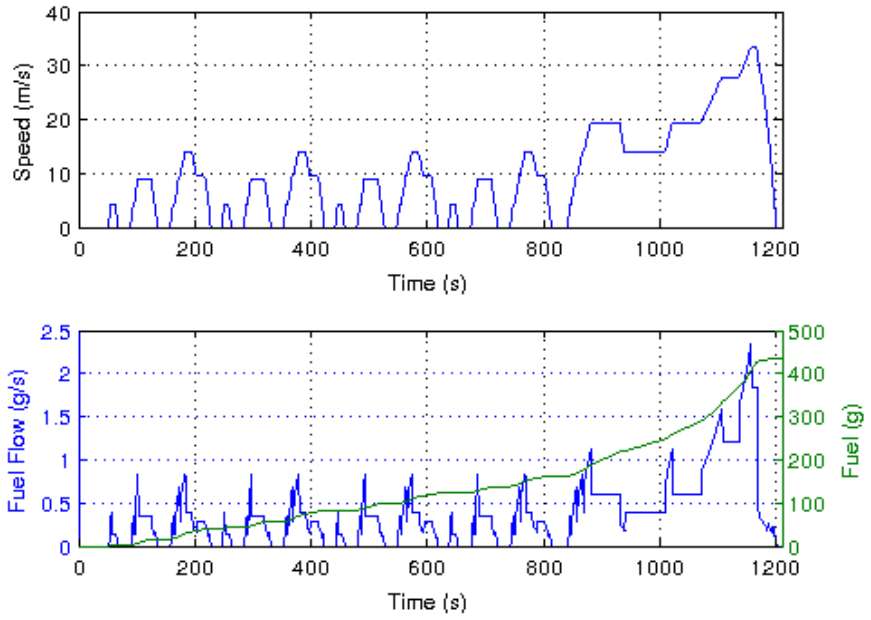

Figure 6.5: Fuel flow (petrol) for Smart drive-train on the NEDC

highest efficiency are identified. Finally for the best operating speed, torque points corresponding to the fuel consumption is determined from the previously derived map. Figure 6.6 shows the BSFC line and the speed, torque points which produce that BSFC line for the same $0.710L$ engine.

$$\eta_{BSFC}(\omega_{apu}, T_{apu}) = min(\eta_{eng}(\omega_e, T_e) \cdot \eta_{em}(\omega_e, T_e)) \tag{6.16}$$

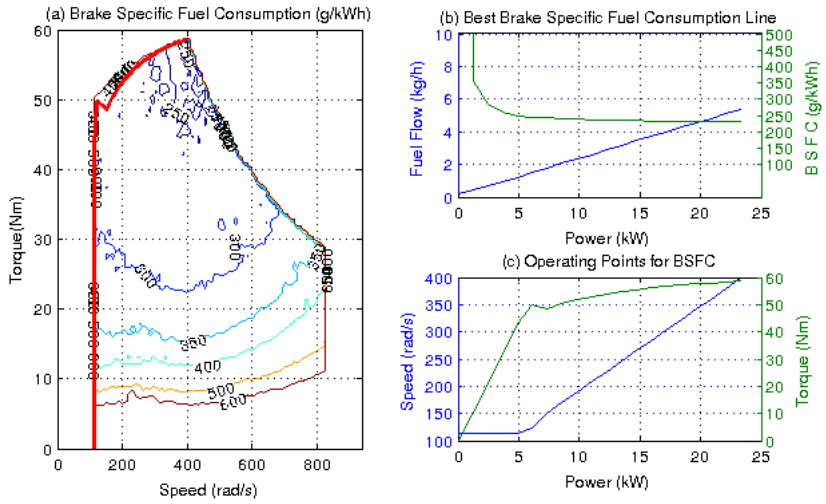

Figure 6.6: Operating line for best specific fuel consumption

6.6 Financial Cost Model

The financial cost of each powertrain component is calculated at Stage 2 of the model execution. Several financial cost metrics have been proposed within the literature to quantify and evaluate different technology options within the automotive sector. As discussed in [78], these include the procurement cost of components, their operating cost and the residual cost or value that may be realized at the vehicle end of life (EOL). The primary aim of this research is to quantify the financial cost of powertrain components installed within the PHEV at the point of sale to the consumer. Research published by the National Renewable Energy Laboratory (NREL) in 2010 [70] quantifies system cost for the HV battery, electrical machine and ICE.

Equation 6.17 defines the installed cost of the battery pack as a function of peak power (P_b) and energy (E_b). Conversely, Equations 6.18 and 6.19 define the financial cost of both the electrical machine and the ICE as a function of their respective peak power requirements. A full derivation of the financial weightings was completed in [70] and will therefore not be repeated here. However, it is noteworthy that the authors include factors such as market segmentation, vehicle class, and the expected profitability within their analysis. Validation of the empirical relationships is provided, where the authors verify the financial cost equations for existing commercially available EVs and HEVs:

$$Battery\ Cost = \frac{\$22.00}{kW} \cdot P_b + \frac{\$700.00}{kWh} \cdot E_b + \$680 \tag{6.17}$$

$$Motor\,Cost = \frac{\$21.70}{kW} \cdot P_m + \$480 \tag{6.18}$$

$$Engine\,Cost = \frac{\$14.50}{kW} \cdot P_e + \$531 \tag{6.19}$$

$$P_b = Peak\ Power\ of\ battery \quad E_b = Energy\,Capacity\ of\ battery$$
$$P_m = Peak\ Power\ of\ motor \qquad P_e = Peak\ Power\ of\ engine$$

6.7 Model Summary

A complete summary of the equations are given in this section. The model is a discretised model of time $t = 0, 1, 2, 3, 4...$ seconds. The discretisation interval of 1s is chosen because the drive-cycle data available is 1s and energy management problems which track fuel consumption and SOC are fairly low dynamics.

The objective of the model is to calculate the amount of fuel used, the trajectory of the SOC and financial cost of the powertrain for a given size of electric motor, battery and engine to complete a drivecycle. The parameters chosen for scaling these components are :

$$\begin{aligned} P_{em(peak)} &= \text{ Peak power of elecrtic machine (kW)} \\ n_p &= \text{Number of parallel strings of the battery} \\ V_d &= \text{ Volumetric displacement of the ICE (l)} \end{aligned} \tag{6.20}$$

Therefore for a given size of $P_{em(peak)}$,n_p and V_d, the mass of the vehicle M_v which is the sum of the powertrain components and the chassis mass is given as :

$$M_v(P_{em(peak)}, n_p, V_d) = 700 + (3 \cdot P_{em(peak)} - 100) + n_p \cdot 9 + V_d \cdot 67.6 \tag{6.21}$$

The road tractive force $F_r(t)$ of the PHEV is given below. It is the same equation as the EV. It is assumed the wind resistance and the rolling resistance of the vehicle which contributes to the road tractive force should be similar for the same class of vehicle.

$$F_r(t) = 8 \cdot 10^{-5} \cdot v^3(t) + 0.0241 \cdot v^{*2}(t) + 0.1456 \cdot v(t) + 146.8 \cdot \cos(\alpha) \tag{6.22}$$

from the tractive force the wheel torque can be calculated as:

$$T_w(t) = (M_v \cdot \frac{dv}{dt} + F_r(t) + M_v \cdot grav \cdot sin(\alpha)) \cdot r_w \tag{6.23}$$

The wheel speed can be calculated as:

$$\omega_w(t) = \frac{v(t)}{r_w} \tag{6.24}$$

Based on the wheel speed and torque the electric machine speed and torque can be calculated as :

$$T_{em}(t) = T_w(t) * g_{fd} \tag{6.25}$$

$$\omega_{em}(t) = \frac{\omega w}{g_{fd}} \tag{6.26}$$

where the same final drive gear ratio g_{fd} of 8.67 as the EV is used. Now that the electric machine torque and speed are known the electric machine power can be calculated as :

$$P_{em}(t) = \frac{T_{em}(t) \cdot \omega em(t)}{\eta em(T_{em}, \omega em, P_{em(peak)})} \tag{6.27}$$

The efficiency of the machine η_{em} is the scaled version of the look-up table shown on Figure 5.8. The torque axis is scaled proportional to the peak power. At this point the total power demand can be calculated as :

$$P_{dmd}(t) = P_{em}(t) + P_{acc}(t) \tag{6.28}$$

The auxiliary power demand of $1kW$ is carried over from the EV model. At this point the contol input β at time t needs to be considered. The control input can range from 0-1 and it sets the ratio of power between the engine and the ICE. Based on the control input β the engine power and the battery power can be calculated as :

$$P_{ICE}(t) = P_{dmd}(t) \cdot \beta P_{bat}(t) = P_{dmd}(t) \cdot (1 - \beta) \tag{6.29}$$

Obviously during simulation, the value of β needs to be chosen such that the peak power of the engine or the battery is not exceeded. During the component sizing optimisation algorithms described in Chapter 9, these constraints are included by penalising the minimisation function. The current at the battery is obtained by solving the equation shown below.

$$R_b \cdot i_b(t)^2 - v_{oc}(SOC(t-1)) \cdot i_b(t) + P_{bat}(t) = 0 \tag{6.30}$$

where $R_b \cdot i_t(t)^2$ is the battery efficiency losses and R is the resistance of the battery which is calculated as shown below. The number 8.84 is the amount of resistance of a single series string of batteries.

$$R_b = \frac{n_p}{8.84} \tag{6.31}$$

$v_{oc}(SOC(t-1))$ is the open circuit voltage of the battery which is a function of the SOC similar to the EV model. When the current i_b is known the SOC of the battery at time t can be calculated as :

$$SOC(t) = \frac{SOC(t-1) \cdot Q_b \cdot 3600 - \int_{t-1}^{t} i_b \cdot dt}{Q_b \cdot 3600} \tag{6.32}$$

Where Q_b is the capacity of the battery. At the beginning of the drive-cycle time $t = 0$, the SOC is stored as the initial SOC_{init}. The amount of fuel used can be calculated based on the best operating line derived from the Willans line model described in Section 6.5.

$$\dot{m} = \text{Best operationg line}(V_d, P_{ICE}) \tag{6.33}$$

Finally the cost of the powertrain can be calculated based on Section 6.6

6.8 Discussion and Conclusions

As discussed in Chapter 5, the parametrisation of the electrical components of the PHEV model was done using experimental data obtained from a fleet of EVs operating in the real-world. This model was then extended with scalable components so that it can be evaluated within an optimisation framework. At this point, it has to be understood that the design space has become quite large and the model will not be able to sufficiently capture variations in efficiency of the system based on external factors such as temperature. However, the author's assertion is that the underlying trend would be the same as the results presented in the thesis.

Data for the scalable model of the ICE were obtained from previously published research [32]. While the results presented in [32] have been experimentally validated, engine technology has advanced in recent years [10]. As a result, if models of such systems were included within the optimisation routine, then it is conceivable that the use of ICEs would be more efficient leading to further downsizing within the battery and electrical machine.

The method of component scaling within the optimisation framework employed within this study is widely accepted within the literature [73, 95]. Many studies have provided experimental validation of the functions used. Within the optimization framework presented here, the primary consideration for component scaling was component mass as a function of the respective power requirements. The assumption was made that this relationship is linear. However, in practice the inclusion of secondary mass compounding effects and the use of ancillary devices may well result in a non-linear relationship between component peak power and mass. The assertion is made that irrespective of the exact nature of the function, the validity of the final optimisation framework holds true. It is within the context of this thesis, to understand the methodology and the trends within the technology. As discussed in Chapter 10, further research may wish to explore this relationship to a higher level of detail. In addition, consideration may also be given to other system attributes such as component volume, particularly with respect to the battery that may constitute a pertinent design constraint.

The financial cost equations presented in this thesis represent the installed cost of the main powertrain components. While the report highlights the underlying trend between the respective components, it is noteworthy that absolute values may vary between manufacturer and component technology.

In conclusion a framework has been built by which various PHEV can be designed based on three key parameters: the engine volumetric size (V_d), peak power of electric machine ($P_{em(peak)}$) and the number of parallel battery strings (n_p). The developed PHEV model can be simulated over a given drive-cycle for a given control strategy. The strategies employed are discussed in detail in Chapter 7. Finally, this framework is used to calculate the value for various cost functions such as TTW emissions and the evaluation of Regulation 101 in Chapters 8 and 9.

Chapter 7

Control Strategies

The aim of this chapter is to evaluate the various control strategies used as part of this study. As described in the literature review in Section 2.2, a PHEV will typically have two primary modes of operation, mainly a charge depleting mode (CD) and a charge sustaining mode (CS). Within a CD mode the vehicle operates as a zero emissions vehicle and the battery is depleted until it reaches a lower threshold. Conversely within a CS mode, the ICE or equivalent is used to maintain the battery SOC within the required range. For a given journey that exceeds the zero emissions range of the vehicle, a number of publications describe a PHEV operating initially in its CD mode until the battery has depleted and then transitioning to the CS mode until the vehicle has reached its destination. However, research published in [39] advocates a third mode of operation, the charge blended (CB) mode in which both the ICE and the electrical subsystems are optimally used throughout the entire journey. Because the ICE is able to operate in its most efficient region for comparatively longer, simulation results presented in [39] demonstrate an overall reduction in TTW emissions for the journey.

The instantaneous power split between the electrical subsystems and the ICE is calculated using the established ECMS of local cost function optimization. However, the ECMS is extended by means of integrating it with a PI controller in order to obtain the required SOC trajectory for the battery throughout the trip. In order to benchmark the performance of this new approach, the resulting powertrain efficiency is compared against that achieved with both a global optimal solution approach (Dynamic Programming) and a rule-based approach (thermostat strategy) in which the ICE is only activated during the CS mode of vehicle operation.

The different control strategies considered are therefore:

- Dynamic Programming (DP).
- PI-ECMS following a linear line based on journey distance (PI-ECMS-LIN).

- PI-ECMS following a NN based predicted trajectory (PI-ECMS-NN).
- PI-ECMS following the trajectory given by DP. (PI-ECMS-DP)
- Thermostat Strategy (THERMO)

For all the various control strategies, the same vehicle model has been utilised. The vehicle parameters are given in Table 7.1 for reference.

Table 7.1: Vehicle parameters for evaluation of control strategies

Parameters	Value
Engine size	$5.5x10^{-4}m^3(0.55l)$
Peak engine power	$36kW$
Electric machine power	$50kW$
Number of parallel strings	12
Battery energy capacity	$11.76kWh$
Initial SOC	90%
Target final SOC	20%

The performance metric chosen for comparison is the TTW emissions of the vehicle because it is the objective of the legislative requirements such as Regulation 101 [87]. This term is directly proportional to the vehicle's fuel consumption. In order to compare the vehicles performance for different journey distances, the drive-cycles are repeated several times. The results for the different control strategies are presented in chapter 8. The drive-cycles employed have been previously discussed in Section 3.3.

7.1 Dynamic Programming

7.1.1 Background

The method of dynamic programming (DP) , developed by Bellman [41] has been predominantly used in existing literature as discussed in chapter 2.3 for the purposes of benchmarking control strategies. The DP approach is a powerful tool to find the optimal solution of a nonlinear dynamic problem for a given set of boundary conditions. Although, it can obtain the ideal control trajectory, it is a very computing intensive task and therefore its real-time application is limited [31]. Further, the drive-cycle has to be known apriori to calculate the global optimal solution hence it is not deemed to be practical for real-time implementation.

To apply DP in control, the states of the system and time have to be discretized. After discretization, a control trajectory has to be calculated such that one state transforms to another state at each time step. The key principle around DP is that the optimal control for each of the remaining states does not depend on the previous ones or control decisions. Bellman has called this property the principle of optimality [5]:

> "An optimal policy has the property that whatever the initial state and the initial decisions are, the remaining decisions must constitute an optimal policy with regard to the state resulting from the first decision."

Therefore, there exists a recursive relationship which has to be executed backwards in which the cost of each decision at time t is calculated, provided the cost has already been calculated for stage $t + \Delta t$. The optimal cost is given as the minimum value of the sum of costs at t and $t + \Delta t$.

In this chapter DP is used in order to find the maximum achievable fuel economy to compare the performance between the different real-time controllers. Using this DP process and a NN based power demand prediction algorithm, an ideal trajectory is generated for PI-ECMS-NN.

7.1.2 Formulation of the DP Problem

In order to apply DP the system dynamics are written in discrete time form, and the state and control input is also discretised. Based on the resolution chosen for discretisation the solution space can be quite large, but a finite solution exists which gives the optimal trajectory of control decisions. Consider a control policy of π decisions which chooses the split in power between the engine and the battery through the drive-cycle of total time t_end. The total control policy is the reduction in the amount of fuel used across the drive-cycle, which can be written as :

$$J_0 = \phi(SOC_{final}) + \sum_{t_{end}}^{t_0} \dot{m}_f(SOC_k, P_{ICE,k}, t_k) \tag{7.1}$$

and the optimal policy is

$$\pi^* = \arg\min_{\pi} J_0(\pi) \tag{7.2}$$

The cost-to-go $J_k(\pi)$ is defined as the cost incurred in moving from the time step k to the end of the optimal horizon, following the control decisions pi. DP is applied in an iterative fashion every time step k, from t_{end} to t_0 as follows :

$$J_k^*(SOC) = J_{k+1}^*(SOC) + \min_{u_k \subset U_k} \dot{m}_f(SOC_k, P_{ICE,k}, t_k) \tag{7.3}$$

if a particular SOC needs to be reached at end of the trip the initial step in DP is given as $\phi(SOC_{final})$ and it is as follows :

$$\phi(SOC_{final}) = \begin{cases} 10^{10} & \text{if} SOC \neq SOC_{final} \\ 0 & \text{if} SOC = SOC_{final} \end{cases} \tag{7.4}$$

Since DP is a computationally intensive process and the system has to be executed backwards, the PHEV model developed in chapter 6 had to be simplified for efficient calculation. Irrespective of the control decision the power demand of the driver does not change for a given drive-cycle. In other words the power drawn by the electric machine can be calculated and stored in advance. This calculation is based on equations 5.3, 5.4 and 5.5 listed earlier. For convenience the EM power P_{em} is called the power demand (P_{demand}). It is calculated for every $1s$ interval since the drive-cycle has a resolution of $1s$.

Now that the power demand has been calculated, the control variable has been assumed as P_{ICE}. Therefore, on knowing the P_{ICE}, assuming the engine is always working on the BSFC line, the fuel consumed can be calculated from Figure 6.6.

Further, since P_{ICE} is known battery power, P_{bat} can be calculated by :

$$P_{bat} = P_{demand} - P_{ICE} + P_{aux} \tag{7.5}$$

For a given P_{bat} value, the change in SOC is calculated based on equations 5.8 and 5.10. During each time step and each SOC state, the integrators in the model are repopulated with initial values to calculate the change in SOC. Although Simulink has the capability to process discrete states, this specific requirement of calculation at every time step and SOC state of DP would lead to opening and closing the Simulink model frequently. This would result in additional memory overhead and makes it computationally unnecessarily inefficient . Therefore, it was found that converting the Simulink model into Matlab scripts led to faster execution. In order to verify the new script model, the change in SOC and P_{demand} were compared between the two forms of the same model when executing over the NEDC. The results of the simulation is shown in Figure 7.1.

The only model state which needs to be calculated every time step is the SOC of the battery. SOC was descretised with sufficient resolution, to capture the change in SOC for the range of control inputs. Finer resolution leads to a more accurate result but requires a longer calculation time. It was determined in existing literature that the minimum level of resolution needed is 0.001% [14]. However with such a high level of resolution it was impractical to simulate large drive-cycles due to simulation time and the memory limitations of the computer. Several techniques were suggested in [41, 14] to reduce simulation time which are discussed below:

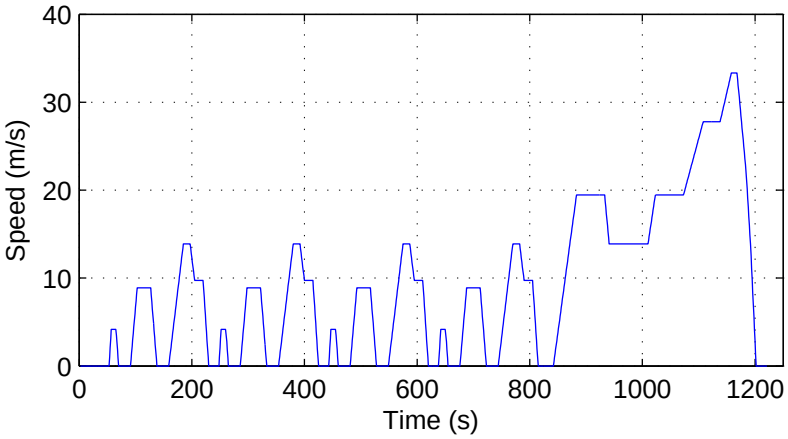

(a) drive-cycle

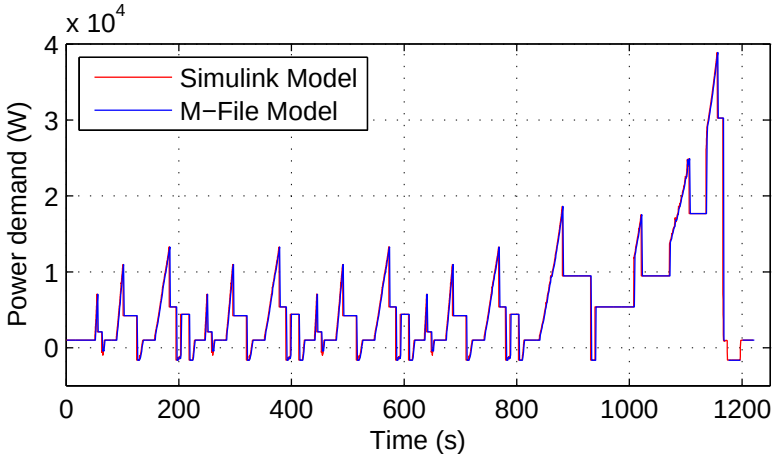

(b) Comparison of power demand

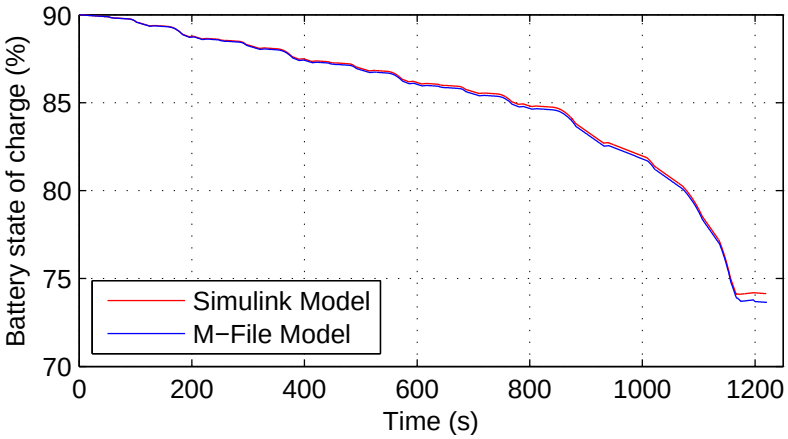

(c) Comparison of state of charge

Figure 7.1: Comparison of M-file model to Simulink model

7.1.3 Calculation

The execution of the DP algorithm is shown in Figure 7.2. The execution of the DP algorithm is split into four steps :

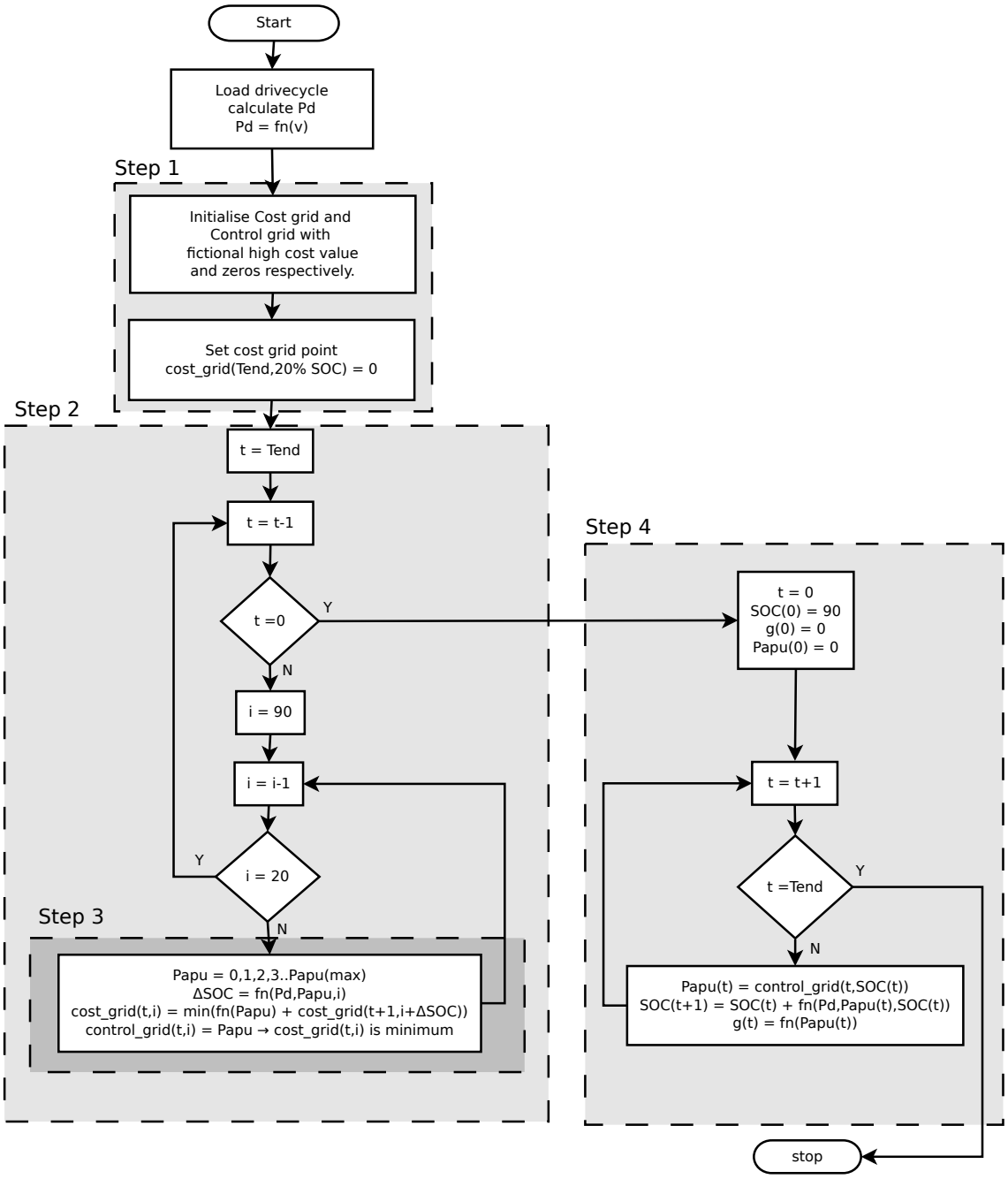

Figure 7.2: Flowchart for DP algorithm

Step 1: The first step of the DP process is to initialise two large matrices with dimensions of 100 points on the Y axis and one point per second. Figure 7.3 shows the cost grid for a resolution of 100 divisions and 100 seconds. The first

matrix is called the cost grid and it stores the cost associated for each decision at a particular state and time. During initialisation, individual elements within the cost grid are stored with artificially high values. The end point at the last time step where the SOC is targeted to finish the cost value is assumed as zero ($cost(T, 20\%SOC) = 0$). The second matrix is called the control grid and it stores the corresponding control decisions.

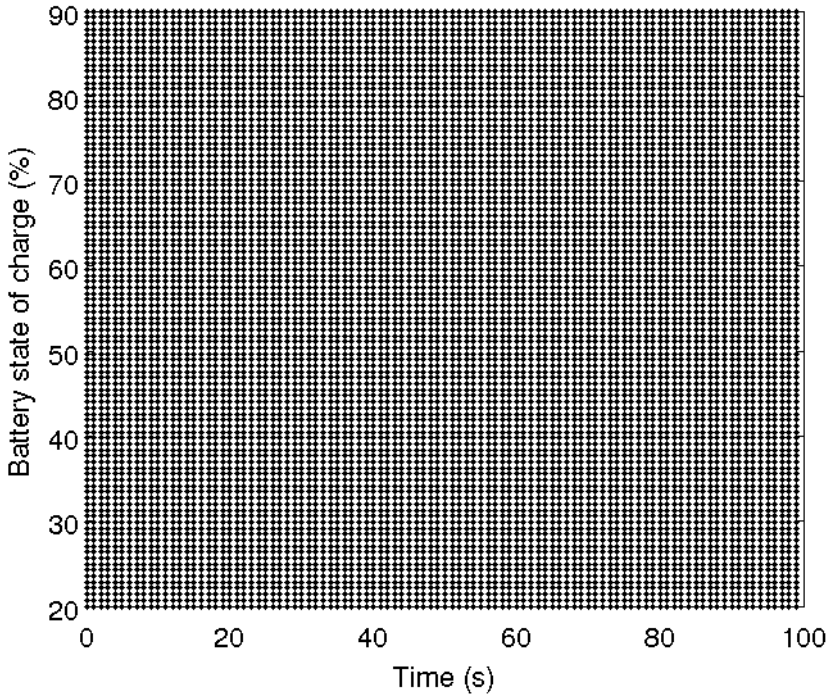

Figure 7.3: Discretisation of dynamic programming cost grid

Step 2: The second step of the DP execution is the use of two nested loops. The outer loop is configured such that the time index is executed in reverse from T-1 to 0. The inner loop is configured such that it executes from 20% SOC to 90% SOC.

Step 3: The third step or the inner execution step is to determine the cost for that particular SOC state and time. Since the objective is to reduce TTW emissions which are directly proportional to the fuel consumed, the cost function is taken as the amount of fuel used throughout the trip. The cost at each SOC state and time k can be calculated as the cumulative minimum of all control decisions at time k. This cost is represented as equation 7.6. The final minimum cost value is stored in the cost grid and the control decision taken at each point is stored in the control grid. The function which relates power used by the ICE to fuel consumed is given in Figure 6.6. This process is repeated for each grid

point and the cumulative cost is stored. Figure 7.4 shows the surface plot for one such cost matrix with a resolution of 100 and 10 repetitions of the NEDC (12000 seconds).

$$J_k^*(SOC) = J_{k+1}^*(SOC) + \min_{u_k \subset U_k} \dot{m}_f(SOC_k, P_{ICE,k}, t_k) \tag{7.6}$$

Step 4: In the final step, after obtaining the cost and control grid, the simulation is run forwards with an initial SOC. Each decision at time t, depends on the value stored in the control grid for that particular SOC. This set of control decisions gives the global optimal solution across time.

Although computing power has increased dramatically over the years, it is not possible to have grid resolution fine enough to account for every control decision. Therefore, several techniques were adopted to speed up computation.

7.1.4 Calculation Domain

Consider a single run of the DP process over the NEDC, with a resolution of 0.01% for battery SOC and the model is executed with a time rate of 1s. Assume the controller has a resolution of 50 different operating points which means, the APU with a peak power of $40kW$ has a resolution of $800W$. Every DP run for the formulation of the cost matrix involves $10000 \times 1200 \times 50$ calculations. The time saving and efficient memory handling, ideas from [41, 14] have been adopted. These techniques are listed below:

- In this research it has been assumed that the range of operation of the battery is from 90% to 20%. Therefore, the battery SOC outside this range is not considered. If the model is led to operation outside this range an artificially high cost is included with the cost function calculation to penalise the use of this region.

$$J_k^*(SOC) = \begin{cases} 10^{10} & SOC < SOC_{MIN} \\ J_k^*(SOC) & SOC_{MIN} \leq SOC \leq SOC_{MAX} \\ 10^{10} & SOC > SOC_{MAX} \end{cases} \tag{7.7}$$

- Based on the performance limits of the various powertrain systems, the control vector calculated for every grid point can be reduced. For example, if the battery limit is to be exceeded for a particular APU power the change in state for that control point is not calculated.

$$max(P_{ICE(min)}, P_{demand} - P_{bat(max)}) \leq P_{ICE} \tag{7.8}$$

$$P_{ICE} \leq min(P_{ICE(max)}, P_{demand} - P_{bat(min)}) \tag{7.9}$$

- The control strategy itself can be considered as an additional constraint. When the vehicle is braking, the power demand is negative and fixed, based on the regenerative braking strategy. In these conditions the change in SOC is calculated for one control point corresponding to the negative power demand. The constraints are mathematically expressed in Equations 7.7, 7.8 and 7.10.

$$P_{ICE} = \begin{cases} P_{ICE} = 0, & P_{demand} \leq 0 \\ P_{ICE} = P_{ICE}, & P_{demand} > 0 \end{cases} \tag{7.10}$$

- Finally, the step which led to the maximum benefit is the use of interpolation [41]. When calculating the cost for a particular grid point at time t, even if there is no value stored for a grid point at $t + \Delta t$ for a particular control input due to poor resolution, the neighbouring grid point values are interpolated. It was found that by using this method it is possible to reduce the grid resolution considerably.

Based on all these additional conditions the simulation time can be reduced. To illustrate the earlier example with a SOC resolution of 0.1%, assuming 10% of the computations violate one of the constraints and assuming 50% of the time the vehicle is either stationary or braking, the number of computations reduces to $800 \times 45 \times 600$. For a SOC grid resolution of 100 divisions and 20 control point evaluations, a 2.27 GHz, 4 core processor was able to complete 10 NEDC repetitions in the region of 3 hours.

7.1.5 Discussion

The reason for the best performance of DP is analysed further in the case of 10 repetitions of the NEDC. Figure 7.4 shows the cost grid computed with DP for 10 repetitions of the NEDC. As it can be observed from Figure 7.4 in the case of the start of the trip (t=0) the cost value is at the minimum when the battery is fully charged at 90% SOC. This is because in the case of a lower SOC starting point the control trajectory is influenced by not having the same amount of "free" energy from the electrical grid. Figure 7.5 shows the corresponding control matrix. As before, in the case of low SOC conditions the ICE would have to charge the battery to complete the drive-cycle leading to large P_{ICE} values.

The power demands across the trip when executing the model forward from 90% SOC are shown in Figure 7.6. In order to understand the Figure better, a snippet of

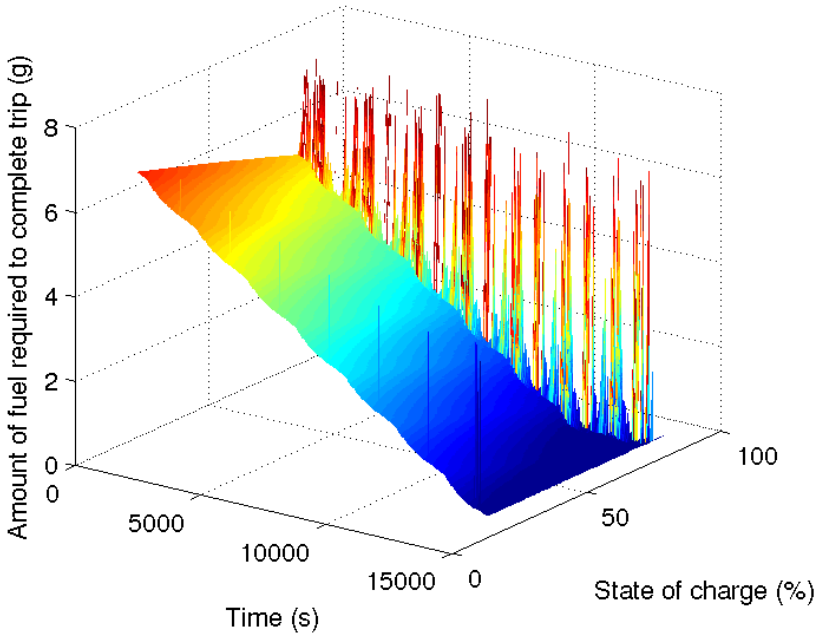

Figure 7.4: Dynamic programming cost grid

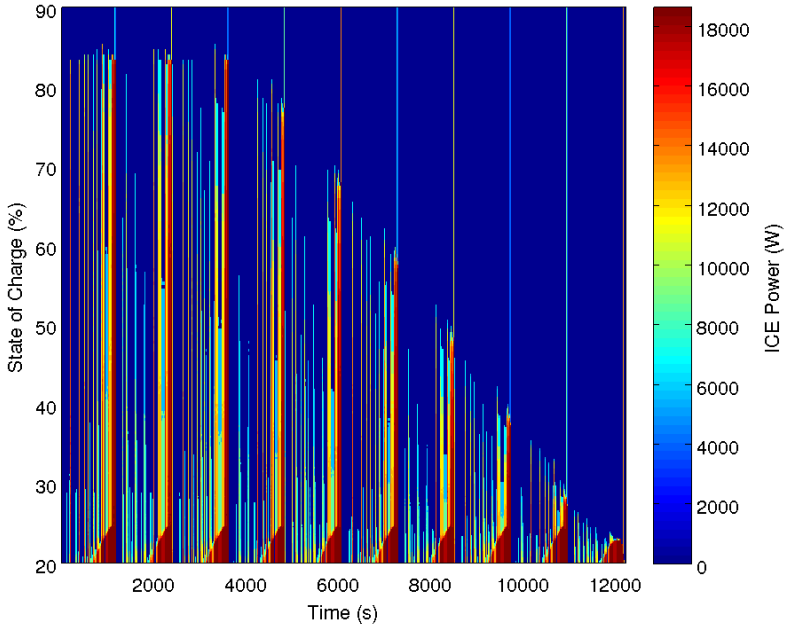

Figure 7.5: Dynamic programming control grid

the 3rd repetition of the NEDC is shown in Figure 7.7 for reference. It is noteworthy that rather than operating the ICE at the component's best efficiency point which is 18kW, the control trajectory is actively attempting to avoid charging the battery. On further investigation it was identified that the efficiency path from the ICE to the battery and then to the wheels is lower than the path from the ICE to the wheels directly. There have been several studies such as [32] which use a rule based control strategy that operates the ICE at the component's best efficiency point. The advantage of such a rule based strategy is that it can be applied in real-time and it is simple to implement. However it is argued that these controllers would have a degraded performance within these regions of vehicle operation.

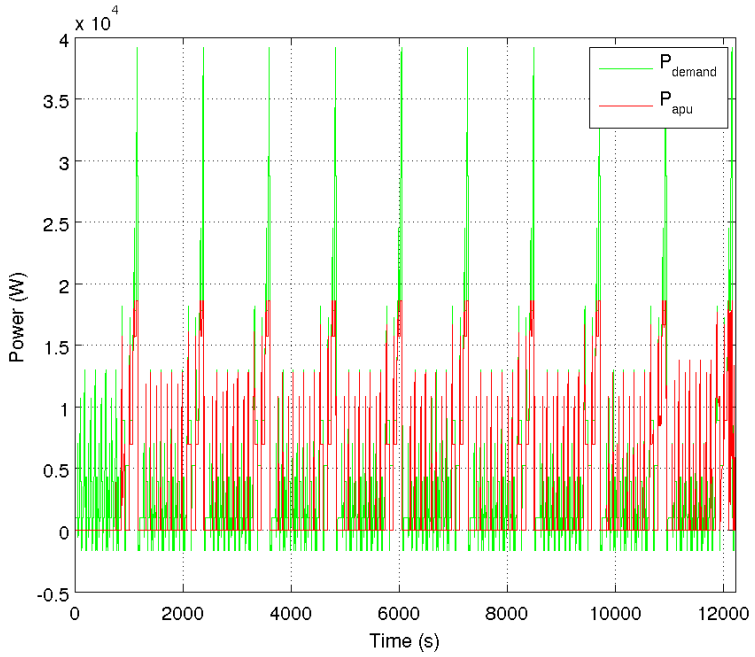

Figure 7.6: Dynamic programming power over 20 repetitions of NEDC

An important factor which has to be taken into account is that the grid resolution may affect the global optimum result. In order to understand the impact of the grid resolution, a study was undertaken in which 20 NEDCs are repeated for the given PHEV, with different grid resolutions. The impact of which is shown in Figure 7.8. Due to interpolation, it is possible to achieve a DP solution with a very low grid resolution of 20. However, as the grid size is increased the TTW emissions decrease by as much as 7% when the resolution is 200. This is because when the grid resolution is low the APU does not respond quickly to changes in SOC. The SOC traces for different grid resolutions are shown in Figure 7.9. As it can be seen with a resolution of 20, the PHEV has to charge sustain from $4000s$ to complete the drive-cycle. Figure 7.10 shows that the APU power delivered for SOC grid resolutions 20 and 200. To

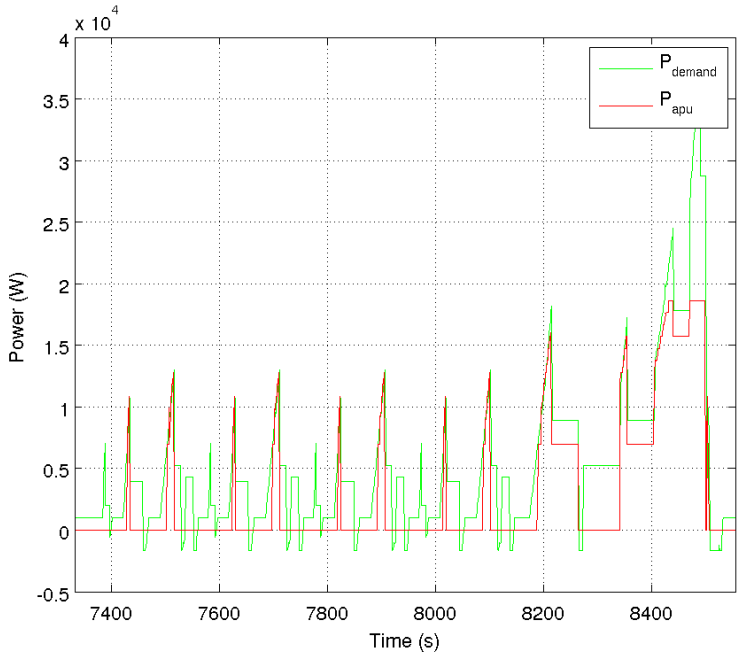

Figure 7.7: Dynamic programming power over 3rd repetition of NEDC

understand the effect of different resolutions, the 6th NEDC repetition is shown in Figure 7.11. It can be observed that the APU is delivering power for longer periods causing the increase in fuel consumption and the corresponding increase in TTW emissions. It was found that with further improvement in grid resolution, beyond 200 the global optimal result does not change by more than 0.1%. Therefore a grid resolution of 200 was selected for further simulations.

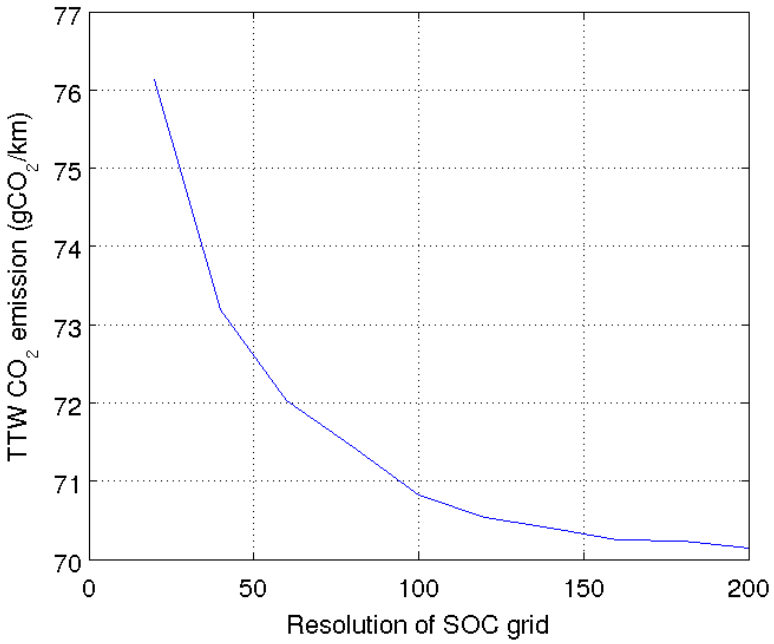

Figure 7.8: Dynamic programming result for different grid resolutions - TTW emissions

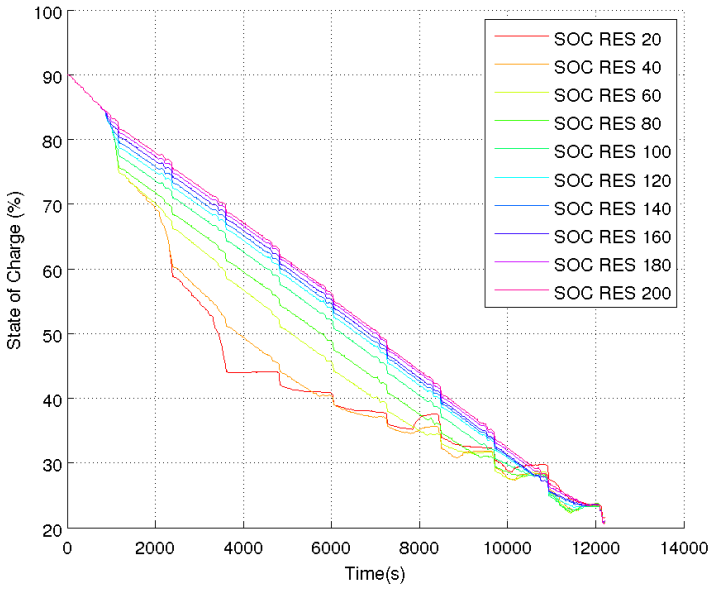

Figure 7.9: Dynamic programming result for different grid resolutions - SOC

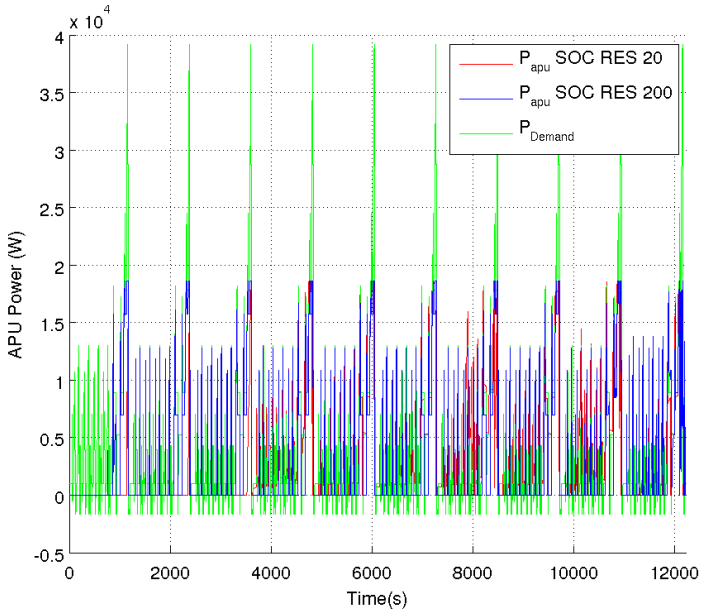

Figure 7.10: P_{ICE} for different grid resolutions and 10 NEDC repetitions

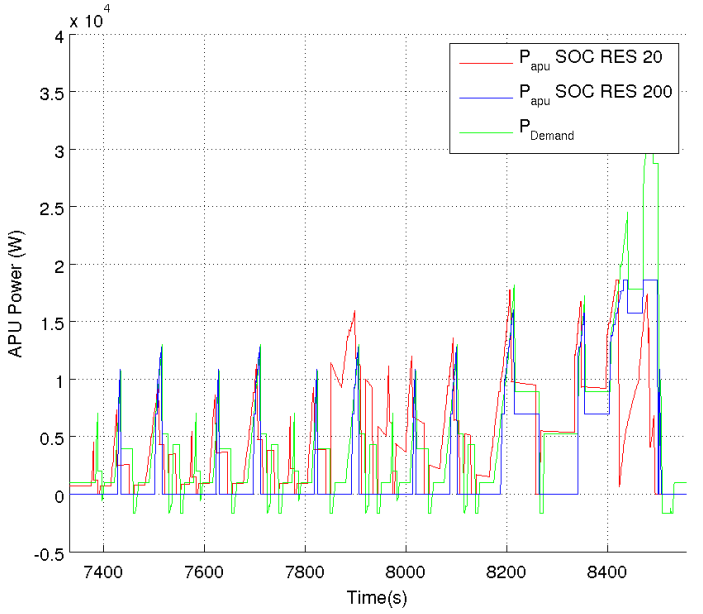

Figure 7.11: P_{ICE} for different grid resolution and the 6th NEDC repetition

7.2 Equivalent Fuel Consumption Method

The ECMS of local cost function optimization was first proposed by [69] for a HEV and later refined and extended within a number of research publications [62, 28, 29, 31, 30]. For a given value of driver demand power P_{dmd}, optimization of the energy consumption within the PHEV is achieved by selecting the optimal instantaneous power split (β) between the APU (P_{ICE}) and HV battery (P_{bat}) while adhering to the minimum and maximum power constraints within the PHEV. The local optimiser evaluates the sum of fuel (g) used by the ICE and the equivalent amount of fuel (g_{equiv}) used to charge and discharge the battery at a future time. The local optimisation problem is written as:

$$
\begin{aligned}
\min_{\beta} \quad & \dot{m}(P_{ICE}(\beta)) + \dot{m}equiv(P_{bat}(\beta)) \cdot \zeta \\
\text{subject to} \quad & P_{ICE} = \beta \cdot P_{dmd} \\
& P_{bat} = (1-\beta) \cdot P_{dmd} \\
& P_{ICE_{MIN}} \leq P_{ICE} \leq P_{ICE_{MAX}} \\
& P_{bat_{MIN}} \leq P_{bat} \leq P_{bat_{MAX}}
\end{aligned}
\tag{7.11}
$$

where

β is a ratio which determines the amount of power from ICE and battery

ζ is an external tuning parameter which needs to be set to maintain a constant SOC

The term $\dot{m}$ represents the instantaneous mass flow rate of fuel from the ICE and $\dot{m}_{equiv}$ represents the equivalent amount of fuel used by the battery to deliver P_{bat}. Finally ζ defines the charge-sustaining penalty function. The value of ζ can be expressed as a penalty term which influences the use of the battery. Figure 7.12 shows the cost curve for a power demand of 10kW and different values of ζ. As the value of ζ increases the cost of using the battery increases causing the minimum value of β to become greater than 1. In this case the ICE is charging the battery. As described in the Literature Review in Section 2.3, the value of ζ is typically expressed as a static lookup table which is a linear or sigmoidal function of the SOC. This is done so that the HEV will charge sustain within a particular SOC range. An important consideration is the zero power point of the ICE or $\zeta = 0$. In this research the value of ζ is calculated from an outer proportional plus integral (PI) control loop. The output from the integral term of the controller is saturated between the values of 0 and 10 in order to avoid potential instability through the

occurrence of integral windup. However, it is noteworthy that for the drive-cycles evaluated the controller limits were never exceeded.

Figure 7.13 presents the structure of the improved PI-ECMS control system. Having an outer control loop based on SOC trajectory gives an improvement of 4%-7% compared to the base ECMS strategy.

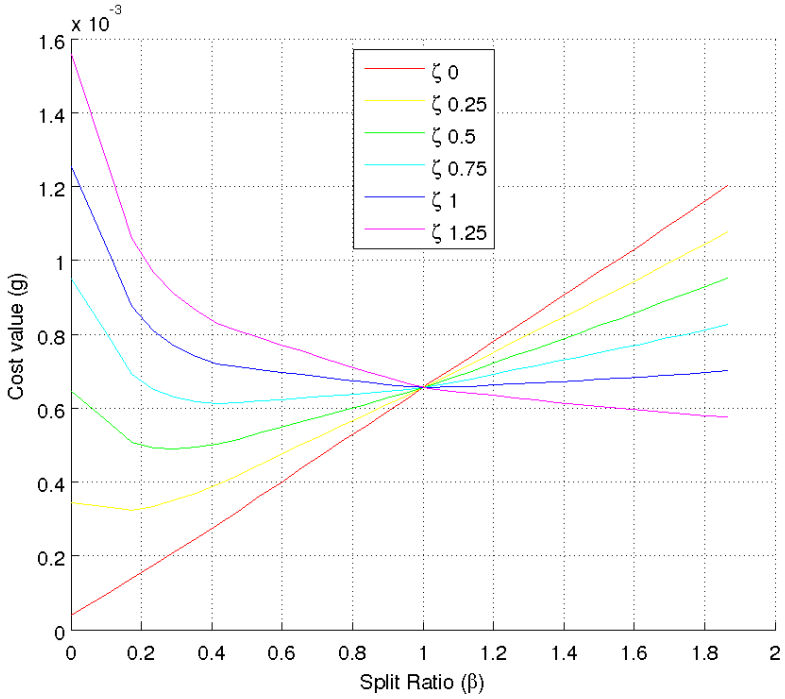

Figure 7.12: Cost function values for different values of ζ

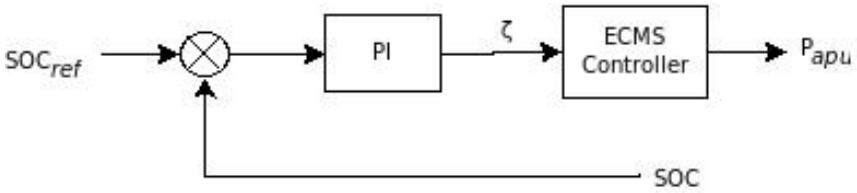

Figure 7.13: Layout of PI-ECMS controller

In order for this technique to be successfully applied to a PHEV as part of a CB energy management strategy, the desired set-point trajectory of SOC across the trip (SOC_{ref}) must be known in advance.

7.2.1 PI-ECMS Following a Linear Line Based on Journey Distance (PI-ECMS-LIN)

The authors in [39] state that the performance of a CB controller is maximum when the battery energy is completely used at the end of the trip. The theory was verified by the authors using DP to find the ideal trajectory. Based on this fact a linear trajectory was developed based on journey distance. Figure 7.14 presents the reference trajectory, in which SOC is a linear function of journey distance.

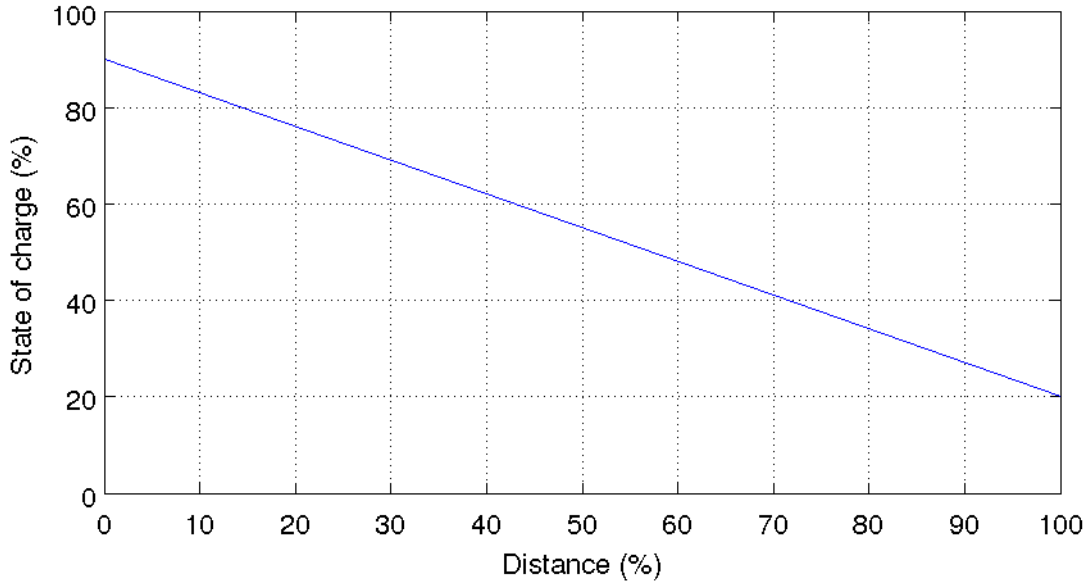

Figure 7.14: Linear SOC trajectory based on distance

Comparison of ECMS and PI-ECMS

In order to compare the ECMS controller to the PI-ECMS controller, consider the repetition of 10 NEDC runs as a case-study. In the case of the PI-ECMS controller, the SOC_{ref} is a linear trajectory based on distance. The ECMS controller is designed to charge sustain at 30% SOC. The engine ON-OFF periods and the corresponding power demands are shown in Figure 7.15 (a) and (b) for the ECMS controller and (c) and (d) for the PI-ECMS controller respectively. As it can be observed from Figure 7.15(a) and (c), the engine is ON for longer periods with the PI-ECMS controller. However, on comparing Figure 7.15 (b) and (d), in the case of PI-ECMS, P_{ICE} never exceeds the driver power demand. Due to this the overall efficiency of the powertrain across the drive-cycle is improved. The TTW emissions in the case of PI-ECMS ($69.76 gCO_2/km$) when compared to ECMS ($77.55 gCO_2/km$) has an improvement of 10%.

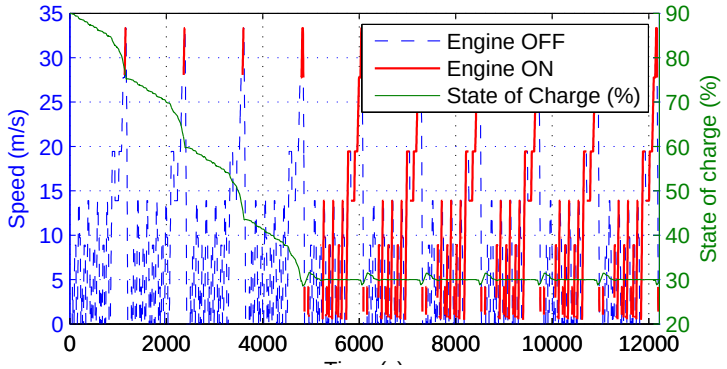

(a) Engine ON-OFF - ECMS

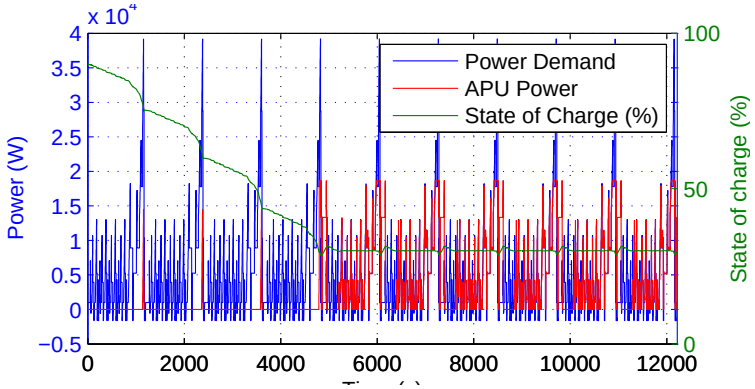

(b) Power - ECMS

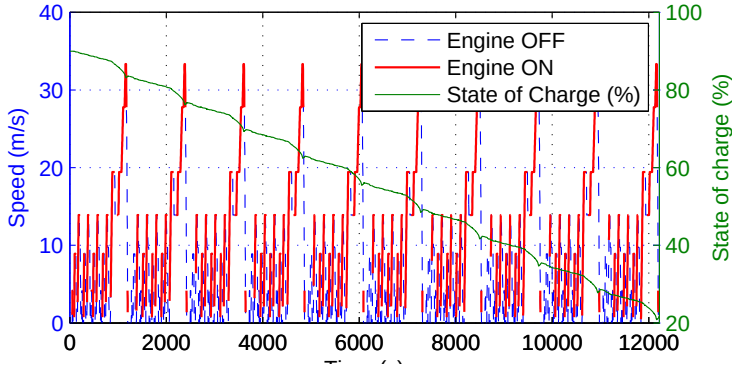

(c) Engine ON-OFF - PI-ECMS

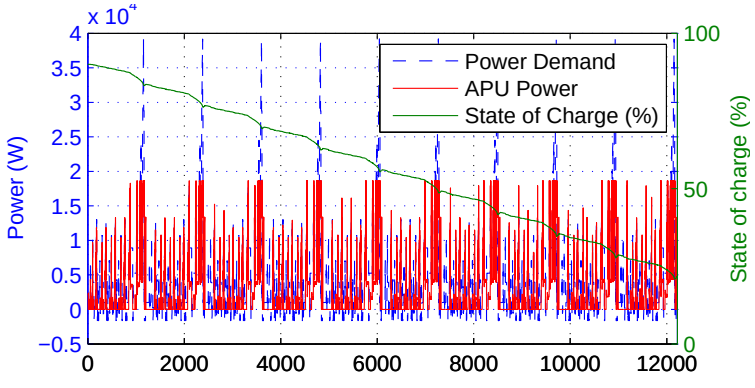

(d) Power - PI-ECMS

Figure 7.15: Comparison of ECMS and PI-ECMS

7.2.2 PI-ECMS Following a NN Based Predicted Trajectory (PI-ECMS-NN)

In the second case, it has been assumed that with current and future GPS and tracking technology the road-type covered for particular distances would be known in advance. As a case study one NEDC is presented. Based on the road-type and distance covered it is possible to build a predicted power demand based on average power and speed of the drive-cycle employed. The three drive-cycles chosen for analysis are different in terms of speed and acceleration. Therefore, the average powers were calculated as three different usage profiles. The values for the various road-types are shown in Table 7.2. On comparing the different drive-cycles in Figure 7.16 and 7.17 the variations in power demand are clear. This is true specifically in the motorway section. The real-world route has particularly low power demands due to the fact that the original vehicle was under-powered and had a low top-speed. It is important to note that the power values are specific for this particular vehicle configuration and would have to be recalculated based on the PHEV model generated.

Table 7.2: Average values of speed and power for different drive-cycles

		NEDC		Real-World Route		Artemis	
		Average Speed (m/s)	Average Power (W)	Average Speed (m/s)	Average Power (W)	Average Speed (m/s)	Average Power (W)
Urban	Stop-Start	1.09	2156	2.16	5612	1.21	2787
	Congested	3.03	1162	4.65	497	3.72	1764
	Free-Flowing	4.16	2963	9.11	3796	5.53	2439
B-Road	Stop-Start	3.35	2394	9.04	2595	1.40	2264
	Congested	0.00	1000	9.73	1000	6.61	10565
	Free-Flowing	12.14	4907	15.45	6948	14.47	7268
A-Road	Stop-Start	9.94	5250	3.52	8269	4.29	7877
	Congested	11.39	8870	3.59	5744	7.93	12755
	Free-Flowing	12.42	10975	15.38	8708	19.74	16592
Motorway	Stop-Start	13.75	10730	11.63	9221	17.28	15097
	Congested	20.27	12883	8.27	11260	23.43	18084
	Free-Flowing	23.78	14416	22.12	10370	29.30	21251

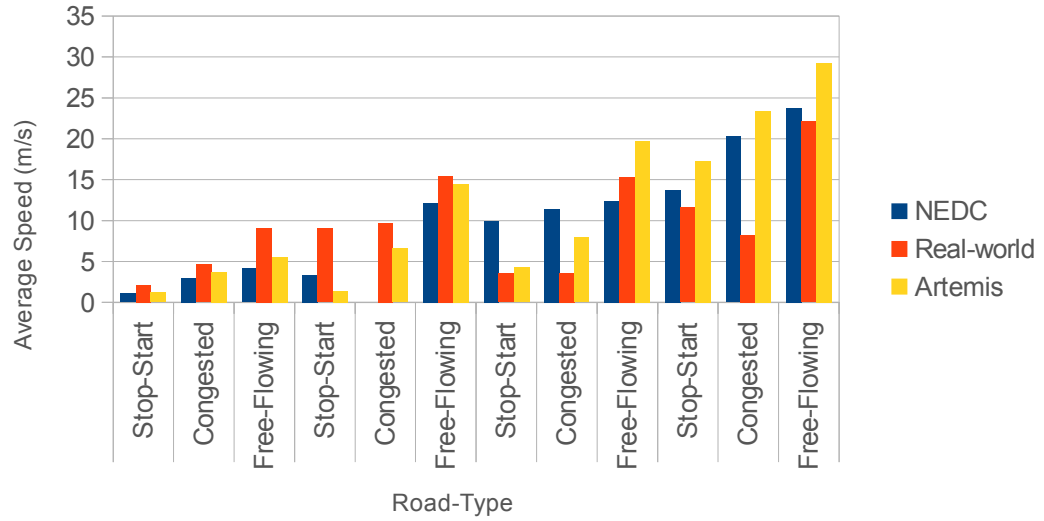

Figure 7.16: Average speed values used for prediction in PI-ECMS-NN

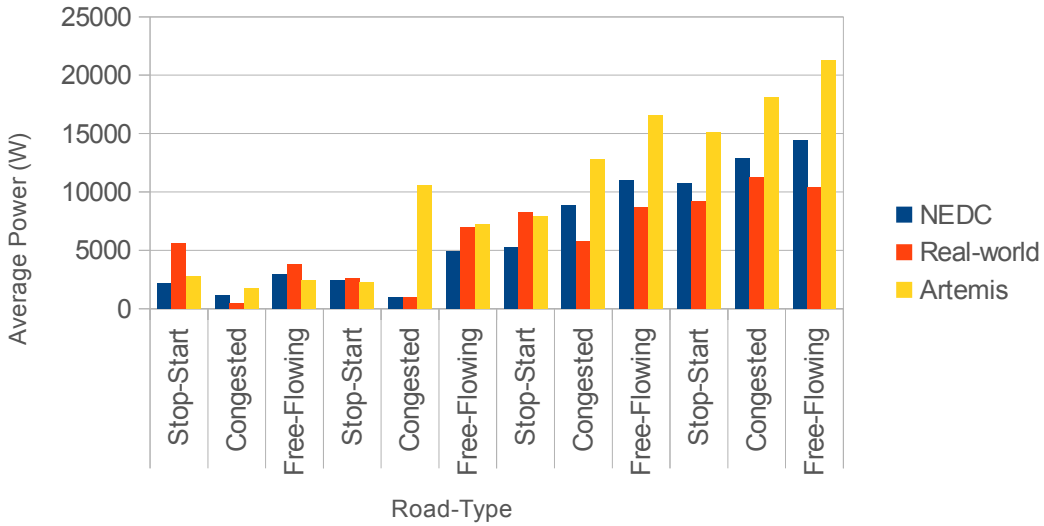

Figure 7.17: Average power values used for prediction in PI-ECMS-NN

Figure 7.18 shows the predicted road-type and the corresponding average speed for one NEDC. In order to predict the power demand across time, the first step is to integrate the average speed values with respect to distance to calculate time. Finally, based on this new time vector and populating the corresponding average power values the new power demand is predicted. This is shown in Figure 7.19. Since the estimated power demand is based on average values, the peaks of instantaneous power demands are not matched. However, it is important to note in terms of energy used, as shown in Figure 7.20, that the trends are very similar. This fact is significant since this enables the ECMS controller to achieve a battery depletion rate that finishes exactly at the end of the trip.

By running a DP algorithm for this predicted power demand an ideal battery

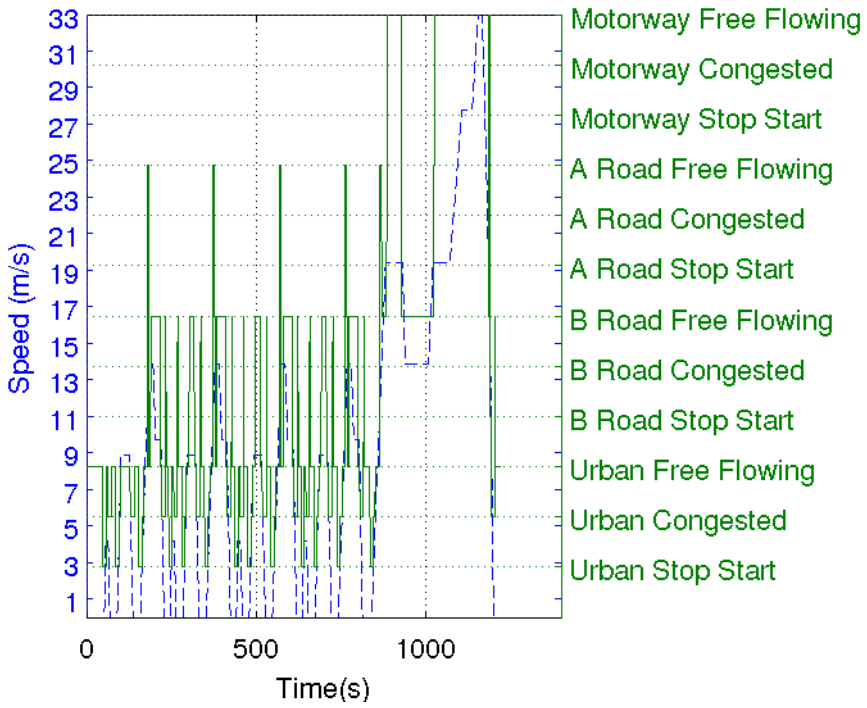

Figure 7.18: Predicted average speed values based on road-type

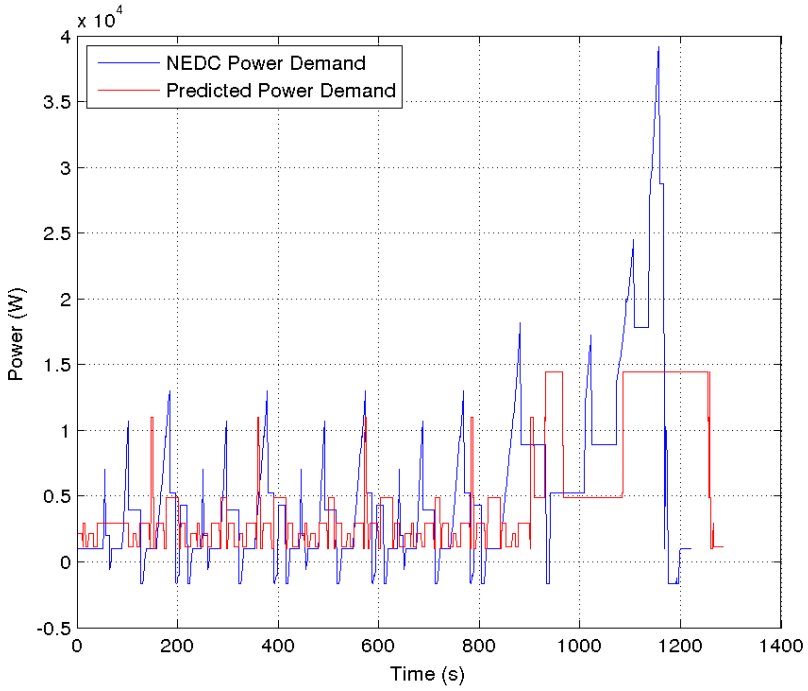

Figure 7.19: Predicted power demand across time

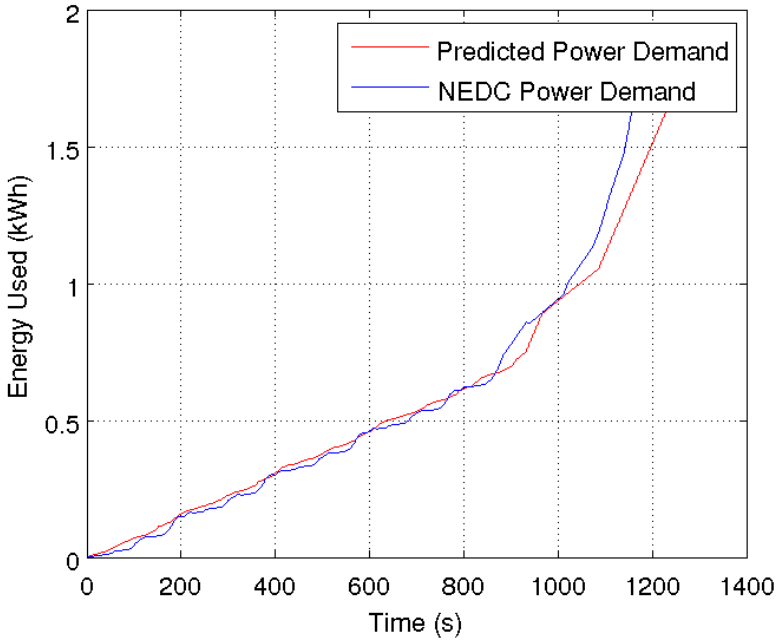

Figure 7.20: Predicted energy demand across time

SOC trajectory can be generated as the set-point for the ECMS controller. However, in order to implement a realistic scenario, the DP algorithm would have to generate the SOC trajectory within the first few minutes of the journey. In order to achieve this the SOC grid resolution was reduced to 100 i.e: 1% SOC and the time axis was interpolated every 10s. With this setup 10 repetitions of the NEDC were completed in 3.5 minutes on a standard desktop machine. It is conceivable, when implementing such a system in the real-world that the PHEV would be able to download the ideal trajectory over the internet or through some form of intelligent transport infrastructure.

7.2.3 PI-ECMS Following the Trajectory Given by DP (PI-ECMS-DP)

As a final variation of the ECMS, the ideal trajectory from a DP simulation is used as the target set-point for the controller. This value can be used to evaluate the performance of the PI-ECMS feedback loop. Further discussion on the performance of this controller is provided in chapter 8 and will therefore not be repeated here. The trajectory was included as a benchmark of the ECMS controller's performance against the DP's in order to evaluate the best performance of the ECMS controller if the ideal trajectory is known. The gains of the PI controller were obtained from experimentation to match the performance of the DP solution. However, the most

appropriate values for the gains were also drive-cycle dependent. Nevertheless, the overall variation in TTW emissions from the DP trajectory were less than one percent, as discussed in chapter 8. Therefore, the tuning of these values can be ignored.

7.3 Thermostat Control Strategy

A rule based thermostat controller has been used for comparison. Specifically when implementing a component sizing framework in chapter 9, it is not possible to implement DP due to the prohibitive computational load. The thermostat controller turns on the engine when the battery reaches 20% SOC and turns off the engine at 30% SOC. The upper threshold point can be tuned to improve the performance of the controller. By this method the controller achieves the two typical operation modes for the vehicle, the CD mode and the CS mode. The controller operated the engine at the best efficiency point of the engine except when the limits of the battery have been exceeded. Figure 7.21 shows the working of the controller for the real-world route.

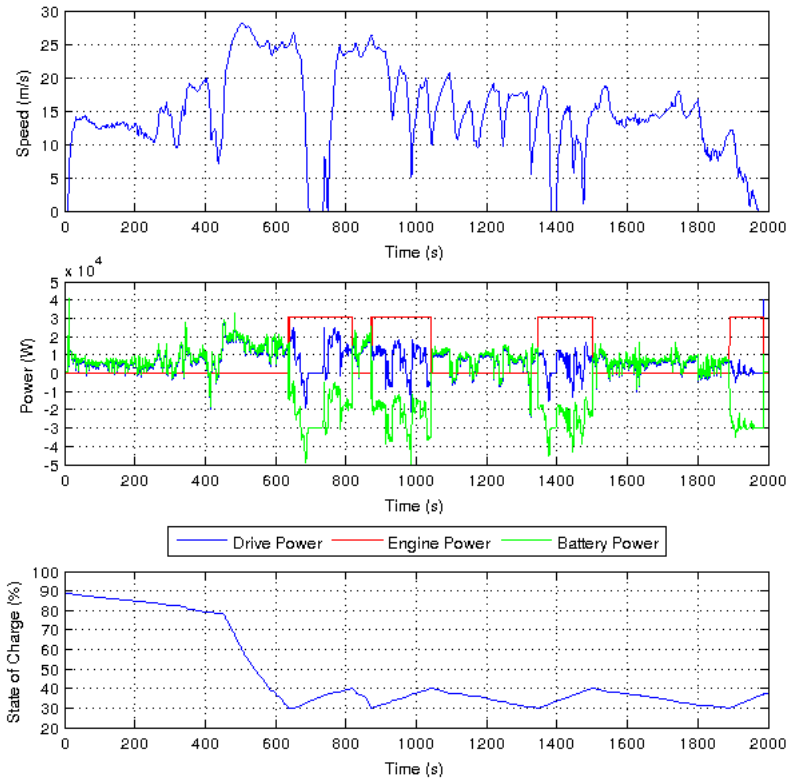

Figure 7.21: Operation of the controller over one of the recorded drive-cycles

7.4 Conclusions

The objective of this chapter was to describe the various control strategies used in this thesis. As described in chapter 2, the global optimal solution was determined using the DP method. This method will then be used as a benchmark for comparison in chapter 8. A novel control strategy was proposed based on the established ECMS controller. The addition of an outer PI loop to the instantaneous optimal controller enabled the addition of a journey predictive target based on SOC. The key finding would be to determine the ideal SOC trajectory across a journey to minimise the fuel consumption across a trip. This SOC trajectory was obtained using several methods, including a linear line method based on journey distance (PI-ECMS-LIN) and a NN based predictive method (PI-ECMS-NN). Finally, a traditional thermostat based method is also described for evaluation. This method due to its simplicity and reduced computational load will be used as the benchmark for the component size optimisation algorithim in chapter 9. The evaluation of these controllers and the comparison of the advantages and disadvantages of each are described in chapter 8.

Chapter 8

Evaluation of a PHEV

The aim of this chapter is to evaluate the various control strategies proposed and the "best" solution is adopted within the optimisation framework. The three different drive-cycles proposed in Section 3.3 are used to consider duty-cycle variations. The PHEV parameters previously stated in Table 7.1 are used for comparison of the various control strategies. As discussed in chapter 2, establishment of a gCO_2/km for a PHEV becomes very difficult, since the value is very closely linked to the driver usage pattern. For example, consider two different usage patterns. In one case, the PHEV has an AER which is larger than the commute distance of the driver and the driver charges the vehicle everyday. The TTW gCO_2/km will be zero, since the ICE is never used. But, in the second case, the PHEV may have the same AER but the commute distance of the second driver is larger than the AER and the driver does not charge the vehicle everyday. This implies that the gCO_2/km will be higher since he would have to make use of the ICE for his daily commute.

In order to evaluate the performance of the controllers the drive-cycles are repeated for increasing distances. By interpolating these distances for a given weekly usage profile it is possible to determine the average gCO_2/km for each driver. The dataset for the weekly usage profile is taken from the Mini Dataset described in Section 3.2. These results are compared to the legislative test result of gCO_2/km. The legislative standard used is from the United Nations Economic Commission for Europe and is termed as Regulation 101. The methodology of how it is applied to the simulation is given in Section 8.2. A more in-depth study of Regulation 101, is presented in Section 8.2.

8.1 Evaluation over Drive-Cycles

For each of the three drive-cycles, the TTW emissions and the relative performance of the controller to the solution provided by DP is shown. Table 8.1 shows the

Table 8.1: Repetitions of different drive-cycles

drive-cycle	Number of repetitions	Total Distance (km)
NEDC	[2 4 6 8 10 12 14 16 18 20 22 24 26 28 30 35 40]	437.2
Real-World	[1 3 5 7 9 11 13 15]	420.6
ARTEMIS	[1 2 3 4 5 6]	438.12

number of repetitions covered for each of the drive-cycles.

Figures 8.1 and 8.2 show the performance of the controllers over the NEDC. During the first two repetitions of the NEDC, there are zero TTW emissions. Therefore, these cycles are within the AER of the PHEV. For the next repetition of the NEDC (6 repetitions) the $gC0_2/km$ varies by only 6 gCO_2/km between the DP and the thermostat, but in terms of percentage it varies by more than 15%. This is influenced by the relatively shorter distance, which amplifies the percentages of the gCO_2/km when compared to longer distances. The PI-ECMS-DP has a mean increase of 1.7% gCO_2/km for the various repetitions when compared to the DP solution. Therefore these results indicate that given the ideal SOC trajectory, it is possible to achieve the global optimal solution in real-time. The algorithm PI-ECMS-NN is a DP solution that is based on average power values, and the fuel consumption is within 3.5% compared to the DP solution. It is envisaged that if the controller is implemented in real-time (where the table of power values per road-type can be updated), this controller's performance would further improve. All the controllers perform better than the traditional thermostat, which has a mean increase of 13% compared to the solution provided by DP. It is noteworthy that PI-ECMS-LIN performs within 1.5% to PI-ECMS-NN. Hence, it is possible to improve the performance of a controller by simply knowing only the distance of the trip.

On comparing Figure 8.3 and 8.1, it was observed that the average gCO_2/km for this particular PHEV configuration is lower for the real-world route when compared to the NEDC. This is primarily attributed to the regenerative braking opportunities available during the real-world route. Again it can be observed from Figure 8.4 that the trends are similar to the thermostat controller and benefits from 17% to 5% can be realised.

Finally, the TTW emissions for the ARTEMIS drive-cycle are shown in Figures 8.5 and 8.6. The TTW emissions have increased by approximately 10% compared to the NEDC. It is interesting to note that due to the high power demands there is no AER for the vehicle. The performance of the PI-ECMS-DP when comparing to the DP solution is within 0.15%. This implies that with specific tuning of the PI controller for a given drive-cycle, it is possible to achieve the global optimal solution.

Figure 8.7 shows the different SOC trajectories for 5 repetitions of the ARTEMIS drive-cycle. It is important to note that the linear SOC trajectory is made to be linear with distance and not linear with time.

In conclusion, the ECMS based controllers are close to the global optimal solution ($1\% - 5\%$). Therefore, on implementation of these controllers in the real-world they would be able to achieve the maximum capabilities of the system for the given usage profile. It has to be noted that the difference in performance between DP and PI-ECMS-DP solutions, though they have the same reference SOC trajectory, is due to the tuning of the gain values of the PI controller. A high value for these two constants makes the controller react aggressively causing unnecessary charging events (power flows from the APU to the battery). A very low value for the gains means the controller is not able to follow the SOC trajectory accurately giving a sub-optimal performance. It was possible to tune the values such that the PI-ECMS-DP is able to achieve the global optimum, however it was found these values where sensitive to the distance of the trip and the characteristics of the drive-cycle. Therefore, as a realistic tuning scenario the values where tuned manually such that they worked across the different drive-cycles compromising the performance to within 2% of the DP solution.

The results presented imply that there is only a very marginal difference between the PI-ECMS-LIN and PI-ECMS-NN. For the NEDC this could be attributed to the fact that the drive-cycle is quite short ($11km$) and repetitive. This difference is also not seen in the ARTEMIS cycle which is a relatively long cycle ($73km$). The difference between the control strategies is less than 1%. On considering component sizing in chapter 9, where computational load is a significant priority, the PI-ECMS-LIN controller has therefore been adopted.

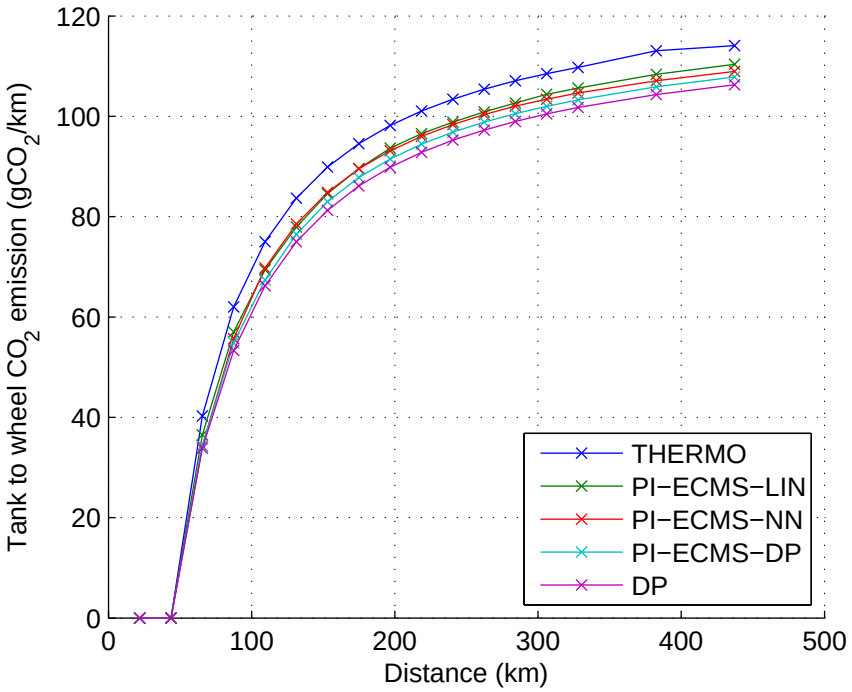

Figure 8.1: TTW emissions - NEDC

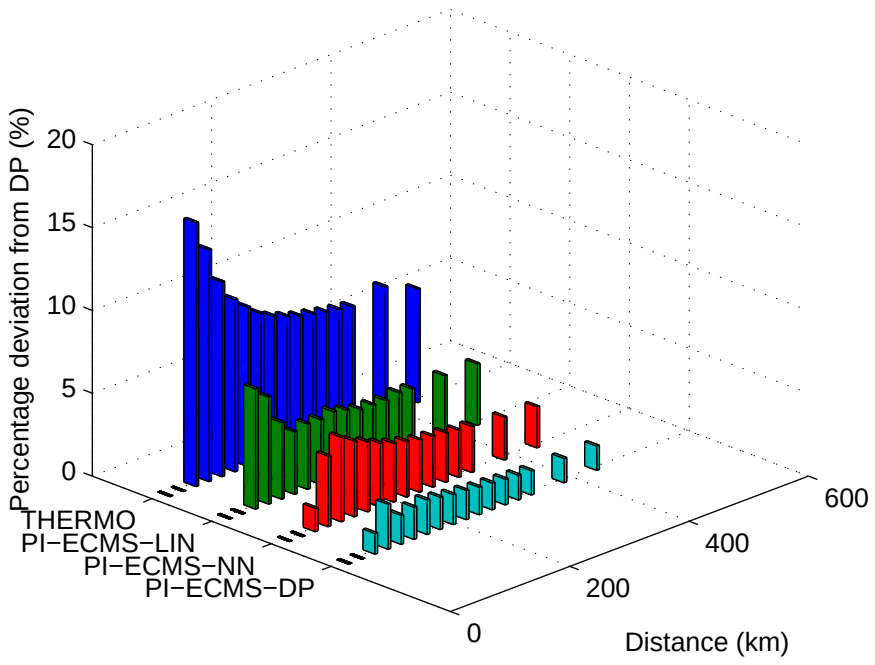

Figure 8.2: Percentage improvement - NEDC

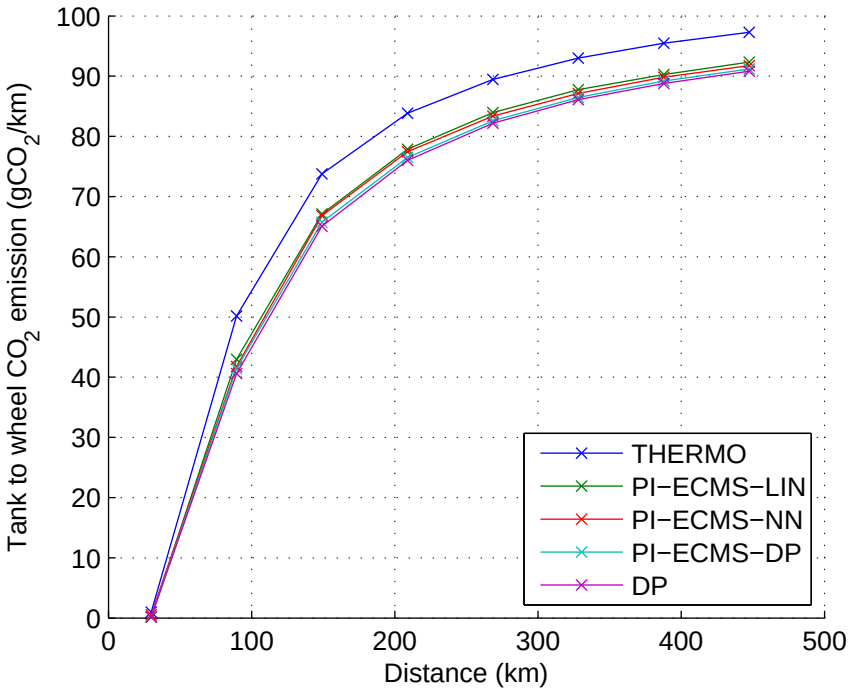

Figure 8.3: TTW emissions - Real-World drive-cycle

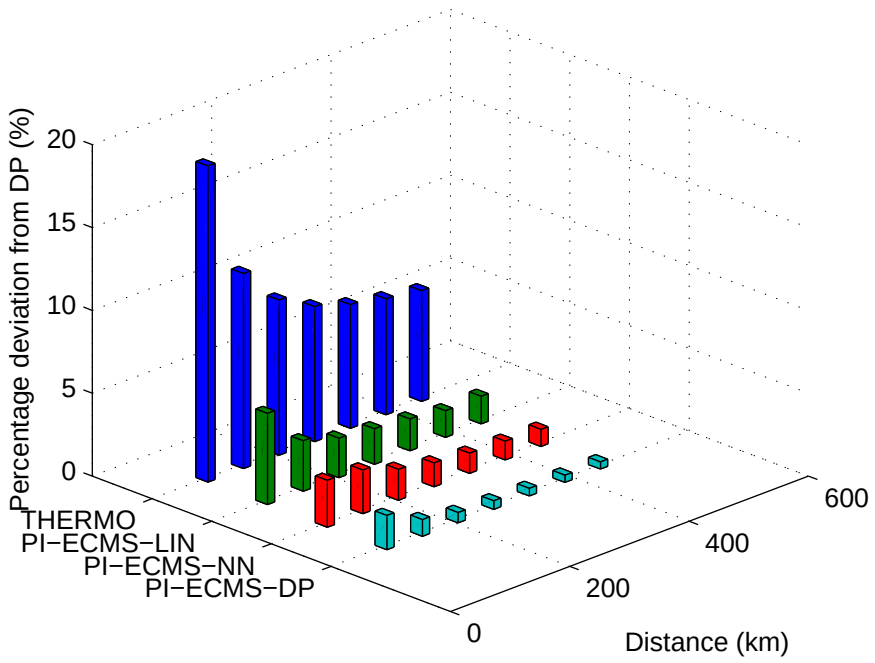

Figure 8.4: Percentage improvement - Real-World drive-cycle

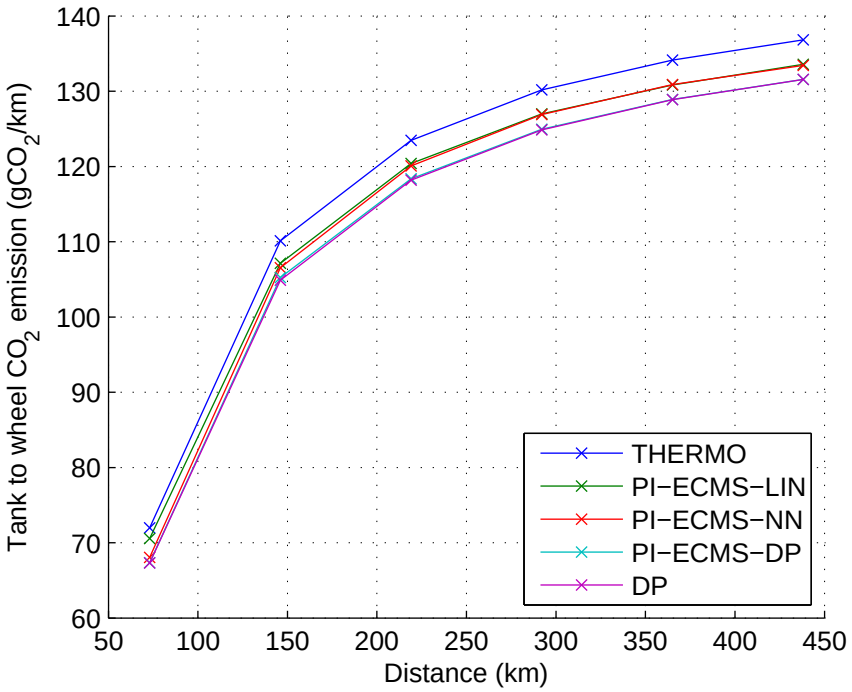

Figure 8.5: TTW emissions - ARTEMIS drive-cycle

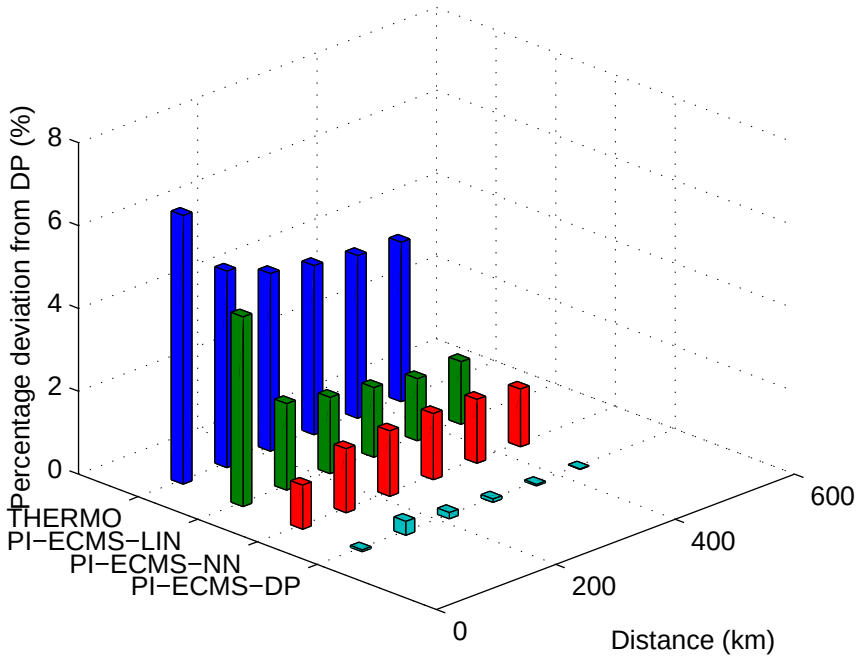

Figure 8.6: Percentage improvement - ARTEMIS drive-cycle

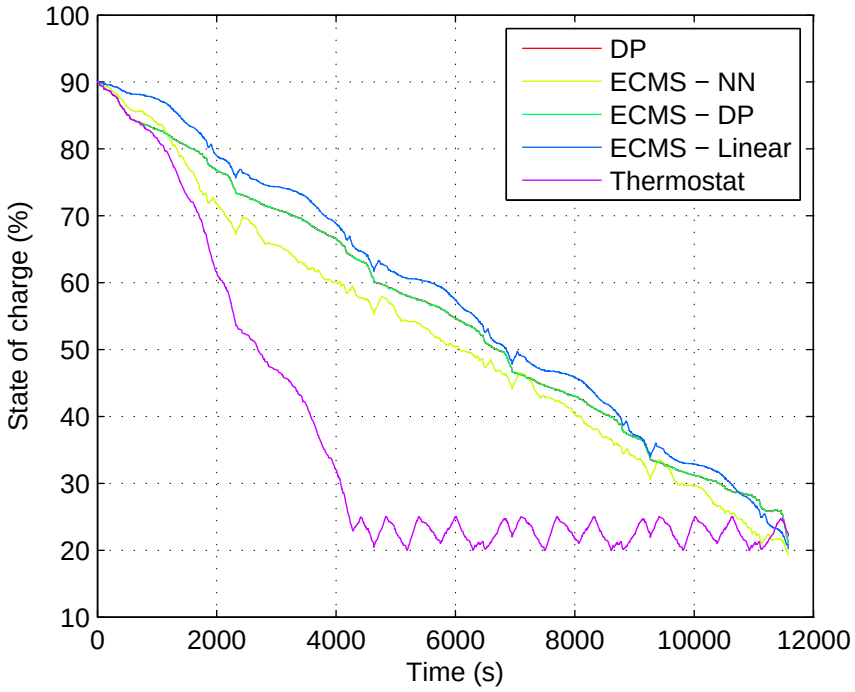

Figure 8.7: SOC trajectories for different control strategies (5 repetitions of ARTEMIS)

8.2 Regulation 101

For the purposes of implementation of Regulation 101, the vehicle parameters implemented are given in Table 7.1. The procedure of how Regulation 101 is applied is given below.

1. The vehicle is first run in pure electric mode to establish the AER of the vehicle. In this case the drive-cycle is repeated until the battery is completely depleted to the minimum SOC (20%) from maximum SOC (90%). The value is recorded as (De). In this case it was determined as 74 km.

2. In the second run the vehicle is in operation as a hybrid vehicle and it is run over the same drive-cycle once, from the maximum SOC (90%). It establishes the $g_{eq}CO_2/km$ ($M1$) and fuel consumption $L/100km$ ($C1$) for that cycle. After the cycle is completed the amount of electric energy needed to charge the vehicle back to (90%) is noted and is recorded as $E1$. The values calculated for the PHEV under investigation are $M1 = 0 g_{eq}CO_2/km$, $C1 = 0 L/100km$ and $E1 = 199.37 Wh/km$. The fuel consumption is zero because the vehicle is able to complete the cycle as a pure EV. Figure 8.9 shows the run and the APU power throughout the cycle is zero.

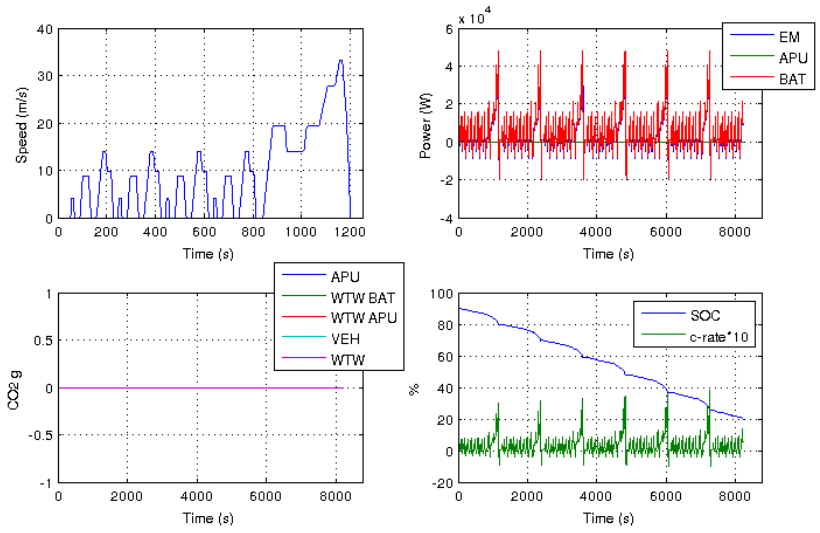

Figure 8.8: Establishment of All-Electric Range of Vehicle

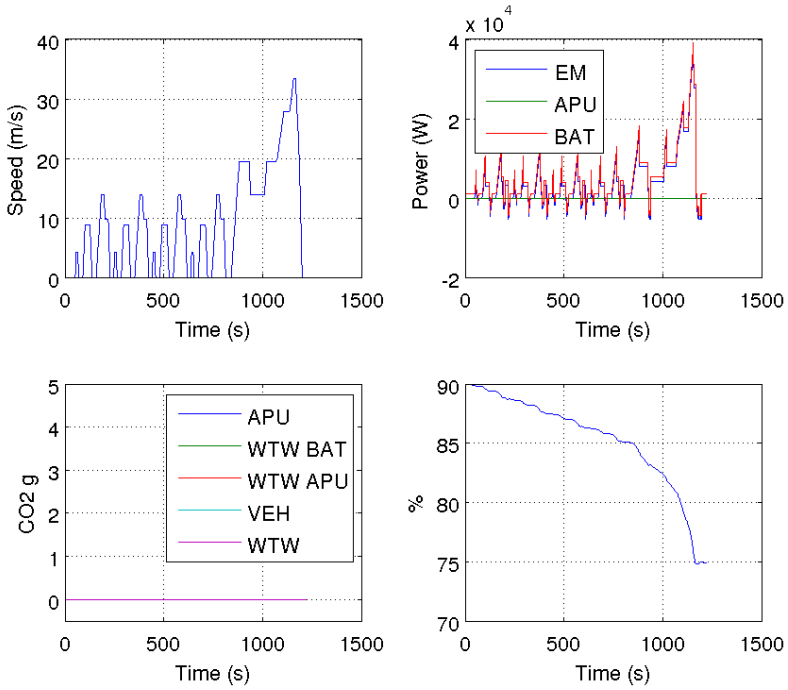

Figure 8.9: Second stage of establishing consumption figures based on Regulation 101

3. In the third run the vehicle is evaluated over the same drive-cycle in hybrid mode. However, the initial SOC is the minimum SOC of the battery (20%). Figure 8.10 shows the vehicle running over the NEDC with a low SOC. The APU turns on at the start of the drive-cycle when there is a low SOC and turns off when SOC reaches 30%. A new set of figures $M2$, $C2$ and $E4$ are established. In this case, at the end of the cycle, the battery is recharged to the maximum SOC ($E2$). Then, $E4$ is the difference in electric energy consumption between charging the battery from minimum SOC ($E3$) and $E2$. The values calculated for the PHEV model under investigation are $M2 = 124 g_{eq}CO_2/km$, $C2 = 5.2L/100km$ and $E4 = 0Wh/km$. In this scenario, the vehicle is performing much lower than a typical EV or a conventional ICE powered vehicle since the PHEV is carrying a heavy empty battery pack. It is noteworthy that the fuel consumption during this cycle has a strong relationship with the supervisory control strategy implemented on the vehicle. As discussed in chapter 2, there could potentially be significant improvement in vehicle performance by improving the supervisory control strategy.

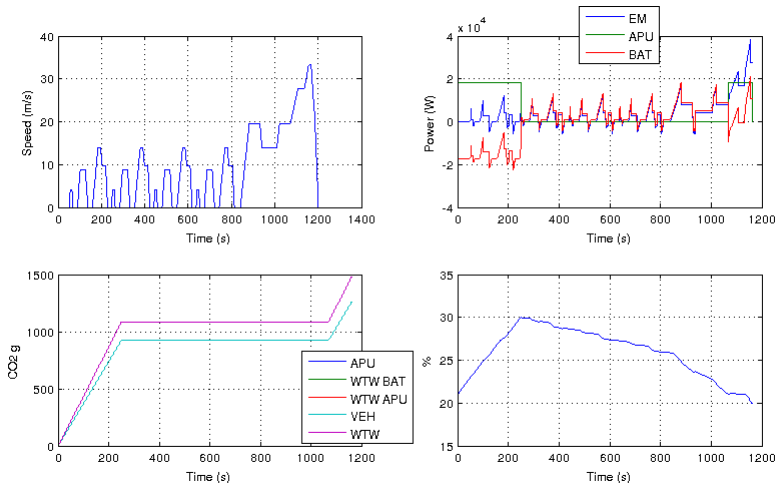

Figure 8.10: Second stage of establishing consumption figures based on Regulation 101

4. Finally, the various figures are calculated based on the formulas 8.1, 8.2 and 8.3. The value Dav is stated as $25km$ [87]. Regulation 101 considers this to be the average distance the vehicle will be driven with a low SOC and in hybrid mode. In this case, since the PHEV has a considerably large AER (De is 70km). The overall emission figures are small when compared to a conventional vehicle. The vehicle will be rated with $31.35 g_C O_2/km$ carbon dioxide emission, $1.33L/100km$ fuel consumption and an electric energy

consumption of $149.2Wh/km$.

$$M = \frac{M1 \cdot De + M2 \cdot Dav}{De + Dav} \tag{8.1}$$

$$31.35 = \frac{0 \cdot 74 + 124 \cdot 25}{74 + 25}$$

$$C = \frac{C1 \cdot De + C2 \cdot Dav}{De + Dav} \tag{8.2}$$

$$1.33 = \frac{0 \cdot 74 + 5.2 \cdot 25}{74 + 25}$$

$$E = \frac{E1 \cdot De + E4 \cdot Dav}{De + Dav} \tag{8.3}$$

$$149.2 = \frac{199.37 \cdot 74 + 0 \cdot 25}{74 + 25}$$

In the regulations, there are further conditions such as maintenance methods and procedures for discharging the batteries. However, the above method manages to capture some of the most important procedures for establishing the fuel economy figures. As discussed below, it becomes apparent there are a number of different ways in which it is possible to trade electric range and fuel consumption within a PHEV design.

8.3 Regulation 101 Response Surface

To understand the effects of component selection on the vehicle's fuel economy over Regulation 101, various parameters are shown as contour plots. Different engine sizes and battery sizes were considered to form the response surface. Although it does not cover the entire solution space of all the design parameters (size of the drive EM, size of the EM in the APU, number of series cells in the battery and the final drive gear ratio can be altered in the model but are not considered for this optimisation) it provides a valid trend of the implications of sizing components within the context of Regulation 101. Since the response surface can be depicted as a surface for only two parameters, the engine size of the APU and the number of parallel strings of the battery are altered to plot the response surface. The engine size is varied from $500cc$ to $1200cc$ in steps of $200cc$ and the battery energy capacity is varied from $5kWh$ to $25kWhh$ in steps of 1kWh. The EM is fixed at 40kW

so that the EM is always powerful enough to meet the driver demands. The fuel consumption and energy consumption figures were calculated based on Regualtion 101 and the results for different powertrain configurations are shown in Figures 8.11 to 8.15.

Regarding Figure 8.11, if considered from bottom to top, as the battery energy capacity increases the gCO_2/km decreases. However, the differences are quite marginal after the battery size increases over $16kWh$. The initial steep drop for battery sizes up to $10kWh$ is the decrease in the value of $M1$ in Regulation 101. For battery sizes beyond $10kWh$, $M1$ is 0. After $20kWh$ the gCO_2/km is fairly constant with increasing battery energy capacity and the same engine size. Therefore, from a pure legislative point of view, a battery size of more than $20kWh$ is not needed. Two PHEV cars with different market categories are the Fisker Karma and the Chevrolet Volt. They have a battery capacity of $20.1kWh$ and $16kWh$ respectively. The legislative cycle could have had an influence in the selection of the drive-train components.

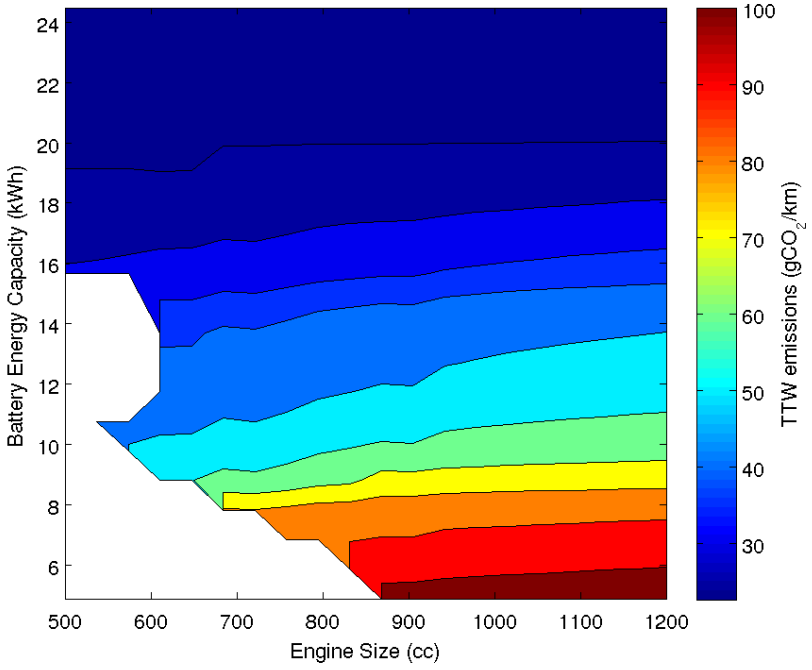

Figure 8.11: gCO_2/km emissions from tank to wheel for different vehicle configurations

An important consideration to be made is that Regulation 101 does not favour a CB approach. Because, of the way the test procedure is structured it is split into a CD mode and CS mode, hence the advantages of a CB approach cannot be observed.

It is interesting to note that there are quite a large number of combinations that can produce the same gCO_2km^{-1}. Therefore, there could be choices in which the peak vehicle power can be increased with a bigger engine (900cc - 1200cc) with no appreciable difference in the fuel economy. This flexibility could be exploited by vehicle OEMs for different user requirements.

The electric energy consumption is shown in Figure 8.12. As the battery energy capacity increases, the electric energy consumption increases. This is primarily due to the increase in mass of the vehicle.

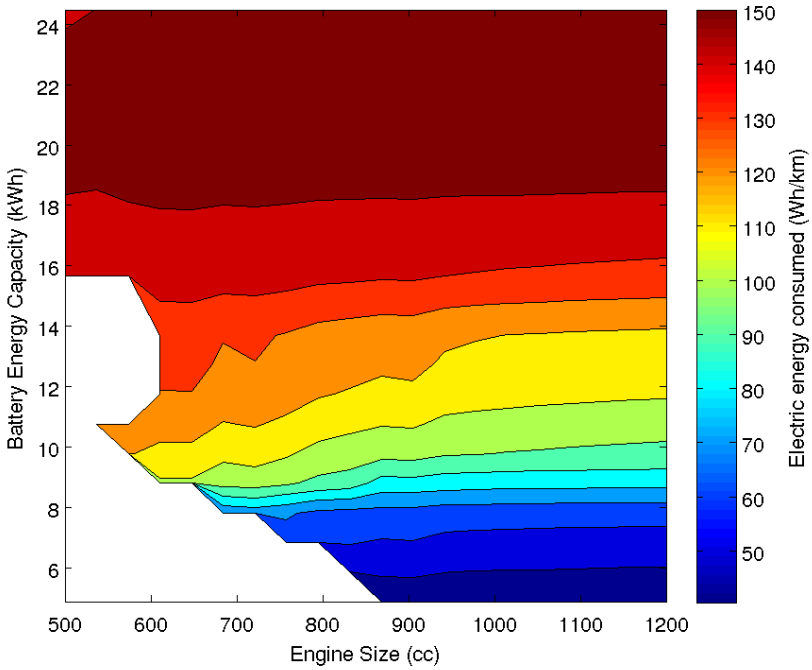

Figure 8.12: Electric energy consumption for different vehicle configurations

The AER is shown in Figure 8.13 as is proportional to the battery energy capacity. It is fairly insensitive to engine weight increases.

The final two graphs 8.14 and 8.15 show the cost and the mass of the various powertrain combinations. The financial cost represents the cost of the powertrain, and as can be expected, the cost is biased towards the battery and increases sharply with increase in battery size. The mass equations penalise batteries more than ICE which can be observed in Figure 8.15.

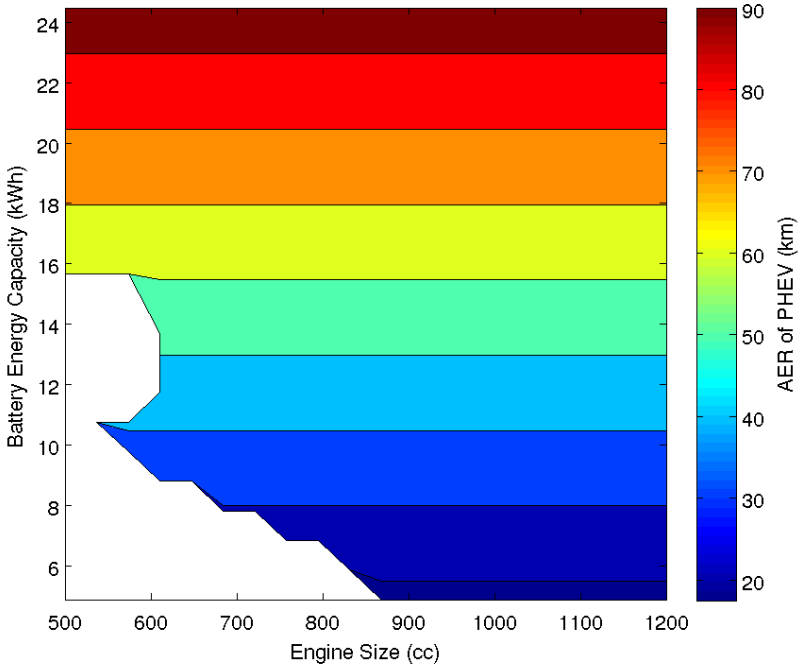

Figure 8.13: AER for different vehicle configurations

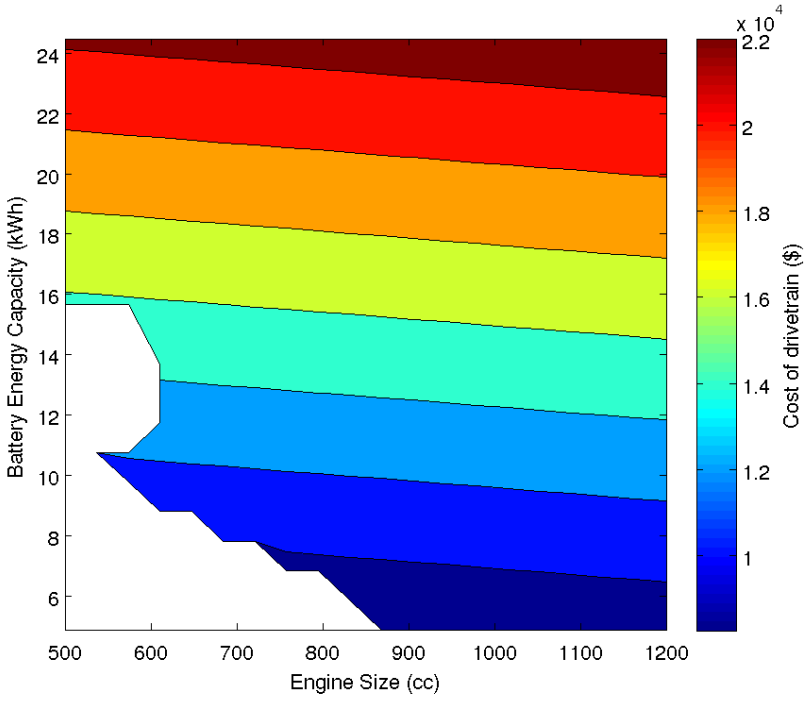

Figure 8.14: Cost for different vehicle configurations

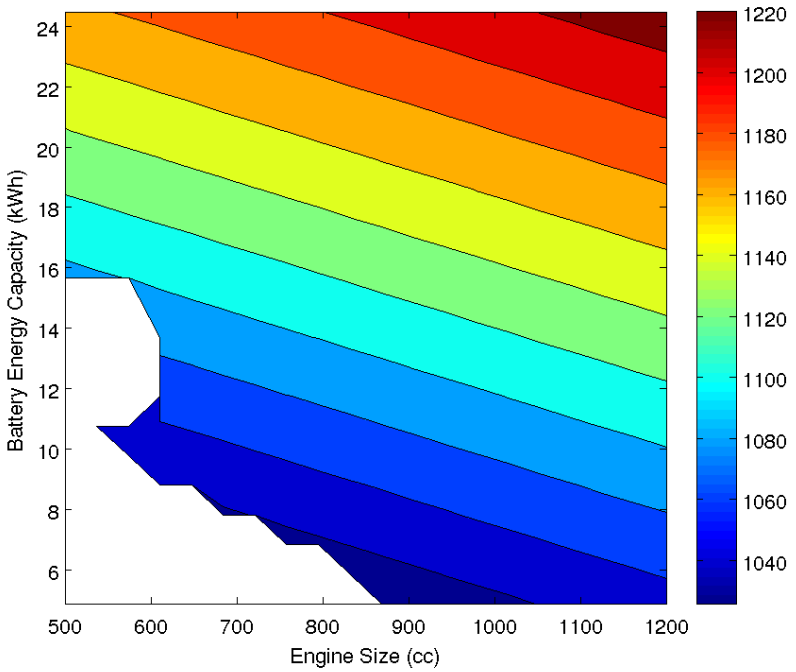

Figure 8.15: Mass for different vehicle configuration

8.4 Evaluation in the Real-World

To compare the potential performance of the PHEV in the real-world to the Regulation 101 cycle, the Mini programme data is used. The PHEV chosen for comparison contains the same case study parameters in Table 7.1. For that particular PHEV configuration, it was determined that the Regulation 101 result was $31.35 gCO_2/km$. From Figure 8.3, based on interpolation the gCO_2/km for each individual trip can be calculated for comparison. The driver aggressions, usage profile is assumed to be similar to NEDC. Based on the total gCO_2 emitted the gCO_2/km per week can be calculated. Figure 8.16, shows the spread of gCO_2/km per week for 40 drivers of the Mini programme. As it can be observed, the CB approach is very close to the DP solution. The thermostat solution performs 16% worse off when compared to the CB approach when calculated across the week. It is interesting to note that the Regulation 101 when considered across the week performs worse off by more than 35%

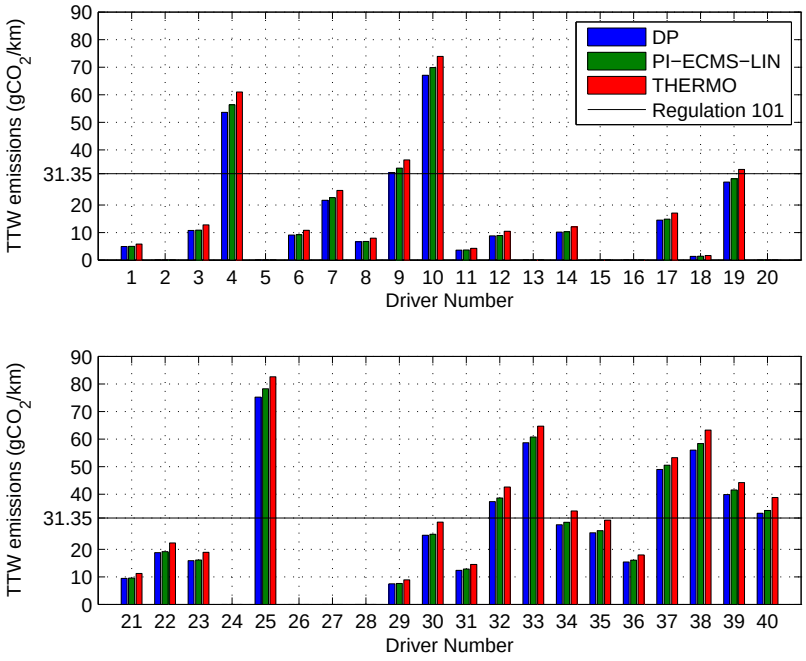

Figure 8.16: Performance of the PHEV in the real-world

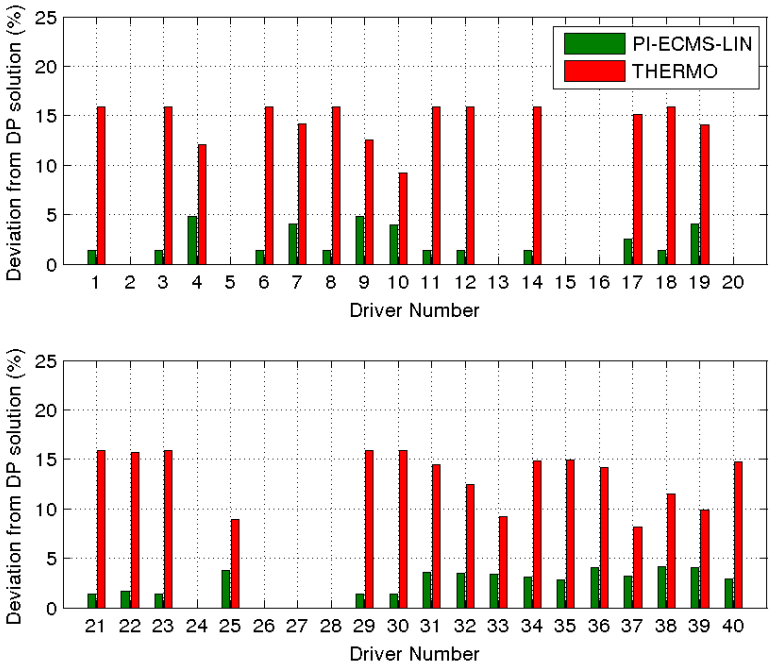

Figure 8.17: Performance of the PHEV in the real-world - percentage variation

Table 8.2: Comparison of performance of control strategies with AVL data

	DP	PI-ECMS-LIN	THERMO	Regulation 101
Average $gC0_2/km$	19.51	20.20	22.24	31.35
Variation from DP	N/A	3%	12%	38%
Variation from Reg 101	38%	36%	29%	N/A

8.5 Conclusions

The various control strategies which were developed in chapter 7 were evaluated for a number of different case studies in chapter 8. It was determined that the journey distance is one of the key factors which affects the performance of the controllers. On comparison of traditional thermostat method to the global optimal solution the fuel consumption reduces by as much as 15%. The novel control strategy proposed in chapter 7 was consistently within 5% of the DP solution. The PI-ECMS-LIN strategy performs within 1.5% of the PI-ECMS-NN. Therefore, PI-ECMS-LIN was assumed to have the ideal trade-off between computational load and predictive capabilities. This strategy is then used within an optimisation framework in chapter 10. The thermostat controller was on average 17% worse off than the PI-ECMS-LIN method. The research presented in chapter 10 shows the potential benefits of downsizing due to the adoption of a journey predictive energy management strategy.

Chapter 9

Component Sizing of PHEV

9.1 Introduction

The objective of this chapter is to present the optimisation framework by which component downsizing can be realized. It can be achieved by adoption of an advanced control strategy. The first part presents the case study and the framework. The second part of the chapter focusses on the analysis of the results for a range of different vehicle usage profiles.

9.2 Case-Study for Component Sizing

Three different drive-cycles were employed as part of the analysis; the NEDC, the ARTEMIS cycle and a real-world cycle previously discussed in Section 3.3 and in Table 9.1. For each drive-cycle, four optimisation studies have been undertaken using the PHEV model presented in chapter 7 and comparing the various control strategies from chapter 8. For each optimisation run, the AER of the PHEV was changed from 48, 64, 80 and finally 96 km (30, 40, 50 and 60 miles). Each of these AER values are classified as Design Cases 1, 2, 3 and 4 respectively. As discussed in 2.3, when considering the application of a CB strategy within a PHEV, the term AER is no longer applicable. Within the context of the results presented in this research, the baseline for comparison between the different energy management approaches is the equivalent CO_2 production over the drive-cycle.

Table 9.1: Characterization of the different drive-cycles

Parameters	NEDC	Real-World	ARTEMIS
Distance	10.93 km	29.83 km	73.02 km
Top Speed	33.33 m/s	28.04 m/s	36.60 m/s
Maximum Acceleration	1.04 m/s2	3.23 m/s2	2.86 m/s2
Number of repetitions	10	7	2
Total distance covered	109.32 km	208.81 km	146.04 km

9.3 The Optimisation Algorithm

The optimisation algorithm employed in this chapter is a local optimiser. This method has been adopted due to the fact that it is iteratively possible to work out the optimal solution. As described in the literature review in chapter 2 commercial software such as PSAT and Advisor have a prescribed rule-based algorithm to determine the best feasible size. However, the iterative algorithm does not extend to optimising the control strategy. A local optimal solution which is present within MATLAB as the function; fminsearch and represents a derivative-free local optimisation routine is selected. For a given set of initial values of the free parameters, the optimiser makes use of a neighborhood search method to identify the local optimal solution. From a review of existing literature, this algorithm has not been previously employed for optimising the powertrain components within a PHEV. However, within the broader context of automotive design, the algorithm has been successfully used for parameter estimation to predict capacity degradation within a battery [81] and for identifying the optimal transmission ratios within a hydraulic hybrid vehicle [13].

A full description of the optimisation routine underpinning fminsearch and the method for detecting convergence is provided in [47]. The optimisation method employs the Nelder-Mead simplex algorithm. A simplex is defined as a set of n + 1 points, where n represents the number of parameters to be optimised. For example, in the case where n = 2, the simplex forms a triangle around the initial solution. For a given cost function, the optimisation routine evaluates each point on the simplex to identify if it represents a better performing solution. If one is found, then a new simplex is created around that individual. Convergence is reached, when the size of the simplex has been sufficiently reduced and a better performing individual cannot be identified within the local search space [47].

9.3.1 The Optimisation Framework

As shown in Figure 9.1, in order to quantify the component downsizing opportunities associated with the use of a CB energy management approach within a PHEV, a three stage optimisation process has been employed:

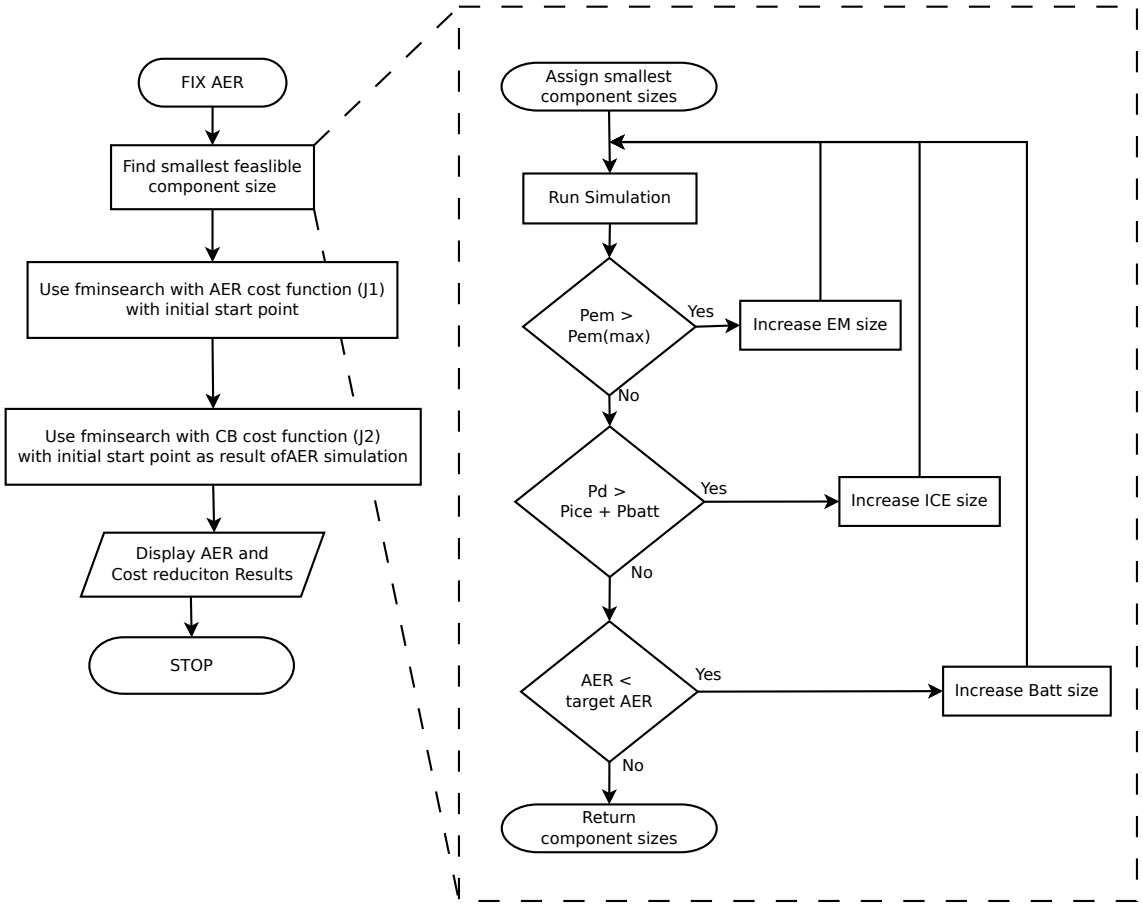

Figure 9.1: Overall component sizing procedure

Stage 1: Firstly, for a given AER and drive-cycle, the PHEV model developed in chapter 7, is executed within an iterative loop. Initial conditions for the energy capacity of the HV battery, the peak power rating of the electrical machine and volumetric size of the ICE are defined as; 9 kWh, 10 kW and 0.5 L respectively. For each execution of the model, if a component constraint is exceeded, the simulation terminates and then restarts with an increased component size. If the PHEV is able to meet the power requirements of the drive-cycle, and the HV battery is depleted to the lower threshold, the simulation terminates and the parametrisation set for the powertrain is deemed to represent the smallest feasible set of components for that drive-cycle and target AER. For this initial simulation the upper threshold of the thermostat strategy is fixed at 30% SOC. It is noteworthy that a similar approach

is adopted within the commercially available PSAT simulation environment for the sizing of EV and HEV powertrain components.

Stage 2: In the second stage the objective is to find the optimal component sizes with CD control strategy. Each vehicle combination is denoted as X with these parameters as an array.

- Engine volumetric size (Vd);
- Electric machine power ($P_{em(peak)}$);
- Battery number of strings in parallel (np);
- Upper threshold calibration for the thermostat controller (SOC_{UP}).

The cost function to be optimized is given as.

$$\begin{aligned}
&\min_{X} && J2 \\
&\text{subject to} && 0 \leq P_{ICE} \leq P_{ice(peak)} \\
& && T_{em} \leq T_{em(scaled)} \\
& && P_{b(min)} \leq P_b \leq P_{b(max)} \\
& && \text{where X is the vector of free parameters given by} \\
& && X = [V_d, P_{em(peak)}, np, SOC_{UP}] \\
& && \text{and the cost function J2 is defined by} \\
& && J2 = fn1(AER(X)) + fn2(CO_2(X)) \\
& \text{where} && \\
& && \text{fn1 and fn2 mappings are shown in figure 9.2}
\end{aligned} \tag{9.1}$$

The results from Stage 1 provide the initial conditions for each of the above input parameters. For each iteration of the optimiser, the PHEV model derived in Section 3 is executed to ascertain the vehicles AER and CO_2 emissions. These values are then weighted by parabolic functions fn1 and fn2 within J2 which are presented in Figure 9.2a and 9.2b. The weighting of the two parameters of the cost function were calibrated such that the optimisation returned the desired AER. If any of the constraints are violated an artificially high number is returned to the optimiser to deem the set of inputs as infeasible. For the final set of PHEV powertrain components, Equations 6.17 6.18 and 6.19 were used to calculate the financial cost of the powertrain.

For a given drive-cycle and target AER, the output from Stage 2, is a re-optimised set of PHEV powertrain components, including the upper threshold calibration for

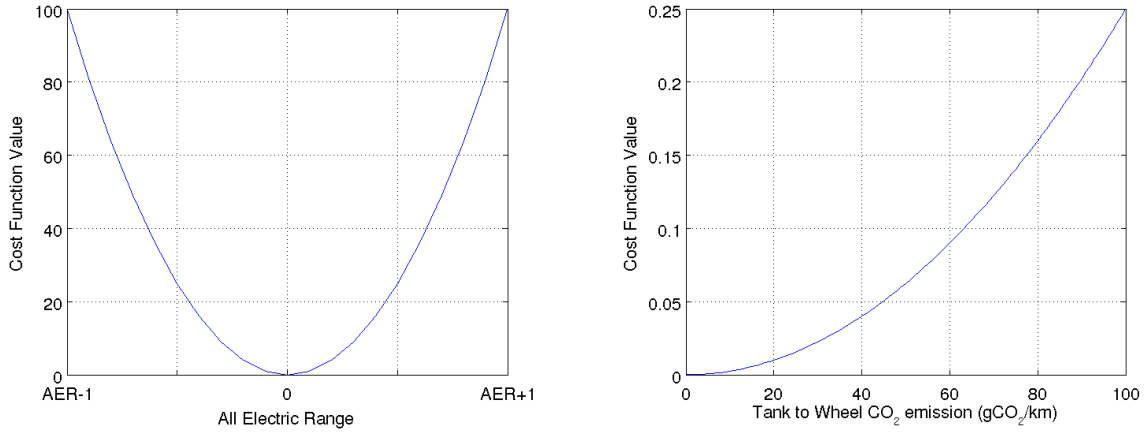

(a) Parabolic equation fn1

(b) Parabolic equation fn2

Figure 9.2: Cost function curves fn1 and fn2 for component sizing

the thermostat strategy. When comparing the results from Stage 1 and Stage 2, it is noteworthy that the optimised set of PHEV powertrain components does not necessarily equate to the smallest feasible component sizes. For example, it has been observed that the optimisation routine may return a larger electrical machine, to facilitate greater levels of regenerative braking during the drive-cycle.

Stage 3: For the same drive-cycle and AER, the final stage (Stage 3) of the optimisation framework is to quantify if further PHEV component downsizing can be realized through the use of a CB energy management strategy. The optimisation routine is seeded using the resultant values from Stage 2. Once again, for each data-set of engine volumetric size, number of parallel strings and EM peak power, the PHEV model is executed with the improved ECMS (PI-ECMS-LIN) approach. The same constraints are applied as Stage 2. With the CB approach, a linear line defines the target SOC profile across the drive-cycle. The ECMS defines the instantaneous optimal power split between the ICE and the HV battery. For each PHEV solution, the resultant CO_2 emissions and the financial cost of the hybrid powertrain are calculated, using Equations 6.17 6.18 and 6.19. In order to solve J3,

the weighting functions fn3 and fn4 are applied within the cost function J3:

$$
\begin{aligned}
&\min_{X} && J3 \\
&\text{subject to} && 0 \leq P_{ICE} \leq P_{ice(peak)} \\
& && T_{em} \leq T_{em(scaled)} \\
& && P_{b(min)} \leq P_b \leq P_{b(max)} \\
& && \text{where X is the vector of free parameters given by} \\
& && X = [V_d, P_{em(peak)}, np, SOC_{UP}] \\
& && \text{and the cost function J3 is defined by} \\
& && J3 = fn3(CO_2) + fn4(cost) \\
& \text{where} && \\
& && \text{fn1 and fn2 mappings is shown in figure 9.3}
\end{aligned}
\tag{9.2}
$$

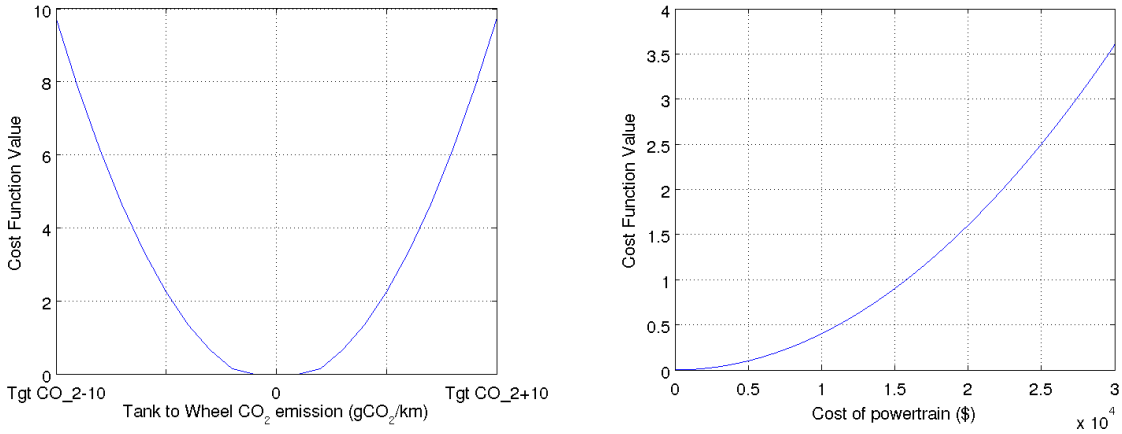

(a) Parabolic equation fn3

(b) Parabolic equation fn4

Figure 9.3: Cost function curves fn3 and fn4 for component sizing

The constraints applied to the optimisation are as previously defined by Equations 9.2. A plot of the parabolic functions, fn3 and fn4, are presented in Figure 9.3a and 9.3b. The relatively high weighting of fn3, ensures that the required target CO2 values are achieved, thereby facilitating an equitable cost comparison to be made between those PHEV solutions that employ the traditional thermostat strategy and those that have been re-optimised using the improved ECMS approach to energy management.

9.4 Results

The results of the optimisation study are shown in Table 9.2. As stated in Section 9.2 four different case studies are considered with AERs 30, 40, 50 and 60 miles respectively. For each of these case studies the three different drive-cycles NEDC, Real-world and ARTEMIS are considered. In Table 9.2, the case studies are arranged as columns and drive-cycles are arranged as rows. For illustration, the Design Case 2 with the NEDC is discussed in detail.

Table 9.2: Centroid values for each of the categories

Drivecycle: NEDC

Parameters	Design Case 1			Design Case 2			Design Case 3			Design Case 4		
	Thermostat	Improved ECMS	Change	Thermostat	Improved ECMS	Change	Thermostat	Improved ECMS	Change	Thermostat	Improved ECMS	Change
AER (miles)	30			40			50			60		
Vd (cc)	538.13	650.28	21.00%	507.82	531.9	5.00%	541.43	500.06	−8%	537.36	500.01	−7%
Pice (kW)	18.02	21.54	20.00%	16.98	17.79	5.00%	18.14	16.75	−8%	17.99	16.75	−7%
Pem (kW)	38.95	36.5	−6%	41.52	36.8	−11%	38.88	37.35	−4%	40.49	37.3	−8%
Pbat (kW)	27.32	24.33	−11%	33.21	31.95	−4%	40.19	39.12	−3%	47.88	46.51	−3%
Qbat (kWh)	13.02	11.59	−11%	15.82	15.22	−4%	19.15	18.64	−3%	22.81	22.16	−3%
TTW (gCO2/km)	69.99	70.51	1.00%	54.68	55.26	1.00%	39.62	40.12	1.00%	23.29	23.61	1.00%
Cost ($)	13538.67	12607.44	−7%	15635.85	15126.79	−3%	18118.63	17633.27	−3%	20877.84	20260.4	−3%

Drivecycle: Real−World

Parameters	Design Case 1			Design Case 2			Design Case 3			Design Case 4		
	Thermostat	Improved ECMS	Change	Thermostat	Improved ECMS	Change	Thermostat	Improved ECMS	Change	Thermostat	Improved ECMS	Change
AER (miles)	30			40			50			60		
Vd (cc)	528	562.91	7.00%	546.26	584.83	7.00%	532.27	500.57	−6%	554.58	500.42	−10%
Pice (kW)	17.65	18.66	6.00%	18.32	19.39	6.00%	17.81	16.77	−6%	18.44	16.76	−9%
Pem (kW)	41.17	40.74	−1%	44.05	42.35	−4%	44.95	41.82	−7%	46.06	43.05	−7%
Pbat (kW)	22.6	19.53	−14%	28.24	24.75	−12%	35.53	31.84	−10%	41.77	39.08	−6%
Qbat (kWh)	10.77	9.3	−14%	13.46	11.79	−12%	16.93	15.17	−10%	19.9	18.62	−6%
TTW (gCO2/km)	83.17	83.61	1.00%	77.23	77.82	1.00%	68.4	68.98	1.00%	59.97	60.55	1.00%
Cost ($)	11890.76	10846.26	−9%	13990.67	12776.07	−9%	16578.49	15143.13	−9%	18856.06	17744.06	−6%

Drivecycle: Artemis

Parameters	Design Case 1			Design Case 2			Design Case 3			Design Case 4		
	Thermostat	Improved ECMS	Change	Thermostat	Improved ECMS	Change	Thermostat	Improved ECMS	Change	Thermostat	Improved ECMS	Change
AER (miles)	30			40			50			60		
Vd (cc)	534.05	500.02	−6%	553.96	501.71	−9%	539.05	501.35	−7%	545.27	500.12	−8%
Pice (kW)	17.87	16.75	−6%	18.49	16.81	−9%	18.06	16.79	−7%	18.28	16.75	−8%
Pem (kW)	50.59	45.24	−11%	50	46.58	−7%	46.77	43.39	−7%	48.94	44.25	−10%
Pbat (kW)	29.52	27.62	−6%	34.87	33.57	−4%	42.79	41.33	−3%	50.81	49.77	−2%
Qbat (kWh)	14.07	13.16	−6%	16.61	15.99	−4%	20.39	19.69	−3%	24.21	23.71	−2%
TTW (gCO2/km)	81.98	83.37	2.00%	71.48	72.99	2.00%	57.6	59.17	3.00%	43.54	45.1	4.00%
Cost ($)	14565.78	13716.97	−6%	16486.78	15863.46	−4%	19210.74	18554.4	−3%	22117.47	21570.86	−2%

Execution for Design Case 2 and NEDC Drive-cycle

1. The first stage of execution is the iterative algorithm to determine the smallest feasible component sizes which would complete the drive-cycle with the traditional thermostat control strategy. The working of this algorithm is shown in Figure 9.1. The algorithm was executed with the upper threshold fixed at 30. The output of that iterative algorithm returned an engine size of 525cc (17.5kW) , 38 kW EM and 17 strings in parallel (16.6 kWh).

2. The second stage of execution is to use the component sizes from the previously executed iterative algorithm as the initial condition for optimisation with fminsearch. Equation 9.1 is used as the cost function and as before the objective was to obtain the lowest gCO_2/km with 40 miles AER. The main difference is that one of the control parameters is also one of the input parameters for the optimisation, therefore the best performing individual with a "tuned" thermostat controller is obtained. Figure 9.4 shows the convergence for the optimisation. In the first two iterations the AER was exceeded due to the simple sizing strategy executed in Stage 1, which caused a high cost function value. From Figure 9.5 it is observed that after obtaining the correct AER the algorithm then optimises for fuel consumption. The optimised values for the thermostat as shown in Table 9.2 is engine size of 507cc, EM size of 41 kW and battery energy capacity of 15.82 kWh. An important consideration when execution of Design Case 1 was the energy and power ratio of the battery was linked, causing the AER of 30 miles to be exceeded by 1.5 miles.

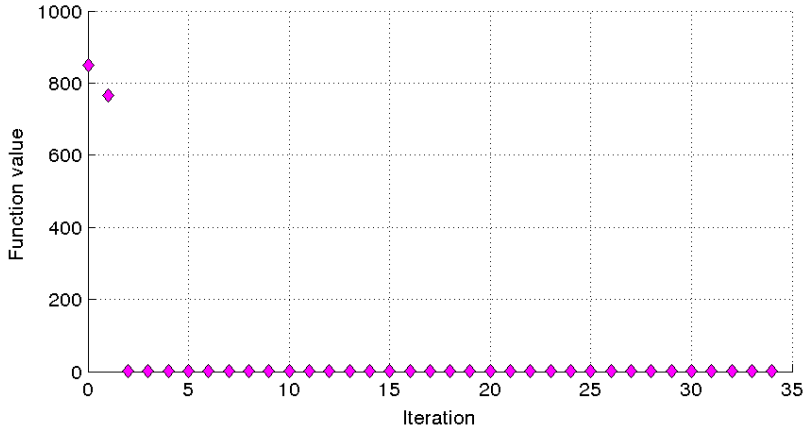

Figure 9.4: Fminsearch algorithm with cost function J2

3. The final stage of execution is the optimisation of the powertrain components with the CB strategy. The optimised values from Stage 2 are used as inputs

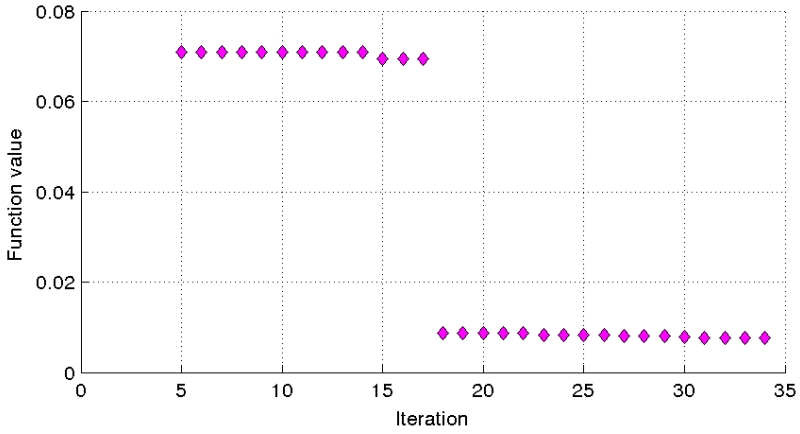

Figure 9.5: Fminsearch algorithm with cost function J2 - expanded

to the simulation. The improvement of the cost function value through the iterations is seen in Figure 9.6. As shown in Table 9.2, with CB strategy the new component sizes are engine size of 531cc, 36kW EM size and 15.22 kWh battery. Therefore, from Stage 2 to Stage 3, the engine size has increased by 5% but the battery size has reduced by 4%. The implication of this reduction in battery size is that it is possible to reduce the financial cost of the drive-train by 3% by adopting a CB strategy.

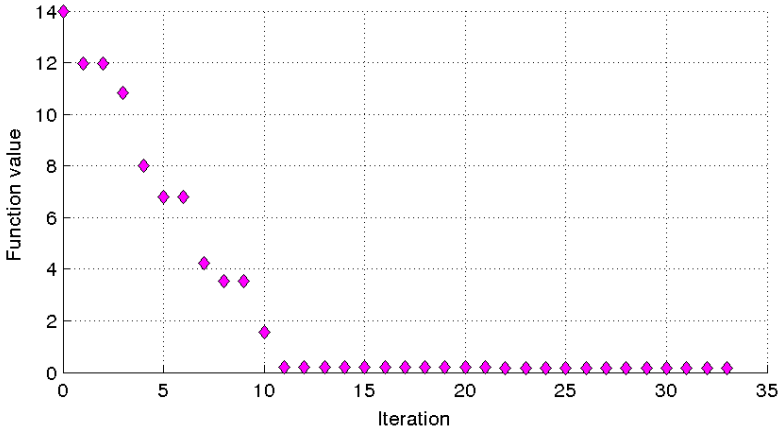

Figure 9.6: Fminsearch algorithm with cost function J3

9.4.1 PHEV Powertrain Cost Reduction

Figure 9.7 presents the total financial cost of the PHEV powertrain for the different CO_2 thresholds corresponding to the AERs of 48, 64, 80 and 96 km (30, 40, 50 and 60 miles) respectively. As it can be seen, the financial cost of the powertrain

increases as the aggressiveness of the drive-cycle increases. Inline with [82] within the context of this research, aggressiveness relates to the levels of vehicle acceleration and braking experienced within the drive-cycle. For the same energy management strategy, the PHEV powertrain cost can increase by as much as 15% when comparing the two solutions; one optimised for the NEDC and the other optimised for the more aggressive, ARTEMIS cycle. In all instances as the required AER for the PHEV increases so does the financial cost of the powertrain. For twice the AER the financial cost of the powertrain increases by a factor of 1.5. Furthermore, Figure 9.8 clearly shows that the HV battery system dominates the financial cost of the hybrid powertrain.

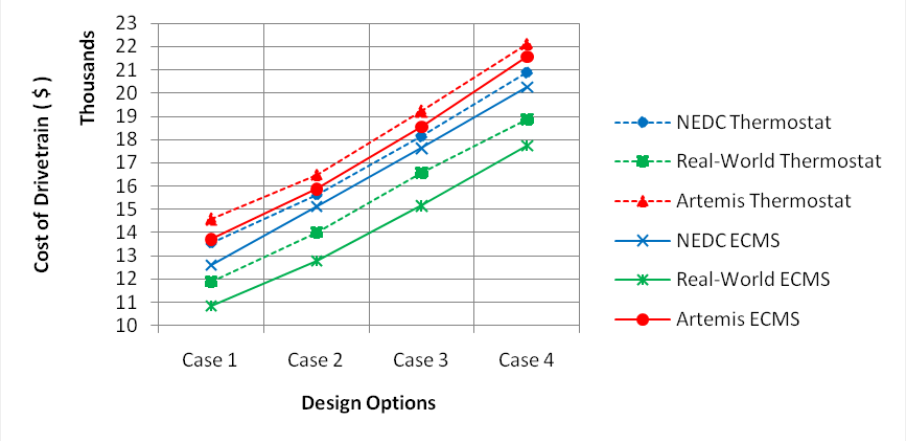

Figure 9.7: Cost reduction drive-train for CB strategy

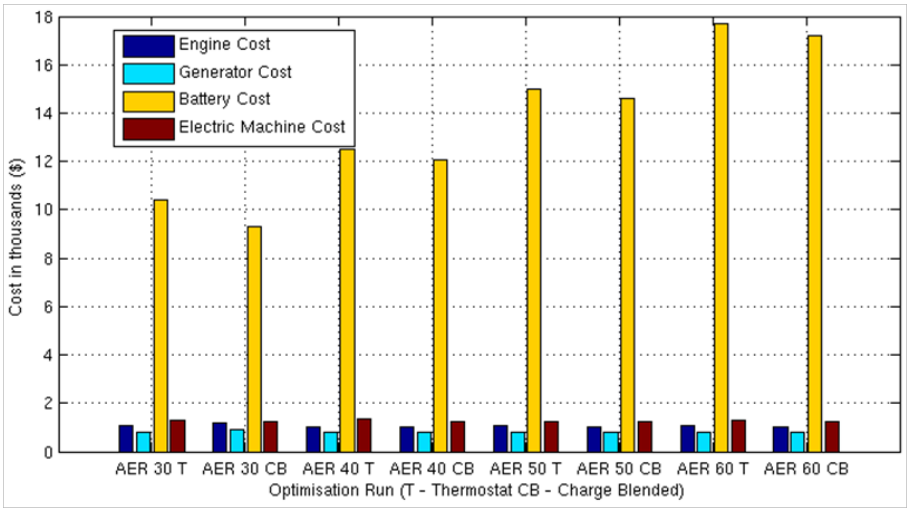

Figure 9.8: Component cost reduction for CB strategy

When comparing the impact of the energy management strategy on the financial

cost of the powertrain, Figure 9.7 highlights that optimisation of the powertrain using the improved ECMS, consistently delivers cost reductions in the order of 3% to 7%. Table 9.2 quantifies the financial cost reductions that may be achieved at the component level.

9.4.2 Downsizing of the HV Battery

Figures 9.9 and 9.10, present the downsizing opportunities within the HV battery both in terms of energy capacity and power capacity. Given the dominant cost of the HV battery system, there is a high degree of correlation between Figures 9.8, 9.9 and 9.10. When considering the different drive-cycles; (NEDC, Artemis and Real-World) for design Case 2 and CO_2 thresholds of 55, 71 and 77 g CO2/km the size of the HV battery system may be reduced by up to 3.7%, 4% and 10% respectively. The reduced requirement for energy storage onboard the vehicle, stems directly from the improved ECMS philosophy and the optimal use of both the ICE and the battery for the duration of the journey.

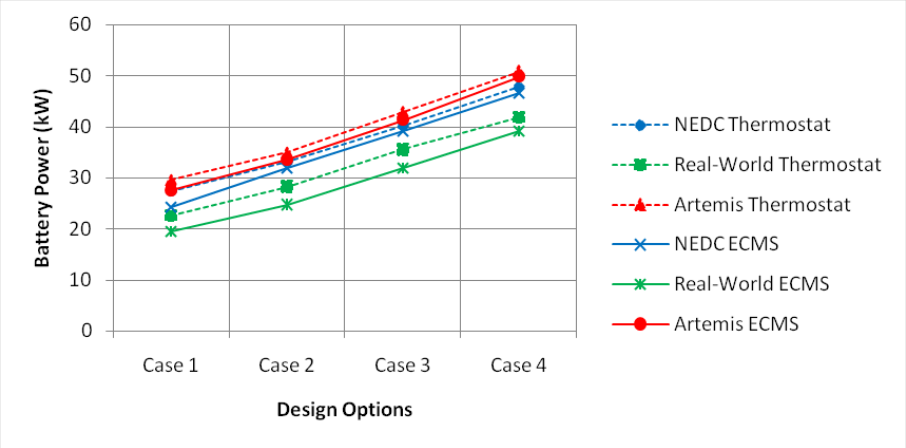

Figure 9.9: Battery power for different options

9.4.3 Optimisation of the Electrical Machine and ICE

Figure 9.11 presents a reduction in the power requirements of the electrical machine through the use of CB energy management strategy. With respect to Table 9.2 for a given drive-cycle and CO_2 threshold, reductions in the order of 3% to 7% may be realised.

As a result of the optimisation, it is noteworthy that the peak power requirement of the electrical machine may not necessarily be the same as the HV battery. When both the ICE and the battery are delivering power to the wheels, the ICE can

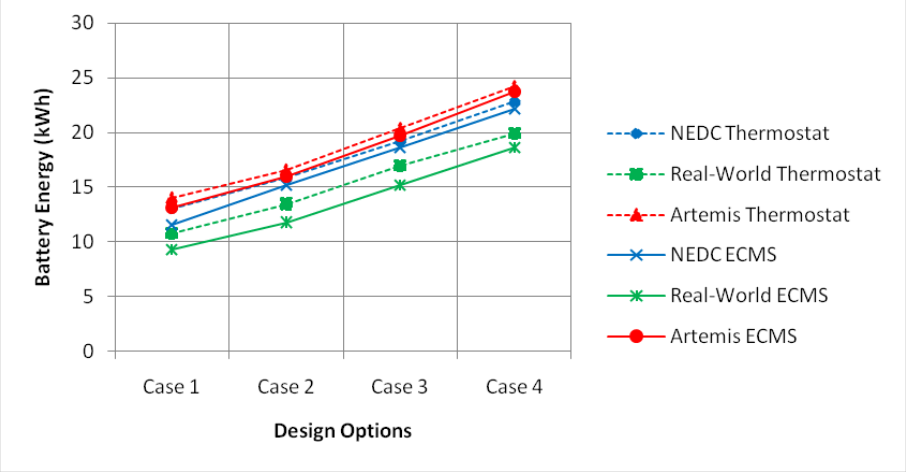

Figure 9.10: Battery energy for different options

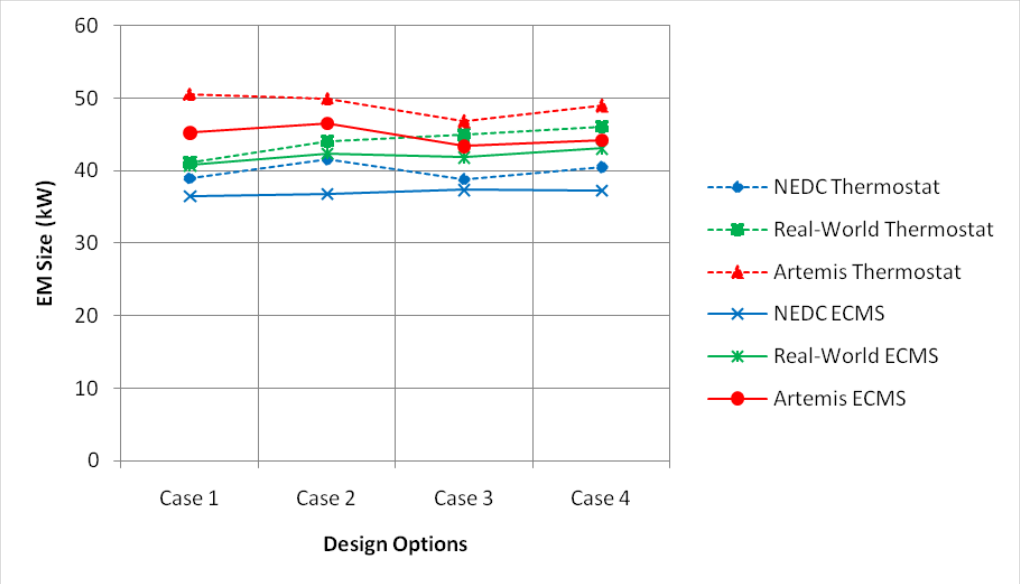

Figure 9.11: Variation of EM power for different options

assist the battery during periods of high power demand. If the PHEV employs a thermostat control strategy, this can only occur when the vehicle is operating in a CS mode. However, within a CB approach the ICE is continually able to augment the power demands placed on the electrical subsystems.

With respect to regenerative braking, depending upon the aggressiveness of the drive-cycle, it has been observed that the optimisation framework may select an electrical machine with a larger peak power rating. Under these conditions the potential to recapture energy under vehicle braking outweighs the relative disadvantages associated with a larger and heavier electrical machine.

For a volumetric capacity of 0.5 L, the optimisation framework continually limits the size of the ICE to smaller values. Across the different drive-cycles and design options only a marginal increase in the ICE is suggested by the optimiser. Figure 9.12 shows the constant value of ICE power across the different design cases.

This limitation in ICE size is due to the high penalty in emissions for its increase in size. It is interesting to note the total power to the optimiser is a constraint and different combinations of EM, battery and ICE are able to meet this power limit. However, because it is a backward facing model and the dynamic response of each of these components are not considered it would need further investigation to confirm if this down-sizing is feasible. Further, the reduced power requirements of NEDC has a negative effect on real-world performance. The vehicles would have to be resized for meeting special conditions such as gradeability. The Artemis cycle is more representative of a real-world cycle and the power demand to complete this cycle means larger battery power as seen in Figure 9.9.

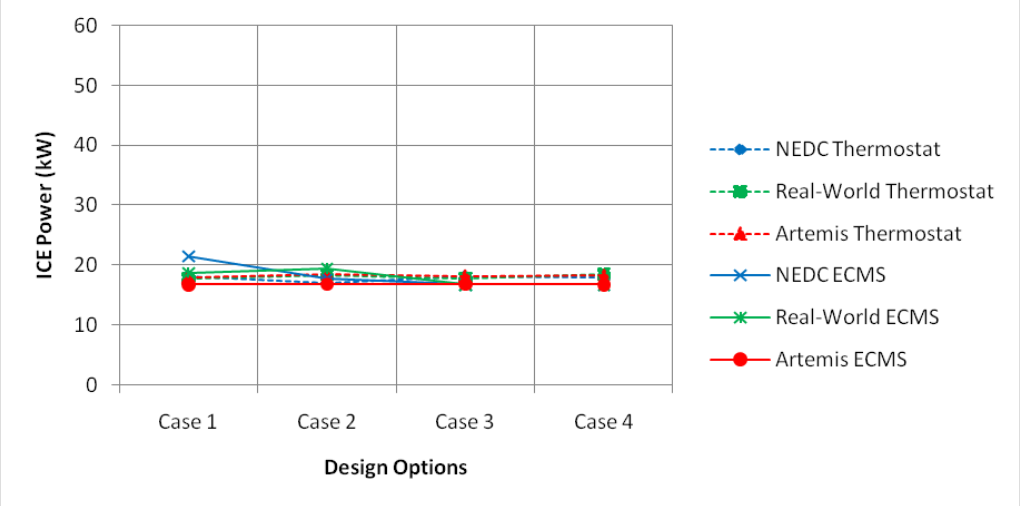

Figure 9.12: Variation of ICE power for different options

9.4.4 Balance between ICE and Battery

One of the interesting points to be noted is the balance in size of the ICE and the battery. As mentioned in the previous section the ICE increases in size as the power demand increases. The increased power demand is due to the aggressiveness of the cycle. The battery however does not correspondingly increase in size based on power demand, this is due to the consideration of the cost of the powertrain. The optimiser increases the battery size only if there is a benefit in the TTW emissions of the vehicle. This is seen with the increase in battery size as the AER increases.

9.4.5 Gradient Implications

As discussed in the previous section, the total power demand required to complete the cycle does not change. Therefore the down-sized vehicle would also be able to complete the drive-cycle. However, the overall peak power capability of the vehicle maybe reduced. This could have an effect on the grading performance of the vehicle. The height data for the real-world route is shown in Figure 9.13. The data was obtained from the on board GPS logger but the accuracy of this data is not known, however, it can be used to draw some conclusions for variations in performance based on height data. Figure 9.14 shows the wheel torque and wheel power needed to complete the real-world route with and without the gradient loads for 1046 kg mass vehicle. As can be seen around 600s the power demand is significantly higher, this was later found to be the on-ramp onto the motorway.

Clearly the down-sized vehicle will not be able to complete this drive-cycle due to the higher power demand. However, if this new power demand was considered and if the components were to be sized for the PHEV, the new ECMS strategy would reduce the component sizes and meet the new power demand compared to the conventional thermostat strategy. There is further scope to study the implications of the ultimate performance of the vehicle and component down-sizing.

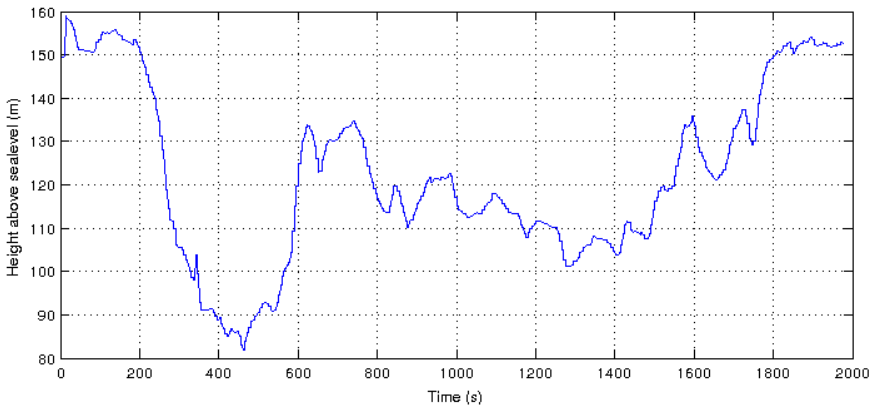

Figure 9.13: Height data for Cranfield Route

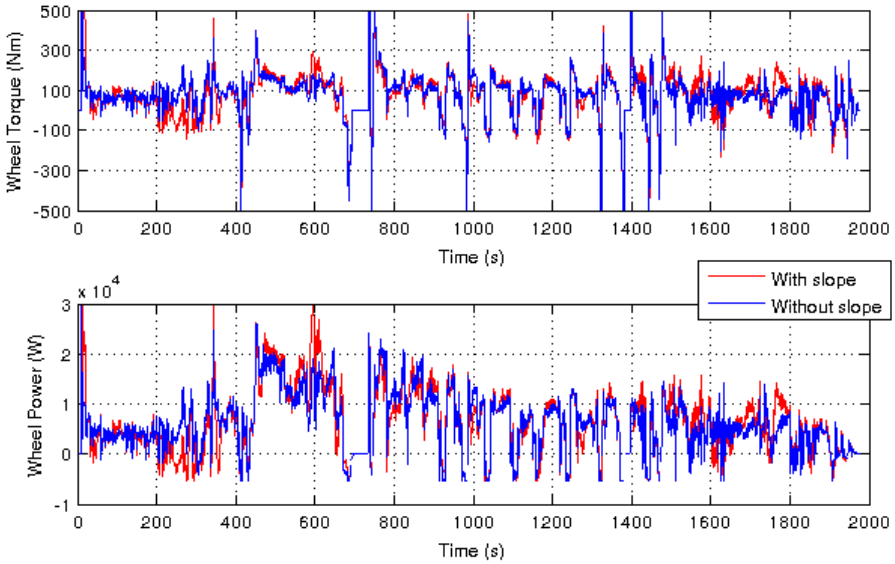

Figure 9.14: Wheel power and torque of PHEV with and without slope data

9.5 Conclusions

Contained within this chapter is an optimisation study in which the use of a CB control strategy is used to reduce the financial cost of key PHEV powertrain components. In order to properly evaluate the downsizing opportunities, comparisons are made against PHEV designs that employ a traditional thermostat strategy, in which the component sizes and controller switching thresholds have been optimised to deliver a specific AER over a drive-cycle. The results presented support those published in comparable studies which highlight that the CB approach facilitates a more energy efficient design of PHEV. For a target CO_2 value and drive-cycle, the co-optimisation of the PHEV components and the ECMS strategy has resulted in between 3% and 14% reductions in the energy and power requirements of the HV battery. Since the HV battery represents the single largest contributor to vehicle mass and powertrain cost, it is proposed that potential cost reductions in the order of 3% 9%, would further support the adoption of PHEVs.

Chapter 10

Conclusions

The thesis presented a design process for the evaluation of a journey predictive type energy management strategy for a PHEV. The aim was to evaluate the potential benefit of predictive journey information on fuel economy and powertrain financial cost. It was found that this approach gave lower TTW emissions compared to standard rule-based controllers. Further, this benefit could then be translated to financial cost reduction of key powertrain components through a process of systems optimisation and downsizing.

The work presented in this thesis focusses on the intersection of three research areas. A summary of the novelty and contribution to science is presented in Table 10.1.

10.1 Real-World Usage Analysis

The real-world usage analysis was performed using the Smart ED dataset from the EV evaluational programme and as such the results are constrained to the class of the vehicle employed. Two different approaches were evaluated.

- The first approach made use of a homogeneous classification scheme based on euclidean distance. This method was previously proposed in [23] and [82]. The classification method was applied to the Smart ED dataset and compared to the results presented in [82]. However, it was found this method is effective only if there is a large data-set with equal representation of the various road categories. Further, since the classification scheme is not based on any pre-established categories it becomes difficult to compare the final results to previous publications.
- The second approach made use of a NN. The NN was used to identify the four road categories and a set of rules was proposed to identify the traffic

conditions within the sub-categories. From comparison of the real-world classification to existing drive-cycles it was determined that the framework and dataset is transferable to other vehicle classes within an urban environment. Further, the NN framework can be re-trained for different vehicle classes and is highly transferable. The NN framework was extended by means of an energy prediction algorithm. Experimental results, exploring the feasibility of this concept, show a good correlation and accuracy within 20% to 30% when comparing predicted and measured energy consumptions for over 800 real-world journeys.

10.2 Scalable PHEV Model

In order to evaluate the downsizing opportunities available due to the adoption of a more effective energy management strategy, a scalable backward PHEV model was developed. Parametrisation of the electrical components within the PHEV model was done using data obtained experimentally by Cenex from a fleet of EVs operating in the real-world. One of the main limitations associated with the data-set is the restricted power range over which data was recorded. The accuracy of the base model was verified by comparison of the real-world change in SOC to the simulated change in SOC. The drop in overall accuracy of the model (68%) could be primarily attributed to the erroneous height data which did not allow accurate estimation of the torque at the wheels.

Data for the scalable model of the ICE was obtained from previously published research [32]. The model was verified by building a conventional Smart drive-train and comparing the fuel consumption to the published legislative rating.

10.3 Energy Management Control System

To investigate the overall additional improvement potential available by control strategy, DP was used in order to find the global optimal solution for different drive-cycles and varying lengths.

It was identified that the fuel economy benefits by DP was by as much as 15% on comparison to standard rule-based algorithms such as the thermostat approach. A novel control strategy was proposed based on the established ECMS to include journey predictive capabilities within the controller. A feedback path based on distance and SOC were included which improved the performance of the base controller. Various derivatives of the controller were studied and it was found that overall the ECMS based controllers were within 5% of the DP solution.

The NN based solution for the prediction of energy consumption across a trip was integrated into the control system to identify the best SOC trajectory. This controller (PI-ECMS-NN) was within 3.5% of the DP solution and it is envisaged that by further online tuning of this controller, the performance can be further improved.

A simpler strategy to PI-ECMS-NN was PI-ECMS-LIN for which only the journey distance had to be known a priori. Only with this information PI-ECMS-LIN performs within 1.5% PI-ECMS-NN. Therefore, this controller was adopted as a suitable compromise so that the components could be sized within an optimisation framework. Therefore, a novel control strategy was proposed which performs within 5% of the DP solution and benefits by as much as 17% can be realised on comparison to a traditional thermostat controller.

An interesting addition to the study was the evaluation of the PHEV over Regulation 101. The ideal component configuration to obtain the best fuel consumption over the legislative procedure was done using GA. One of the main drawbacks discussed was the non-applicability of a CB strategy for Regulation 101. The PHEV performance during Regulation 101 was compared to 40 drivers operating in the real-world for a two week period. It was determined that the TTW emissions vary significantly based on user behaviour and in this case the Regulation 101 was on average 38% worse off than the DP solution. A key conclusion is that across the 40 drivers the TTW emissions of PI-ECMS-LIN are within 3% of the DP solution.

10.4 Component-Sizing and Optimisation

A new optimisation framework was proposed which enabled the reduction of the financial cost of key PHEV powertrain components by adoption of a CB control strategy. In order to properly evaluate the downsizing opportunities, comparisons are made against PHEV designs that employ the thermostat strategy, in which the component sizes and controller switching thresholds have been optimized to deliver a specific AER over a drive-cycle. The results presented support those published in comparable studies which highlight that the CB approach facilitates a more energy efficient design of PHEV. For a target CO_2 value and drive-cycle, the co-optimization of the PHEV components and the ECMS strategy has resulted in between 3% and 14% reductions in the energy and power requirements of the battery. Since the battery represents the single largest contributor to vehicle mass and powertrain cost, it is proposed that potential cost reductions in the order of 3%–9%, would further support the sustainable market introduction of this variant of low carbon vehicle.

Table 10.1: Claim of novelty

Area of Novelty	Research to date	Novelty
Energy prediction across trip	Studies have acknowledged the importance of energy prediction. However, to date the solutions built are based on probabilistic approaches or based on readily available information such as speed limits. Some research publications assume they would be available in the future with the development of transport infrastructure.	A NN based framework is proposed to analyse existing data and determine the road-type in Chapter 4. This methodology was extended to predict the energy across a trip. The NN based framework has applications in the transport sector, as fleet management tools, journey predictive energy management controllers and online range estimators which would aid the adoption of EVs.
Journey predictive ECMS	Several strategies have been proposed to improve the performance of the ECMS controller. They include the use of complex sigmoidal functions to constant values to represent the equivalence ratio.	Several approaches have been studied in detail in Chapter 7 and 8. A novel control strategy was developed using journey distance as a key variable. Performance was found to be close to the DP solution.
Component size optimisation	Few studies were published with a rule-based sizing approach. No comprehensive study has been done with an optimisation framework.	An optimisation framework has been proposed in Chapter 9 which addresses the advantages of use of journey predictive energy management strategy. Components could be down-sized with no significant increase in TTW emissions.

10.5 Further Work

Further work would be the investigation of the performance of such a controller in a forward model with the additional dynamics of the drive-train included. In particular, the ICE is assumed to operate instantaneously and this could have implications on the final solution. Some initial studies were done in [37] where the emissions of the PHEV increased by 2% with the additional dynamics of engine inertia and manifold air.

Throughout the research the thermal aspect had been ignored due to non-availability of useful data. A parameter varying model of the battery and integration of cold-start maps of the ICE into the ECMS strategy would be a key addition to improve the performance of the controller in the real-world.

Regenerative braking affects the amount of "free-energy" available and hence has a significant effect on the TTW emissions. Unfortunately, with the given dataset it was not possible to determine the strategy employed and hence the true potential of the system could not be exploited. An interesting area of research would be to identify the further downsizing opportunities with a more aggressive regenerative braking strategy.

On determining the ideal SOC trajectory PI-ECMS is very close to the DP solution. Possible alternatives rather than a mean-value lookup table based solution to predict the energy across the trip could achieve further improvements of the control system.

Finally, it was determined that with the correct tuning of the gains of the PI controller and knowing the ideal SOC trajectory the PI-ECMS could achieve the DP solution. For very high gains the error in SOC trajectory gets reduced at the expense of excessive use of the ICE and the fuel consumption increases. Similarly for very low gain values the deviation becomes significantly large leading to sub-optimal performance. An interesting area of research would be to identify the possible alternatives to the PI controller which has more intelligence and could self-tune to achieve the best trade-off point.

References

[1] Abdollahi, A. (2006). An intelligent control strategy in a parallel hybrid vehicle. In *IEEE Conference on Electric and Hybrid Vehicles*, pages 1 –2. IEEE.

[2] André, M. (2004). The ARTEMIS European driving cycles for measuring car pollutant emissions. *Science of the Total Environment*, 334:73–84.

[3] Bauman, J. and Kazerani, M. (2008). A comparative study of fuel-cell–battery, fuel-cell–ultracapacitor, and fuel-cell–battery–ultracapacitor vehicles. *IEEE Transactions on Vehicular Technology*, 57(2):760–769.

[4] Beachley, H. and Frank, A. (1973). Electric and electric-hybrid cars-evaluation and comparison. *SAE Technical Paper*, 730619.

[5] Bellman, R. E. (1957). *Dynamic Programming*. Princeton University Press.

[6] Bradley, T. and Frank, A. (2009). Design, demonstrations and sustainability impact assessments for plug-in hybrid electric vehicles. *Renewable and Sustainable Energy Reviews*, 13(1):115–128.

[7] Browning, L. and Unnasch, S. (2001). Hybrid electric vehicle commercialization issues. In *The Sixteenth Annual Battery Conference on Applications and Advances*, page 45. IEEE.

[8] Burch, S., Cuddy, M., and Markel, T. (1999). Advisor 2.1 documentation. *National Renewable Energy Laboratory*.

[9] Carroll, S. and Walsh, C. (2011). The smart move case studies. Technical report, Cenex.

[10] Chan, C. (2007). The state of the art of electric, hybrid, and fuel cell vehicles. *Proceedings of the IEEE*, 95(4):704–718.

[11] Chaulieu, O. (2010). Optimal battery sizing for plug-in hybrid electric vehicle. Master's thesis, Cranfield University, Department of Automobile Engineering.

[12] Chen, Z., Kiliaris, L., Murphey, Y., and Masrur, M. (2009). Intelligent power management in SHEV based on roadway type and traffic congestion levels. In *Vehicle Power and Propulsion Conference, 2009. VPPC'09. IEEE*, pages 915–920. IEEE.

[13] Cheong, K. L., Li, P. Y., and Chase, T. R. (2011). Optimal design of power-split transmissions for hydraulic hybrid passenger vehicles. In *American Control Conference (ACC)*, pages 3295–3300. IEEE.

[14] Cho, B. (2008). *Control of a hybrid electric vehicle with predictive journey estimation*. PhD thesis, Cranfield University.

[15] Cocron, P., Buhler, F., Neumann, I., Franke, T., Krems, J., Schwalm, M., and Keinath, A. (2011). Methods of evaluating electric vehicles from a user's perspective-the mini e field trial in Berlin. *Intelligent Transport Systems, IET*, 5(2):127–133.

[16] Contestabile, M., Offer, G., Slade, R., Jaeger, F., and Thoennes, M. (2011). Battery electric vehicles, hydrogen fuel cells and biofuels. which will be the winner? *Energy & Environmental Science*, 4(10):3754–3772.

[17] De Vlieger, I. (1997). On board emission and fuel consumption measurement campaign on petrol-driven passenger cars. *Atmospheric Environment*, 31(22):3753–3761.

[18] De Vlieger, I., De Keukeleere, D., and Kretzschmar, J. (2000). Environmental effects of driving behaviour and congestion related to passenger cars. *Atmospheric Environment*, 34(27):4649–4655.

[19] Deb, K., Pratap, A., Agarwal, S., and Meyarivan, T. (2002). A fast and elitist multiobjective genetic algorithm: NSGA-II. *IEEE Transactions on Evolutionary Computation*, 6(2):182–197.

[20] DEFRA (2012). 2012 guidelines to defra / deccs ghg conversion factors for company reporting. `http://www.defra.gov.uk/publications/files/pb13792-emission-factor-methodology-paper-120706.pdf`.

[21] Egbue, O. and Long, S. (2012). Barriers to widespread adoption of electric vehicles: An analysis of consumer attitudes and perceptions. *Energy Policy*, 48(0):717 – 729.

[22] Ehsani, M., Gao, Y., Guy, S. E., and Emadi, A. (2005). *Modern Electric, Hybrid Electric, and Fuel Cell Vehicles: Fundamentals, Theory and Design*. CRC.

[23] Ericsson, E. (2001). Independent driving pattern factors and their influence on fuel-use and exhaust emission factors. *Transportation Research Part D: Transport and Environment*, 6(5):325–345.

[24] Freyermuth, V., Fallas, E., and Rousseau, A. (2008a). Comparison of powertrain configuration for plug-in hevs from a fuel economy perspective. *SAE Technical Paper*, 2008-01-0461.

[25] Freyermuth, V., Fallas, E., and Rousseau, A. (2008b). Comparison of powertrain configuration for plug-in hevs from a fuel economy perspective. *SAE paper*, pages 01–0461.

[26] Gong, Q., Li, Y., and Peng, Z. (2007a). Optimal power management of plug-in hev with intelligent transportation system. In *IEEE/ASME International Conference on Advanced Intelligent Mechatronics*, pages 1–6. IEEE.

[27] Gong, Q., Li, Y., and Peng, Z. (2007b). Trip based power management of plug-in hybrid electric vehicle with two-scale dynamic programming. In *Vehicle Power and Propulsion Conference*, pages 12–19. IEEE.

[28] Gong, Q., Li, Y., and Peng, Z. (2008a). Trip-based optimal power management of plug-in hybrid electric vehicles. *IEEE Transactions on Vehicular Technology*, 57(6):3393–3401.

[29] Gong, Q., Li, Y., and Peng, Z. (2008b). Trip based optimal power management of plug-in hybrid electric vehicles using gas-kinetic traffic flow model. In *American Control Conference, 2008*, pages 3225–3230. IEEE.

[30] Gong, Q., Li, Y., and Peng, Z. (2009a). Power management of plug-in hybrid electric vehicles using neural network based trip modeling. In *American Control Conference, 2009. ACC'09.*, pages 4601–4606. IEEE.

[31] Gong, Q., Li, Y., and Peng, Z. (2009b). Trip based optimal power management of plug-in hybrid electric vehicle with advanced traffic modeling. *SAE International Journal of Engines*, 1(1):861–872.

[32] Guzzella, L. and Sciarretta, A. (2005). *Vehicle propulsion systems: introduction to modeling and optimization*. Springer Verlag.

[33] Harrington, C. (2012). *Reference Architecture*. Phd thesis, Cranfield University.

[34] Harrington, C., Marco, J., and Vaughan, N. (2012). The design of a reference control architecture to support vehicle hybridisation. *International Journal of Vehicle Design*, 60(3):206–224.

[35] Huang, X., Tan, Y., and He, X. (2011). An intelligent multifeature statistical approach for the discrimination of driving conditions of a hybrid electric vehicle. *IEEE Transactions on Intelligent Transportation Systems*, 12(2):453–465.

[36] Jeon, S., Jo, S., Park, Y., and Lee, J. (2002). Multi-mode driving control of a parallel hybrid electric vehicle using driving pattern recognition. *Journal of Dynamic Systems, Measurement, and Control*, 124(1):141–149.

[37] Kallur Krishnamoorthy, R. (2012). *Real-time local optimal control development for a plug-in hybrid electric vehicle*. Msc thesis, Cranfield University.

[38] Kamble, S. H., Mathew, T. V., and Sharma, G. (2009). Development of real-world driving cycle: Case study of Pune, India. *Transportation Research Part D: Transport and Environment*, 14(2):132–140.

[39] Karbowski, D., Rousseau, A., Pagerit, S., and Sharer, P. (2006). Plug-in vehicle control strategy: from global optimization to real time application. In *22nd Electric Vehicle Symposium, EVS22, Yokohama, Japan*.

[40] Kelly, K., Mihalic, M., and Zolot, M. (2002). Battery usage and thermal performance of the Toyota Prius and Honda Insight during chassis dynamometer testing. In *Battery Conference on Applications and Advances, 2002. The Seventeenth Annual*, pages 247–252. IEEE.

[41] Kirk, D. (2004). *Optimal Control Theory: an Introduction*. Dover Publications.

[42] Kohonen, T. (1990). The self-organizing map. *Proceedings of the IEEE*, 78(9):1464–1480.

[43] Koo, E., Lee, H., Sul, S., and Kim, J. (1998). Torque control strategy for a parallel hybrid vehicle using fuzzy logic. In *Industry Applications Conference, 1998. Thirty-Third IAS Annual Meeting. The 1998 IEEE*, volume 3, pages 1715–1720. IEEE.

[44] Kuhler, M. and Karstens, D. (1978). *Improved driving cycle for testing automotive exhaust emissions*. Society of Automotive Engineers.

[45] Kurani, K., Axsen, J., Caperello, N., Davies, J., and Stillwater, T. (2010). Plug-in hybrid electric vehicle (phev) demonstration and consumer education, outreach, and market research program, volumes i and ii. *Plugin Hybrid Electric Vehicle Research Center. Institute of Transportation Studies, University of California, Davis*.

[46] Kwon, J., Kim, J., Fallas, E., Pagerit, S., and Rousseau, A. (2008). Impact of drive cycles on phev component requirements. *SAE paper*, pages 01–1337.

[47] Lagarias, J. C., Reeds, J. A., Wright, M. H., and Wright, P. E. (1998). Convergence properties of the Nelder–Mead simplex method in low dimensions. *SIAM Journal on Optimization*, 9(1):112–147.

[48] Langari, R. and Won, J. (2003). Integrated drive cycle analysis for fuzzy logic based energy management in hybrid vehicles. In *The 12th IEEE International Conference on Fuzzy Systems*, volume 1, pages 290–295. IEEE.

[49] Langari, R. and Won, J. (2005). Intelligent energy management agent for a parallel hybrid vehicle-part i: system architecture and design of the driving situation identification process. *IEEE Transactions on Vehicular Technology,*, 54(3):925–934.

[50] Liaw, B. and Dubarry, M. (2007). From driving cycle analysis to understanding battery performance in real-life electric hybrid vehicle operation. *Journal of Power Sources*, 174(1):76–88.

[51] Lin, C., Jeon, S., Peng, H., and Lee, J. (2004). Driving pattern recognition for control of hybrid electric trucks. *Vehicle System Dynamics*, 42(1-2):41–58.

[52] Lin, J. and Niemeier, D. (2003). Regional driving characteristics, regional driving cycles. *Transportation Research Part D: Transport and Environment*, 8(5):361–381.

[53] Markel, T. and Wipke, K. (2001). Modeling grid-connected hybrid electric vehicles using ADVISOR. In *The Sixteenth Annual Battery Conference on Applications and Advances*, pages 23–29. IEEE.

[54] Daimler AG. (2012). Technical data - smart.

[55] Department of Transport (2010). Plug-in car grant. `http://www.dft.gov.uk/publications/plug-in-car-grant/`.

[56] Mathworks Inc. (2013). kmeans. `http://www.mathworks.co.uk/help/stats/kmeans.html`.

[57] Zytek Automotive (2013). Smart electric drive. `http://www.zytekautomotive.co.uk/Products/CaseStudies/smartElectricDrive.aspx`.

[58] Montazeri-Gh, M., Ahmadi, A., and Asadi, M. (2008). Driving condition recognition for genetic-fuzzy hev control. In *3rd International Workshop on Genetic and Evolving Systems*, pages 65–70. IEEE.

[59] Moura, S., Callaway, D., Fathy, H., and Stein, J. (2010). Tradeoffs between battery energy capacity and stochastic optimal power management in plug-in hybrid electric vehicles. *Journal of Power Sources*, 195(9):2979–2988.

[60] Moura, S., Fathy, H., Callaway, D., and Stein, J. (2011). A stochastic optimal control approach for power management in plug-in hybrid electric vehicles. *IEEE Transactions on Control Systems Technology*, 19(3):545–555.

[61] Murphey, Y., Chen, Z., Kiliaris, L., Park, J., Kuang, M., Masrur, A., and Phillips, A. (2008). Neural learning of driving environment prediction for vehicle power management. In *IEEE International Joint Conference on Neural Networks (IEEE World Congress on Computational Intelligence)*, pages 3755–3761. IEEE.

[62] Musardo, C., Rizzoni, G., Guezennec, Y., and Staccia, B. (2005). A-ecms: An adaptive algorithm for hybrid electric vehicle energy management. *European Journal of Control*, 11(4-5):509.

[63] Newman, P., Kenworthy, J., and Lyons, T. (1992). The ecology of urban driving iidriving cycles across a city: their validation and implications. *Transportation Research Part A: Policy and Practice*, 26(3):273–290.

[64] O'Keefe, M. and Markel, A. (2006). Dynamic programming applied to investigate energy management strategies for a plug-in hev. Technical report, National Renewable Energy Laboratory.

[65] ordnancesurvey.co.uk (2011). Road type esri shape files.

[66] Paganelli, G., Delprat, S., Guerra, T., Rimaux, J., and Santin, J. (2002). Equivalent consumption minimization strategy for parallel hybrid powertrains. In *Vehicular Technology Conference, VTC Spring. IEEE 55th*, volume 4, pages 2076–2081. IEEE.

[67] Paganelli, G., Ercole, G., Brahma, A., Guezennec, Y., and Rizzoni, G. (2001a). General supervisory control policy for the energy optimization of charge-sustaining hybrid electric vehicles. {*JSAE*} *Review*, 22(4):511 – 518.

[68] Paganelli, G., Guerra, T., Delprat, S., Santin, J., Delhom, M., and Combes, E. (2000). Simulation and assessment of power control strategies for a parallel hybrid car. *Proceedings of the Institution of Mechanical Engineers, Part D: Journal of Automobile Engineering*, 214(7):705–717.

[69] Paganelli, G., Tateno, M., Brahma, A., Rizzoni, G., and Guezennec, Y. (2001b). Control development for a hybrid-electric sport-utility vehicle: strategy,

implementation and field test results. In *Proceedings of American Control Conference*, volume 6, pages 5064–5069. IEEE.

[70] Pesaran, A. (2010). *Battery Ownership Model: A Tool for Evaluating the Economics of Electrified Vehicles and Related Infrastructure*. National Renewable Energy Laboratory.

[71] Pesaran, A., Markel, T., Tataria, H., and Howell, D. (2009). *Battery Requirements for Plug-in Hybrid Electric Vehicles–analysis and Rationale*. National Renewable Energy Laboratory.

[72] Piccolo, A., Ippolito, L., and Vaccaro, A. (2001). Optimisation of energy flow management in hybrid electric vehicles via genetic algorithms. In *IEEE/ASME International Conference on Advanced Intelligent Mechatronics*, volume 1, pages 434–439. IEEE.

[73] Rizzoni, G., Guzzella, L., and Baumann, B. (1999). Unified modeling of hybrid electric vehicle drivetrains. *IEEE/ASME Transactions on Mechatronics*, 4(3):246–257.

[74] Rousseau, A., Pagerit, S., and Gao, D. (2008). Plug-in hybrid electric vehicle control strategy parameter optimization. *Journal of Asian Electric Vehicles*, 6(2):1125–1133.

[75] Sanna, L. (2005). Driving the solution, the plug-in hybrid vehicle. *EPRI Journal*, pages 8–17.

[76] Sciarretta, A. and Guzzella, L. (2007). Control of hybrid electric vehicles. *Control Magazine, IEEE*, 27(2):60–70.

[77] Serrao, L., Onori, S., and Rizzoni, G. (2011). A comparative analysis of energy management strategies for hybrid electric vehicles. *Journal of Dynamic Systems, Measurement, and Control*, 133(3):031012.

[78] Simpson, A. et al. (2006). *Cost-benefit analysis of plug-in hybrid electric vehicle technology*. National Renewable Energy Laboratory.

[79] Sisternes, F. J. (2010). Plug-in electric vehicle introduction in the eu. Master's thesis, Massachusetts Institute of Technology.

[80] Staackmann, M., Liaw, B., and Yun, D. (1997). Dynamic driving cycle analyses using electric vehicle time-series data. In *Energy Conversion Engineering Conference, 1997. IECEC-97., Proceedings of the 32nd Intersociety*, volume 3, pages 2014–2018. IEEE.

[81] Stamps, A. T., Holland, C. E., White, R. E., and Gatzke, E. P. (2005). Analysis of capacity fade in a lithium ion battery. *Journal of Power Sources*, 150:229–239.

[82] Standley, G., Marco, J., and Cho, B. (2010). The impact of vehicle usage and recharging infrastructure on the energy storage requirements of a plug-in hybrid electric vehicle. *International Journal of Electric and Hybrid Vehicles*, 2(3):222–239.

[83] Tara, E., Shahidinejad, S., Filizadeh, S., and Bibeau, E. (2010). Battery storage sizing in a retrofitted plug-in hybrid electric vehicle. *IEEE Transactions on Vehicular Technology*, 59(6):2786–2794.

[84] Tate, E. and Boyd, S. (2000). Finding ultimate limits of performance for hybrid electric vehicles. *SAE Transactions*, 109(6):2437–2448.

[85] Tulpule, P., Marano, V., and Rizzoni, G. (2010). Energy management for plug-in hybrid electric vehicles using equivalent consumption minimisation strategy. *International Journal of Electric and Hybrid Vehicles*, 2(4):329–350.

[86] Turrentine, T., Garas, D., Lentz, A., Woodjack, J., Ejlalmaneshan, S., Kurani, K., and Nicholas, M. (2011). The UC Davis mini e consumer study. Technical report, UC Davis.

[87] UNECE (2005). Regulation no. 101 emissions of carbon dioxide and fuel consumption. Technical report, United Nations.

[88] Unnasch, S., Kassoy, E., Counts, R., Powars, C., Browning, L., Santini, D., Vyas, A., Taylor, D., Smith, J., Markel, T., Kalhammer, F., Graham, R., Miller, A., Frank, A., Schurhoff, R., Duvall, M., Reisen, S., Kosowski, M., Bush, R., and Warf, W. (2001). Comparing the benefits and impacts of hybrid electric vehicle options. Technical report, EPRI.

[89] VoltStats (2012). Tracking real world usage of Chevrolet Volts in the wild.. `http://www.voltstats.net/`.

[90] Wang, R. and Lukic, S. (2011). Review of driving conditions prediction and driving style recognition based control algorithms for hybrid electric vehicles. In *Vehicle Power and Propulsion Conference (VPPC)*, pages 1–7. IEEE.

[91] Williamson, S. (2007). Electric drive train efficiency analysis based on varied energy storage system usage for plug-in hybrid electric vehicle applications. In *Power Electronics Specialists Conference*, pages 1515–1520. IEEE.

[92] Wipke, K. B., Cuddy, M. R., and Burch, S. D. (1999). Advisor 2.1: a user-friendly advanced powertrain simulation using a combined backward/forward approach. *IEEE Transactions on Vehicular Technology*, 48(6):1751–1761.

[93] Wirasingha, S. and Emadi, A. (2011). Classification and review of control strategies for plug-in hybrid electric vehicles. *IEEE Transactions on Vehicular Technology*, 60(1):111–122.

[94] Wirasingha, S., Schofield, N., and Emadi, A. (2008). Plug-in hybrid electric vehicle developments in the US: Trends, barriers, and economic feasibility. In *Vehicle Power and Propulsion Conference, 2008. VPPC'08*, pages 1–8. IEEE.

[95] Wu, X., Cao, B., Li, X., Xu, J., and Ren, X. (2011). Component sizing optimization of plug-in hybrid electric vehicles. *Applied Energy*, 88(3):799–804.

[96] Wu, X., Cao, B., Wen, J., and Bian, Y. (2008). Particle swarm optimization for plug-in hybrid electric vehicle control strategy parameter. In *Vehicle Power and Propulsion Conference, 2008. VPPC'08. IEEE*, pages 1–5. IEEE.

[97] Yi, T., Xin, Z., Liang, Z., and Xinn, Z. (2009). Intelligent energy management based on driving cycle identification using fuzzy neural network. In *Second International Symposium on Computational Intelligence and Design*, volume 2, pages 501–504. IEEE.

[98] Yushan, L., Qingliang, Z., Chenglong, W., and Yuanjie, L. (2010). Research on fuzzy logic control strategy for a plug-in hybrid electric city public bus. In *International Conference on Measuring Technology and Mechatronics Automation (ICMTMA)*, volume 3, pages 88–91. IEEE.

[99] Zhang, C. and Vahid, A. (2010). Real-time optimal control of plug-in hybrid vehicles with trip preview. In *American Control Conference (ACC*, pages 6917–6922. IEEE.

[100] Zhang, C. and Vahidi, A. (2012). Route preview in energy management of plug-in hybrid vehicles. *IEEE Transactions on Control Systems Technology*, 20(2):546–553.

Chapter 11

Appendix

11.1 Schedule of the Training Dataset for the Smart

	Driver	1	2	3	4	5	6	7	8	9	10		Driver	1	2	3	4	5	6	7	8	9	10
	M 9:45 AM	x											M 9:45 AM										
16/02/2011	A 1:15 PM											03/03/2011	A 1:15 PM		x								
	E 4:45 PM												E 4:45 PM			x							
	M 9:45 AM												M 9:45 AM										
17/02/2011	A 1:15 PM											04/03/2011	A 1:15 PM				x						
	E 4:45 PM		x										E 4:45 PM						x				
	M 9:45 AM			x									M 9:45 AM										
18/02/2011	A 1:15 PM				x							05/03/2011	A 1:15 PM										
	E 4:45 PM												E 4:45 PM										
	M 9:45 AM												M 9:45 AM										
19/02/2011	A 1:15 PM											06/03/2011	A 1:15 PM										
	E 4:45 PM												E 4:45 PM										
	M 9:45 AM												M 9:45 AM						x				
20/02/2011	A 1:15 PM											07/03/2011	A 1:15 PM							x			
	E 4:45 PM												E 4:45 PM								x		
	M 9:45 AM									x			M 9:45 AM										
21/02/2011	A 1:15 PM								x			08/03/2011	A 1:15 PM										
	E 4:45 PM				x								E 4:45 PM										
	M 9:45 AM					x							M 9:45 AM										
22/02/2011	A 1:15 PM			x								09/03/2011	A 1:15 PM										
	E 4:45 PM	x											E 4:45 PM										
	M 9:45 AM												M 9:45 AM						x				
23/02/2011	A 1:15 PM						x					10/03/2011	A 1:15 PM										
	E 4:45 PM					x							E 4:45 PM				x						
	M 9:45 AM		x										M 9:45 AM				x						
24/02/2011	A 1:15 PM					x						11/03/2011	A 1:15 PM										
	E 4:45 PM			x									E 4:45 PM										
	M 9:45 AM										x		M 9:45 AM										
25/02/2011	A 1:15 PM							x				12/03/2011	A 1:15 PM										
	E 4:45 PM										x		E 4:45 PM										
	M 9:45 AM												M 9:45 AM										
26/02/2011	A 1:15 PM											13/03/2011	A 1:15 PM										
	E 4:45 PM												E 4:45 PM										
	M 9:45 AM												M 9:45 AM										
27/02/2011	A 1:15 PM											14/03/2011	A 1:15 PM										x
	E 4:45 PM												E 4:45 PM										x
	M 9:45 AM										x		M 9:45 AM							x			
28/02/2011	A 1:15 PM										x	15/03/2011	A 1:15 PM										
	E 4:45 PM										x		E 4:45 PM										
	M 9:45 AM							x					M 9:45 AM										
01/03/2011	A 1:15 PM								x			16/03/2011	A 1:15 PM	x									
	E 4:45 PM									x			E 4:45 PM										
	M 9:45 AM				x								M 9:45 AM										
02/03/2011	A 1:15 PM			x								17/03/2011	A 1:15 PM		x								
	E 4:45 PM	x											E 4:45 PM										